SCALING OF ENTANGLEMENT ENTROPY IN SOME CONDENSED MATTER SYSTEMS

BY

XIAO CHEN

DISSERTATION

Submitted in partial fulfillment of the requirements
for the degree of Doctor of Philosophy in Physics
in the Graduate College of the
University of Illinois at Urbana-Champaign, 2016

Urbana, Illinois

Doctoral Committee:

Assistant Professor Shinsei Ryu, Chair
Professor Eduardo Fradkin, Director of Research
Assistant Professor Thomas Faulkner
Professor Lance Cooper

Abstract

The following thesis focuses on the scaling of entanglement entropy in lower dimensions and is divided into three main parts. Chapter 2 studies the thermal reduced density matrices in fermion and spin systems on ladders. Chapter 3 studies the many-body localization phase transition in a Rokhsar-Kivelson type wave function. Chapter 4 studies the subleading correction term of entanglement entropy in 2+1 dimensional scale invariant systems. Chatper 5 studies the bulk-boundary correspondence in $3+1$ dimensional topological phases and its entanglement entropy.

In chapter 2, we investigate the reduced density matrices for a model of free fermions on a two-leg ladder (gapped by the inter-chain tunneling operator) and in 1/2 spin systems on a ladder with a gapped ground state using exact solutions and several controlled approximations. We calculate the reduced density matrix and the entanglement entropy for a leg of the ladder (i.e. cut made between the chains). In the fermionic system we find the exact form of the reduced density matrix for one of the chains and determine the entanglement spectrum explicitly. Here we find that in the weak tunneling limit of the ladder the entanglement entropy of one chain of the gapped ladder has a simple and universal form dictated by conformal invariance. In the case of the spin system, we consider the strong coupling limit by using perturbation theory and get the reduced density matrix by the Schmidt decomposition. The entanglement entropies of a general gapped system of two coupled conformal field theories (in 1+1 dimensions) is discussed using the replica trick and scaling arguments. We show that 1) for a system with a bulk gap, the reduced density matrix has the form of a thermal density matrix, 2) the long-wavelength modes of one subsystem (a chain) of a gapped coupled system are always thermal, 3) the von Neumann entropy equals to the thermodynamic entropy of one chain, and 4) the bulk gap plays the role of effective temperature.

In chapter 3, we construct a family of many-body wave functions to study the many-body localization phase transition. The wave functions have a Rokhsar-Kivelson form, in which the weight for the configurations are chosen from the Gibbs weights of a classical spin glass model, known as the Random Energy Model, multiplied by a random sign structure to represent a highly excited state. These wave functions show a phase transition into an MBL phase. In addition, we see three regimes of entanglement scaling with subsystem

size: scaling with entanglement corresponding to an infinite temperature thermal phase, constant scaling, and a sub-extensive scaling between these limits. Near the phase transition point, the fluctuations of the Rényi entropies are non-Gaussian. We find that Rényi entropies with different Rényi index transition into the MBL phase at different points and have different scaling behavior, suggesting a multifractal behavior.

In chapter 4, we study the universal scaling behavior of the entanglement entropy of critical theories in 2+1 dimensions. We specially consider two fermionic scale-invariant models, free massless Dirac fermions and a model of fermions with quadratic band touching, and numerically study the two-cylinder entanglement entropy of the models on the torus. We find that in both cases the entanglement entropy satisfies the area law and has the subleading term which is a scaling function of the aspect ratios of the cylindrical regions. We test the scaling of entanglement in both the free fermion models using three possible scaling functions for the subleading term derived from a) the quasi-one-dimensional conformal field theory, b) the bosonic quantum Lifshitz model, and c) the holographic AdS/CFT correspondence. For the later case we construct an analytic scaling function using holography, appropriate for critical theories with a gravitational dual description. We find that the subleading term in the fermionic models is well described, for a range of aspect ratios, by the scaling form derived from the quantum Lifshitz model as well as that derived using the AdS/CFT correspondence (in this case only for the Dirac model). For the case where the fermionic models are placed on a square torus we find the fit to the different scaling forms is in agreement to surprisingly high precision.

In chapter 5, we discuss (2+1)-dimensional gapless surface theories of bulk (3+1)-dimensional topological phases, such as the BF theory at level K, and its generalization. In particular, we put these theories on a flat (2+1) dimensional torus T^3 parameterized by its modular parameters, and compute the partition functions obeying various twisted boundary conditions. We show the partition functions are transformed into each other under $SL(3,\mathbb{Z})$ modular transformations, and furthermore establish the bulk-boundary correspondence in (3+1) dimensions by matching the modular $\mathcal{S}$ and $\mathcal{T}$ matrices computed from the boundary field theories with those computed in the bulk. We propose the three-loop braiding statistics can be studied by constructing the modular $\mathcal{S}$ and $\mathcal{T}$ matrices from an appropriate boundary field theory. We also study the EE for $3+1$-dimensional topological phase with or without three-loop braiding phase.

To Father and Mother.

Acknowledgments

I would like to start by thanking my advisor, Eduardo Fradkin for his guidance and support in advising me in my research and my career development. He is a brilliant role model and an inspiring mentor to me. I am thankful because he encourages me to think critically and independently in my research, meanwhile he keeps me motivated to explore the field of condensed matter physics with passion and perseverance. Most importantly, he listens to my original ideas and works patiently to plant seeds in them, until they grow into mature trees of wisdom. Apart from enlightening me in research, he also inspired me to cultivate a sense of humor and love for my life, which have helped me keep the work life balance from time to time.

I would like to thank Shinsei Ryu for instructing me patiently when I was a beginning graduate student. From the numerous discussions with him, I came to understand the physics about conformal field theory (CFT). His deep insight about CFT helped me to understand the connection between CFT and topological phases. When I was ready to move forward, Shines gave me several projects at my level in a considerate way. He guided me throughout the projects by explaining the physics in detail to me and reading my calculation carefully. Every time when I was stuck in some calculation and went to Shinsei, he would help me sort through ideas and simplify the calculation. Shinsei works tirelessly 7 days a week (except the time he spends sleeping and babysitting) and his working style also inspires me to persevere and working hard.

I would like to thank Jeffrey Teo for the discussions we've had when he was a postdoc in UIUC. Jeffrey is like an Iron man. When he was in Urbana, we used to have long blackboard discussion on the third floor of ESB from afternoon to evening every week. It was amazing to see everything works out on blackboard. Jeffrey taught me a lot on topological defect by directly drawing them on blackboard in an intuitive way. Apart from physics, I also enjoyed sharing running skills, watching movies and having trips with him in and outside Illinois.

I am grateful towards Thomas Faulkner for sharing with me his understanding on AdS/CFT. Tom often gave me insightful suggestions when I was asking him questions. I benefit much from the numerous discussion sessions with him. I would like to thank Gil Cho for collaborating with me on various projects of entanglement entropy and giving me helpful suggestions about finding postdoc positions. I am also thankful

to Lance Cooper for assigning teaching positions to me in the last several years, and for supporting me going to several conferences by giving me travel awards.

I would like to thank Benjamin Hsu for giving me suggestions in my first year as a fresh graduate student. He kindly help me by introducing his project on entanglement entropy to me. With him, I finished my first project in UIUC, which turned out to be a nice starting point for my graduate school research, and it means a lot to me. In the meantime, I express sincere gratitude to Taylor Hughes, Bryan Clark, Michael Stone and other members in ICMT for their collaborations and invaluable discussions with me.

I would like to thank two former graduate students from physics department, Ching-Kai Chiu and Po-Yao Chuang. Ching-Kai taught me a lot of rock climbing skills when I was a first year graduate student and later on we became climbing partners. Rock climbing enriches my leisure activities beyond physics. We solved several "big" projects together. I also enjoyed several (climbing) trips to national parks with Ching-Kai in the last several years. Po-Yao is my running partner when he was in Urbana. He helped me discover my potential in running marathon. I enjoyed chatting on physics and other interesting topics in the country road of corn fields, where we trained for of Chicago marathon together every summer.

During the last six years, I made a lot of friends from physics department. Just to mention some of them: Abhishek Roy, Apoorv Tiwari, Atma Chan, Bo Han, Can Zhang, Chang-Tse Hsieh, Dalmau, David Luitz, Di Zhou, Gil Cho, Jackson Fliss, Huihuo Zheng, Krishna, Mao-Chuang Yeh, Mayukh, Pei-Wen Tsai, Rodrigo, Xiongjie Yu, Xueda Wen, Wathid, Wenchao Xu, Tianci Zhou, Vasilios Passias, Ye Zhuang and Zihe Gao. I thank them for discussion on physics, many dinners, soccer games, board games and laser tag games we played together in the last several years.

I would like to thank my parents and other relatives for their advice and love in the last six years. My parents Jie Chen and Yinshun Liu support and encourage me along the way to this point.

Finally, and more importantly, to my beloved wife Shengmei Xu, her love, care and company have been the most important during the last several years.

Funding Agencies: This work was supported in part by the National Science Foundation grants, under grants DMR-1064319 and DMR-1408713 at the University of Illinois.

Academic Disclaimer: The author wrote this dissertation in support of requirements for the degree Doctor of Philosophy in Physics at University of Illinois, Urbana-Champaign.

Table of Contents

List of Tables

List of Figures

List of Abbreviations

EE	Entanglement entropy
QBT	Quadratic band touching
CFT	Conformal field theory
MBL	Many-body localization
QBT	Quadratic band touching
RK	Rokhsar-Kivelson
REM	Random energy model
SPT	Symmetry protected topological phase

Chapter 1

Introduction

Entanglement entropy (EE) is an important concept defined in quantum mechanics and quantum information. It distinguishes the quantum state from the classical state. For the pure quantum state, the entanglement entropy is a measure of the quantum entanglement between the subsystem A and its complement B and is defined as follows. In a pure state $|\Psi\rangle$, the density of matrix is

$$\rho_{A\cup B} = |\Psi\rangle\langle\Psi| \tag{1.1}$$

by tracing out the degree of freedom in region B, we obtain the reduced density matrix in subsystem A,

$$\rho_A = \mathrm{Tr}_B \rho_{A\cup B}, \tag{1.2}$$

Therefore, the (von Neumann) entanglement entropy is given by

$$S_{vN}(A) \equiv -\mathrm{Tr}\rho_A \ln \rho_A \tag{1.3}$$

Since the full system $A \cup B$ is in a pure state, $|\Psi\rangle$, the von Neumann entanglement entropy is the same for both members of the partition, $S_{vN}(A) = S_{vN}(B)$. Similarly, the Rényi entropies S_n are given by $(n > 1)$

$$S_n = \frac{1}{1-n} \ln \mathrm{Tr}\rho_A^n \tag{1.4}$$

and are also symmetric under the exchange of regions A and B. In the limit $n \to 1$, the Rényi entropy goes back to S_{vN}.[Callan and Wilczek, 1994, Holzhey et al., 1994, Calabrese and Cardy, 2004]

Von Neumann entanglement entropy for a pure state has some nice properties. For instance, for two subsystem A and B of quantum state $|\Psi\rangle$, the entanglement entropy satisfies triangle inequality,

[Araki and Lieb, 1970]

$$|S(\rho_A) - S(\rho_B)| \leq S(\rho_{AB}) \leq S(\rho_A) + S(\rho_B) \tag{1.5}$$

The right hand inequality can be further generalized to the strong subadditivity constraint for any three subsystem A, B and C,

$$S(\rho_{ABC}) + S(\rho_B) \leq S(\rho_{AB}) + S(\rho_{BC}) \tag{1.6}$$

This constraint has important application for entanglement entropy of many-body state and we will discuss it later.

1.1 EE for $1+1$ dimensional critical system

In the last two decades, people started to study the entanglement entropy for quantum field theory and found that it can be used to successfully capture universal properties of many-body wave function. One celebrated example is $1+1$-dimensional conformal field theories (CFT), which describes the critical point between phase transition in $1+1$-dimensional system. For CFT, it was shown that the von Neumann EE of a subregion A of a partition $A \cup B$ has the universal form[Callan and Wilczek, 1994, Holzhey et al., 1994, Calabrese and Cardy, 2004, Calabrese and Cardy, 2009] $S_{vN} = \frac{c}{3} \log \frac{\ell}{\epsilon}$, where c is the central charge of the CFT, ϵ is the short-distance cutoff, and ℓ is the length of a large subregion A (provided $\epsilon \ll \ell \ll L$, where L is the linear size of the system). Although formally this logarithmic scaling law is consistent with the formal $d \to 1$ limit of the area law, it represents the long-range entanglement properties of $1+1$-dimensional CFTs instead of the short-ranged entanglement reflected in the area law for $d > 1$. Finite sub-leading contributions (as a function of the size of the region) to the EE (in the form of multi-region partitions, mutual information and entanglement negativity) are also known to be determined by the structure of the CFTs and reflect the structure of the large-scale entanglement encoded in their ground state wave functions.[Caraglio and Gliozzi, 2008, Calabrese et al., 2009, Calabrese et al., 2012, Cardy, 2013]

In general, it is very had to calculate entanglement entropy for many-body state analytically since the dimension of the reduced density matrix is divergent in thermodynamic limit. In last two decades, different approaches has been developed to study entanglement entropy for $1+1$ dimensional CFT. One method is to directly calculate the reduced density matrix ρ_A and then study the EE. This method works only for free boson and free fermion system. [Callan and Wilczek, 1994, Holzhey et al., 1994, Vidal et al., 2003,

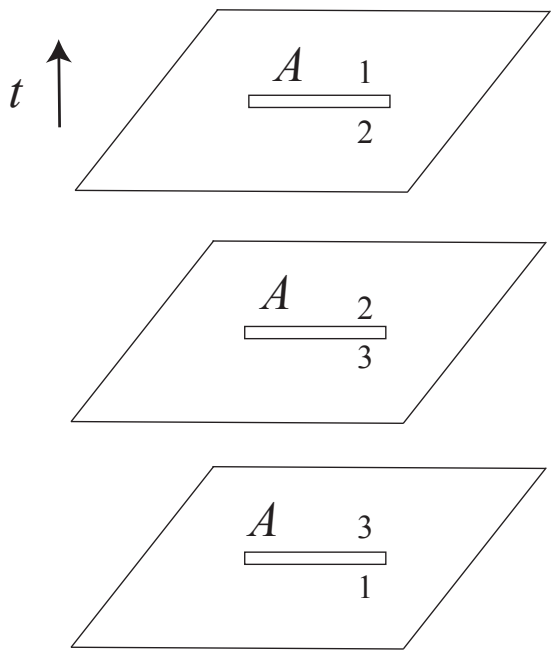

Figure 1.1: stitching three copies together by gluing the boundaries along A

Peschel, 2003, Jin and Korepin, 2004]

A more standard method is to use the replica trick method and express the von Neumann EE as

$$S_{vN} = -\frac{d}{dn}\mathrm{Tr}\rho_A^n|_{n=1} \tag{1.7}$$

where $\mathrm{Tr}\rho_A^n|_{n=1}$ is equal to

$$\mathrm{Tr}\rho_A^n = \frac{Z_n}{Z^n} \tag{1.8}$$

where Z_n is the partition function of a two dimensional Riemann surface formed by gluing the boundaries in region A as shown in Fig. 1.1.[Callan and Wilczek, 1994, Calabrese and Cardy, 2004] Since the partition function for CFT on any manifold can be calculated with the help of the conformal mapping, we can shown that $S_{vN} \sim \frac{c}{3}\log\ell$. The replica trick method can be generalized to higher dimension. However, the partition function is hard to calculate in this case.

According to the Bisognano-Wichmann Theorem,[Bisognano and Wichmann, 1976] in a relativistic quantum field theory in $d+1$ dimensions, for a planar partitioning surface at $x_1 = 0$, the reduced density matrix

for $x_1 > 0$ is

$$\rho_A \sim e^{-\int_{x_1>0} d^d x (2\pi x_1) H} \tag{1.9}$$

In the above equation, the reduced density looks like the thermal density. The entanglement Hamiltonian is the same as the real Hamiltonian with extra prefactor $2\pi x_1$. This extra prefactor can be treated as the inverse temperature and the local temperature at position x_1 is $1/2\pi x_1$. The local temperature is divergent at $x_1 = 0$ and decreases to zero when we go deep into the bulk. Here we would like to apply this formula to $1+1$ dimensional CFT defined on $\mathbb{R}^2$. If the subsystem A is half line $x_1 > 0$, the reduced density matrix is

$$\rho_A \sim e^{-\int_{x_1>0} dx_1 (2\pi x_1) H_{CFT}} \tag{1.10}$$

By using the knowledge of thermal entropy for CFT, [Affleck, 1986, Blote et al., 1986] we can calculate EE for half line. This result can be generalized to any finite single interval by performing conformal mapping.[Casini et al., 2011]

Another interesting example in $1+1$ dimension is the infinite-randomness fixed point for the disordered spin chain,[Fisher, 1994] where the EE also displays a similar $\log \ell$ scaling behavior. By analogy, it was proposed that these models may have very unconventional values for the "effective" central charge.[Refael and Moore, 2009]

1.2 Entanglement Hamiltonian and thermalization of ρ_A

For the reduced density matrix ρ_A, it can always be written in this form,

$$\rho_A = \frac{1}{Z} e^{-H_E} \tag{1.11}$$

where H_E is the entanglement Hamiltonian and is a Hermitian operator. Different from the Hamiltonian defined in region A, H_E in general is not always local and does not have connection with the Hamiltonian H. Only in some special cases, H_E has physical meaning. For instance, as we showed in the previous section in Eq.(1.10), H_E of half line for any $1+1$d CFT is proportional to xH, which actually is $H_{Rindler}$ and therefore we have

$$\rho_A = \frac{1}{Z} e^{-2\pi H_{Rindler}} \tag{1.12}$$

Therefore H_E is a local operator and the reduced density takes a thermal form in Rindler space at temperature $1/2\pi$. In this geometry, the subsystem A and its complement has the same system size and the total Hilbert space can be decomposed into two copies of Rinder Hilbert space. Therefore the total wave function can be written in this way,

$$|\Psi_{CFT}\rangle = \sum_n e^{-\pi E_n} |n\rangle_R |n\rangle_{\bar{R}} \tag{1.13}$$

where E_n is the energy spectrum for the Rindler Hamiltonian $H_{Rindler}$ and $\bar{R}$ means CPT conjugate.

Following the same idea, we can always start with a thermal density matrix ρ_T for system A and construct a pure state by introducing an auxiliary Hilbert space $\bar{H}$, so that the reduced density matrix ρ_A takes a thermal form and $\bar{H}$ can be treated as the heat bath. This model is called thermal double model and has important application in both high energy physics (black hole dynamics) [Asplund et al., 2015, Hartman and Maldacena, 2013] and the bulk boundary correspondence in the topological phase in the condensed matter physics.[Kitaev and Preskill, 2006, Li and Haldane, 2008a, Qi et al., 2012] In chapter 2, we will discuss this toy model in detail in a two-leg ladder chain. We will show that the reduced density matrix for one leg in some situations can take a thermal form.

The thermal double model is an artificial model where we need to couple H_A and $\bar{H}_A$ in a special way so that ρ_A can take a thermal form. In general, for the ground state of a local Hamiltonian, the EE for a ground state satisfies the area law due to some constraints and ρ_A cannot take a thermal form. However, it turns out that for a highly excited state of a generic Hamiltonian, the reduced density matrix for a small subsystem A is expected to take a thermal form where the energy difference with the ground state is related with the effective temperature. Therefore, the isolated quantum wave function decoupled from the environment can act as its own heat bath. This phenomenon is called quantum thermalization and is closed related with a conjecture called eigenstate thermalization hypothesis (ETH). [Srednicki, 1994, Deutsch, 1991] The reduced density matrix takes a thermal form and therefore the entanglement entropy satisfies the volume law. This hypothesis can break down if we introduce strong quench disorder in the system and therefore the system fails to thermalize. This phenomenon is called many-body localization (MBL) and we will discuss it in chapter 3. [Basko et al., 2006, Oganesyan and Huse, 2007, Pal and Huse, 2010] We will show a class of model wave function which can explicitly show MBL phase transition in it.

1.3 EE in spatial dimension $d > 1$

Large-scale entanglement is expected to be found in topological phases of matter (described by topological field theories) and in scale-invariant field theories (which are at a fixed point of the renormalization group) in spatial dimension larger than one. In the cases of topological phases and topological quantum field theories in two spatial dimensions, the EE was shown to obey the scaling law,

$$S_{vN} = \alpha \frac{\ell}{\epsilon} - \gamma_{\text{topo}} \tag{1.14}$$

where α is non-universal and ℓ is the linear size of the macroscopic subregion A, and for a topologically-trivial simply-connected entangling region with smooth boundary $\gamma_{\text{topo}} = \ln \mathcal{D}$ where $\mathcal{D}$ is the effective quantum dimension of the underlying topological field theory,[Kitaev and Preskill, 2006, Levin and Wen, 2006] which is a topological invariant. In fact, in $d = 2$ spatial dimensions, the von-Neumann EE and the Rényi EEs have a rich structure since they also depend on the topology of the entangling regions and, for non-trivial topologies, γ_{topo} depends on the full structure of the topological field theory and not just on the effective quantum dimension.[Dong et al., 2008] This scaling law (and its generalizations) has been verified in many systems including fractional quantum Hall fluids [Zozulya et al., 2009, Zozulya et al., 2007, Li and Haldane, 2008a], $\mathbb{Z}_2$ topological phases of quantum dimer models on non-bipartite lattice [Furukawa and Misguich, 2007, Papanikolaou et al., 2007, Stéphan et al., 2009] and the related Kitaev's Toric Code model (equivalent to the $\mathbb{Z}_2$ gauge theory in its deconfined phase), [Hamma et al., 2005b, Hamma et al., 2005a, Levin and Wen, 2006, Castelnovo and Chamon, 2008] and in the chiral spin liquid phases of $d = 2$ frustrated quantum antiferromagnets [Zhang et al., 2012]. Similar ideas have been generalized to 3+1d topological phases, where EE also has a constant piece correction term and can be used to classify different topological phases (with three-loop braiding phase) [Grover et al., 2011, Chen et al., 2015b]. We will discuss this constant piece correction in detail in chapter 5.

For the scale-invariant systems with spatial dimensions $d > 1$, EE is expected to obey the area law $S_{vN} = \alpha\left(\frac{L_A}{\epsilon}\right)^{(d-1)}$ where L_A is the linear size of the subsystem A. The coefficient α is non-universal and depends on the detail of the model. The area law scaling behavior is coming from the short-range entanglement on the boundary between A and its complement. Apart from the non-universal leading term, there can be possible subleading corrections and it is proposed to be universal.[Casini and Huerta, 2007, Casini and Huerta, 2009, Casini et al., 2011, Ryu and Takayanagi, 2006a, Ryu and Takayanagi, 2006b, Fradkin and Moore, 2006]

Recently, there has been much progress in understanding of this subleading correction in $(2 + 1)$ dimensional CFTs on subsystem with various geometries. It was shown that in the infinite two dimensional

plane, if the subsystem A has the shape of a disk, the subleading correction for the von Neumann EE is a finite constant and is called F in the literature.[Jafferis et al., 2011, Casini et al., 2011, Casini et al., 2015] This F equals to the regulated free energy on S^3 and decreases along RG flow. This constant term is replaced by a scaling function if the whole system is a finite disk instead of infinite plane and is constrained by the strong subadditivity. On the other hand, logarithmic contributions to the EE are found when the entangling region has cusp-like conical singularities with the coefficient representing the effective degree of freedom.[Casini and Huerta, 2007, Bueno et al., 2015] This term depends on the short-distance cutoff and is divergent in the thermodynamic limit. Furthermore, the scaling of EE in cylindrical section of a torus also has a finite subleading term.[Casini and Huerta, 2009, Chen et al., 2015a] This finite term is shown to be scale-invariant and only depends on the aspect ratios of the entangling region. In the thin slice limit, the subleading correction is connected to the corner correction through conformal transformation.[Bueno and Myers, 2015, Witczak-Krempa et al., 2015] These results are found in several different CFTs and are confirmed by the results derived from the Ryu-Takayanagi formula.[Ryu and Takayanagi, 2006a, Ryu and Takayanagi, 2006b]

For the more general scale invariant systems in $2+1$ dimensions without spacetime conformal invariance, such as quantum Lifshitz model and fermionic quadratic band touching model, there can also be subleading correction depending on the geometry of the subsystem.[Fradkin and Moore, 2006, Hsu et al., 2009, Hsu and Fradkin, 2010, Stéphan et al., 2009, Oshikawa, 2010, Chen et al., 2015a] Quantum Lifshitz model is a compact free boson model with dynamical scaling exponent $z = 2$ and the ground state is a Rokhsar-Kivelson type wave function with Gibbs weight of 2d free boson. [Ardonne et al., 2004, Fradkin et al., 2004]. The finite term here can be computed analytically by using the knowledge of conformal field theory. For the fermionic quadratic band touching model having two bands with quadratic band touching point, in the low energy limit, this system is equivalent to a theory of massless Dirac spinor with a quadratic dispersion and hence have $z = 2$. Although these two models do not have Lorentz invariance, it turns out that the subleading correction term has the similar scaling behavior as that for CFTs. [Chen et al., 2015a] We will discuss this subleading correction on torus in detail in chapter 4.

1.4 Organization of this thesis

The rest of this thesis is organized as follows:

In chapter 2, we will study the reduced density matrix of one chain in a two-leg ladder model. This chapter will follow the paper [Chen and Fradkin, 2013]. We first consider a system of free fermions on a ladder model gapped by relevant inter-chain coupling. Since this model is exactly solvable, we will calculate

the reduced density matrix explicitly and show that ρ_A for one leg can take a thermal form. We then consider the spin ladder problem in the strong inter-chain coupling limit and we show that in this limit H_E for one leg is the same as the spin-1/2 quantum Heisenberg chain. After that, we consider a more general case where we formulate a scaling ansatz for the form of entanglement entropy for a system of two weakly coupled CFT. We show that the ρ_A for subsystem of one leg takes the thermal form if the coupling term is relevant. Finally, we consider a counter-example where two coupled Luttinger liquids is in a gapless phase.

In chapter 3, we will discuss the many-body localization phase transition in a Rokhsar-Kivelson type wave function with random sign structure in it. This chapter will follow the paper [Chen et al., 2015c]. We first construct a Rokhsar-Kivelson-type wave function and introduce a random sign structure into it to represent a typical excited state. In the Rokhsar-Kivelson type wave function, the weight is associated with the Gibbs weight of a classical model. The classical model we are using here is the random energy model. Next we analytical calculate the lower bound and upper bound for the Rényi entropies and show that there are thermalized phase and many-body localized phase in it. Furthermore, we identify the MBL phase transition in the wave function numerically by finite size scaling and demonstrate the importance of the sign structure.

In chapter 4, we will study the subleading correction of entanglement entropy for $2+1$-dimensional scale invariant systems on torus and we will focus on two fermionic models with different dynamical exponent. This chapter will follow the paper [Chen et al., 2015a]. We first introduce and explain three possible scaling functions for the subleading correction. The first one is from the holographic calculation, the second one is the exact result for quantum Lifshitz model and the third one is logarithmic correction based on $1+1$ dimensional CFT. Then we numerically calculate the entanglement entropy of Dirac fermion and fermion model quadratic banding touching on the torus with various aspect ratios and test these three possible scaling functions. Finally, we conclude that there is a universal scaling function of the subleading term of the EEs for critical systems.

In chapter 5, we will study the (gapless) boundary-bulk correspondence in $(3+1)$-dimensional topological phase and we use the $\mathcal{S}$ matrix calculated for the boundary theory to investigate the EE for the bulk topological phase. This chapter will follow the paper [Chen et al., 2015b]. We first discuss the partition function for the compactified free boson theory in $(2+1)$ dimensions. Then we study the gapless surface theory of the $(3+1)$d BF theory at level K. We will calculate the $\mathcal{S}$ and $\mathcal{T}$ matrices for the surface theory and use the partition function to compute the constant piece correction for the bulk theory. Later on, we introduce the axion term to the $(3+1)$d BF theory and study the gapless surface state over there. Furthermore, we study the coupled BF theory and its gapless surface state. We will show that this coupled

BF theory realizes the three-loop braiding process and we will also calculate the partition function on the surface. We will compute the $\mathcal{S}$ and $\mathcal{T}$ matrices for the surface theory and use them to extract the constant piece correction of EE for the bulk topological phase.

Chapter 2

Thermal Reduced Density Matrices in Fermion and Spin Systems on Ladders

2.1 Introduction

In this chapter, we investigate the relation between *reduced density matrix* ρ_A and *thermal density matrix* ρ_T. We will study under what condition can reduced density matrix ρ_A of a subsystem of a system in its *ground state* take a *thermal form* ρ_T. Before we go into the detail, we briefly explain the definition of ρ_A and ρ_T.

The thermodynamic entropy is a key concept in Statistical Mechanics, and measures disorder and randomness in a macroscopic system. The thermodynamic entropy S_T for a quantum system in thermal equilibrium at temperature T is defined as

$$S_T \equiv -\mathrm{Tr}\rho_T \ln \rho_T \tag{2.1}$$

where

$$\rho_T \equiv \frac{1}{Z} e^{-\beta H} \tag{2.2}$$

is (thermal density) matrix, of the Gibbs ensemble at temperature T, and $Z \equiv \mathrm{Tr}\exp(-\beta H)$ is the Gibbs partition function with $\beta = 1/T$. At zero temperature, the system is in its ground state (with an at most finite degeneracy) and in this limit the thermodynamic entropy vanishes, $S_T = 0$.

On the other hand, the entanglement entropy is a measure of the non-local correlations of a pure quantum state. The entanglement entropy for subsystem A is a measure of the quantum entanglement between A and B (and viceversa). and it is defined as follows. Let us consider an extended system in a pure state $|\Psi\rangle$, and define a partition of system into two subsystems, A and B with common boundary $\Gamma = \partial A = \partial B$. We will denote by

$$\rho_{A\cup B} = |\Psi\rangle\langle\Psi| \tag{2.3}$$

the density matrix of the pure state $|\Psi\rangle$, and by

$$\rho_A = \mathrm{Tr}_B \rho_{A\cup B}, \quad \rho_B = \mathrm{Tr}_A \rho_{A\cup B}, \tag{2.4}$$

the (normalized) reduced density matrices of the subsystems A and B of the partition (which satisfy $\mathrm{Tr}\rho_A = \mathrm{Tr}\rho_B = 1$). Then, the (von Neumann) entanglement entropy is given by

$$S_{vN}(A) \equiv -\mathrm{Tr}\rho_A \ln \rho_A \tag{2.5}$$

Since the full system $A \cup B$ is in a pure state, $|\Psi\rangle$, the von Neumann entanglement entropy is the same for both members of the partition, $S_{vN}(A) = S_{vN}(B)$. Similarly, the Rényi entropies S_n are given by ($n > 1$)

$$S_n = \frac{1}{1-n} \ln \mathrm{Tr}\rho_A^n \tag{2.6}$$

and are also symmetric under the exchange of regions A and B. In the limit $n \to 1$, the Rényi entropy becomes S_{vN}.[Callan and Wilczek, 1994, Holzhey et al., 1994, Calabrese and Cardy, 2004]

The behavior of the entanglement entropy has been the focus of study in several areas of physics. A particular focus of interest has been the scaling of the entanglement entropy with the linear size ℓ of the subsystem, assumed to be much smaller than the linear size L of the system as a whole, $\ell \ll L$. It is known that for a generic state in spatial dimension d, the entanglement entropy scales with the area of the subsystem $S_{vN}(\ell) = \alpha \ell^{d-1}$ where α is a non-universal constant determined by the short-distance correlations of the wave function.[Bombelli et al., 1986, Srednicki, 1993, Eisert et al., 2010] This result is reminiscent of the area law of the entropy of black holes[Bekenstein et al., 1973, Hawking, 1975] where the constant is instead determined by the Planck scale. Of particular interest is the fact that quantum entanglement also encodes universal information of the non-local correlations of the many-body wavefunction of the macroscopic quantum system.[Calabrese and Cardy, 2004, Kitaev and Preskill, 2006, Levin and Wen, 2006, Fradkin and Moore, 2006, Wen, 2012]

Although the von Neumann *entanglement* entropy S_{vN} has the same formal definition as the *thermodynamic* entropy S_T, these are conceptually different quantities. In this chapter we will be interested in under what circumstances can the *reduced density matrix* ρ_A of a subsystem of a system in its *ground state* $|\Psi\rangle$ define an effective Gibbs ensemble for the subsystem at some effective temperature T_{eff}. For this equivalence to be meaningful it should be possible to express the reduced density matrix, whose spectrum is by definition non-negative, in terms of an effective *local* so-called entanglement Hamiltonian, that we will denote by H_E, whose spectrum is the entanglement spectrum.[Li and Haldane, 2008b] If this equivalence holds, then the reduced density matrix takes the thermal form

$$\rho_A = \frac{1}{Z_{\mathrm{eff}}} e^{-\beta_{\mathrm{eff}} H_E} \tag{2.7}$$

where $\beta_{\rm eff} = 1/T_{\rm eff}$, and the normalization factor $Z_{\rm eff}$ plays the role of an effective partition function. Since the reduced density matrix is, by definition, a Hermitian matrix it is obvious that a suitable Hermitian operator H_E can always be defined. However it is not obvious, and in general it is not true, that H_E should also be local and, even more, what connection it may bear, if any, with the Hamiltonian H of the combined quantum system of which the state $|\Psi\rangle$ is its ground state or with the Hamiltonian H_A of subsystem A (and similarly with B).

In this chapter we will consider systems made of two identical subsystems which are coupled to each other in the bulk. In this case, both subsystems are thermodynamically large and neither can be regarded as a "heat bath" for the other. Here we will focus on the special (and interesting) problem in which the two identical subsystems are one-dimensional and are separately at quantum criticality. The problem that we want to address is under what circumstances can the reduced density matrix of one of these subsystems have a Gibbs form at some effective temperature $T_{\rm eff}$ with a local (and Hermitian) entanglement Hamiltonian H_E. We are motivated by some recent numerical results by Poilblanc[Poilblanc, 2010] who used an exact diagonalization technique to determine the entanglement Hamiltonian for one leg of spin-1/2 quantum antiferromagnet on a two-leg ladder. Over some range of values of the inter-leg exchange interaction, Poilblanc found that the reduced density matrix of one leg is the same as the thermal (Gibbs) density matrix of a spin-1/2 quantum Heisenberg *chain* at an effective temperature (determined by the spin gap of the ladder). Similar results have also been found in other fully gapped systems such as AKLT models on ladders[Katsura et al., 2010, Lou et al., 2011] and in the entanglement of spin and orbital degrees of freedom in Kugel-Khomski models in one dimension.[Lundgren et al., 2012] To this end we examine this question first in an exactly solvable system of free fermions on a ladder, with a gapped ground state. Next we examine the same problem in the spin-1/2 ladder in the strong inter-leg coupling regime, a system recently discussed also by Laüchli and Schliemann[Lauchli and Schliemann, 2012] and by Qi, Katsura and Ludwig[Qi et al., 2012] in 2D topological phases. Next we formulate a scaling hypothesis for the entanglement entropy in the weak coupling limit, where the combined system can be regarded as being a perturbed conformal field theory, and test its validity in the free-fermion system. We finally compare with results in a system of two coupled Luttinger liquids in a gapless combined ground state.[Furukawa and Kim, 2011]

An important question is whether the effective entanglement Hamiltonian H_E is local and what is its relation with the (local) Hamiltonian of the decoupled subsystems. We will see below that if we insist that the entanglement Hamiltonian H_E be fully local (i.e. at the scale of the lattice spacing) the energy gap of the coupled system has to be much larger than the coupling constants (end hence the energy scales) of the subsystems. In this regime all the degrees of freedom of the subsystem are thermal. However we

will see in an explicitly solvable free-fermion example that in regimes in which the gap is small (compared with other scales of the problem), the reduced density matrix for the *long wavelength* degrees of freedom of subsystem A is thermal with a *local* effective *continuum* effective entanglement Hamiltonian which is the same as the Hamiltonian H_A of the low-energy conformal field theory of the decoupled subsystem A. Moreover, in this regime the structure of the effective long-wavelength entanglement entropy has a form which is determined entirely by conformal invariance. This observation leads us to conjecture that this result and not a peculiarity of the free fermion system but it is actually a general property of gapped systems of this type. The separation of the entanglement spectrum into a long-wavelength universal (and thermal) piece and a short-distance non-universal piece that we found in this free-fermion model is in line with what was found by Li and Haldane.[Li and Haldane, 2008b] These authors showed that the low-(pseudo)energy modes of the entanglement Hamiltonian of fractional quantum Hall fluids of a two-dimensional electron gas have the same universal structure as the low-energy states of the edge states of the same fractional quantum Hall state (on a disk geometry).

We should note that the question we are asking here is conceptually different from the central axiom of Statistical Mechanics stating that a subsystem weakly coupled to a much larger system (the "heat bath") can reach thermal equilibrium at a temperature determined by the larger system. It is an axiom of Statistical Mechanics that the equilibrium state of the subsystem is in the Gibbs Ensemble, and that this equilibrium state is universally reached irrespective of the specific dynamics. It is known rigorously that the reduced density matrix of a subsystem has a Gibbs form if the total system is in a "typical state", *i.e.* a state drawn from some statistical ensemble, which is assumed to be a typical state of the spectrum of the full (and generic) Hamiltonian H.[Tasaki, 1998, Goldstein et al., 2006, Popescu et al., 2006] However the ground state of the Hamiltonian is hardly a typical state and one generally does not expect to find a Gibbssian reduced density unless the ground state has special properties.

This chapter is organized as follows. In Section 2.2 we consider a system of free fermions on a ladder which is gapped by the inter-chain tunneling amplitude. This problem is exactly solvable and the reduced density matrix can be determined explicitly.[Peschel, 2003, Peschel and Eisler, 2009, Peschel and Chuang, 2011] In Section 2.3 we consider the spin ladder problem in the strong inter-chain coupling limit and we show that in this limit the reduced density matrix is that of a spin-1/2 quantum Heisenberg chain. In Section 2.4 we use the insights obtained in the free-fermion system of Section 2.2 to formulate a scaling ansatz for the form of the entanglement entropy for a system of two weakly coupled quantum critical systems (which can be regarded as a perturbed conformal field theory). Here we conjecture a general form of the the scaling behavior of the entanglement entropies, and infer that the reduced density matrix for the low energy degrees of freedom of

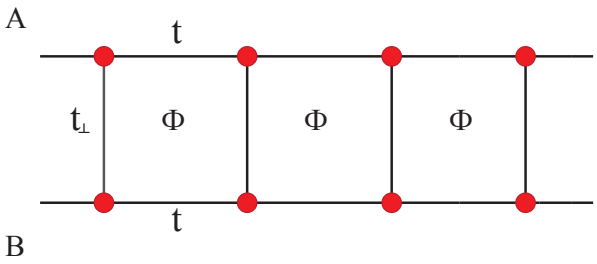

Figure 2.1: The schematic for the two-leg ladder model of free fermions

the subsystem is the thermal Gibbs density matrix of the conformal field theory at a temperature determined by the gap scale. In Section 2.5 we consider the case of two coupled Luttinger liquids with a joint gapless ground state. Our conclusions are summarized in Section 3.5.

2.2 A Free Fermion Model

In this section we will consider a two-leg ladder model of free fermions which are gapped by the inter-chain tunneling.

As shown in Fig., the two-leg ladder model has Hamiltonian [Jaefari and Fradkin, 2012]

$$\begin{aligned} H = \quad & -t\sum_j (e^{i\Phi/2} c^\dagger_{A,j+1} c_{A,j} + e^{-i\Phi/2} c^\dagger_{B,j+1} c_{B,j} + h.c.) \\ & + t_\perp \sum_j (c^\dagger_{A,j} c_{B,j} + c^\dagger_{B,j} c_{A,j}) \end{aligned} \tag{2.8}$$

in which $c_{A,j}$ and $c_{B,j}$ are the fermion operators on chain A and on chain B, respectively. Here t is the hopping amplitude along the chains and $t_\perp$ is the hopping amplitude along the rungs (between the chains). For each plaquette of the ladder there is a flux Φ introduced in the Hamiltonian through minimal coupling (the Peierls substitution). As the flux per plaquette Φ varies from 0 to π the spectrum evolves continuously from a regime with two gapless branches (for $\Phi \sim 0$) to a fully gapped spectrum (for $\Phi \sim \pi$). Since in this chapter we are interested in the gapped case, we consider only the simple case in which the flux per plaquette is half of the flux quantum and hence $\Phi = \pi$ (in units in which $\hbar = c = e = 1$). The behavior of entanglement in the gapless regime is similar to what is discussed in Section 2.5.

In momentum space, the Hamiltonian of this model becomes:

$$H = \int_{-\pi}^{\pi} \frac{dk}{2\pi} \mathcal{H}(k) \tag{2.9}$$

For flux $\Phi = \pi$, the Hamiltonian $\mathcal{H}(k)$ of Eq.(2.9) is

$$\begin{aligned}\mathcal{H}(k) =& 2t \sin k \ \left(c_A(k)^\dagger c_A(k) - c_B(k)^\dagger c_B(k)\right) \\ & - t_\perp \left(c_A(k)^\dagger c_B(k) + c_B(k)^\dagger c_A(k)\right)\end{aligned} \tag{2.10}$$

The Hamiltonian can be diagonalized by a change of basis

$$\begin{aligned}c_A(k) =& \cos\left(\frac{\xi(k)}{2}\right) c^a(k) - \sin\left(\frac{\xi(k)}{2}\right) c^b(k) \\ c_B(k) =& \sin\left(\frac{\xi(k)}{2}\right) c^a(k) + \cos\left(\frac{\xi(k)}{2}\right) c^b(k)\end{aligned} \tag{2.11}$$

where b and a label the bonding and the anti-bonding bands of the ladder, respectively, and $\xi(k)$ is defined as

$$\begin{aligned}\sin\left(\frac{\xi(k)}{2}\right) =& \frac{u(k)}{\sqrt{1+u^2(k)}} \\ \cos\left(\frac{\xi(k)}{2}\right) =& \frac{1}{\sqrt{1+u^2(k)}}\end{aligned} \tag{2.12}$$

where $u(k)$ is given by

$$t_\perp u(k) = 2t \sin k + \sqrt{(2t \sin k)^2 + t_\perp^2} \tag{2.13}$$

The dispersion relations for the bonding and anti-bonding bands are

$$E(k) = \pm\sqrt{(2t \sin k)^2 + t_\perp^2} \tag{2.14}$$

At half filling, the bonding band is filled and the anti-bonding band is empty. As can be seen from Eq.(2.14), the excitation energy $E(k)$ is smallest at $k = 0, \pi$, where the spectrum has an energy gap of $2t_\perp$.

As in all fermionic systems in 1D, this system can also be put in the form of 1D Dirac fermions with two two-component spinor fields, with the components being the right and left moving amplitudes near the two Fermi points at $k = 0, \pi$. Therefore the low-energy degrees of freedom of this ladder (with flux $\Phi = \pi$) are described by two species (bonding and anti-bonding) Dirac spinors each with velocity $v = 2t$ and mass gap $mv^2 = t_\perp$. This can be done, more formally, by combining the right moving fermion from the A chain (with $k \sim 0$), $R_A(k)$ and the left-moving fermion from the B chain (also with $k \sim 0$), $L_B(k)$, into a two-component (Weyl) spinor. Similarly a second spinor can be constructed where $\tilde{R}_B(k)$ is the right-moving component of the fermion on the B chain with momentum $-\pi + k$ and $\tilde{L}_A(k)$ is the left-moving fermion from the A chain

with momentum $\pi - k$.

$$\psi_1(k) = \begin{pmatrix} R_A(k \\ L_B(k) \end{pmatrix}, \qquad \psi_2(k) = \begin{pmatrix} \tilde{R}_B(k) \\ \tilde{L}_A(k) \end{pmatrix} \tag{2.15}$$

The tunneling matrix element $t_\perp$, which mixes right and left movers with the same momenta on both chains, opens the (same) mass gap $m \propto t_\perp$ in both Dirac spinors. The effective (continuum) low energy Hamiltonian density for this system is

$$\mathcal{H} = \sum_{a=1,2} \left(\psi_a^\dagger \sigma_3 iv \partial_x \psi_a + m v^2 \psi_a^\dagger \sigma_1 \psi_a \right) \tag{2.16}$$

where $a = 1, 2$ labels the two spinors and σ_1 and σ_3 are the two 2×2 Pauli matrices (which act on the components of each spinor).

Below we will calculate the reduced density matrix for chain A by making a cut between the chains and trace out chain B. We can now use the results of Peschel [Peschel, 2003] for free-fermion system to find the entanglement Hamiltonian

$$\widetilde{H}_E \equiv -\ln \rho_A \tag{2.17}$$

for subsystem A, which has the explicit form

$$\widetilde{H}_E = \sum_{i,j=1}^{N} \widetilde{H}_{ij} c_i^\dagger c_j \tag{2.18}$$

where the matrix $\widetilde{H}_{ij}$ takes the form

$$\widetilde{H}_{ij} = \left(\ln \left[(C^{-1} - 1) \right] \right)_{ij} \tag{2.19}$$

The creation and annihilation operators $c_I^\dagger$ and c_i in Eq.(2.18) are labelled by the sites of subsystem A. In Eq.(2.19) C_{ij} is the correlation function matrix (the fermion propagator at equal times) whose matrix elements in momentum space are

$$\begin{aligned} C_{kk'} =& \langle c_A^\dagger(k) c_A(k') \rangle = 2\pi \delta(k - k') \sin^2 \left(\frac{\xi(k)}{2} \right) \\ =& 2\pi \delta(k - k') \frac{u^2(k)}{1 + u^2(k)} \end{aligned} \tag{2.20}$$

Combining the above two equations, we find that the entanglement Hamiltonian (in momentum space) has the standard form

$$\widetilde{H}_E = \int_{-\pi}^{\pi} \frac{dk}{2\pi} \, \omega(k) \, c^\dagger(k) c(k) \tag{2.21}$$

where

$$\omega(k) = \ln u^2(k) \tag{2.22}$$

By inspection of Eq.(2.13) we see that as $k \to 0$ the quantity $u(k) \simeq 1 + vk/t_\perp + O(k^2)$, and similarly as $k \to \pi$. Thus the one-particle spectrum $\omega(k)$ vanishes linearly as $k \to 0, \pi$. In other terms, the long-wavelength modes (with $k \sim 0, \pi$) of the one-particle entanglement spectrum is that of a system of massless fermions, $\omega(k) \simeq 2vk/t_\perp$, with the modes near $k = 0$ representing right-movers and the modes near $k = \pi$ representing left movers, respectively.

If we define the inverse temperature $\beta_{\text{eff}} = (t_\perp/2)^{-1}$, we can rewrite the reduced density matrix ρ_A as

$$\rho_A = \rho_{T_{\text{eff}}} = \frac{1}{Z} e^{-\beta_{\text{eff}} H_A} \tag{2.23}$$

We can see that ρ_A has the same form as ρ_T for chain A with $T_{\text{eff}} = t_\perp/2$ playing the role of the temperature. Therefore, the entanglement Hamiltonian for the long-wavelength modes (near $k = 0$ and $k = \pi$, always has the form (regardless of the strength of the tunneling amplitude $t_\perp$)

$$\begin{aligned} \widetilde{H}_E =& \int_{-\Lambda}^{\Lambda} \frac{dk}{2\pi} \frac{4ta}{t_\perp} k\big(R^\dagger(k)R(k) - L^\dagger(k)L(k)\big) \\ =& \beta_{\text{eff}} H_A \end{aligned} \tag{2.24}$$

where $R(k)$ represent the right-moving modes (with $k \sim 0$) and $L(k)$ the left-moving modes (with wave vector $\pi - k$), respectively, $v = 2ta$ is the velocity of the modes, and $\Lambda \sim \pi/a$ is a momentum cutoff (and a is the lattice spacing which we have set to 1). In other terms, the long-wavelength entanglement Hamiltonian for chain A is the same as the low-energy Hamiltonian H_A for the Dirac fermions of the decoupled chain. Therefore the long-wavelength reduced density matrix is the Gibbs density matrix of a system of a massless Dirac fermion (with velocity $2t$) at temperature $T_{\text{eff}} = \beta_{\text{eff}}^{-1} = t_\perp/2$.

On the other hand, in the strong coupling (tunneling) limit $t_\perp \gg t$, in which there is a large energy gap in the spectrum of the fermions, the entanglement Hamiltonian has the simple form

$$\begin{aligned} \widetilde{H}_E =& \int_{-\pi}^{\pi} \frac{dk}{2\pi} \frac{4t}{t_\perp} \sin k \; c^\dagger(k)c(k) \\ =& \beta_{\text{eff}} \; it \sum_{n=1}^{N} \; c(n)^\dagger c(n+1) + \text{h.c.} \end{aligned} \tag{2.25}$$

In this limit the reduced density matrix for leg A is that of a single chain of free fermions with hopping amplitude it at an effective temperature $T_{\text{eff}} = t_\perp/2$.

This effective temperature is in fact much higher than the bandwidth $4t$ of the fermionic spectrum of the chain. Thus, the statistical ensemble of the chain defined by the strong tunneling limit is essentially the classical Gibbs ensemble. In the strong tunneling limit the entanglement Hamiltonian is a local operator of the chain degrees of freedom. Clearly the corrections to this strong tunneling limit lead to an effective entanglement Hamiltonian which becomes increasingly non-local. Nevertheless, these apparently non-local lattice operators only contribute with irrelevant operators in the long-wavelength regime.

In summary, in this free fermion ladder model the reduced density matrix of a chain has a Gibbs form with an effective entanglement Hamiltonian H_E, given in Eq.(2.21). Since the reduced density matrix for chain A is thermal, the von Neumann entanglement entropy is equal to the thermodynamic entropy of the 1D quantum system described by the Hamiltonian H_E. As the strength of the tunneling matrix element $t_\perp$ increases, the fraction of the entanglement spectrum that is thermal also increases ranging from only the long-wavelength modes of chain A for $t_\perp \ll t$ to all of the modes for $t_\perp \gg t$, with an effective temperature $T_{\rm eff} = t_\perp/2$. Nevertheless, the long-wavelength modes, i.e. the lowest eigenvalues of the entanglement Hamiltonian, which are always thermal, have universal properties.

The free energy of a system of 1D massless Dirac fermions (in a system of length L in the thermodynamic limit) at temperature T is that of a conformal field theory with central charge $c = 1$ (see Refs. [Affleck, 1986, Blote et al., 1986])

$$F = -T \ln Z = \varepsilon_0 L - \frac{\pi c}{6v} T^2 L \tag{2.26}$$

where ε_0 is the (non-universal) ground state energy density, c is the central charge of the conformal field theory and v is the velocity of the modes. The last term in Eq.(2.26) is universal and it is well known low temperature (the Casimir term) contribution to the free energy of a conformal field theory. The form of this term is determined by the conformal anomaly of the conformal field theory.[Affleck, 1986, Blote et al., 1986] From here it follows that the thermodynamic entropy S_T of this 1D quantum critical system is

$$S_T = -\frac{\partial F}{\partial T} = \frac{\pi c}{3v} T L \tag{2.27}$$

Depending on the boundary conditions, the entropy S_T may have the finite limiting value $\ln g$ as $T \to 0$, where g is a universal number that depends on the boundary conditions and can be interpreted as a ground state "degeneracy" (even though it is generally not an integer). [Affleck and Ludwig,]

Since we have shown that the reduced density matrix of a leg of the fermion ladder with flux $\Phi = \pi$ per plaquette is, in the long wavelength limit, identical to the Gibbs density matrix of a system of massless Dirac fermions in 1D, we can apply the above results from CFT to the present case. It then follows that the

thermodynamic entropy of a system of 1D massless Dirac fermions at finite temperature T is the same as the von Neumann entanglement entropy S_{vN} of chain A (also in the long wavelength limit) with a temperature $T = T_{\rm eff} = M$, given by the mass gap of the fermion ladder.

It is an elementary excercise to compute the Rényi entropies, S_n. Indeed in this system the trace of the nth power of the (unnormalized) reduced density matrix ρ_A is now equal to the partition function of a free Dirac fermion at temperature $T_{\rm eff}/n$,

$$\begin{aligned} {\rm Tr}\rho_A^n =& Z_F\left(T = \frac{T_{\rm eff}}{n}\right) \\ =& \exp\left(-\frac{n}{T_{\rm eff}}\varepsilon_0 L + \frac{\pi c}{6v}\frac{T_{\rm eff}}{n}L\right) \end{aligned} \tag{2.28}$$

where we have purposely left the explicit dependence on the central charge c of the CFT (although for the free fermion case $c = 1$). We will return to this expression in Section 2.4. Therefore

$$\frac{{\rm Tr}\rho_A^n}{({\rm Tr}\rho_A)^n} \equiv {\rm Tr}\hat{\rho}_A^n = \exp\left[\frac{\pi c}{6v}\left(\frac{1}{n} - n\right)T_{\rm eff}L\right] \tag{2.29}$$

where we denoted by $\hat{\rho}_A$ the normalized reduced density matrix, i.e. ${\rm Tr}\hat{\rho}_A = 1$. From here we find that the von Neumann entanglement entropy S_{vN} is given by

$$S_{vN} = -\frac{\partial}{\partial n}{\rm Tr}\hat{\rho}_A^n\Big|_{n\to 1} = \frac{\pi c}{3v}T_{\rm eff}L = S(T_{\rm eff}) \tag{2.30}$$

which agrees with the thermodynamic entropy $S(T_{\rm eff})$ at temperature $T_{\rm eff}$ (as it should). Similarly, the Rényi entropy S_n is given by the result (valid for $n > 1$)

$$S_n = \frac{\pi c}{6v}\left(1 + \frac{1}{n}\right)T_{\rm eff}L \tag{2.31}$$

Notice that $S_1 = \lim_{n\to 1} S_n = S_{vN}$ as it should.

We close this section with a comment of the correlators. The equal-time fermionic correlators, i.e. the equal time propagators (or Green functions), of a theory of massive fermions in $1+1$ dimensions has an asymptotic exponential decay $\exp(-m|x|)$ (where m is the mass gap) with a power law correction prefactor $(m|x|)^{-1/2}$. This behavior is correctly reproduced by Eq.(2.20) (as it should). However the equal-time correlation function of gapless Dirac fermions at temperature T has a pure exponential decay of the form $\pi T/\sinh(2\pi T|x|)$, which does not have a power law prefactor correction. This apparent difference is the result of the long-wavelength approximation used in the entanglement Hamiltonian of Eq.(2.24).

2.3 Entanglement in Strongly Coupled Systems

For a free fermion model, such as the one discussed in Section 2.2, we can exactly calculate the reduced density matrix for any value of the coupling constant. For the general case of two arbitrary coupled systems which are not free the computation of the reduced density matrix is non-trivial. However, in the strong coupling limit we can still use the perturbation theory to calculate the reduced density matrix. This is the approach we will follow here. A similar calculation was done by Laüchli and Schliemann.[Lauchli and Schliemann, 2012]

In general the Hamiltonian will have the form $H = H_0 + H_{\rm pert}$, where H_0 is the (local) inter-chain coupling between chains A and B and $H_{\rm pert}$ represents the Hamiltonian of the two decoupled chains. The ground state of the coupled system, to zeroth order in perturbation theory is the product state $\left|\Psi_0\right\rangle = |1\rangle \times |2\rangle \times \ldots \times |N\rangle$ where $\{\left|n\right\rangle\}$ (with $n = 1, \ldots N$ for chains of N sites) are the states of the degrees of freedom of the two chains at the nth rung of this ladder. This ground state is non-degenerate and has a finite (and large) energy gap to all excitations. Since it is a product of singlet states, it is also "maximally entangled" even though in this basis the ground state is a product state. This is a simple example showing that the degree of entanglement of a state depends on how the question is posed, i.e. on the choice of the entangling region. Thus if we choose as the entangling region the left half of the ladder we would conclude that its entanglement entropy would be trivially zero. In contrast, if we choose one chain of the ladder as the entangling region the entanglement entropy will be (trivially) maximal).

We can compute next the corrections to the unperturbed ground state $\left|\Psi_0\right\rangle$ using an expansion in powers of the intra-chain interactions. Since we start with a gapped phase, the strong coupling expansion works well. For the sake of definiteness we will consider the problem of a quantum Heisenberg antiferromagnetic model with $S = 1/2$ on a two-leg ladder as an example. Other models can be treated using a similar procedure.

The unperturbed Hamiltonian H_0 now contains only the inter-chain exchange interactions (with coupling constant $J_\perp$) on the rungs of the ladder,

$$H_0 = J_\perp \sum_{n=1}^{N} \vec{S}_A(n) \cdot \vec{S}_B(n) \tag{2.32}$$

The coupling between the chains A and B is anti-ferromagnetic with $J_\perp > 0$. For H_0, the ground state is the product of N spin singlets on the rungs

$$\left|\Psi_0\right\rangle = \prod_{i=n}^{N} \left|0,0\right\rangle_n \tag{2.33}$$

where

$$\big|0,0\rangle_n = \frac{1}{\sqrt{2}}\big(\big|\uparrow_A,\downarrow_B\rangle_n - \big|\downarrow_A,\uparrow_B\rangle_n\big) \tag{2.34}$$

is the spin singlet state on the nth rung of the ladder. In the first excited state of the ladder, $\big|\Psi_1\rangle$, the spin singlet state of one rung is replaced by a spin triplet state $\big|1,m\rangle$, with $m=\pm1,0$ given by their standard expressions, $\big|1,1\rangle = \big|\uparrow_A,\uparrow_B\rangle$, $\big|1,-1\rangle = \big|\downarrow_A,\downarrow_B\rangle$, and $\big|1,0\rangle = (\big|\uparrow_A,\downarrow_B\rangle + \big|\downarrow_A,\uparrow_B\rangle)/\sqrt{2}$. The excitation energy is $E_1 - E_0 = J_\perp$. For the second excited state $\big|\Psi_2^{i,j}\rangle$, two singlets at rungs i and j become triplets, etc. For the kth excited state $\big|\Psi_k\rangle$, the excitation energy is $kJ_\perp$.

The perturbing Hamiltonian $H_{\rm pert}$ is the sum of the Hamiltonians of the quantum Heisenberg antiferromagnets of the two chains

$$\begin{aligned}
H_{\rm pert} =& J\sum_{n=1}^{N}(\vec{S}_A(n)\cdot\vec{S}_A(n+1) + \vec{S}_B(n)\cdot\vec{S}_B(n+1)) \\
=& \frac{J}{2}\sum_{n=1}^{N}\big(\sigma_A^+(n)\sigma_A^-(n+1) + \sigma_A^-(n)\sigma_A^+(n+1)\big) \\
&+\frac{J}{4}\sum_{n=1}^{N}\sigma_A^z(n)\sigma_A^z(n+1) \\
&+\frac{J}{2}\sum_{n=1}^{N}\big(\sigma_B^+(n)\sigma_B^-(n+1) + \sigma_B^-(n)\sigma_B^+(n+1)\big) \\
&+\frac{J}{4}\sum_{n=1}^{N}\sigma_B^z(n)\sigma_B^z(n+1)
\end{aligned} \tag{2.35}$$

where we have expressed the spin operators in terms of the Pauli matrices.

Let us compute the ground state of the ladder to first order in perturbation theory in $H_{\rm pert}$. By inspection of Eq.(2.35) we see that the only non vanishing contribution involves breaking the spin singlets on pairs of nearest-neighbor rungs at a time, i.e. only $\langle\Psi_2^{n,n+1}\big|H_{\rm pert}\big|\psi_0\rangle \neq 0$. The perturbed ground state is

$$\begin{aligned}
\big|\Psi\rangle =& \big|\Psi_0\rangle + \sum_n \frac{\langle\Psi_2^{n,n+1}\big|H_{\rm pert}\big|\Psi_0\rangle}{E_0 - E_2}\big|\Psi_2^{n,n+1}\rangle \\
=& \big|\Psi_0\rangle \\
&-\sum_n\left(-\frac{J}{16J_\perp}\big|\phi_1^{n,n+1}\rangle - \frac{J}{16J_\perp}\big|\phi_2^{n,n+1}\rangle + \frac{J}{4J_\perp}\big|\phi_3^{n,n+1}\rangle\right)
\end{aligned} \tag{2.36}$$

where $\{\big|\phi_{1,2,3}^{n,n+1}\rangle\}$ are three different types of excited states of the unperturbed Hamiltonian H_0. In these

excited states spins on pairs of nearest-neighbor rungs are put in triplet states. They are given by

$$\begin{aligned}
\big|\phi_1^{n,n+1}\big\rangle &= \ldots \big|1,1\big\rangle_n \big|1,-1\big\rangle_{n+1} \ldots \\
\big|\phi_2^{n,n+1}\big\rangle &= \ldots \big|1,-1\big\rangle_n \big|1,1\big\rangle_{n+1} \ldots \\
\big|\phi_3^{n,n+1}\big\rangle &= \ldots \big|1,0\big\rangle_n \big|1,0\big\rangle_{n+1} \ldots
\end{aligned} \tag{2.37}$$

where $\ldots$ represents product of singlets on the other rungs. We have

$$\begin{aligned}
\langle\phi_1^{n,n+1}\big|H_{\rm pert}\big|\Psi_0\rangle &= -J/8 \\
\langle\phi_2^{n,n+1}\big|H_{\rm pert}\big|\Psi_0\rangle &= -J/8 \\
\langle\phi_3^{n,n+1}\big|H_{\rm pert}\big|\Psi_0\rangle &= J/2
\end{aligned} \tag{2.38}$$

The wavefunction of Eq.(2.36) is written in the basis of states of total spin state on the rungs. However in order to compute the reduced density matrix of one chain we will need to express the wave function in the basis of the spin projections of each chain, $\big|S^z(1),\ldots,S^z(N)\big\rangle_A$ for chain A, and $\big|S^z(1),\ldots,S^z(N)\big\rangle_B$ for chain B, respectively. Let us denote the spin configurations in chain A by $\big|\phi\big\rangle_A$ and the spin configurations of chain B by $\big|\phi\big\rangle_B$.

In this basis the unperturbed wave function $\big|\Psi_0\big\rangle$ of Eq.(2.33) is given by

$$\begin{aligned}
\big|\Psi_0\big\rangle &= \sum_{C(B)} \left(\frac{1}{\sqrt{2}}\right)^N (-1)^{m_d(C(B))} \big|\phi\big\rangle_A \big|\phi\big\rangle_B \\
&= \sum_{C(B)} \left(\frac{1}{\sqrt{2}}\right)^N (-1)^{m_d(C(B))} \big|\uparrow\downarrow \ldots \downarrow\uparrow \ldots\big\rangle_A \,\big|\downarrow\uparrow \ldots \downarrow\uparrow \ldots\big\rangle_B
\end{aligned} \tag{2.39}$$

where we have denoted by $C(B)$ the set of all spin configurations in chain B, and by $m_d(C(B))$ the number of down spins $\downarrow$ in the configuration of chain B. Notice that in this basis the spin configurations $\big|\phi\big\rangle_A$ of chain A are antiparallel to the spin configurations $\big|\phi\big\rangle_B$ in chain B at every rung of the ladder. Although this is a product state, this state is maximally entangled when the cut is made between the chains.

Similarly, when we add $H_{\rm pert}$ to H_0, in the basis of the spin projection of each chain, the perturbed

wavefunction $|\Psi\rangle$ defined in Eq.(2.36) can be rewritten in the following form:

$$\begin{aligned}
|\Psi\rangle &= \sum_{C(B)} \left(\frac{1}{\sqrt{2}}\right)^N (-1)^{m_d(C(B))} \left[(1 - \frac{J}{4J_\perp}M_1 + \frac{J}{4J_\perp}M_2)|\phi\rangle_A - \sum_{C(A)'} \frac{J}{8J_\perp}|\phi'\rangle_A\right] |\phi\rangle_B \\
&= \sum_{C(B)} \left(\frac{1}{\sqrt{2}}\right)^N (-1)^{m_d(C(B))} \left[(1 - \frac{J}{4J_\perp}M_1 + \frac{J}{4J_\perp}M_2)|\uparrow ... \uparrow\downarrow ...\rangle_A \right. \\
&\quad \left. - \sum_{C(A)'} \frac{J}{8J_\perp}|\uparrow ... \downarrow\uparrow ...\rangle_A\right] |\downarrow ... \downarrow\uparrow ...\rangle_B
\end{aligned} \tag{2.40}$$

where $C(B)$ represents all the spin configurations $|\phi\rangle_B$ of chain B (which are presented schematically in Eq.(2.40)). For each $|\phi\rangle_B$, the spin configuration $|\phi\rangle_A$ of chain A is antiparallel with the spin configuration in chain B. $|\phi'\rangle_A$ is defined by flipping the neighboring antiparallel spin paris ($\uparrow\downarrow$ or $\downarrow\uparrow$) in $|\phi\rangle_A$ and $C(A)'$ represents all possible spin configurations for $|\phi'\rangle_A$. $m_d(C(B))$ is the number of down spins $\downarrow$ in the states of the B chain, M_1 and M_2 are the numbers of pairs for parallel spins ($\uparrow\uparrow$ or $\downarrow\downarrow$) and antiparallel spins ($\uparrow\downarrow$ or $\downarrow\uparrow$) in $|\phi\rangle_A$.

To get the reduced density matrix for chain A, we need to use the Schmidt decomposition to trace out the states in chain B. The resulting (unnormalized) reduced density matrix for chain A is

$$\begin{aligned}
\rho_A &= \sum_{C(A)} \frac{1}{2^N} \left[\left(1 - M_1\frac{J}{2J_\perp} + M_2\frac{J}{2J_\perp}\right)|\phi\rangle_A\langle\phi|_A - \sum_{C(A)'}\left(\frac{J}{4J_\perp}|\phi\rangle_A\langle\phi'|_A + \text{h.c.}\right)\right] \\
&= \sum_{C(A)} \frac{1}{2^N} \left[\left(1 - M_1\frac{J}{2J_\perp} + M_2\frac{J}{2J_\perp}\right)|\uparrow ... \downarrow\uparrow ...\rangle_A\langle\uparrow ... \downarrow\uparrow ...|_A \right. \\
&\quad \left. - \sum_{C(A)'}\left(\frac{J}{4J_\perp}|\uparrow ... \downarrow\uparrow ...\rangle_A\langle\uparrow ... \uparrow\downarrow ...|_A + \text{h.c.}\right)\right]
\end{aligned} \tag{2.41}$$

(2.42)

where $C(A)$ are all the spin configurations in chain A and $C(A)'$ are the spin configurations obtained by flipping neighboring antiparallel spin pairs in $|\phi\rangle_A$.

The reduced density matrix for chain A can be computed straightforwardly at this (first) order in perturbation theory in $J/J_\perp$. It has the form

$$\rho_A = \frac{1}{Z}(1 - \beta_{\text{eff}}H_E + \ldots) \simeq \frac{1}{Z}e^{-\beta_{\text{eff}}H_E + \ldots} \tag{2.43}$$

where Z normalizes the reduced density matrix, and H_E is the entanglement Hamiltonian. Notice that in

Eq.(2.43), in the square bracket, there are two terms, the first term $|\phi\rangle_A\langle\phi|_A$ can be understood as the potential term and the second term $|\phi\rangle_A\langle\phi'|_A$ represents the hopping term between neighboring sites. Thus H_E (at this order) is the Hamiltonian of the spin-1/2 antiferromagnetic quantum Heisenberg chain,

$$\begin{aligned} H_E =& \frac{J}{4}\sum_n \Big(2\sigma^z(n)\sigma^z(n+1) \\ &+ \sigma^+(n)\sigma^-(n+1) + \sigma^-(n)\sigma^+(n+1)\Big) + \dots \\ =& J\sum_n \vec{S}_A(n)\cdot\vec{S}_A(n+1) + \dots \end{aligned} \tag{2.44}$$

Thus, in the strong coupling limit, $J_\perp \gg J$, the reduced density matrix ρ_A of chain A is equal to the thermal density matrix ρ_T of the chain with an effective (very high) temperature $T_{\text{eff}} = 2J_\perp \gg J$. In this limit the entanglement entropy equals to thermal entropy of the chain.

The result we derived is a general consequence of the strong coupling limit and it is not peculiar to a ladder system. It is straightforward to see that, for instance, it also applies to a 2D bilayer antiferromagnet in the regime of strong inter-layer exchange interactions. In this regime the bilayer system is gapped and the ground state is also well approximated by a product of singlets on the inter-layer couplings. By construction, in all cases the resulting reduced density matrix always describes a system at very high temperature. Thus we obtain that the reduced density matrix is thermal with an effective local Hamiltonian which that of a 2D quantum Heisenberg antiferromagnet. Since the effective temperature is much larger than the intra-layer exchange interaction, the reduced density matrix of layer A describes the paramagnetic phase of a single-layer antiferromagnet. However, this result does not imply that the entanglement Hamiltonian must necessarily always be equal to the Hamiltonian of the subsystem. For instance, Laüchli and Schliemann have also shown that at second order in perturbation theory the entanglement Hamiltonian acquires a next-nearest-neighbor exchange interaction. Higher order terms in perturbation theory will generate more non-local terms in the effective Hamiltonian.

2.4 Weak Coupling Limit

From the discussion in Section 2.2 we see that for the free fermion model, in the strong tunneling limit, the reduced density matrix of one chain has thermal form, $\rho_A = \rho_T$. However, in the same section we also saw that for the low energy modes of a chain of the ladder, i.e. those with wave vectors around $k = 0$ and $k = \pi$, the reduced density matrix of one chain is also thermal regardless of the strength of the tunneling matrix element $t_\perp$. Also in section 2.3 we saw that in the case of antiferromagnets on ladders, the reduced density

matrix of one chain of the ladder is also thermal in the strong inter-ladder coupling, albeit with a temperature large compared with the scale of the entanglement Hamiltonian (which has the quantum Heisenberg form). By comparison with the results of Section 2.2 we would also expect that the reduced density matrix for the long-wavelength degrees of freedom of a chain of the ladder should also have a thermal form. This issue cannot be addressed by a direct calculation from the inter-chain strong-coupling regime of the ladder.

In this section, we will consider the general case in the weak coupling limit. We consider a system with two critical chains with the same Hamiltonian which in the low-energy and long-wavelength limit describes a conformal field theory (CFT) in $1+1$ dimensions. We will further assume that, when coupled by some relevant operator $O(A,B)$ of the CFT, the combined system flows to a fixed point with a finite energy gap in its spectrum. Our goal is to determine if the reduced density matrix of one subsystem, A, has a thermal form.

Formally, the Hamiltonian of the coupled CFTs has the form

$$H = H_A + H_B + \int dx\, g\, O(A,B) \tag{2.45}$$

where $H_A \simeq H_B$ describe the two critical subsystems (the "legs"), $O(A,B)$ is a suitable local relevant operator, and g is a coupling constant. We will assume that this operator has the form $O(A,B) = \phi(A)\phi(B)$ where $\phi(A)$ and $\phi(B)$ are local operators of A and B each with (the same) scaling dimension $\Delta_{\phi(A)} = \Delta_{\phi(B)} \equiv \Delta/2$. This perturbation is relevant if its scaling dimension $\Delta_{\phi(A)} + \Delta_{\phi(B)} = \Delta \leq 2$ (where 2 is the space-time dimension). Under these assumptions this perturbation drives the combined system into a massive phase with a finite mass gap $M(g)$ which obeys the scaling relation $M(g) \sim \text{const.}\ g^{\nu z}$ where $\nu = 2 - \Delta$. These CFTs are "relativistic" and hence have dynamical exponent $z = 1$. The case $\Delta = 2$ is special in that the operator $O(A,B)$ is marginal. We will further assume that in this case it is marginally relevant.

In the case of the fermionic ladder of Section 2.2 the CFT of the decoupled chains is a theory of two massless Dirac (Weyl) fermions (and hence with central charge $c = 2$). The scaling dimension of the tunneling operator (i.e. the fermion mass term) is $\Delta = 1$ which is relevant. In this case, the exponent is $\nu = 1$. In the case of the two-leg ladder, the decoupled ladder is a theory of two spin-1/2 quantum Heisenberg antiferromagnetic chains and hence are critical. The CFT of the spin-1/2 quantum Heisenberg antiferromagnetic chain is an $SU(2)_1$ Wess-Zumino-Witten (WZW) model.[Affleck,] Hence the decoupled ladder is a product of two $SU(2)_1$ WZW models (with total central charge $c = 2$). The most relevant operator in the inter-ladder exchange interaction is the coupling of the Néel order parameters of each chain,

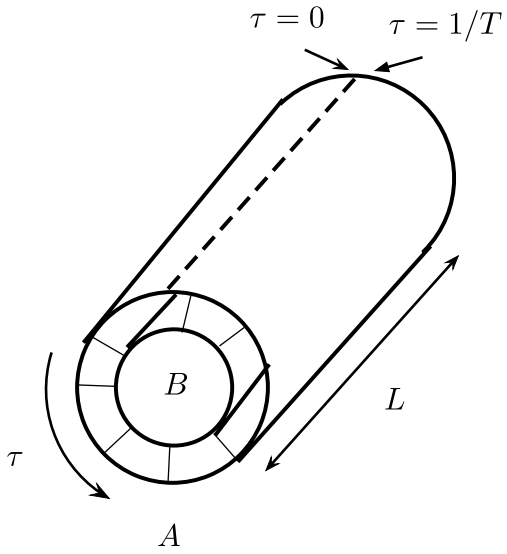

Figure 2.2: Spacetime manifold with a cut required for the computation of ρ_A. The cut (the broken line) only affects the spacetime for subsystem A (the outside cylinder) whose configurations are discontinuous across the cut. The configurations on region B (the inside cylinder) are periodic and smooth. The interactions between the fields on regions A and B is depicted by the thin radial lines.

$\vec{N}_A(x) \cdot \vec{N}_B(x)$. In the SU(2)$_1$ CFT the Néel order parameters of each chain are represented by the primary field whose scaling dimension is 1/2 (for a detailed discussion see, e.g. Ref.[Fradkin, 2013]). Hence, the scaling dimension of the inter-chain exchange interaction in the spin-1/2 ladder is $\Delta = 1$, and hence the exponent is $\nu = 1$ (albeit for different reasons than in the case of the fermionic ladder).

The computation of the reduced density matrix of a subsystem (in this case a perturbed CFT) is in general a very difficult problem. In principle it is possible to compute the reduced density matrix using methods of quantum field theory which reduces this computation to an imaginary time path integral over the field configurations $\phi(x, \tau)$, with $0 \leq x \leq L$ and $0 \leq \tau \leq 1/T$ (in the limits $L \to \infty$ and $1/T \to \infty$), with suitable boundary conditions. For the matrix element $\langle \phi_A^{\rm in}(x) \big| \rho_A \big| \phi_A^{\rm out}(x) \rangle$, the boundary conditions are that the field configurations for region B are periodic in imaginary time, $\phi_B(x, 0) = \phi_B(x, 1/T)$, whereas on region A the field configurations are discontinuous across the x axis between $\tau = 0$ and $\tau = 1/T$, and hence satisfy $\phi_A(x, 0) = \phi_A^{\rm in}(x)$ and $\phi_A(x, 1/T) = \phi_A^{\rm out}(x)$ (see Ref. [Calabrese and Cardy, 2004]). For the type of problems we are discussing here the result is a path integral on two concentric cylinders each of length L and and circumference $1/T$, with the cylinder for region A having a cut along the x axis representing the discontinuity of the field configurations, as shown in Fig.2.2.

Alternatively, we can compute the moments of the reduced density matrix of the subsystem (needed for

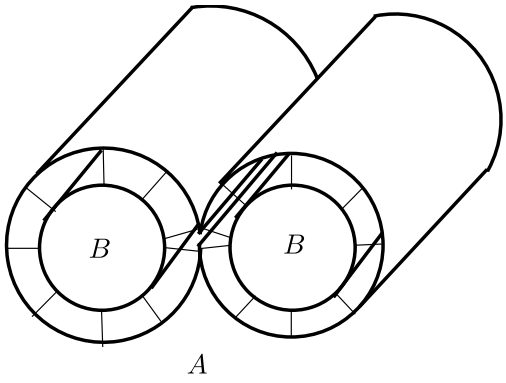

Figure 2.3: The spacetime manifold needed for the computation of $\mathrm{Tr}\rho_A^2$. The inside cylinders represent the replicated regions B (which are integrated out) and the outer surface which wraps around them is the replicated A region. The interactions between the A and B regions are shown as thin radial lines.

the computation of the Rényi and von Neumann entropies) using the replica trick[Callan and Wilczek, 1994, Holzhey et al., 1994, Calabrese and Cardy, 2004]

$$\mathrm{Tr}\rho_A^n = \frac{\mathcal{Z}_n}{\mathcal{Z}^n} \tag{2.46}$$

from which the Rényi entropies S_n and the von Neumann entropy can be determined,

$$S_n = \frac{1}{1-n}\ln \mathrm{Tr}\rho_A^n, \qquad S_{vN} = \lim_{n\to 1} S_n \tag{2.47}$$

In Eq.(2.46) we have denoted by $\mathcal{Z}$ the partition function of the coupled system (with coupling constant g) defined on a cylinder of length $L \to \infty$ and circumference $1/T \to \infty$. $\mathcal{Z}_n$ is the partition function of the coupled system (with subsystems A and B) on a spacetime manifold obtained by stitching together n copies of the path integral of the reduced density matrix. In the case at hand this leads to the manifold shown in Fig.2.3 (for the case $n = 2$), where the B region are the inside cylinders whereas the A region is obtained by gluing together the n path integrals along the n cuts. Therefore, $\mathcal{Z}_n$ is a path integral in which the fields on the n copies of the region B are periodic with period $1/T$. Instead the fields on region A are stitched together in such a way that they are periodic with period n/T (see Fig. 2.3). The partition function $\mathcal{Z}$

should not be confused withe the normalization Z of the reduced density matrix.

This procedure requires the introduction of a set of twist fields that connect the Hilbert spaces two at a time. In the case of spatial cuts there are a finite number of such twist fields. In the case of a conformally invariant theory the twist fields behave as local operators with non-trivial scaling dimensions and uniquely determine the singularities of the path-integral.[Calabrese and Cardy, 2004] However in the case in which two conformal field theories (on regions A and B) are coupled everywhere we are led to the "body" cuts we described above (and shown in Fig.2.2) which require the introduction of a line of twist fields defined along these cuts.

The introduction of this line of twist fields complicates the calculation of the replicated partition function, and we will not pursue this approach here. Another option is to use the approach introduced by Qi, Katsura and Ludwig[Qi et al., 2012] who made the observation that upon physically splitting regions A and B suddenly, i.e. upon setting the coupling constant $g \to 0$ after some (real) time $t = 0$, the reduced density matrix of subsystem A becomes the density matrix of the (now decoupled) system A. These authors used this approach to relate the entanglement entropy of a simply connected region of a 2D chiral topological phase to the behavior of its edge states.

In this section we will formulate instead a scaling argument to generalize the results of Section 2.2. There we saw that the reduced density matrix of the long-wavelength modes of a chain of a gapped free fermion system on a ladder is thermal and that the von Neumann entropy of the chain is the thermal entropy of an isolated chain at a finite effective temperature set by the gap in the fermion spectrum. We also saw that the resulting expressions for the entanglement entropies (von Neumann and Rényi) depend only on the Casimir term that gives the form of the finite size correction to the free energy in a conformal field theory. The structure of the universal Casimir term is determined by conformal invariance and by the conformal anomaly[Blote et al., 1986, Affleck, 1986] (through the central charge c). We are thus led to conjecture that this behavior of the entanglement entropies holds for any system of two coupled conformal field theories in a massive phase with a mass gap $M(g) \sim g^{\nu}$.

The scaling argument is based on the observation that the quantity $\mathcal{F}_n = -T \ln \mathcal{Z}_n$ is the *free energy* of the replicated system and, as such, it is a function of L, T and n (as well as of the coupling constant g). The scaling behavior is expected to hold since we are dealing with a perturbed conformal field theory which, due to the effects of the relevant perturbation, is driven into a massive phase. Since the coupled theory now has a finite mass gap $M(g)$ and a finite correlation length $\xi(g)$, the singular part of $\ln \mathcal{Z}$ of the coupled system, whose Hamiltonian is given in Eq.(2.45), should be, as in all theories of critical behavior,[Cardy, 1996] an

extensive homogeneous function of the form (known in the theory of Critical Phenomena as Widom scaling)

$$\left(\ln \mathcal{Z}\right)_{\rm sing} = \text{const.}\, TL\, \xi^{-2}(g)\, f(g) \tag{2.48}$$

where $f(g)$ is a function such that $f(0) = 1$.

Turning now to the replicated partition function, $\mathcal{Z}_n$, we notice that on the A region the stitched cuts act only at imaginary times $\tau = p/T$ (with $p = 1, \ldots, n$) and for all values of x. The partition function of the replicated system, $\mathcal{Z}_n$, differs from the partition function of a single copy by the action of the lines of twist fields at n equally spaced boundaries in imaginary time. We are interested in the limit in which both $L \to \infty$ and $T \to \infty$ for fixed and finite n. In this limit $\mathcal{Z}_n$ should have a bulk contribution which is asymptotically the same as the bulk contribution of n decoupled copies.

By examining the free energies $-T \ln \mathcal{Z}_n$ and $-nT \ln \mathcal{Z}$, we notice that in the thermodynamic limit $L \to \infty$ and $T \to 0$, the bulk contributions should cancel exactly each other out and that the only surviving contributions come from the "defects" (associated with the twist fields). Thus, the piece we are interested in is a finite size correction in $\mathcal{Z}_n$ which defines a type of boundary field theory. Furthermore, since for any finite value of the coupling constant g the theory is in a massive phase, the subtracted quantity $(\ln \mathcal{Z}_n - n \ln \mathcal{Z})$ (needed to compute the Rényi entropies) has contributions only from a strip of width $\xi = 1/M(g)$ and length L. The length scale ξ is the "extrapolation length" invoked in Refs.[[Gambassi and Calabrese, 2011, Qi et al., 2012]].

Therefore, again in the thermodynamic limit $L \to \infty$ and $T \to 0$, we expect to obtain the scaling behavior

$$\lim_{T\to 0, L\to\infty} \left(\ln \mathcal{Z}_n - \ln \mathcal{Z}^n\right) = LM(g)\, \tilde{f}_n(g) \tag{2.49}$$

where $\tilde{f}_n(g)$ is another function with the limit $\widetilde{f}_n(0) = f_n$. By demanding consistency with the results from Section 2.2, we will conjecture that the quantities f_n are given by

$$f_n = \frac{\pi c}{6v}\left(\frac{1}{n} - n\right) \tag{2.50}$$

where c is the central charge of each of the two conformal field theories at $g = 0$ and v is the velocity of their long-wavelength modes.

We are then led to conjecture that the von Neumann entanglement entropy of subsystem A of a gapped

system $A \cup B$ is extensive and has the scaling behavior

$$S_{vN} = \frac{\pi c}{3v} M(g) L \tag{2.51}$$

where $M(g) \sim g^{2-\Delta}$, c is the central charge c of the decoupled CFTs which are coupled by a local relevant operator of scaling dimension Δ, and v is the velocity of the modes. These arguments also imply that the Rényi entropies S_n should be given by an expression of the form

$$S_n = \frac{\pi}{6} \frac{c}{v} \left(\frac{1}{n} + 1 \right) M(g) L \tag{2.52}$$

2.5 Gapless Coupled Luttinger Liquids

For completeness, in this Section we will consider a situation where the coupling operator $O(A, B)$ is marginal and therefore will not open a gap in the spectrum. The entanglement entropy thus should be different from the thermal entropy. As a simple example we consider two Luttinger liquids coupled with a marginal operator. The Rényi entropy for this model has been calculated before by Furukawa and Kim, using the replica trick. They showed that the von Neumann entanglement entropy has, in addition to a term proportional to the length of the subsystem, there is a constant term determined by Luttinger parameter.[Furukawa and Kim, 2011] Here we will arrive to the same result using a different (and simpler) method. We will obtain this result directly by computing the reduced density matrix ρ_A. This can be done since the Luttinger liquid model is essentially a free scalar (compactified) (Bose) field.

The Hamiltonian density for this model is

$$\mathcal{H} = \mathcal{H}_A + \mathcal{H}_B + \mathcal{H}_{AB} \tag{2.53}$$

where $\mathcal{H}_A$ and $\mathcal{H}_B$ are the Hamiltonian densities for the two Luttinger liquids

$$\mathcal{H}_{AB} = \frac{v}{2} \left[\frac{\Pi^2}{K} + K (\partial_x \phi)^2 \right] \tag{2.54}$$

In momentum space the Hamiltonians have the form

$$H_{AB} = \sum_{p \neq 0} v|p| \left(a_p^\dagger a_p + \frac{1}{2} \right) + \frac{v}{2LR^2} M^2 + \frac{2v}{L} R^2 N^2 \tag{2.55}$$

where ϕ is a compactified boson with compactification radius r and $R = r\sqrt{K} = 1/\sqrt{4\pi}$, where K is the Lut-

tinger parameter, and Π is the canonical momentum conjugate to the the field ϕ. Here M and N take integer values. (For a summary of the Luttinger model see, e.g., Refs. [Fradkin, 2013] and [Gogolin et al., 1998]).

The coupling term $\mathcal{H}_{AB}$ takes the form

$$\mathcal{H}_{AB} = uK\partial_x\phi_A\partial_x\phi_B - \frac{u}{K}\Pi_A\Pi_B \tag{2.56}$$

where u is the coupling constant. In momentum space the inter-chain coupling Hamiltonian is

$$\begin{aligned} H_{AB} =& \sum_{p\neq 0} u|p|(a_p^\dagger b_{-p}^\dagger + a_p b_{-p}) \\ & -\frac{u}{LR^2}M_A M_B + \frac{4u}{L}R^2 N_A N_B \end{aligned} \tag{2.57}$$

where a_p and b_p are the boson operators for chain A and chain B, respectively.

The inter-chain coupling term of Eq.(2.56), has scaling dimension 2 and hence it is a marginal operator. In the case of the Luttinger model it is an exactly marginal operator. Its main effects are to change (continuously) the scaling dimensions of the operators of the physical observables, as well as a finite renormalization of the velocities of the modes (see, e.g., Refs.[Vishwanath and Carpentier, 2001] and [Emery et al., 2000]). The coupled Luttinger models are stable provided $|u| < v$.

Since $|u| < v$, the ground state of this system is in the sector where the winding modes are absent, $N_A = N_B = M_A = M_B = 0$. Thus, we only need to solve the following Hamiltonian:

$$H = \sum_{p\neq 0}\Big[v|p|(a_p^\dagger a_p + b_p^\dagger b_p) + u|p|(a_p b_{-p} + a_p^\dagger b_{-p}^\dagger)\Big] \tag{2.58}$$

which is a bilinear form in the bosons. Since the number of bosons in the separate chains are not conserved, the diagonalization of the Hamiltonian then proceeds through the standard Bogoliubov transformation

$$\begin{aligned} a_p^\dagger =& f_+ c_p^\dagger + f_- d_{-p} \\ b_{-p}^\dagger =& f_+ d_{-p}^\dagger + f_- c_p \end{aligned} \tag{2.59}$$

By diagonalizing the Hamiltonian, we can get the new spectrum for the bosons

$$E(p) = |p|\sqrt{v^2 - u^2} \tag{2.60}$$

The parameters $f_\pm$ are given by

$$f_\pm^2 = \frac{1}{2}\left((1-u^2/v^2)^{-1/2} \pm 1\right) \tag{2.61}$$

Since the coupled Luttinger model has been reduced to a free bosonic model, the reduced density matrix for chain A can be calculated similarly as in free fermionic model. The entanglement Hamiltonian here too has the form $\widetilde{H}_E = \sum_{ij} \widetilde{H}_{ij} a_i^\dagger a_j$ with

$$\widetilde{H}_{ij} = \left(\ln[C^{-1}+1]\right)_{ij} \tag{2.62}$$

where C_{ij} is the correlation matrix. Its matrix elements in momentum space (and in the thermodynamic limit $L \to \infty$) are

$$C_{pp'} = 2\pi\delta(p-p')f_-^2 \tag{2.63}$$

Since f_-^2 is a constant, the matrix $\widetilde{H}_{ij}$ is proportional to the identity matrix. Hence the entanglement Hamiltonian is proportional to the number operator and it is not equal to the Hamiltonian of one of the subsystems. Consequently the reduced density matrix is no longer thermal.

This difference is also reflected in the different behavior of the von Neumann entanglement entropy S_{vN} and thermal entropy S_T. Let us define the parameter κ,

$$\kappa = \frac{K_+ - K_-}{K_+ + K_-} = \frac{u}{v} \tag{2.64}$$

where

$$K_\pm = K\left(\frac{v \pm u}{v \mp u}\right)^{1/2} \tag{2.65}$$

are the Luttinger parameters for the fields $\phi_\pm = (\phi_A \pm \phi_B)/\sqrt{2}$ that diagonalize the Hamiltonian of the coupled system, Eq.(2.53). We will now obtain the expressions of the entanglement entropies as functions of κ.

In the weak coupling limit $|u| \ll v$ (i.e. $\kappa \ll 1$) and in momentum space, the correlation matrix is

$$C_{pp'} \simeq \frac{\kappa^2}{4} 2\pi\delta(p-p') \tag{2.66}$$

It follows that the Rényi entropies S_n are equal to

$$\begin{aligned} S_n &= \frac{1}{1-n}\ln \mathrm{Tr}\rho_A^n \\ &= \frac{1}{1-n}\left(\frac{L}{a}-1\right)\ln\left[\frac{(1-e^{-E})^n}{1-e^{-nE}}\right] \\ &\approx \frac{1}{1-n}\left(\frac{L}{a}-1\right)\left(-n\frac{\kappa^2}{4}+\left(\frac{\kappa}{2}\right)^{2n}\right) \\ &= -\gamma_n\frac{L}{a}+\gamma_n \end{aligned} \tag{2.67}$$

where $E=\ln\left((4/\kappa^2)-1\right)$, a is a short-distance cutoff and

$$\gamma_n = \frac{1}{(1-n)}\left[n\frac{\kappa^2}{4}-\left(\frac{\kappa}{2}\right)^{2n}\right] \tag{2.68}$$

From the above equation, we see that besides a term proportional to the length L of the system, there is also a constant term related to the Luttinger liquid parameter. When n is large, $\gamma_n = \frac{n\kappa^2}{4(1-n)}$. These results agree with those of Ref.[Furukawa and Kim, 2011]. Similarly, the von Neumann entanglement entropy equals to

$$S_{vN} = \left(\frac{L}{a}-1\right)\frac{\kappa^2}{4}\left[1-\ln\left(\frac{\kappa^2}{4}\right)\right] = -\gamma_1\frac{L}{a}+\gamma_1 \tag{2.69}$$

where $\gamma_1 = -\frac{\kappa^2}{4}(1-\ln\frac{\kappa^2}{4})$. We can see that the von Neumann entanglement entropy S_{vN} for this system is extensive but it is totally different from the thermal entropy S_T which is given by Eq.(2.27) (with $c=1$).

2.6 Conclusions

In conclusion, in this chapter we obtained the reduced density matrix in some two-leg ladder systems. We find that when the two chains that are critical and are coupled by some relevant operator which opens a finite energy gap in the spectrum, the reduced density matrix for one chain takes the same form as the thermal density matrix with the energy gap playing the role of the effective temperature. This idea is verified at both the strong coupling limit and the weak coupling limits. We also noted that although the entanglement Hamiltonian is generally non-local, the reduced density matrix for the long-wavelength modes of the subsystem is of the Gibbs form with a local effective Hamiltonian with a finite effective temperature. The fraction of modes which are thermal increases as the strength of the coupling increases. We showed that the entanglement von Neumann entropy for the long wavelength modes has a universal form which is equal to the thermodynamic entropy of the decoupled conformal field theory with central charge c. We verified

the validity of this conjecture by explicit calculations in a ladder fermionic system with a gap. The strong coupling results are generally valid and also hold in higher dimensional systems

Chapter 3

Many-body Localization Transition in Rokhsar-Kivelson-type wave functions

3.1 Introduction

In the previous chapter, we have showed that for a coupled two-leg ladder system, the reduced density matrix for one leg can take a thermal form. However, this is a special situation and in general, for a typical ground states of local Hamiltonian, under some constraints, the EE of subsystem satisfies area law. [Bombelli et al., 1986, Srednicki, 1993, Eisert et al., 2010] An interesting question is whether or not the reduced density matrix can take a thermal form?

It is proposed that for a generic system, the reduced density matrix for the subsystem of a highly excited state can take thermal form. This phenomenon is called the eigenstate thermalization hypothesis (ETH) in the literature and has been verified in numerous numerical calculations and experiments. Therefore, for an isolated quantum many-body system totally decoupled from the environment, the system can act as its own heat bath.[Srednicki, 1994, Deutsch, 1991] One way to distinguish systems which reach the thermalized state from those which don't is by studying the entanglement entropy of a subsystem. If a subsystem is in thermal equilibrium, the entanglement and thermal entropies must be the same and thus must satisfy a volume law, i.e. , the entropy should scale like L_A^d in d dimensions.

Evidence has recently accumulated for a certain class of interacting systems with quenched disorder which fail to thermalize. These systems go under the name many-body localization[Basko et al., 2006, Oganesyan and Huse, 2007, Pal and Huse, 2010] (MBL) and are the interacting analogue of Anderson insulators. [Anderson, 1958] This failure to thermalize has been attributed to an extensive number of locally conserved charges. [Serbyn et al., 2013, Huse and Oganesyan, 2014, Imbrie, 2014, Ros et al., 2015, Chandran et al., 2015] For a review of MBL phases, see the recent review of Ref. [Nandkishore and Huse, 2015]. In an Anderson insulator, all single-particle eigenstates are exponentially localized in real space, quantum diffusion is impossible at zero temperature and the system is an insulator on macroscopic scales.[Anderson, 1958] In such a state thermalization is not possible (without an external heat bath). It has been suggested that many-body localization results from a similar localization of states in Hilbert space.[Monthus and Garel, 2010,

Canovi et al., 2011]

The phenomenon of MBL is principally (and theoretically) observed in states deep in the excited state spectrum of a macroscopic system, and hence have an extensive *excitation energy* which, following standard (but somewhat inexact) terminology, we will call 'finite energy density' states. As a function of some tuning parameter (typically disorder), there can be a phase transition from an ergodic (thermalized) phase to an MBL phase. In contrast to its non-interacting counterpart (the Anderson insulator), an MBL phase transition can occur at finite temperature.[Basko et al., 2006] We should note that phonons may interfere with the observation of an MBL phase in solids, but MBL may be physically realized in optical lattice systems, see e.g. Ref. [Morong and DeMarco, 2015].

In this chapter we consider the problem of the MBL phase transition by constructing an ensemble of simple 'model' many-body wave functions with a simple structure parameterized by a 'disorder' strength, and study the phase transition as a function of this parameter. We will show that, in spite of their simple structure, these model wave function can represent both thermal states and MBL states. The wave functions that we consider have a structure similar to the Rokhsar-Kivelson (RK) states[Rokhsar and Kivelson, 1988] and their generalizations.[Ardonne et al., 2004, Fradkin, 2013] More specifically, we consider states that are linear superpositions of quantum states labeled by the classical configurations of a system of N Ising spins, and have the form

$$|\Psi_{REM}\rangle = \sum_{\{\mathcal{C}\}} W[\mathcal{C}]|\mathcal{C}\rangle, \tag{3.1}$$

Here the quantum mechanical amplitude $W[\mathcal{C}]$ for a configuration $\mathcal{C}$ of the Ising spins is given by the Gibbs weight of a classical spin glass model known as the Random Energy Model, i.e.

$$W[\mathcal{C}] \propto e^{-\beta E[\mathcal{C}]} \tag{3.2}$$

where the 'energy' $E[\mathcal{C}]$ assigned to the configuration $\mathcal{C}$ is taken to be a random number drawn from a Gaussian distribution. By construction, the amplitudes of these states $W[\mathcal{C}]$ are positive real numbers. The associated classical spin glass model in infinite space dimension (since each spin is coupled to all the other $N-1$ spins) is known to have a classical thermodynamic phase transition to a spin glass state.[Derrida, 1980] The parameter β, which in the classical spin glass model is the inverse temperature, but in this work will be used as a parameter of the wave function. Notice that we have not defined a quantum Hamiltonian for which the wave function of Eq.(3.1) is an eigenstate and, hence, we have not actually defined an energy for the quantum system. Thus, the 'energy' of the Random Energy Model should not be confused with the energy of the quantum state.

The quantum state $|\Psi_{REM}\rangle$ has the manifestly positive weights shown in Eq.(3.2). Such a state can be a natural candidate for a ground state of a Hamiltonian but not for a typical excited state whose amplitudes are generally non-positive. To mimic a 'typical' state deep in the spectrum of a quantum system, we generalize this construction so that, for a given configuration C, the amplitudes for these new states are just a *random sign* multiplied by the amplitude $W(\mathcal{C})$ discussed above (a similar approach has been used in Ref.[Grover and Fisher, 2014a] and Ref.[Grover and Fisher, 2014b].) We will denote the new wave functions by $|\Psi_{REM+\text{sign}}[\beta]\rangle$. Here we will also consider the wave function without random signs denoted by $|\Psi_{REM}[\beta]\rangle$ and compare the physical properties of both types of wave functions.

An advantageous aspect of our approach is that we have more analytical control over this system then is typical in interacting disorder systems. In addition we are able to perform numerical calculations with a system size ($\gtrsim 30$) which can only be achieved in other numerical MBL studies with the use of matrix-product states [Khemani et al., 2015, Yu et al., 2015]. These wave functions are also conceptually simple, making them an ideal setting to further our understanding of MBL.

Laumann, Pal and Scardicchio studied numerically the MBL state in the *quantum* Random Energy Model and found that the MBL quantum phase transition is distinct from the quantum phase transition to the spin-glass phase.[Laumann et al., 2014] Here we will find that in the RK wave functions $|\Psi_{REM+\text{sign}}\rangle$, although they are not actual eigenstates of the quantum REM model, the MBL and spin-glass transitions are also separate.

In this work we will be focused on three particular aspects of the problem- the transition to the MBL phase, the scaling of the entanglement entropy with subsystem size and the transition from being geometrically delocalized to localized in the Hilbert space. To identify the ergodic and MBL phases, we use the Rényi entanglement entropies S_n (where n is the Rényi index)

$$S_n = \frac{1}{1-n} \log \text{Tr} \rho_A^n \tag{3.3}$$

of a subsystem A whose size $N_A < N/2$ is smaller than half of the entire system. In the limit $n \to 1$, S_n converges to the von Neumann entropy. In an ergodic system, there is a regime where the Rényi entropy obeys a volume law which changes linearly as a function of N_A. Bauer and Nayak have argued that, for most states in an MBL phase, their entanglement entropy scales at most as an area law of the subsystem size.[Bauer and Nayak, 2013] We will show below that, in our MBL phase, the Rényi entropy is sub-extensive as a function of subsystem size and is bounded by a finite constant deep inside the MBL phase (Fig. 4.1). We take particular note of volume laws at an energy density that corresponds to infinite temperature (ITV)

which scales as $N_A \log 2$. The scaling behavior of the entanglement entropy may depend on the subsystem size often showing a crossover from ITV to sub-extensive as the subsystem gets larger. An important subtlety of our model comes from the lack of correlation length in the REM (inherent in a system at infinite dimension). This makes the relevant parameter to consider in looking for such a crossover not the absolute size N_A but the ratio $t \equiv N_A/N$ and our results will be quoted as a function of this parameter.

While entanglement entropy can be used to distinguishing MBL from ergodic phases, geometric localization is a measure of compactness of the wave function in Hilbert space. In an Anderson insulator, the localization is of the single-particle wave function in real space and can be characterized by the inverse participation ratio defined as

$$Y_n = \int d^d x |\psi(x)|^{2n} \tag{3.4}$$

where $|\psi(x)|^2$ is the probability distribution of single-particle state in real space.[Thouless, 1974] Generically, Y_n takes the scaling form

$$Y_n \sim N^{-\tau(n)} \tag{3.5}$$

where the exponent $\tau(n) = D_n(n-1)$. For the extensive (delocalized) state, $D_n = d$, while for the localized state $D_n = 0$. For the critical single-particle wave function at the mobility edge, D_n has a non-trivial dependence on n, and it indicates that the critical wave function has a multifractal nature. [Evers and Mirlin, 2008, Wegner, 1980, de C. Chamon et al., 1996, Castillo et al., 1997, Gruzberg et al., 2011, Kravtsov et al., 2015] For non-interacting systems, this multifractal behavior [Halsey et al., 1986, Jensen et al., 1987] is also manifest in the Rényi entropy for the single-particle critical wave function.[Jia et al., 2008, Chakravarty, 2010, Chen et al., 2012]

Here we will present evidence that multifractal behavior also appears in the entanglement near the phase transition into the MBL phase by looking at the scaling behavior of the Rényi entropies. Loosely speaking the many-body generalization of this multifractality measures the degree of localization of states in the multi-dimensional Hilbert space (in a real-space basis) and not just those of a single particle orbital. Multifractal behavior of weight of a state in a Hilbert space has been studied recently by several authors.[Luitz et al., 2014, Torres-Herrera and Santos, 2015] In these studies multifractality is used to characterize the geometry of a state in Hilbert space, i.e. its degree of localization in the Hilbert space. In those works, the Shannon-Rényi entropies used to quantify the multifractal behavior of the many-body states is a measure of the statistical properties of the wave functions as probability distributions and are unrelated to the concept of quantum entanglement. Multifractality has also been discussed in connection with the fidelity of the ground state wave functions in systems at the infinite-disorder fixed point.[Vasseur and Moore, 2015] So far as we know,

multifractal behavior of quantum entanglement in wave functions close to the MBL transition has not been discussed previously in the literature. This is one of the main questions that we address in our work.

3.1.1 Short summary of this chapter

In this chapter, we consider the MBL transition, the value of $\overline{S(N_A, N)} \equiv \langle S(N_A, N)\rangle$ and the geometric localization of the wave function $|\Psi_{REM+\text{sign}}[\beta]\rangle$. We show that the wave-function geometrically localizes in Hilbert space at $\beta = 1.18$. We also find three regimes of entanglement scaling for $\overline{S_2(N_A; N = \infty)}$: a thermalized regime (at infinite temperature) where the entanglement entropies for a partition show volume law scaling as a function of the subsystem size N_A; a regime bounded by constant entanglement entropy; and a regime which is sub-extensive but not constant. The transition from sub-extensive to constant happens at, or before, the geometric localization transition. Notice that the presence of extensive scaling for any $N_A > 0$ implies that the finite size scaling of $\overline{S_2(N; N_A)}$ as a function of N at a fixed N_A is also extensive. Because $\overline{S_2(\rho_A)}$ is hard to compute exactly, we analytically calculate lower and upper bounds for it. In addition, we identify the MBL transition (with respect to the second R ényi entropy) via a numerical scaling collapse with $\langle S_2\rangle$ and $\langle \delta S_2\rangle$ [Kjall et al., 2014, Vosk et al., 2014] (see Section 3.4.1). We find that the the MBL transition is different from the geometric localization transition and therefore the wave-function is still geometrically delocalized in Hilbert space at the MBL transition [Luca and Scardicchio, 2013, Luitz et al., 2015] . While the entanglement entropy $\overline{S_2(N_A, N = \infty)}$ scales sub-extensively with N_A at the MBL transition, the transition to sub-extensive scaling doesn't correspond to the MBL transition. In addition, the numerical evidence suggests that the MBL transition (for S_2, at $N_A/N = 1/2$) happens at a β where $\overline{S_2(N; N_A/N = 1/2)}$ as a function of N still scales extensively. While these statements hold for S_2, we also consider S_n, finding that the MBL transition as well as the analytic bounds for sub-ITV scaling happen for different n at different β. The former of these appears to scale linearly in $(n-1)/n$. In addition, the scaling exponents identified from scaling collapse are different for different n. This is an indication of multifractal behavior. We further study the entanglement spectrum in this regime and observe an entanglement gap between the lower continuous band and the other higher eigenvalues and show that this feature explains transitions which differ for different n. In Fig.4.1 a and b, we give a succinct and broad summary of the phase diagram (including the phase diagram of the classical REM for comparison).

We also explain the importance of the random sign structure. This effect we compare the behavior of the second Rényi entropies $\langle S_2(\rho_A)\rangle$ for $|\Psi_{REM+\text{sign}}\rangle$ with $|\Psi_{REM}\rangle$ without random sign. The difference, ΔS_2, is found to decrease monotonically as a function of disorder strength. In the low disorder regimes, $\langle S_2(\rho_A)\rangle$ for $|\Psi_{REM}\rangle$ is a constant and thus their difference ΔS_2 takes the maximal value. At the values of $t \leq 1/3$,

the difference disappears before entering into the MBL phase.

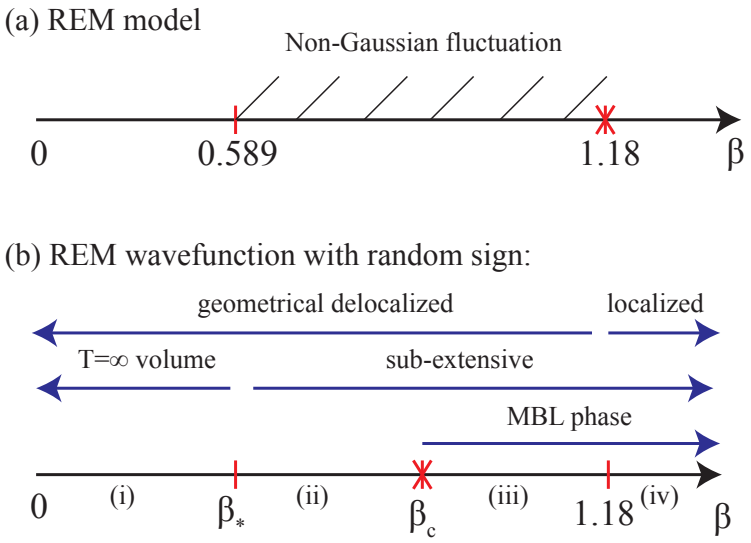

Figure 3.1: (Color online). (a) Phase diagram for the classical REM model as a function of β. The spin glass phase transition occurs at $\beta = \sqrt{2\log 2}$. The shaded region between $\sqrt{\log 2/2}$ and $\sqrt{2\log 2}$ has non-Gaussian fluctuation. (b) Schematic phase diagram for the REM wave function in terms of the entanglement entropy showing different scaling behaviors in four different regimes as a function of β. In the regime (i) $\langle S_n \rangle$ is equal to $N_A \log 2$ for all N_A. In the intermediate regime (ii), $\langle S_2 \rangle$ is sub-extensive but does not saturate to a constant. Regime (iii) is the MBL phase. In this regime, the wavefunction is not localized in the Hilbert space. (iv) is also the MBL phase with the wavefunction localized in Hilbert space.

The rest of this chapter is organized as follows. In Section 3.2, we explain the construction of a Rokhsar-Kivelson-type wave function which assigns to the amplitude of a quantum many-body state the Gibbs weight of a classical spin glass model (the Random Energy Model) and introduce a random sign structure into it to access represent typical excited states with a *finite excitation energy density*. In Section 3.3.1 we briefly review the classical random energy model (REM) and interpret the classical spin glass phase transition in it. In the Section 3.3.2 we construct a REM wave function with a random sign structure to mimic a highly excited state for a Hamiltonian with disorder. We will analytically compute the Rényi entropy to show that there is a thermalized regime and a many-body localized phase. In Section 3.4 we calculate the Rényi entropy numerically and find the location of MBL phase transition by finite size scaling. In the Section 3.4.4 we study the Rényi entropy for the REM wave function without random sign and demonstrate the importance of the sign structure. In the Section 3.5 we summarize our results and conclude that there is a MBL phase transition in the REM wave function with random sign structure.

3.2 Rokhsar-Kivelson Model wave functions

In the physics of strongly correlated systems there are many examples in which the properties of a new state of matter can be represented by simple 'model' wave functions. The best known examples of such model wave functions include the BCS wave function for the ground state of a superconductor and the Laughlin wave function for the fractional quantum Hall fluid.

3.2.1 RK-type wave functions

In this chapter we will give a description of the MBL states using a particularly simple class of model wave functions with a structure similar to the one proposed by Rokhsar and Kivelson (RK) to capture the physics of the ground states of strongly frustrated quantum antiferromagnets.[Rokhsar and Kivelson, 1988] In the RK construction the quantum mechanical amplitude of a many-body state is given by a local function of the degrees of freedom, as expressed in the orthonormal basis set $\{|\mathcal{C}\rangle\}$ where $\mathcal{C}$ is the 'configuration space'. In the RK problem the configuration space is the set of dimer coverings of a 2D lattice. While in the RK case the dimers are a qualitative representation of spin singlets on each bond of the lattice, a picture of this type has been generalized to many other systems, including Kitaev's Toric Code state,[Kitaev, 2003] which represents the topological (or deconfined) phase of a $\mathbb{Z}_2$ gauge theory.

Since the weights of the RK wave functions are local and positive, they can also be regarded as the Gibbs weights of a related problem in classical statistical mechanics with the same degrees of freedom on the same lattice. Thus if the basis of orthonormal states is the set $\{|\mathcal{C}\rangle\}$, i.e. such that $\langle\mathcal{C}|\mathcal{C}'\rangle = \delta_{\mathcal{C},\mathcal{C}'}$, the generalized normalized RK states are

$$|\Psi\rangle = \frac{1}{\sqrt{\mathcal{Z}}} \sum_{\{\mathcal{C}\}} e^{-\frac{\beta}{2}E[\mathcal{C}]} |\mathcal{C}\rangle \tag{3.6}$$

where

$$\mathcal{Z} = \sum_{\{\mathcal{C}\}} e^{-\beta E[\mathcal{C}]} \tag{3.7}$$

Here $E[C]$ and $\mathcal{Z}$ are, respectively, the energy for the classical configuration $\mathcal{C}$ and the partition function for the associated classical problem, and β plays the role of the inverse temperature.

Entanglement entropy for the RK-wave function with classical local Hamiltonian

For the RK state with a classical local Hamiltonian, after partitioning the system into two parts A and B, it can be approximately written in this way,

$$|\Psi_0\rangle = \sum_{\Gamma} \lambda_\Gamma |\Psi_A(\Gamma)\rangle |\Psi_B(\Gamma)\rangle \tag{3.8}$$

where $\Psi_A(\Gamma)$ and $\Psi_B(\Gamma)$ are the RK wave functions defined in region A and region B with the same boundary configuration Γ

$$\begin{aligned} |\Psi_A(\Gamma)\rangle &= \sum_A \frac{e^{-\frac{\beta}{2}H_A(\Gamma)}}{\sqrt{\mathcal{Z}_A(\Gamma)}} |c_A(\Gamma)\rangle \\ |\Psi_B(\Gamma)\rangle &= \sum_B \frac{e^{-\frac{\beta}{2}H_B(\Gamma)}}{\sqrt{\mathcal{Z}_B(\Gamma)}} |c_B(\Gamma)\rangle \end{aligned} \tag{3.9}$$

When $\Gamma \neq \Gamma'$, they satisfy $\langle\Psi_A(\Gamma)|\Psi_A(\Gamma')\rangle = 0$ and $\langle\Psi_B(\Gamma)|\Psi_B(\Gamma')\rangle = 0$. The summation in Eq.(3.8) is the sum over all possible boundary configurations along the cut and $\lambda_\Gamma = \sqrt{\mathcal{Z}_A(\Gamma)}\sqrt{\mathcal{Z}_B(\Gamma)}/\sqrt{\mathcal{Z}}$.

Thus Eq. (3.8) is the Schmidt decomposition of the wave function, the reduced density matrix in regime A is

$$\rho_A = \sum_\Gamma \lambda_\Gamma^2 |\Psi_A(\Gamma)\rangle\langle\Psi_A(\Gamma)| \tag{3.10}$$

Since the dimension of ρ_A only depends on the dimension of the Hilbert space along the boundary, the entanglement entropy should satisfy the area law.

The original RK wave function is an equal-amplitude superposition of all dimer coverings in $2D$. This wave function can be associated with the partition function for the classical dimer model and is also the ground state of the quantum dimer model at critical point [Rokhsar and Kivelson, 1988, Ardonne et al., 2004, Fradkin, 2013] (for 2D bipartite lattices) and a $\mathbb{Z}_2$ topological state[Moessner and Sondhi, 2001] (for non-bipartite lattices). States of these type are exact ground states of a special type of quantum Hamiltonians that are the sum of projection operators and are closely related to classical dynamics.[Henley, 2004, Castelnovo et al., 2004]

The generalized RK wave function $|\Psi_{REM}\rangle$ inherits many properties from the classical model. For instance, the equal time correlation function of the wave function is the same as the correlation function of the classical model, and the quantum critical point in the wave function corresponds to the classical phase transition at temperature $1/\beta_c$.

3.2.2 Random sign wave function

We want to consider our family of wave functions as representing finite energy density states with the possibility of supporting both ergodic and MBL phases. As we noted above, there exists Hamiltonians constructed by projection operators for which the RK wave functions of the form of Eq.(3.6) are the exact ground states. However, we should note that its amplitudes are all strictly positive. If the classical Hamiltonian used to generate the RK state only has local interactions, we can show this state must have an area law. This follows from the fact that one can write a Schmidt decomposition of the state where the number of terms is bounded by the number of classical interactions which are broken (See Appendix A for detail). The entanglement properties of these type of states have been discussed in great detail in the case of the quantum dimer model,[Furukawa and Misguich, 2007, Castelnovo and Chamon, 2007, Stéphan et al., 2009] of the associated quantum Lifshitz model,[Fradkin and Moore, 2006, Hsu et al., 2009, Hsu and Fradkin, 2010] and of the Toric Code state.[Hamma et al., 2005b, Levin and Wen, 2006]

To have the potential for ergodic states, then, we must either use a non-local classical Hamiltonian or introduce directly a more rich sign structure into the wave function as done in Refs. [Grover and Fisher, 2014a, Grover and Fisher, 2014b]. While the classical Hamiltonian we are using for the REM model is non-local, it nonetheless supports an area law at low disorder; in fact, at $\beta = 0$, the entanglement entropy is zero over any cut. Therefore, we introduce a random sign structure in the wave function giving

$$|\Psi_{REM+\text{sign}}\rangle = \frac{1}{\sqrt{\mathcal{Z}}} \sum_{\{C\}} s_{\mathcal{C}}\ e^{-\frac{\beta}{2}E[\mathcal{C}]}|\mathcal{C}\rangle, \tag{3.11}$$

where $s_{\mathcal{C}}$ is a quenched random sign associated to each configuration $\mathcal{C}$. The average ratio between the number of positive and negative signs is one. A similar construction was discussed in Ref. [Khemani et al., 2014], where they showed that the random sign structure can lead to a thermalized phase. In this chapter, we will study the MBL phase transition in a RK-wave function with random sign.

3.3 Many body localization phase transition

In this section we will show that the RK wave function with random signs has an ergodic (thermalized) regime and an MBL phase. We begin with a summary of the properties of the classical Random Energy Model whose Boltzmann weights will enter into the structure our wave function.

3.3.1 The Random Energy Model

The random energy model (REM) is a simple classical model which has a phase transition to a spin glass phase.[Derrida, 1980] This effectively infinite dimensional model has 2^N configurations and is the infinite range coupling limit of the Sherrington-Kirkpatrick spin glass model.[Sherrington and Kirkpatrick, 1975] In the REM model, the energy for each configuration is no longer given by the complicated spin glass Hamiltonian, but rather simply an independent random variable. This random variable has the Gaussian distribution

$$P(E) = (2N\pi)^{-1/2} e^{-\frac{E^2}{2N}}. \tag{3.12}$$

The number of configurations in the energy interval $[N\epsilon, N(\epsilon+\delta)]$, in expectation, is

$$\langle \mathcal{N}(\epsilon, (\epsilon+\delta)) \rangle = \int_{\epsilon}^{\epsilon+\delta} dx e^{Ns(x)} \tag{3.13}$$

where

$$s(x) = \log 2 - \frac{x^2}{2}, \qquad \text{with } x = \frac{E}{N} \tag{3.14}$$

In the thermodynamic limit, $N \to \infty$, this expectation value takes the asymptotic form

$$\lim_{N\to\infty} \langle \mathcal{N}(\epsilon, (\epsilon+\delta)) \rangle = \exp\{N \max_{x\in[\epsilon,\epsilon+\delta]} s(x)\} \tag{3.15}$$

Notice that $s(x) > 0$ only in the interval $x \in [-\epsilon_*, \epsilon_*]$, where $\epsilon_* = \sqrt{2\log 2}$. This means that for $\epsilon \in [-\epsilon_*, \epsilon_*]$, $\langle \mathcal{N}(\epsilon) \rangle$ is exponentially large, and the fluctuations are very small. For ϵ outside the interval $[-\epsilon_*, \epsilon_*]$, $\mathcal{N}(\epsilon)$ is exponentially small.

The partition function for this model is simply given by

$$\mathcal{Z} = \sum_{i=1}^{2^N} e^{-\beta E_i} = \int dE\, \mathcal{N}(E)\, e^{-\beta E} = \int dx\, e^{N\phi(x)}. \tag{3.16}$$

where $\phi(x)$ equals to

$$\phi(x) = \log 2 - \frac{x^2}{2} - \beta x, \tag{3.17}$$

Similar to the calculation for $\langle \mathcal{N}(\epsilon) \rangle$, we can also use the saddle point approximation to calculate the partition function to obtain

$$\mathcal{Z} = \exp\{N \max[\phi(x)]\} \tag{3.18}$$

which is the exact result in the thermodynamic limit, $N \to \infty$. By computing $\phi_{\max} = \max[\phi(x)]$, it is easy

to show that the free energy density equals to

$$\begin{aligned} f(\beta) &= -\frac{\log \mathcal{Z}}{\beta N} = -\frac{\phi_{\max}}{\beta} \\ &= \begin{cases} -\frac{\beta}{2} - \frac{\log 2}{\beta} & \beta < \beta_{sg} \\ -(2\log 2)^{1/2} & \beta \geq \beta_{sg} \end{cases} \end{aligned} \tag{3.19}$$

At $\beta_{sg} = \sqrt{2\log 2}$, there is a discontinuity in the second derivative of the free energy density, showing that there is a phase transition at this point, the spin glass transition. This phase transition can be further studied by computing the inverse participation ratio (IPR), [Derrida, 1981, Mezard and Montanari, 2009]

$$Y_n(\beta) \equiv \sum_i^{2^N} p_i^n = \frac{\sum_i^{2^N} e^{-n\beta E_i}}{(\sum_i^{2^N} e^{-\beta E_i})^n}. \tag{3.20}$$

This quantity measures how many configurations effectively contribute to the partition function and measurable quantities. The expectation value for Y_2 equals to [Mezard and Montanari, 2009]

$$\langle Y_2(\beta) \rangle = \begin{cases} 0 & \beta < \beta_{sg} \\ 1 - \frac{\beta_{sg}}{\beta} & \beta \geq \beta_{sg} \end{cases} \tag{3.21}$$

At low temperatures, $\beta > \beta_{sg}$, the participation ratio takes a finite value. This means that the system is completely frozen to $O(1)$ number of configurations and is in a non-ergodic phase. At high temperature, $\beta < \beta_{sg}$, all configurations will contribute to the thermodynamic properties of the system. For instance, in the high temperature limit $\beta \to 0$, the Boltzmann's measure becomes uniform and the second participation ratio becomes $Y_2(\beta \to 0) = 2^{-N}$. When $N \to \infty$, $Y_2 \to 0$. In general, when $\beta < \beta_{sg}$, Y_n scales with the system size

$$Y_n \sim \mathcal{D}^{-\tau(n)}, \qquad \text{with } \mathcal{D} = 2^N \tag{3.22}$$

From the results on $\log \mathcal{Z}(\beta)$, we can compute the exponent $\tau(n)$ (for $n > 1$)

$$\tau(n) = \begin{cases} (n-1)(1-\gamma n), & 0 \leq \gamma < \frac{1}{n^2} \\ n(1-\sqrt{\gamma})^2, & \frac{1}{n^2} < \gamma < 1 \\ 0, & \gamma > 1 \end{cases} \tag{3.23}$$

where $\gamma = \frac{\beta^2}{2\log 2}$. We will use $\tau(n)$ to give a upper bound for the Rényi entropy of the wave function

$|\Psi_{REM+\text{sign}}\rangle$ later.

Although the REM model is a simple toy model, it has a spin glass phase transition, i.e., it undergoes a localization transition. It also shows a rich structure in the fluctuation of the free energy. According to the results of Ref. [Bovier et al., 2002], for the ergodic phase, which occurs for $\beta < \beta_{sg}$, there are two regimes with different fluctuation behavior of the free energy. When $\beta < \sqrt{\log 2/2}$, the fluctuations of the free energy are Gaussian, and satisfy the central limit theorem. When $\beta_{sg} > \beta > \sqrt{\log 2/2}$, there are non-Gaussian fluctuations of the free energy driven by the Poisson process of the extreme values of the random energies. This regime does not satisfy the central limit theorem. The resulting phase diagram of classical REM model is shown in Fig.4.1 (a).

3.3.2 Random sign REM wave function

We can now construct a quantum state following the procedure of Eq.(3.11),

$$|\Psi_{REM}\rangle = \frac{1}{\sqrt{\mathcal{Z}}} \sum_{\{\mathcal{C}\}} e^{-\frac{\beta}{2}E[\mathcal{C}]} |\mathcal{C}\rangle \tag{3.24}$$

whose amplitudes are the Boltzmann weights of the classical REM. By further introducing the random sign structure, the wave function takes the form

$$|\Psi_{REM+\text{sign}}\rangle = \frac{1}{\sqrt{\mathcal{Z}}} \sum_{\{\mathcal{C}\}} s_{\mathcal{C}} e^{-\frac{\beta}{2}E[\mathcal{C}]} |\mathcal{C}\rangle \tag{3.25}$$

Here both $s_{\mathcal{C}}$ and $E[\mathcal{C}]$ are random variables and are independent of each other. The random sign $s_{\mathcal{C}}$ takes the values ± 1 with equal probability over the entire Hilbert space of 2^N spin configurations.

Before we do any calculations, we can first estimate the scaling behavior of the Rényi entropy for this quantum state in the extreme limits. In this wave function, β is a tuning parameter and has the physical meaning of the disorder strength. The random sign structure is used to represent a highly excited quantum state. When there is no disorder, i.e., $\beta = 0$, the amplitude for every configuration is the same. At this point, the Rényi entropy for the subsystem A with different Rényi index is equal to the thermal entropy at infinite temperature. Thus this wave function is thermalized, and the entanglement entropies obey a volume law.[Grover and Fisher, 2014a] As β increases, the disorder becomes stronger and the entanglement entropy becomes smaller. The wave function is eventually localized to a small fraction of the configurations as $\beta > \beta_{sg}$. As we already showed in the previous section, since the number of these configurations is only $O(1)$, in this regime the Rényi entropy is bounded by a finite constant.

Nomenclature and thermodynamic limit for scaling

The entanglement entropy $\langle S_n \rangle$ at fixed β depends on both the subsystem size N_A as well as the total system size N and there can be separate functional forms for the scaling of $\langle S_n \rangle$ with respect to either of these parameters. While in many physical systems, these scalings coincide, this is not the case in our model and so it is important to be clear about the distinction. Unless otherwise specified, our discussion will always focus on scaling with N_A at fixed system size N.

For the thermodynamic limit considered in this work, we let both N_A and N go to infinity but their ratio $t = N_A/N$ to be a finite value. The changes in entanglement scaling we identify then happen at particular values of t for $0 \leq t \leq 1/2$ for different values of β. The MBL phase in our terminology is identified with scaling collapse.

Analytic Bounds

We now analytically compute bounds to the Rényi entropy. Notice that for a disordered system, we need to take a quenched ensemble average of the Rényi entropy,

$$\langle S_n(\rho_A) \rangle = \frac{1}{1-n} \langle \log \mathrm{Tr} \rho_A^n \rangle \tag{3.26}$$

In this quenched average the disorder is frozen and does not evolve with time. We mainly focus here on the second Rényi entropy, but the results are easily extended to the other Rényi entropies.

We begin by noting that the quenched average in Eq.(3.26) is redundant if, in the thermodynamic limit, the system is self-averaging.[Buffet, 1993] However, this will not always be the case. For brevity, we sometimes will denote $\langle S_n(\rho_A) \rangle \equiv \langle S_n \rangle$.

Let us define a bipartition our system of N spins into two subsets (or regions), A and B. The reduced density matrix for region A is

$$\begin{aligned} \rho^A_{a,a'} &= \frac{1}{\mathcal{Z}} \left(\sum_b s_{a,b} s_{a',b} e^{-\frac{\beta}{2}(E_{a,b}+E_{a',b})} \right) |\mathcal{C}_a\rangle \otimes \langle \mathcal{C}_{a'}| \\ &= \frac{\widetilde{\rho}^A_{a,a'}}{\mathcal{Z}} \end{aligned} \tag{3.27}$$

where $\widetilde{\rho}^A_{a,a'}$ is the unnormalized reduced density matrix.

For the above reduced density matrix, $\langle S_n(\rho_A) \rangle$ equals to

$$\langle S_n(\rho_A) \rangle = \frac{1}{1-n} \left(\langle \log \mathrm{Tr} \widetilde{\rho}^n_A \rangle - n \langle \log \mathcal{Z}(\beta) \rangle \right) \tag{3.28}$$

The second term $\langle \log \mathcal{Z}(\beta) \rangle$ can be calculated by the saddle point approximation and the result is already shown in Eq.(3.19). However, the first term $\langle \log \mathrm{Tr} \widetilde{\rho}_A^n \rangle$ is hard to obtain analytically. Instead of calculating it directly, we compute a lower bound and upper bound for it.

Lower Bound : Consider the *annealed average*

$$S_n(\langle \widetilde{\rho}_A \rangle) = \frac{1}{1-n} \left(\log \langle \mathrm{Tr} \widetilde{\rho}_A^n \rangle - n \langle \log \mathcal{Z}(\beta) \rangle \right) \tag{3.29}$$

which is much easier to compute. By using Jensen's inequality,[Reed and Simon, 1981] when $n > 1$, it is straightforward to see that the annealed average of the Rényi entropy $S_n(\langle \widetilde{\rho}_A \rangle)$ provides a lower bound for the quenched average $\langle S_n(\rho_A) \rangle$, i.e.

$$\langle S_n(\rho_A) \rangle \geq S_n(\langle \widetilde{\rho}_A \rangle) \tag{3.30}$$

To obtain the annealed average $S_2(\langle \widetilde{\rho}_A \rangle)$, we need to calculate $\langle \mathrm{Tr} \widetilde{\rho}_A^2 \rangle$. By means of simple manipulations we find

$$\begin{aligned}
\langle \mathrm{Tr} \widetilde{\rho}_A^2 \rangle =& \sum_{a,a'} \langle (\widetilde{\rho}^A_{a,a'})^2 \rangle \\
=& \sum_a \langle \left(\widetilde{\rho}^A_{a,a} \right)^2 \rangle + \sum_{a \neq a'} \langle \left(\widetilde{\rho}^A_{a,a'} \right)^2 \rangle \\
=& \sum_a \langle \Big(\sum_b e^{-\beta E_{a,b}} \Big)^2 \rangle \\
&+ \sum_{a \neq a'} \langle \Big(\sum_b s_{a,b} s_{a',b} e^{-\frac{\beta}{2}(E_{a,b}+E_{a',b})} \Big)^2 \rangle \\
=& 2^N e^{2N\beta^2} + (2^{N_B} - 1) 2^N e^{N\beta^2} + (2^{N_A} - 1) 2^N e^{N\beta^2}
\end{aligned} \tag{3.31}$$

where the last step is derived by using that for a Gaussian distribution $\langle e^{-\alpha E} \rangle = e^{\alpha^2 N/2}$.

In the thermodynamic limit, when $N_A < N$, the annealed average of the second Rényi entropy becomes

$$S_2(\langle \widetilde{\rho}_A \rangle) = \begin{cases} N_A \log 2, & \beta \leq \beta_1 \\ N(\log 2 - \beta^2), & \beta > \beta_1 \end{cases} \tag{3.32}$$

where $\beta_1 = \sqrt{(1-t)\log 2}$ and t is the ratio N_A/N. The result is plotted in Fig.3.2 (a), where the black dashed curve is the lower bound for $\langle S_2 \rangle / S_T$ at $t = 1/3$. $S_T = N_A \log 2$ is the thermal entropy for subsystem N_A at infinite temperature. Notice that when $\beta \leq \beta_1$, since the lower bound $S_2(\langle \widetilde{\rho}_A \rangle) = S_T$, $\langle S_2(\rho_A) \rangle$ must be equal to $N_A \log 2$. When $\beta > \sqrt{\log 2}$, $S_2(\langle \widetilde{\rho}_A \rangle) < 0$, this lower bound is replaced by zero and is not useful

anymore.

Upper Bound : It is easy to see that $\mathrm{Tr}\rho_A^2$ can be bounded from below by the second participation ratio of the classical REM. Indeed,

$$\mathrm{Tr}\rho_A^2 > \frac{\sum_a (\sum_b e^{-\beta E_{a,b}})^2}{\mathcal{Z}(\beta)^2} > \frac{\mathcal{Z}(2\beta)}{\mathcal{Z}(\beta)^2} = Y_2(\beta) \tag{3.33}$$

Thus, an upper bound for the quenched average $\langle S_2(\rho_A)\rangle$ is given by

$$\langle S_2(\rho_A)\rangle < \tau_2(\beta) N \log 2 \tag{3.34}$$

where $\tau_2(\beta)$ is defined in Eq.(3.23). This upper bound puts a constraint on $\langle S_2(\rho_A)\rangle$, showing that when

$$\beta > \beta_{ub}(n=2) = (1 - \sqrt{\frac{t}{2}})\sqrt{2\log 2} \tag{3.35}$$

then

$$\langle S_2(\rho_A)\rangle < N_A \log 2 \tag{3.36}$$

which is the thermal entropy at infinite temperature. The red solid curve in Fig.3.2 (a) is the upper bound for $\langle S_2\rangle / S_T$ at $t = 1/3$.

Using a similar approach, we can prove that when n is an even number, $\mathrm{Tr}\rho_A^n \geq Y_n(\beta)$, and the quenched averaged nth Rényi entropy satisfies

$$\langle S_n(\rho_A)\rangle < \frac{\tau_n(\beta) N \log 2}{n-1} \tag{3.37}$$

This upper bound indicates that when

$$\beta > \beta_{ub}(n) = (1 - \sqrt{\frac{n-1}{n}t})\sqrt{2\log 2} \tag{3.38}$$

we obtain the bound

$$\langle S_n(\rho_A)\rangle < N_A \log 2 \tag{3.39}$$

which, again, is the thermal entropy at the infinite temperature. The result for the upper bound is shown in Fig.3.2 (b). Notice that when $\beta \leq \beta_{ub}(n=\infty)$, the different curves in Fig.3.2 (b) are overlapping with each other. When $\beta_{ub}(n=\infty) < \beta < \beta_{sg}$, the upper bounds for $\langle S_n\rangle$ show different scaling behavior. Combining

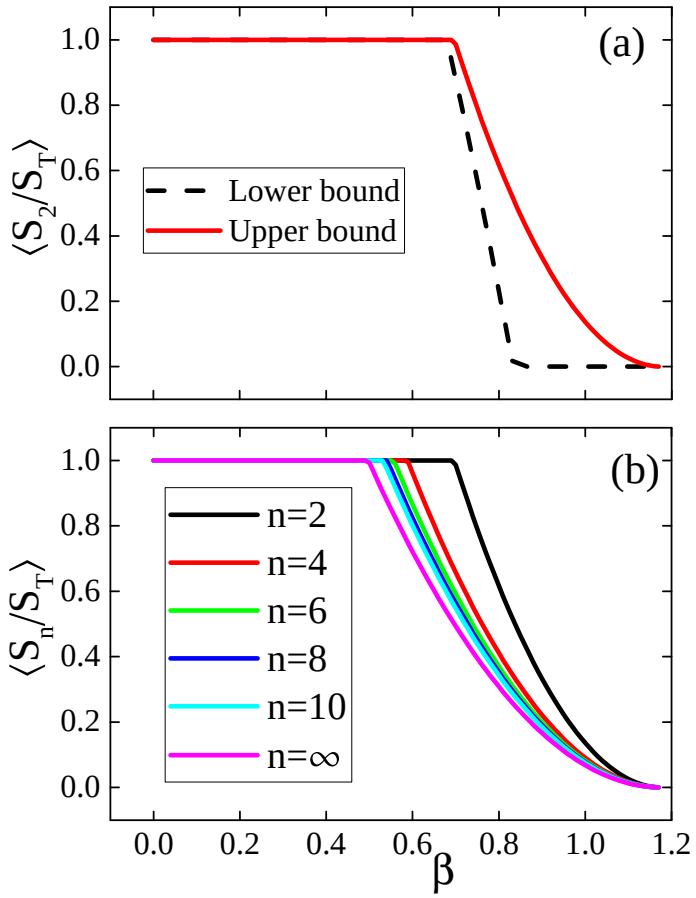

Figure 3.2: (Color online) (a) The lower and upper bound for $\langle S_2 \rangle$. The black dashed curve is for the lower bound and the red solid curve is for the upper bound. The system size $N = 300$ and the ratio $t = 1/3$. (b) The upper bound for $\langle S_n \rangle$. The setup is the same as (a).

the upper and lower bounds for different n leads to a regime where the $n = 2$ Rényi entropy satisfies a volume law and behaves like a thermal entropy at infinite temperature, but for $n > 2$ is strictly below this bound.

Implications from the bounds : From the above results, we find an upper and lower bound for the Rényi entropy. Here we consider $\langle S_2 \rangle$ in detail, which thus has the following behaviors

$$\begin{cases} \langle S_2 \rangle = S_2(\langle \widetilde{\rho}_A \rangle) = N_A \log 2, & \beta \leq \beta_1 \\ N(\log 2 - \beta^2) < \langle S_2 \rangle < N_A \log 2, & \beta_2 < \beta < \beta_{sg} \\ \langle S_2 \rangle < -\log(1 - \beta_{sg}/\beta), & \beta > \beta_{sg} \end{cases} \tag{3.40}$$

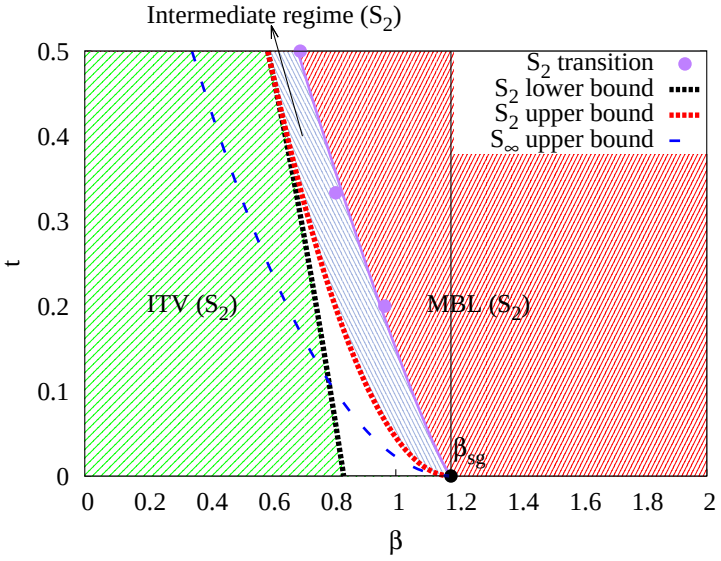

Figure 3.3: (Color online) A summary of our knowledge of the phase diagram of $\Psi_{REM+\text{sign}}$, based on $\langle S_n \rangle$. The dotted black line indicates a bound to the left of which $\langle S_2 \rangle$ analytically follows the $T = \infty$ volume law (ITV). The dotted red line indicates a bound to the right of which $\langle S_2 \rangle$ analytically is strictly below the $T = \infty$ volume law. β_{sg} indicates analytically the transition to a localized Hilbert space for any N_A/N and a guaranteed constant for all $\langle S_n \rangle$. The solid purple dots indicate the numerically computed transition points for $\langle S_2 \rangle$ (the purple line is a fit for the eye). In comparison, the blue dashed line indicates a bound to the right of which $\langle S_\infty \rangle$ analytically is strictly less then ITV, and suggests multifractality.

where $\beta_2 = \beta_{ub}(n = 2) = (1 - \sqrt{t/2})\sqrt{2 \log 2}$.

For $\langle S_2 \rangle$, there is a regime where $\langle S_2 \rangle$ satisfies the volume law and equals the thermal entropy at $T = \infty$. When $\beta > \beta_{sg}$, $\langle S_2 \rangle$ is bounded by a finite constant. A phase transition into the MBL phase is expected to be between $\beta_1 \leq \beta \leq \beta_{sg}$. To find the location of the MBL phase transition, we will use scaling collapse in Section 3.4.

3.3.3 Localization properties of the wave function

We end this Section with a discussion of the statistical properties of the states $|\Psi_{REM}\rangle$ and $|\Psi_{REM+\text{sign}}\rangle$. Given these states, we can define the amplitudes, i.e. their overlap with an eigenstate of the spins $|\mathcal{C}\rangle$. For each state, the square of the amplitude defines a probability distribution for the configuration $\mathcal{C}$ to occur in the state (and hence the random sign does not affect the probability distribution). The resulting probability distribution is thus the same for both states, and it is given by the probability of the configuration $\mathcal{C}$ in the classical REM,

$$P[\mathcal{C}] = |\langle \mathcal{C}|\Psi_{REM}\rangle|^2 = \frac{1}{\mathcal{Z}} e^{-\beta E[\mathcal{C}]} \tag{3.41}$$

Given this probability distribution, we can compute its Shannon-Rényi entropies, which one can immediately see, c.f. Eq.(3.20), to be the same as the IPR of the classical REM. Hence, the localization of wave function in the Hilbert space can be characterized by the IPR defined in the configuration space. For REM wave function,

$$Y_n = \sum_{\{\mathcal{C}\}} |\langle \Psi | \mathcal{C} \rangle|^{2n} = \frac{\sum_{i=1}^{2^N} e^{-n\beta E_i}}{\left(\sum_{i=1}^{2^N} e^{-\beta E_i}\right)^n} \tag{3.42}$$

This is the same as the IPR for the classical REM model defined in Eq.(3.20). Since $\tau(n)$, defined in Eq.(3.22), is the multifractal spectrum, given explicitly in Eq.(3.23), in the regime $0 < \beta < \beta_{sg}$, the wave function itself has multifractal behavior. The multifractality of the wave function indicates the pre-freezing behavior before entering into the MBL phase. Similar phenomenon was also observed in Refs.[Luca and Scardicchio, 2013, Luitz et al., 2015], where they found that at the MBL phase transition point, the whole wave function is still delocalized in the configuration space.

We can now use the results of the inverse participation ratios of the classical REM summarized in section 3.3.1 to draw conclusions on the degree of localization in the 2^N-dimensional Hilbert space of the $|\Psi_{REM}\rangle$ and $|\Psi_{REM+\text{sign}}\rangle$ wave functions. From the results of Section 3.3.1 we find that for $\beta > \beta_{sg} = \sqrt{2\log 2}$ all the inverse participation ratios are finite as $N \to \infty$ and, hence, that the Shannon-Rényi entropies for the wave functions are finite (and are not extensive). Thus, in this regime these wave functions are (exponentially) localized. On the other hand, for $\beta < \beta_{sg}$, the IPRs of the REM vanish exponentially fast as $N \to \infty$, and so do the Shannon-Rényi entropies of the wave functions. In this regime the wave functions are not localized. In this regime the multifractal nature of these wave functions is manifest in the size dependence of their Shannon-Rényi entropies. We should emphasize that, beyond setting the bounds that we have discussed earlier in this section, the knowledge the behavior of the Shannon-Rényi entropies alone yields no information on the scaling of quantum entanglement, which is our main interest.

3.4 Numerical results on MBL phase transition

In the previous section, we were able to analytically establish the existence of a regime in which the quenched averaged second Rényi entropy $\langle S_2 \rangle$ is strictly less than ITV scaling, and happens strictly before the localization transition. Nothing prevents this regime from being one in which $\langle S_2(N_A) \rangle$ still scales linearly but at finite T; in addition, it doesn't separate the MBL transition from the localization transition. To establish this, we numerically identify the transition point via scaling collapse. We explicitly construct different disorder samples from the random sign REM wave function and calculate the quenched average $\langle S_n \rangle$ with at least 1000 disorder realizations. First, we focus on the $n = 2$ case, and then discuss the other values of

n. As a sanity check, we verify that our numerical results are consistent with the analytical results above at large and small β.

The following is a summary of our numerical results.

At small β : Analytically we anticipate ITV for $n = 2$. In Fig. 3.4, we concretely consider $\beta = 0.3$ at $N = 30$ with 2000 disorder realizations. We see that it corresponds to the expected $\langle S_2 \rangle = N_A \log 2$.

As $N_A \log 2$ is the maximal entanglement entropy for any given realization, for a $T = \infty$ volume law to hold, essentially all but a measure zero fraction of configurations must have this entropy. From the inset of Fig.3.7b, one can see that the standard deviation of $\langle S_2 \rangle$ at $\beta = 0.3$ is zero showing this is indeed the case. Similar behavior can be observed for $\langle S_n \rangle$ with other Rényi indices, where $\langle S_n \rangle = N_A \log 2$ and $\langle \delta S_n \rangle$ is close to zero as $\beta \leq \beta_*$.

At large $\beta > \beta_{sg}$: We find analytically that $\langle S_n \rangle$ with $n \geq 2$ is bounded by a finite constant and, hence, in this range the state is in the MBL phase. Note that a constant for small n gives a bound for the entanglement entropy for all larger m as $S_n > S_m$ if $m > n$. In Fig.3.4 the numerical results for $\beta = 1.5$ are presented, and show that when N_A increases, $\langle S_n \rangle$ saturates to some constant value. Notice also from the inset of Fig.3.7b, that as we move deeper into the localized phase, the standard deviation is monotonically decreasing.

The change from ITV to constant in the entanglement entropy can be seen in Fig.3.5, which shows $d\langle S_2 \rangle / dN_A$ as a function of β. As system sizes increases, the slope quickly approaches $\log 2$ for $\beta < 0.5$, and approaches 0 for $\beta > 1.2$. The slopes for all 5 values of N start to drop around $\beta = 0.6$, which is less than the $\beta_2 = (1 - \sqrt{1/6})\sqrt{2 \log 2} \approx 0.6967$ in Eq.(3.40) for subsystem ratio $t = 1/3$ and is consistent with the analytical result.

3.4.1 Finite-size scaling

To locate the MBL phase transition, we use both $\langle S_2 \rangle$ and its standard deviation, δS_2.[Kjall et al., 2014, Vosk et al., 2014] For instance, in the bottom inset of Fig. 3.7, it is shown that when $\beta > 0.5$, $\delta S_2 / S_T$ will increase rapidly and reach the maximum value at some β. Fig. 3.7 (bottom) shows that the standard deviation at intermediate values of β is actually a non-trivial fraction of the maximum thermodynamic entropy. In fact, because of the breakdown in the REM of the Central Limit Theorem, the fluctuation of the Rényi entropy is non-Gaussian. This is seen, for example, in the distribution of S_2/S_T at $\beta = 0.72$ shown in Fig.3.6, which is peaked around 1 and has a long tail. This long tail has power law scaling behavior shown in the inset of Fig.3.6, with a power-law exponent between -3 and -2, which implies a well-defined

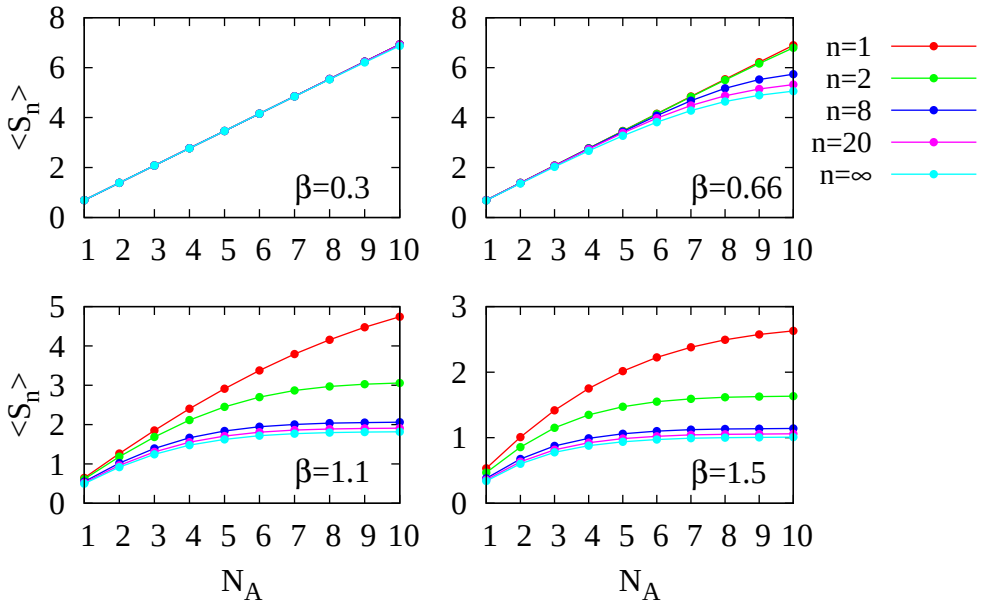

Figure 3.4: (Color online) The numerical results for $\langle S_n \rangle$ with n from 1 to ∞ at different values of β. The total system size is $N = 30$. Each point in the plot is averaged over 2000 disorder realizations. At $\beta = 0.3$, S_n shows ITV behavior for all n. At $\beta = 0.66, 1.1$, $\langle S_n \rangle$ deviates from the ITV with increasing β, but the speed at which it moves away depends on its Rényi index. At $\beta = 1.5$, $\langle S_n \rangle$ is a constant for all n.

average but an infinite variance in the thermodynamic limit (which is consistent with the peak scaling as S_T). This may be related to the quantum Griffiths phase found in Ref. [Vosk et al., 2014, Agarwal et al., 2015, Potter et al., 2015].

While we can use the peak of δS_2 and the transition of $\langle S_2 \rangle$ from maximal to zero to locate the phase transition, these quantities scale with system size. We therefore use finite-size scaling to find the MBL phase transition. In the regime of interest, we perform a scaling collapse of the data for the two ratios $\langle S_2 \rangle / S_T$ and $\delta S_2 / S_T$ separately, using scaling functions of the form

$$N^b \Phi((\beta - \beta_c) N^a) \tag{3.43}$$

and determine the form of the scaling functions $\Phi(x)$ numerically. The exponent b is expected to be very close to 0 for $\langle S_2 \rangle / S_T$. When doing the scaling analysis, we find that the quality of the $\langle S_2 \rangle / S_T$ collapse is better than that of the $\delta S_2 / S_T$. Error analysis is only performed on the scaling parameters obtained from

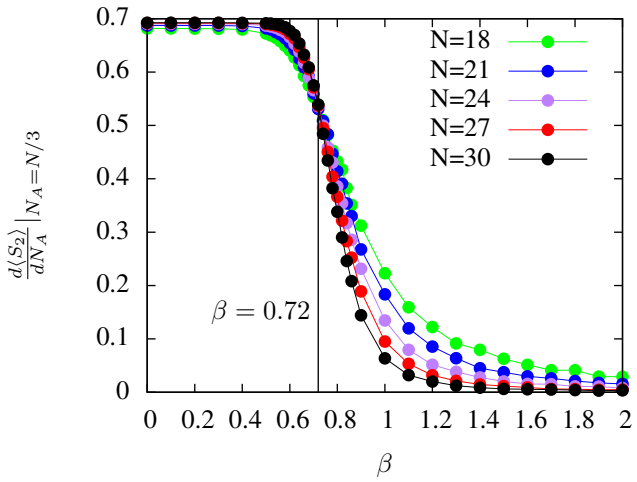

Figure 3.5: (Color online) $\frac{d\langle S_2\rangle}{dN_A}$ vs β graph at $t = 1/3$, where the slopes are obtained from finite differences. As β increases, the slopes drop from $\log 2$ towards 0 for all 5 different system sizes.

$\langle S_2\rangle/S_T$, although generally the $\delta S_2/S_T$ collapse yields similar values for β_c.

Notice that this scaling form assumes the existence of only one transition in spite of the fact that we have analytical bounds that show the presence of ITV, constant, and sub-ITV scaling; numerically the latter appears to be neither constant nor linear with subsystem size.

Fig. 3.7 shows the scaling collapsed for $\langle S_2\rangle$ at $t = 1/3$. In previous work on MBL phase transition, $\nu \equiv a^{-1}$ in Eq.(3.43), is the critical exponent for the localization length and is expected to satisfy Harris inequality $\nu \geq 2/d$, where d is the spatial dimension. However REM model is a highly non-local model and d here is equal to infinity, which suggests that there is no bound for ν. To make sure the scaling parameters obtained are truly associated with this transition, one can use them to scale the $\langle S_n\rangle/S_T$ data following Ref. [Luitz et al., 2015]. For each β, we plot $\langle S_n\rangle$ vs N as shown in the inset of Fig. 3.10 , from which one can see that the scaled curves bifurcate smoothly into the two branches depending on β. Furthermore, Fig. 3.10 indicate that the system experiences a phase transition rather than a crossover, because of the clear separation of the two branches at large N.

We have also done scaling collapse for $\langle S_2\rangle$ with other subsystem ratios. At $t = 1/2$, we get $\beta_c = 0.693$; and at $t = 1/5$, we get $\beta_c = 0.965$. These results are shown as purple dots on Fig. 3.3. All our collapsing results are summarized in Table 3.1.

Based on the above numerical results, we conclude that the MBL transition (both of $\langle S_2\rangle$ and all the other $\langle S_n\rangle$ (see Sec.3.4.3 and Appendix C) happen separately from the localization transition at β_{sg}. The MBL phase transition is at β_c and is smaller than β_{sg}. Between β_c and β_{sg}, although it is in the MBL phase, the whole wave function is still delocalized in the Hilbert space. Only when $\beta > \beta_{sg}$, the wave function

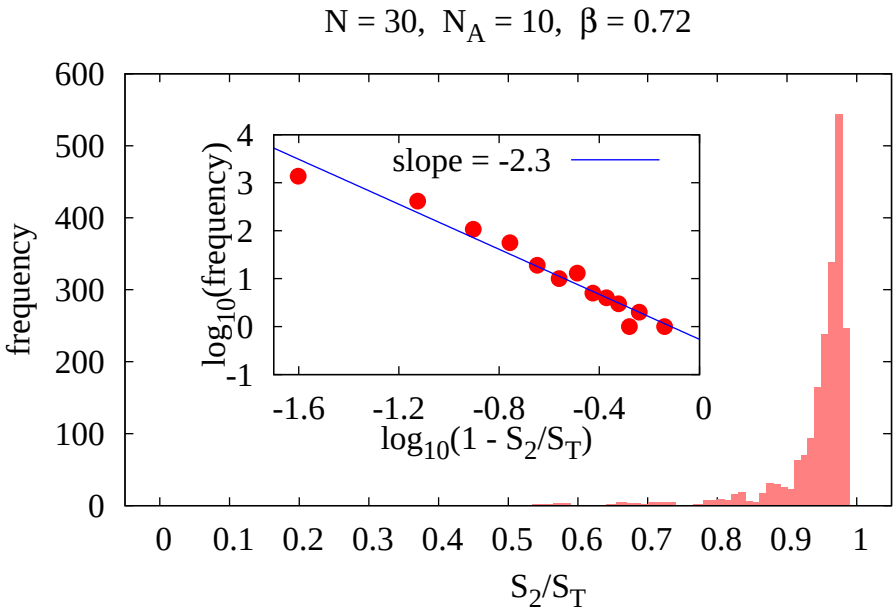

Figure 3.6: (Color online) The distribution of S_2/S_T at $\beta = 0.72$. The total number of samples is 2000. The number of bins used to make the histogram is 100. The inset shows a log-log plot with a linear fit, which indicates a power law distribution. The number of bins in the log-log scale is 20 for S_2/S_T from 0 to 1. However, as many of the bins have 0 sample, some points are not included the log-log plot.

becomes localized in the Hilbert space and is already deep in the MBL phase.

3.4.2 Intermediate regime

According to the scaling collapse in Fig. 3.7, the MBL phase transition for $\langle S_2 \rangle$ happens at around 0.8 at $t = 1/3$. From Eq.(3.35), we also know that when $\beta > 0.697$, $\langle S_2 \rangle < N_A \log 2$. This implies that there is an intermediate regime between ITV and MBL phase (regime (ii) in Fig.4.1 (b)). In this regime, $\langle S_2 \rangle$ is sub-extensive and the slope

$$0 < s(N_A) = \frac{1}{\log 2} \frac{d\langle S_2 \rangle}{dN_A} < 1. \tag{3.44}$$

This regime is not a cross-over but sharply defined with non-analyticities in the curve $s(t)$ signaling its beginning. While a combination of our analytical bounds and numerical results can bound the location of this transition, we are not able to numerically pinpoint its location. It is interesting to note, though, that all

	t	n	a	b	β_c
$\frac{\langle S_n \rangle}{S_T}$	1/3	1	0.811	0.007	0.970
	1/3	1.5	0.897	0.0093	0.8680
	1/3	2	0.906	?0.0006	0.8072
	1/3	3	0.902	0.0095	0.755
	1/3	20	0.8389	?0.025	0.6657
	1/3	∞	0.817	?0.039	0.651
	1/2	2	0.90	?0.070	0.693
	1/5	2	0.766	0.010	0.965
$\frac{\delta S_n}{S_T}$	1/3	1	0.893	0.321	0.983
	1/3	1.5	0.902	0.396	0.861
	1/3	2	0.923	0.400	0.798
	1/3	3	0.908	0.399	0.753
	1/3	20	0.835	0.383	0.655
	1/3	∞	0.824	0.397	0.643
	1/2	2	0.909	0.090	0.678
	1/5	2	0.856	0.147	0.963

Table 3.1: Collected scaling collapse data

the curves in Fig. 3.5 seem to cross at a single point; for $t = 1/3$, this point is approximately $\beta = 0.72$ which is surprisingly close to the β_2 bound. While we can't say anything definitive about the value of the $s(N_A)$ in the intermediate regime, Fig. 3.5 shows only two plateaus suggesting that the $s(N_A)$ in this intermediate regime is not constant. Instead we conjecture that the slope changes continuously as a function of N_A in this regime in a nonlinear way. This means that this regime is non-thermal and doesn't correspond to a thermal density matrix at any temperature. It is not clear whether to call this regime a separate phase, particularly as the data collapse on $\langle S_2 \rangle / S_T$ and $\delta S_2 / S_T$ only identify a single transition.

3.4.3 Multifractality of the Rényi entanglement entropies

While we have identified transitions in $\langle S_2 \rangle$, we can also consider $\langle S_n \rangle$ for $n \neq 2$. The analytical bounds (Fig.3.2) show that there is a regime where S_2 is still ITV where S_∞ scales at a rate less then ITV. We can also use scaling collapse to identify the MBL phase transition in $\langle S_n \rangle$; for example, see Fig. 3.8. More scaling collapse graphs with different n and subsystem ratio t can be found in Appendix C. We summarize the $N_A/N = 1/3$ results for various n in Fig.3.9, from which one can clearly see the transition depends on n. We attribute this as a sign of multifractal behavior similar to the multifractal behavior found in the critical wave function of the Anderson localization phase transition point. [Wegner, 1980] In the Anderson localization problem it is known that multifractality is a feature of the wave function for the mobility edge.[Wegner, 1980] It is not known if this is also the case in MBL or if there is a multifractal phase. From our data we cannot at present make a definitive determination. It is interesting to note that $\beta_c(n)$ is linearly proportional to

$(n-1)/n$. The phase transition point β_c for von Neumann entropy is 0.97 and we identify this as the true MBL transition.

We can understand the different scaling behavior of $\langle S_n \rangle$ by considering the entanglement spectrum. Fig.3.12 is the distribution of eigenvalue λ of ρ_A for a randomly chosen disorder configuration at different β. When $\beta = 0.3$, λ forms a continuous band around 0.001 which is approximately equal to $1/2^{N_A}$. While for $\beta = 0.66, 1.1$ and 1.5, there is an obvious gap between the lower continuous band and the other higher eigenvalues. The entanglement gap increases as β increases.

This inspires us to write down a simplified two-level model for entanglement spectrum which includes a flat band and a single λ_{max}. If we assume that $\langle S_n \rangle$ is approximately equal to its upper bound in Eq.(3.37), by using $S_{n=\infty} = -\log \lambda_{max}$, we have

$$\lambda_{max} = 2^{-(1-\frac{\beta}{\sqrt{2\log 2}})^2 N} \tag{3.45}$$

All the other $\lambda_1 \approx 1/2^{N_A}$ and there is a gap between λ_1 and λ_{max}. This toy model exhibits the multifractal behavior described above with a transition to constant entanglement slope that scales with $n > 2$. The transition in this simplified model is direct from ITV to constant; to capture our intermediate regime, the single λ_{max} can be replaced by a finite number λ_i with each of them are separated by a finite gap. Also the lower flat band can be replaced a continuous band with more complicated band structure. These additional ingredients are required to have an intermediate regime with sub ITV as well as accurately finding the constant $n = 1$ von Neumann entropy.

3.4.4 The random sign structure in the wave function

We have introduced a random sign structure to convert our ground state wave function into one at finite energy density. While for any strictly positive wave function, the introduction of random signs can only increase the entanglement entropy, it is interesting to ask what effect, if any, the random sign has here. This requires computing the Rényi entropy $\langle S_n(\rho'_A) \rangle$ for the REM wave function without the random sign $|\Psi_{REM}\rangle$. Different from $|\Psi_{REM+\text{sign}}\rangle$, the Rényi entropy for $|\Psi_{REM}\rangle$ is not a monotonic function with β and has more complicated scaling behavior. In fact $|\Psi_{REM}\rangle$ has zero entanglement entropy at both $\beta = 0$ and $\beta \to \infty$. It is interesting to note that while $\langle S_2(\rho_A) \rangle$ and $\langle S_2(\rho'_A) \rangle$ have long tails and infinite variance in the thermodynamic limit at intermediate β, their difference $\Delta S_2 = \langle S_2(\rho_A) \rangle - \langle S_2(\rho'_A) \rangle$ appears to have finite variance (as shown in Fig. 3.13).

Since the quenched average $\langle S_2(\rho'_A) \rangle$ is hard to access analytically, we can compute a lower bound via

Eq.(3.29) using Jensen's inequality. [Reed and Simon, 1981]

Lower bound for $\langle S_2(\rho'_A)\rangle$

For the REM wave function without random sign, the quenched average $\langle S_2(\rho'_A)\rangle$ is hard to access analytically, instead we calculate the annealed average $S_2(\langle\rho'_A\rangle)$ defined in Eq.(3.29), which gives the lower bound for $\langle S'_2\rangle$. To obtain $S_2(\langle\rho'_A\rangle)$, we need to know $\langle \mathrm{Tr}(\widetilde{\rho}'_A)^2\rangle$ first, where $\widetilde{\rho}'_A$ is the unnormalized reduced density matrix.

$$\begin{aligned}\langle \mathrm{Tr}(\widetilde{\rho}'_A)^2\rangle =& 2^N e^{2N\beta^2} + (2^{N_B}-1)2^N e^{N\beta^2} \\ &+(2^{N_A}-1)2^N e^{N\beta^2} + (2^{N_A}-1)(2^{N_B}-1)2^N e^{\frac{N\beta^2}{2}}\end{aligned} \tag{3.46}$$

This gives $S_2\langle(\rho'_A)\rangle$ in the thermodynamic limit. When $0 < t \leq 1/3$, there are three regimes,

$$S_2(\langle\rho'_A\rangle) = \begin{cases} \frac{\beta^2 N}{2}, & \beta \leq \sqrt{2t\log 2} \\ N_A \log 2, & \sqrt{2t\log 2} < \beta \leq \sqrt{(1-t)\log 2} \\ N(\log 2 - \beta^2), & \beta > \sqrt{(1-t)\log 2} \end{cases} \tag{3.47}$$

When $1/3 < t < 1/2$, there are two regimes

$$S_2(\langle\rho'_A\rangle) = \begin{cases} \frac{\beta^2 N}{2}, & \beta \leq \sqrt{2\log 2/3} \\ N(\log 2 - \beta^2), & \beta > \sqrt{2\log 2/3} \end{cases} \tag{3.48}$$

From the above calculation, we find that if $t < 1/3$, there is a region $\sqrt{2t\log 2} \leq \beta \leq \sqrt{(1-t)\log 2}$ where $|\Psi_{REM}\rangle$ has ITV entanglement. As this is the maximal allowed value, it then directly follows that there is no difference between $\langle S'_2\rangle$ and $\langle S_2\rangle$ due to the introduction of signs.

Moreover, we conjecture that ΔS_2 decreases monotonically as a function of β. This is consistent with the numerical results shown in Fig.3.14. Following from this conjecture, we would have that $\Delta S_2 = 0$ for all $\beta \geq \sqrt{2t\log 2}$ and $t < 1/3$. This is because, for all $t < 1/3$ both models show ITV between $\beta = \sqrt{2t\log 2}$ and $\sqrt{(1-t)\log 2}$ and hence $\Delta S_2 = 0$. The regions B, C, D in Fig. 3.15 denote where $|\Psi_{REM}\rangle$ and $|\Psi_{REM+\mathrm{sign}}\rangle$ have the same $\langle S_2\rangle$.

Having identified regimes where the introduction of random signs doesn't affect the entanglement entropy, we also identify regimes where the entanglement entropy can be shown to be different. When $\beta = 0$, $|\Psi_{REM}\rangle$ is a constant (actually a product state) whereas $|\Psi_{REM+\mathrm{sign}}\rangle$ is a volume law. We can argue that this extends

to larger β. Defining $X = \mathrm{Tr}\widetilde{\rho}_A^2$ and $Y = \mathrm{Tr}(\widetilde{\rho}'_A)^2$, where $\widetilde{\rho}_A$ is the unnormalized reduced density matrix, we have

$$\langle \log \frac{X}{Y} \rangle \leq \log \langle \frac{X}{Y} \rangle \leq \log \frac{\langle X \rangle}{\langle Y \rangle} \tag{3.49}$$

where the second inequality, while not true in general, appears to be numerical validated in our case. In the thermodynamic limit, $\log \frac{\langle X \rangle}{\langle Y \rangle}$ can be directly computed (see Eq.(3.31) and Eq.(3.46)). We find that when $t < 1/3$ and $\beta \leq \sqrt{2t \log 2}$, $\log \frac{\langle X \rangle}{\langle Y \rangle} = 0$. In this region, $\langle S_2 \rangle$ for $|\Psi_{REM+\mathrm{sign}}\rangle$ continues growing as volume while $|\Psi_{REM}\rangle$ stays constant, indicating that the random sign structure can thermalize the wave function and is responsible for the volume law scaling behavior. Fig. 3.16 is the numerical result for $\langle S'_n \rangle$ at $\beta = 0.4$. We can see that when $n \geq 2$, they all saturate to a constant. This region is highlighted in blue on Fig. 3.15 and marks a region where the models differ maximally.

Finally, we note that ΔS_n can be numerically computed. Fig.3.14 is ΔS_n for $N = 30$ and $N_A = 10$. We find that for all n, $\Delta S_n = 0$ when $\beta > 0.8$. This result, while only for $N = 30$ and so not absent finite-size effects happens to be at the location of the $\langle S_2 \rangle$ MBL phase transition.

3.5 Conclusions

In this chapter, we have studied the many-body localization phase transition in a class of many-body wave functions. We focused our analysis in a class of wave functions, $|\Psi_{REM}\rangle$, whose amplitudes are the Boltzmann weights of a classical spin glass model in infinite dimension, the Random Energy Model. In order to mimic the structure of wave functions of highly excited states with a finite excitation energy density we considered another class of states, $|\Psi_{REM+\mathrm{signs}}\rangle$, whose amplitudes are obtained by multiplying the amplitudes of $|\Psi_{REM}\rangle$ by a random sign for each configuration. We studied the MBL problem in the $|\Psi_{REM+\mathrm{signs}}\rangle$ wave function, for different regime of the parameter β, by using both analytical and numerical approaches.

We showed that there is a direct phase transition into the MBL phase. Here we assume that the MBL phase is characterized that the entanglement entropies, as a function of the size of the observed region N_A, scale to a constant value, a feature that we observed explicitly for large enough values of β. The location of the phase transition point is identified by scaling collapse of Rényi entropy and its standard deviation. In the thermalized regime, there is a regime where the Rényi entropies with different Rényi index all equal to the thermal entropy S_T at $T = \infty$. When $\beta > \beta_c$, the system enters into the MBL phase where the entanglement entropy is sub-extensive. The MBL phase transition point β_c is smaller than β_{sg} and this suggests that the MBL phase transition and the classical spin glass phase transition are different. Upon entering the MBL phase, the random sign structure is not important any more and $\langle \Delta S_n \rangle$ between $|\Psi_{REM+\mathrm{sign}}\rangle$ and $|\Psi_{REM}\rangle$

is zero. For $\beta > \beta_{sg}$, the wave function is deep inside the MBL phase and only $O(1)$ number of the configurations in the REM wave function contributes significantly to the statistical average. The Rényi entropy in this regime will reduce to a finite constant. We find that close to the phase transition point β_c, the fluctuation of Rényi entropy is strong in the finite size system. In this regime, Rényi entropies with different Rényi index show different scaling behavior and are similar to the multifractal behavior observed at the Anderson localization phase transition point. Moreover, $\langle S_n \rangle$ has a phase transition at different β_c. Finally we note that we have refrained ourselves from performing the same extensive studies for the wave function without random signs, $|\Psi_{REM}\rangle$. While we have evidence that this wave function too has a thermalized regime, since it has only strictly positive amplitudes we do not expect it to provide an useful description of the MBL problem. Nevertheless it may be useful to investigate its properties in a separate publication.

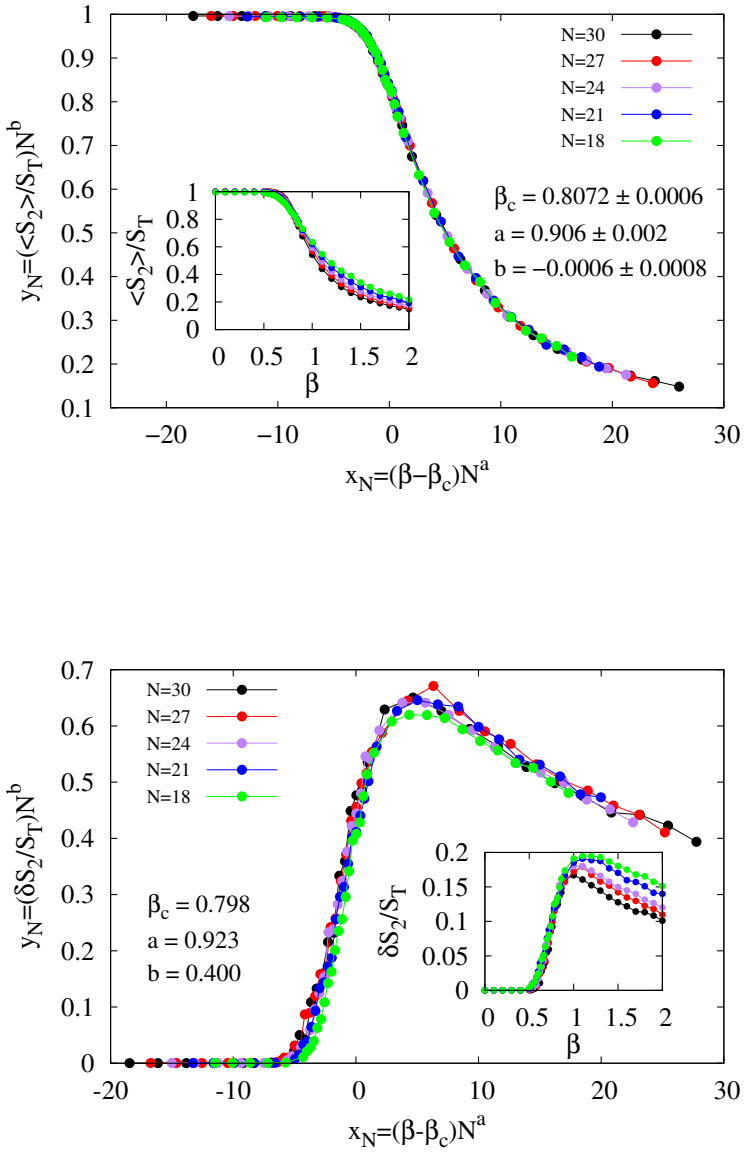

Figure 3.7: (Color online). a) Scaling collapse of $\langle S_2\rangle/S_T$ at $t = 1/3$, where $S_T = N_A \log 2$. It can be noticed that b is very close to 0. b) Scaling collapse of $\delta S_2/S_T$. The left insets show the original curves. Two scaling collapses give very close β_c values. Error analysis is only performed on the scaling collapse of $\langle S_2\rangle/S_T$.

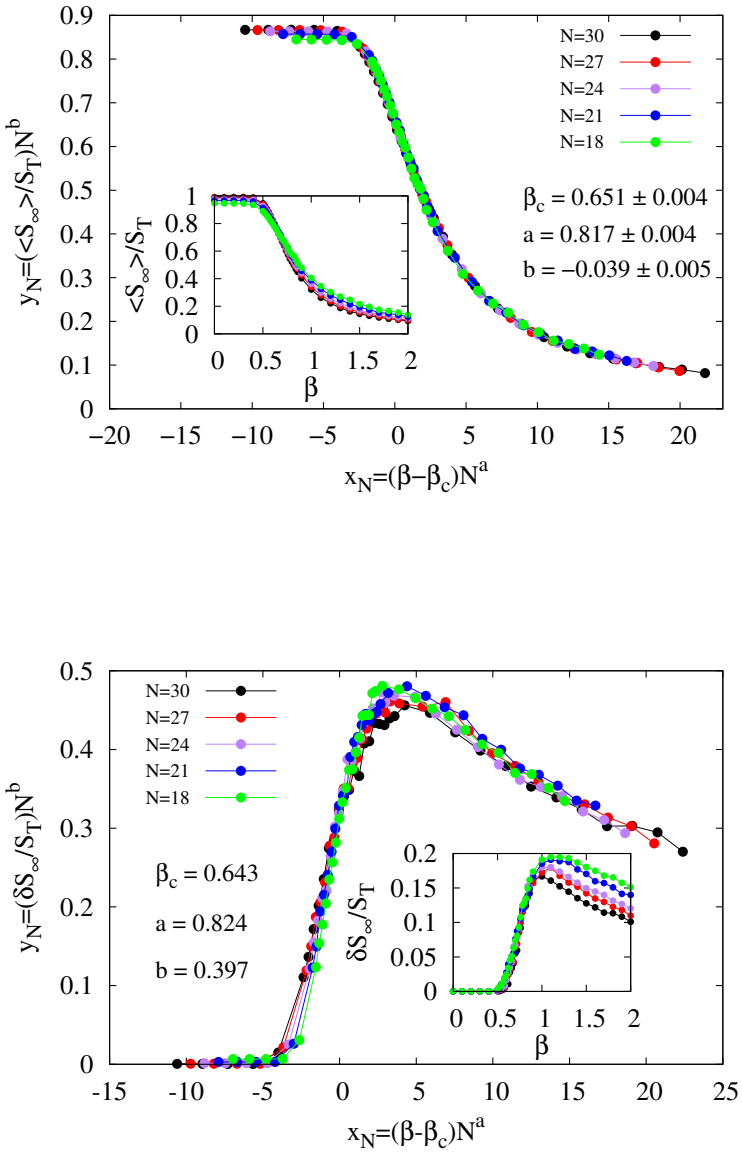

Figure 3.8: (Color online) (a) Scaling collapse of $\langle S_\infty \rangle / S_T$ at $t = 1/3$, where $S_T = N_A \log 2$. It can be noticed that b is very close to 0. (b) Scaling collapse of $\delta S_\infty / S_T$. The left insets show the original curves. Two scaling collapses give very close β_c values. Error analysis is only performed on the scaling collapse of $\langle S_\infty \rangle / S_T$.

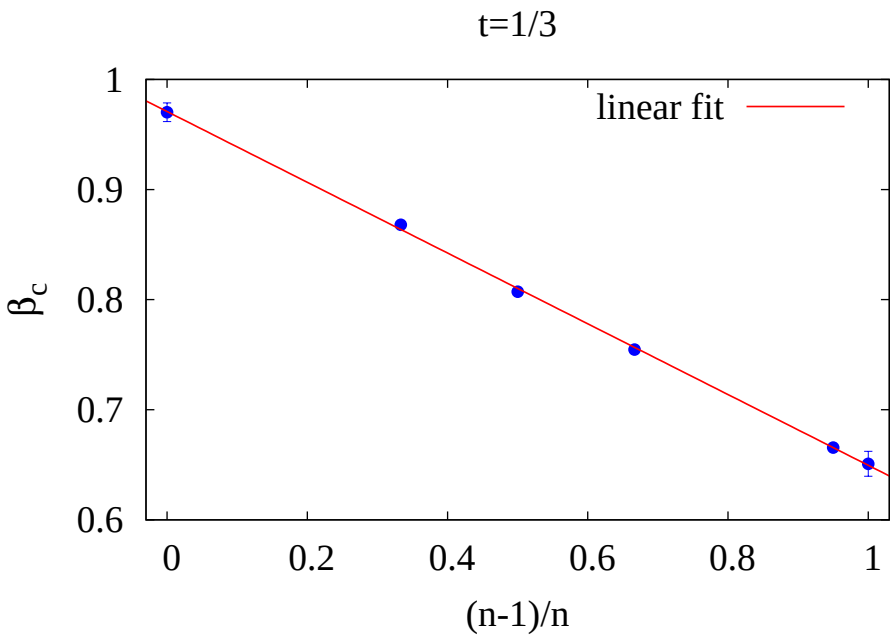

Figure 3.9: (Color online) β_c vs $\frac{n-1}{n}$ curve at $t = 1/3$. The linear fit line's slope is -0.3213 ± 0.0034, and its y-intercept is 0.9709 ± 0.0023.

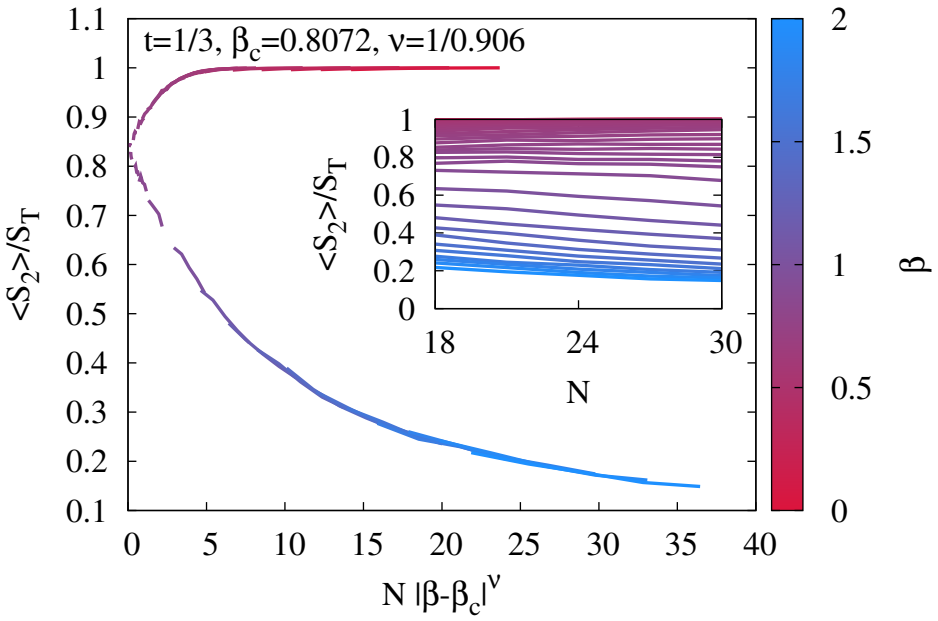

Figure 3.10: (Color online) This graph uses the scaling parameters obtained from Fig. 3.7 to scale the $\langle S_2 \rangle / S_T$ vs N curves for β values ranging from 0 to 2. The scaled graph clearly shows two branches – (1) curves with large β flow to low entanglement entropy; (2) curves with small β flow to $T = \infty$ entanglement entropy, i.e. $N_A \log 2$. The right inset shows the original curves, where each curve corresponds to a different β.

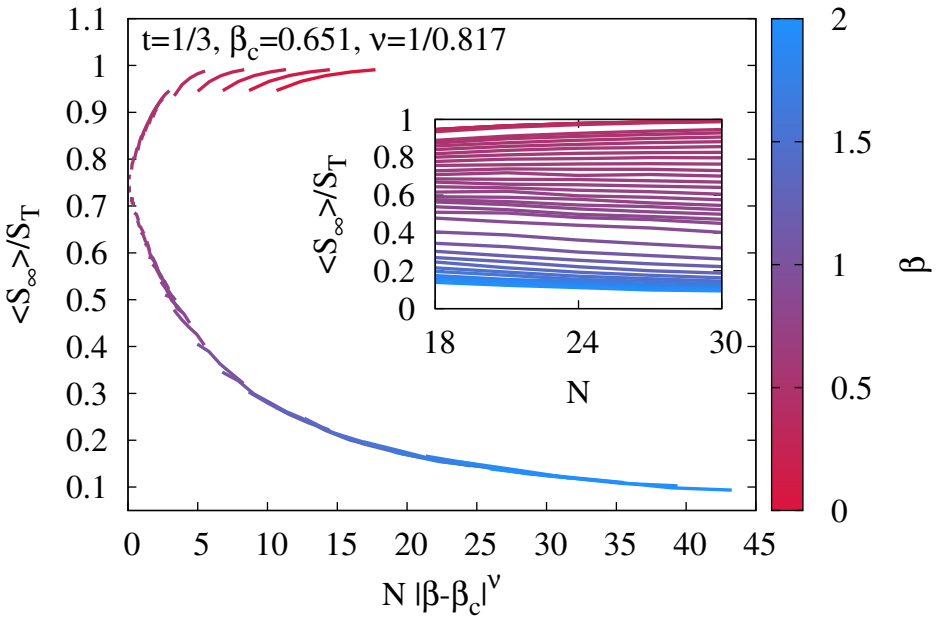

Figure 3.11: (Color online) This graph uses the scaling parameters obtained from Fig. 3.8 to scale the $\langle S_\infty \rangle / S_T$ vs N curves for β values ranging from 0 to 2. The scaled graph clearly shows two branches – (1) curves with large β flow to low entanglement entropy; (2) curves with small β flow to $T = \infty$ entanglement entropy, i.e. $N_A \log 2$. The right inset shows the original curves, where each curve corresponds to a different β.

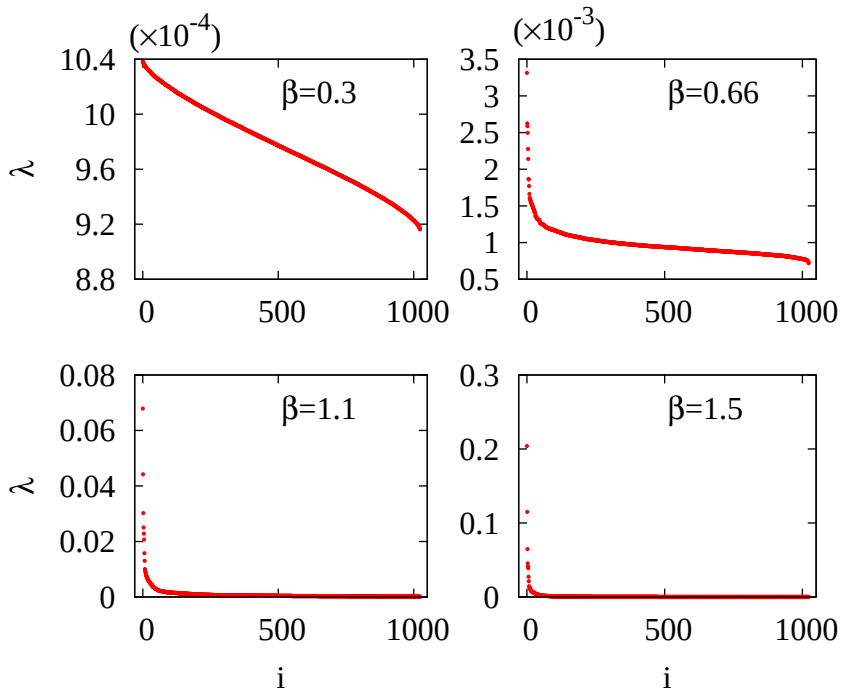

Figure 3.12: (Color online) Entanglement spectrum for one randomly chosen disorder configuration at $\beta = 0.3, 0.66, 1.1$ and 1.5, with $N = 30$, $N_A = 10$. The gaps in the entanglement spectrum become evident when β gets larger.

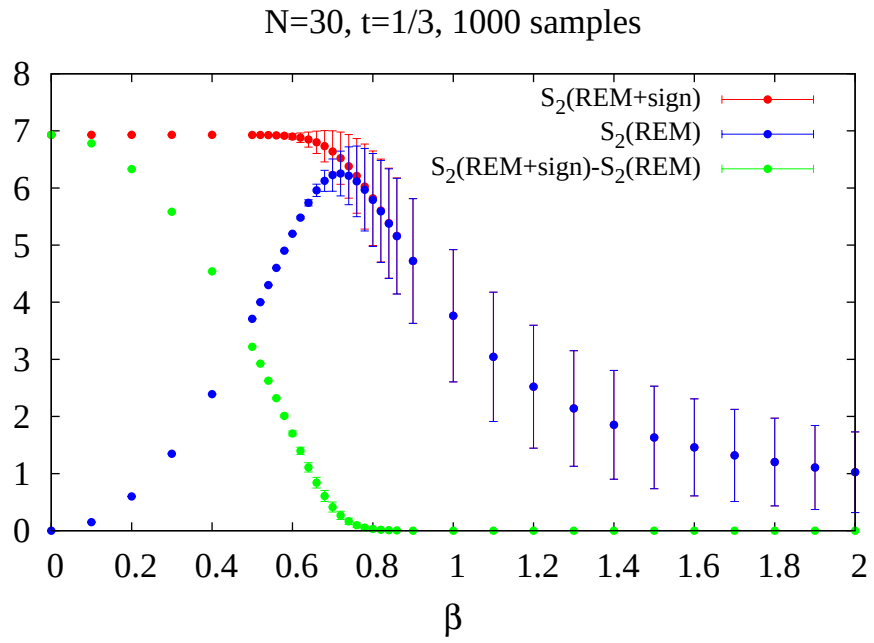

Figure 3.13: (Color online) $\langle S_2 \rangle$ of REM+sign and REM, and their difference. The 1000 disorder configurations are the same for REM+sign and REM. Error bars here represent standard deviations. The difference of the $\langle S_2 \rangle$ has well bounded variance for all β.

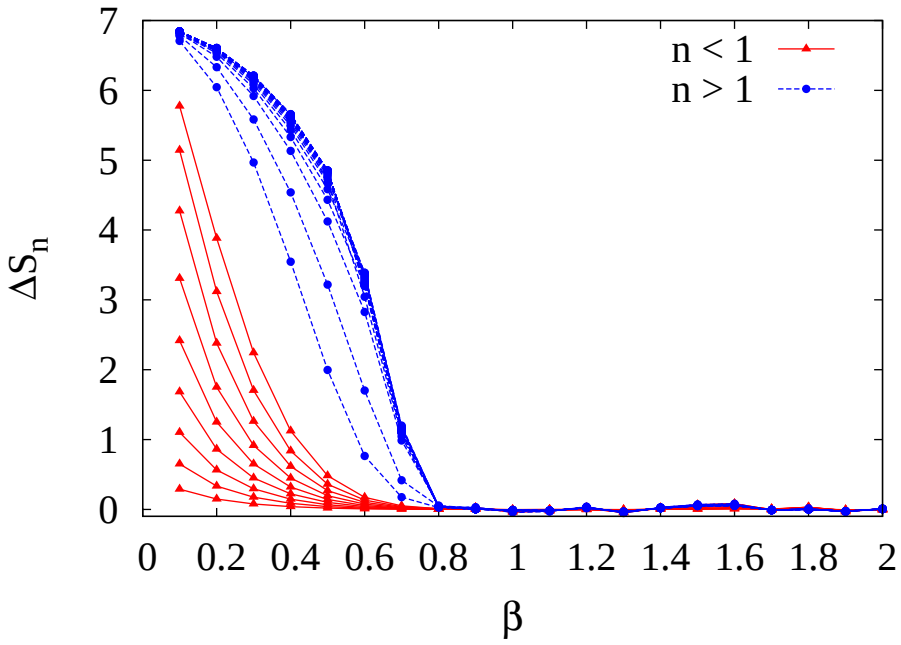

Figure 3.14: (Color online) Difference of $\langle S_n \rangle$ between REM+sign and REM for $n = 0.1, \ldots, 0.9$ in 0.1 steps (triangles), and for $n = 1.5$, $n = 2, \ldots, 20$, and ∞ (full circles), at $N = 30$ and $N_A = 10$. The number of disorder configurations is 2000. The random configurations are not the same for REM+sign and REM.

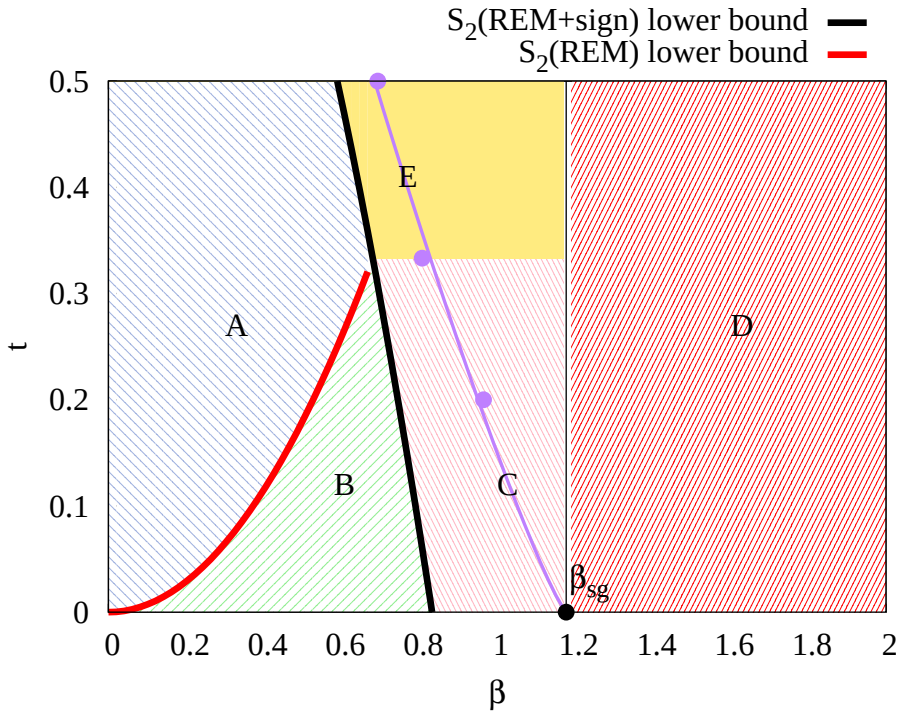

Figure 3.15: (Color online) Different behaviors of $\Delta S_2 = \langle S_2(REM + \text{sign})\rangle - \langle S_2(REM)\rangle$ on the t vs β graph. Region A represents the area where $\langle S_2(REM + \text{sign})\rangle$ follows ITV and $\langle S_2(REM)\rangle$ is a constant, so ΔS_2 obeys ITV. Region B represents the area where $\langle S_2(REM + \text{sign})\rangle$ and $\langle S_2(REM)\rangle$ are both ITV, and ΔS_2 is zero. As a result, ΔS_2 is also zero in Region C based on the monotonicity argument. In Region D, both $\langle S_2(REM + \text{sign})\rangle$ and $\langle S_2(REM)\rangle$ are localized in Hilbert space and ΔS_2 is zero. We do not have enough information to determine the behavior ΔS_2 in Region E.

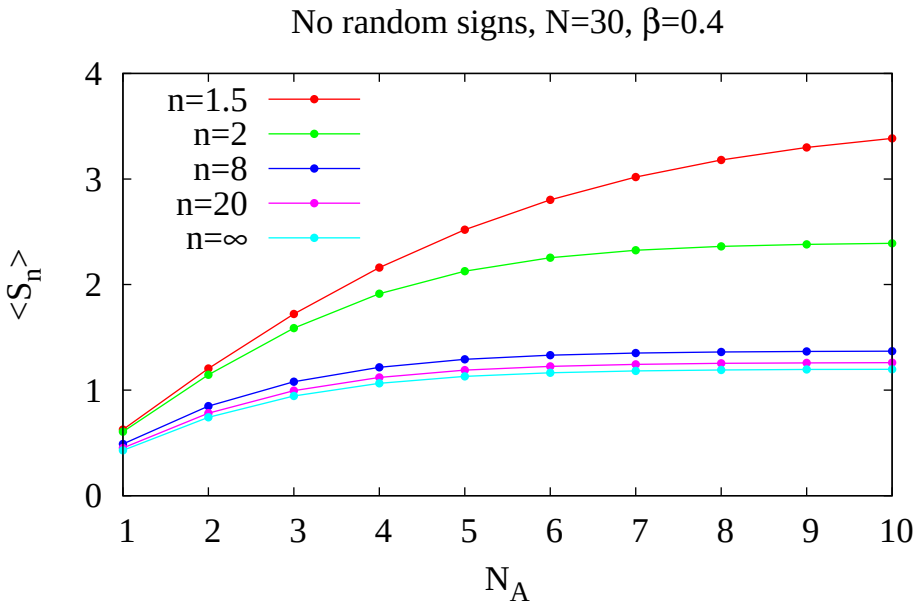

Figure 3.16: (Color online) The numerical results for $\langle S'_n \rangle$ without random sign with n from 1.5 to ∞ at $\beta = 0.4$. The total system size is $N = 30$. Each point in the plot is the average of 2000 disorder realizations.

Chapter 4

Scaling of entanglement in $2+1$-dimensional scale-invariant field theories

4.1 Introduction

The von Neumann entanglement entropy (EE) has proven to be a useful tool to diagnose and characterize strongly coupled field theories and condensed matter systems such as the topologically ordered phases and quantum critical systems. In this chapter, we study the universal scaling behavior of the entanglement entropy of scale-invariant field theories in $2+1$ dimensions. We specially consider two fermionic scale-invariant models, free massless Dirac fermions and a model of fermions with quadratic band touching, and study the two-cylinder entanglement entropy of the models on the torus numerically and analytically.

The von Neumann EE S_{vN} in a massive phase is well understood and it has been shown to satisfy an area law, $S_{vN} = \alpha \left(\frac{\ell}{\epsilon}\right)^{d-1}$, where d is the dimension of space, ℓ is the linear size of the region A being observed, and α is a non-universal (cutoff-dependent) constant.[Bombelli et al., 1986, Srednicki, 1993, Wolf et al., 2008] The EE of massless and in generally scale-invariant field theories in spatial dimensions $d > 1$ is also expected to obey the area law since it reflects the short-range entanglement generally present in the ground-state wave functions of these local field theories. This expectation is confirmed by the general result derived from the AdS/CFT correspondence in relativistic scale-invariant theories,[Ryu and Takayanagi, 2006b] in calculations in free-field theories,[Casini and Huerta, 2009] and in many models in condensed matter physics in one and two spatial dimensions.[Amico et al., 2008, Eisert et al., 2010, Fradkin, 2013]

Much less is known about the scaling of EE in scale-invariant systems in $d > 1$. Dimensional analysis and locality of the field theory suggest that that for scale-invariant systems in $d = 2$ space dimensions with an entangling region with a smooth boundary, the EE again has the same form, $S_{vN} = \alpha \left(\frac{\ell}{a}\right) - \gamma$, where the leading correction to the area law (perimeter in this case) is a finite term γ. The finite term is expected to be scale-invariant which, in general may be a universal function of the aspect ratios of the entangling region.[Fradkin and Moore, 2006, Casini and Huerta, 2007]

This finite term has been computed explicitly in several cases but its general properties are not understood. In the case of the quantum Lifshitz model (QLM) it was computed by several authors.[Hsu et al., 2009,

Hsu and Fradkin, 2010, Stéphan et al., 2009, Stéphan et al., 2011, Stéphan et al., 2012] The QLM is a scalar field theory in $d = 2$ spatial dimensions with dynamical exponent $z = 2$ (and hence not Lorentz invariant) which is the effective field theory of generalized quantum dimer models at their quantum critical points.[Ardonne et al., 2004, Fradkin et al., 2004] Among all these works, of particular interest to us is a result of Ref.[Stéphan et al., 2013a] who gave a full expression of the finite universal subleading term of the EE of the QLM for cylindrical entangling sections of a torus in the form of a scaling function of the aspect ratios of the cylinder.

There has been great progress in understanding of scaling of the von Neumann EEs for entangling regions with the shape of a disk in $2+1$-dimensional relativistic conformal field theories.[Casini and Huerta, 2007, Casini and Huerta, 2010] The result has the same form as the EEs found in the QLM. In this context, in the literature the constant term is called F (see, *e.g.* Ref.[Klebanov et al., 2011]). Casini *et al.*[Casini et al., 2011] have provided a proof in arbitrary dimensions of the holographic entanglement entropy ansatz of Ryu and Takayanagi[Ryu and Takayanagi, 2006b] for the case of spherical entangling regions. In $2+1$ dimensions this result shows that the finite part of the entanglement entropy of a disk with a smooth boundary is universal at a CFT. Additionally it was shown in [Casini and Huerta, 2012] that, when appropriately defined, this finite part of the EE decreases under relevant perturbations of the CFT (and hence obeys a "c-theorem".) Earlier results have given explicit values of F for a disk for a free massless scalar field in $2+1$ dimensions.[Casini and Huerta, 2010, Dowker, 2010] In the case of the CFT of an interacting scalar field at its non-trivial Wilson-Fisher (IR) fixed point, it is known for the case of a spatial split cylinder but only within the $1/N$ and $4-d = \epsilon$-expansions,[Metlitski et al., 2009] and the extrapolation to $2+1$ dimensions is presently not understood. On the other hand, logarithmic contributions to the EE are found when the entangling region has cusp-like conical singularities,[Casini and Huerta, 2007] are also found in the $z = 2$ quantum Lifshitz model,[Fradkin and Moore, 2006, Zaletel et al., 2011, Kallin et al., 2014, Stoudenmire et al., 2014] and at the quantum critical point of the ($z = 1$) two-dimensional transverse field Ising model,[Inglis and Melko, 2013] as well as in broken symmetry states with Goldstone bosons. [Metlitski and Grover, 2011, Ju et al., 2012]

Quantum Monte Carlo simulations have been used recently to compute the Rényi entropy S_2 for several model wave functions of interest in condensed matter physics. [Hastings et al., 2010] Stéphan and coworkers investigated the scaling of S_2 in cylindrical sections of a torus for the case of resonating-valence-bond (RVB) wave functions and for the wave functions of quantum dimer models on the square lattice. [Stéphan et al., 2013a] They also derived an explicit expression for the subleading term in the context of the QLM (which is believed to describe the continuum limit of these critical states), which is a universal

scaling function of the aspect ratios of the cylinder. As expected, in the case of the quantum dimer model on the square lattice, the finite subleading term (for cylinders with aspect ratio 1) extracted from their Monte Carlo results is clearly well fit by the universal scaling function deduced from the QLM. In a separate study,[Inglis and Melko, 2013] this group also investigated the scaling of the Rényi entropy S_2 at the quantum critical point of the two-dimensional Ising model in a transverse field. This system, which is in the same universality class as the classical three-dimensional Ising model, is Lorentz-Invariant at the quantum critical point, where it is described by an interacting one-component relativistic real scalar field theory at its Wilson-Fisher (IR) fixed point. Remarkably, these authors find that the numerically obtained Rényi entropy S_2 is also well fitted (within a precision of a fraction of 1%) by the same scaling function derived from the QLM. This is quite unexpected since the QLM has dynamical exponent $z = 2$ and a global $U(1)$ symmetry whereas the quantum Ising model has a $\mathbb{Z}_2$ global symmetry and dynamical scaling exponent $z = 1$ at the criticality. This apparent agreement is quite puzzling since these different universality classes are described by fixed points with very different scaling behaviors.

In this chapter we re-examine the problem of the scaling of entanglement in two spatial dimensions using two different approaches. Firstly we consider a class of theories with relativistic critical points (CFTs) that have the property that they are dual to a gravitational like theory in one higher dimensions, via the holographic duality. In this case the Ryu-Takayanagi ansatz can be used to derive an explicit expression for the von Neumann EE for cylindrical sections of the torus by mapping the problem to a minimal surface computation in the anti-de Sitter (AdS) geometry (more precisely, we consider the AdS soliton geometry in order to have the torus topology on the boundary). Our result has a leading area law term and a finite sub-leading term which is a function of the aspect ratio of the cylindrical region that is being observed. We argue that in the "thin slice" limit, the pre-factor of the finite term is analogous to a central charge and is intrinsic to the $2 + 1$-dimensional CFT, giving a rough measure of the number of degrees of freedom in the theory. We will then use this "central charge" to rescale the finite sub-leading term, thus allowing comparison of the functional dependence of the sub-leading term across different theories.

Next we examined two simple free fermion field theories in $2 + 1$ dimensions where the different proposals for the scaling of entanglement can be tested directly. The first model is a theory of free Dirac fermions. In this case we used a lattice regularization in the form of spinless fermions on a square lattice with flux π per plaquette, which is a discretization of the Dirac fermion known as the Kogut-Susskind fermion.[Kogut and Susskind, 1975] In two spatial dimensions, the low-energy limit of this model is equivalent to the two species (or "valleys") of massless Dirac fermions with opposite parity,[Fisher and Fradkin, 1985] analogous to the case of graphene.[Semenoff, 1984] All local perturbations of this system are irrelevant op-

erators and this is an infrared stable fixed point of the renormalization group. However, on a cylinder of finite radius this system behaves asymptotically as a system of free Dirac fermions in $1+1$ dimensions which is a CFT. The second free fermion model we considered is a system of fermions with two bands with a symmetry-protected quadratic band touching (QBT).[Sun et al., 2009] In the low-energy limit, this system is equivalent to a theory of massless Dirac spinors with a quadratic dispersion and hence has the dynamical exponent $z = 2$. In contrast to the massless Dirac fermion, this massless "Lifshitz-Dirac" fermion is an infrared unstable fixed point of the renormalization group and, in fact, all four-fermion operators are marginally relevant perturbations. Contrary to the case of free Dirac fermions, the QBT model on a cylinder of finite radius is not a $1+1$-dimensional CFT and has instead ultra-local correlations. Therefore the two fixed point theories have quite different dynamical properties. Since they are free-field theories, the EE can be computed explicitly with great accuracy[Peschel, 2003] where the different proposals can be tested.

The QBT model is also interesting in that it has a finite density of states (DOS) at low energies (while in the relativistic Dirac fermion case the DOS scales linearly with the energy). In this sense, the QBT model is reminiscent of the problem of fermions at finite density which has a finite DOS at the Fermi surface. In this case, it is known [Wolf, 2006, Gioev and Klich, 2006, Swingle, 2010, Ding et al., 2012] that the von Neumann EE has a logarithmic violation of the area law of the form $S_E = \alpha(\frac{l_A}{\epsilon})^{d-1} \log \frac{l_A}{\epsilon}$, where the prefactor α has been argued to be essentially universal provided the scale ϵ is determined by the size of the Fermi surface (see, however, the numerical results of Ref.[[McMinis and Tubman, 2013]]). This result may suggest that the finite DOS of a Fermi liquid at the Fermi surface may be the origin of the logarithmic violation of the area law, and that systems with a finite DOS at asymptotically low energies may also obey a similar scaling law. We will see, however, here that this is not the case.

Keeping the differences in mind, we studied the two-cylinder EEs of both fermionic models by computing the EEs of the cylinder explicitly (albeit numerically). In spite of the differences in physics, we find that the EEs of the models satisfy the area law and, in particular in the case of the QBT, we do not find any logarithmic violation of entanglement scaling from the area law. We further study the scaling behavior of the subleading term in the EEs. In the case of massless Dirac fermions we find that although the expression derived from the QLM fits well with surprising accuracy, the holographic entropy result for the cylinder appears to be essentially exact. In the case of the QBT the finite subleading term in the EE is accurately fitted by the expression derived from the QLM.

The rest of this chapter is organized as following. In the section II, we introduce and explain the three possible scaling functions which will be tested in two free fermion models, namely a free Dirac fermion model and a QBT model. In the section III, we will explain, based on the asymptotic behaviors of equal-time two-

point correlators, why the EE of the QBT cannot have any logarithmic violation of the area law. In the section IV, we numerically calculate the EE of the two fermion models and test the three scaling functions proposed in the section II. In the section V, we summarize our results and conclude that there is a universal scaling function of the subleading term of the EEs for the critical systems.

4.2 Entanglement Entropy Scaling Functions

In this chapter we will discuss three possible EE scaling functions for scale-invariant systems in $d = 2$ space dimensions. We will restrict ourselves to the EE of two cylinders A and B obtained from a partition of a torus. The scaling functions enter as scale-invariant finite corrections of the leading, area law, term of the von Neumann and Rényi entropies. They are: a) a quasi-1D scaling function, b) the quantum Lifshitz model scaling function, and c) a holographic scaling function (which we derive here using the AdS/CFT correspondence).

Different geometries of bipartition may give rise to different subleading terms with different structure. For instance, both numerical and analytical calculations on $2 + 1$-dimensional critical models show that there is a subleading term correction if the boundary of the subregion A is not smooth.[Stéphan et al., 2011, Kallin et al., 2014] The corner will give rise to the logarithmic term in the EE with the coefficient proportional to the low-energy degrees of freedom. [Inglis and Melko, 2013, Kallin et al., 2014, Stoudenmire et al., 2014] Even for the smooth boundary, the curvature on the subregion A may also lead to the logarithmic correction. [Fradkin and Moore, 2006] In this chapter, to avoid both the corner and the curvature corrections, we consider the torus geometry and bipartition the torus into two cylinders with a smooth boundary and calculate the two-cylinder entropy as shown in Fig. 4.1.

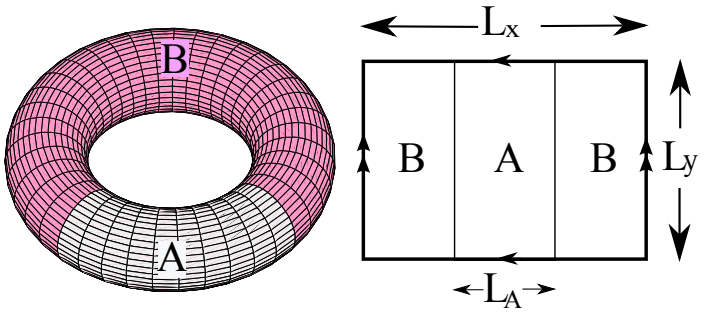

Figure 4.1: The torus is divided into two cylinders A and B with size $L_A \times L_y$ and $(L_x - L_A) \times L_y$.

4.2.1 Quasi-1D Entanglement Scaling Function

This scaling function was introduced heuristically by Ju and coworkers.[Ju et al., 2012] It assumes that in the thin torus limit, $L_y \ll L_x$ (see Fig.4.1), the effectively quasi-one-dimensional system should approximate a $1+1$-dimensional CFT. The posited form of the von Neumann EE is[Ju et al., 2012] (up to a non-universal additive constant)

$$S_{vN} = \alpha L_y + \beta \log \sin(\pi u) \tag{4.1}$$

where $u = L_A/L_x$. Here α is a non-universal coefficient and β is universal.

4.2.2 Quantum Lifshitz Entanglement Scaling Function

This scaling function was derived from the QLM by Stephan and coworkers,[Stéphan et al., 2013a] who tested it in the quantum dimer model (on the square lattice) and in the two-dimensional Ising model in a transverse field.[Inglis and Melko, 2013] For a torus with aspect ratio L_y/L_x, the von Neumann EE is

$$S_{vN} = \alpha L_y + \beta J(u) \tag{4.2}$$

where $J(u)$ is given by[Stéphan et al., 2013a]

$$J(u) = \log\left(\frac{\lambda}{2}\frac{\eta(\tau)^2}{\theta_3(\lambda\tau)\theta_3(\tau/\lambda)}\frac{\theta_3(\lambda u\tau)\theta_3(\lambda(1-u)\tau)}{\eta(2u\tau)\eta(2(1-u)\tau)}\right) \tag{4.3}$$

where $\theta_3(z)$ is the Jacobi theta-function, $\eta(z)$ is the Dedekind eta-function, $\tau = iL_x/L_y$ is the modulus of the torus, and λ is a parameter. For the case of the quantum dimer model at its Rokhsar-Kivelson quantum critical point the parameter is $\lambda = 2$. In this chapter we will test this scaling function in two free fermion models in $2+1$-dimensions and use λ as a fitting parameter. As we will see this scaling function works surprisingly well even in relativistic systems.

4.2.3 Holographic Relativistic Entanglement Entropy

To get a handle on the surprising universality of the scaling function $J(u)$ we now turn to another set of quantum systems whose EE can be efficiently calculated, *i.e.*, strongly-interacting relativistic (with dynamical exponent $z = 1$) quantum field theories which are described by a weakly-coupled dual gravity theory. There is a large class of such examples and we will concentrate on a subset which can be effectively described by (rather, truncated to) AdS gravity in $3+1$ dimensions. Since $J(u)$ is defined on a torus geometry, we must pick the appropriate solution to Einstein's equations with torus boundary topology (in the spatial

directions). This is the AdS soliton metric.[E.Witten, 1998, Horowitz and Myers, 1998] There are actually two possible metrics that we can use, depending on which torus direction (x or y) we allow to contract in the bulk - picking the smallest direction describes the ground state of the system.

The EE is sensitive to which cycle of the torus contracts because the cut is always along the y-direction. We will study both cases in detail. In the case where $L_y < L_x$ and the y-cycle contracts one finds that the EE saturates for large enough L_A (but still smaller compared to L_x) - this can be understood by taking the thin torus limit $L_y \ll L_x$ where it is clear that the saturation indicates the effective low energy $1+1$-dimensional theory is gapped. The reason for this can be traced to the anti-periodic boundary conditions for fermions around the torus cycles, which is forced upon us just by the fact that we allow such gravitational solutions with contracting spatial cycles [E.Witten, 1998]. Periodic boundary conditions could also be studied, however this presumably would involve more stringy ingredients (for example the application of T-duality to the contracting cycle) and the calculation of EE in such situations is not developed.

We will eventually compare the strongly interacting holographic model to the free Dirac model with periodic boundary conditions at $L_x = L_y$ and so not surprisingly the geometry where the y-cycle contracts does not do a good job due to this saturation. However it turns out that the phase where the x-cycle contracts, which is not continuously connected to the phase showing the aforementioned gap, has an incredibly similar form to the Dirac answer. We consider this case taking $L_y \geq L_x^+$ and return to the other case later.

AdS soliton geometry with $L_y \geq L_x$

According to the Ryu-Takayanagi conjecture,[Ryu and Takayanagi, 2006b] the EE takes the very simple form:

$$S = \frac{\mathcal{A}}{4G_N} \tag{4.4}$$

where $\mathcal{A}$ is the Area of the minimal surface ending on the boundary where the QFT lives at $\partial\mathcal{A}$ and falling into the bulk AdS-soliton geometry. There is by now have ample evidence for this formula and so we will take it as a given.[Lewkowycz and Maldacena, 2013]

The AdS soliton metric is given by:

$$ds^2 = \frac{1}{z^2}\left(\frac{dz^2}{f} + f dx^2 + dy^2 - dt^2\right) \tag{4.5}$$

where $f = 1 - (z/z_h)^3$. This geometry looks like a cigar in the (x, z) directions, where the tip is at $z = z_h$ and x is the angular direction. To avoid the conical singularity at the tip, we need to impose the constraint: $x \sim x + \frac{4\pi}{3} z_h$. Since x has the periodicity $x \sim x + L_x$, we require $z_h = \frac{3}{4\pi} L_x$.

The minimal surface for the subregion $\mathcal{A}$ can be calculated by assuming an ansatz which is translationally invariant in the y direction and has profile: $x(z)$.

$$\begin{aligned}\mathcal{A} &= \int \sqrt{G}dzdy = \int dzdy \left[\frac{1}{f} + f(x')^2\right]^{1/2} \frac{1}{z^2} \\ &= 2L_y \int_\epsilon^{z_\star} dz \left[\frac{1}{f} + f(x')^2\right]^{1/2} \frac{1}{z^2} \\ &= 2L_y \int_\epsilon^{z_\star} L(x, x', z) \end{aligned} \tag{4.6}$$

where $x' = dx/dz$ and G is the induced metric on the co-dimension 2 surface $(t = 0, x = x(z))$.

The minimal area profile can be found using standard Lagrangian mechanics: $\delta L/\delta x = 0$ from which the equation of motion is $E = \frac{\partial L}{\partial x'} = x' f \left[1/f + f(x')^2\right]^{-1/2} /z^2$. This leads to

$$(x')^2 = \frac{1}{f^2} \frac{E^2}{f/z^4 - E^2} \tag{4.7}$$

We have defined the point $z = z_\star$ such that $x' = \infty$ which will be the largest z obtained by the surface. $z_\star$ satisfies $f_\star/z_\star^4 = E^2$, where $f_\star = 1 - (z_\star/z_h)^3$.

Integrating the above differential equation we can solve for $z_\star$ in terms of L_A:

$$\begin{aligned}\frac{L_A}{2} &= \int_{-L_A/2}^0 dx = \int_0^{z_\star} \frac{E}{f} \left(\frac{1}{f/z^4 - E^2}\right)^{1/2} dz \\ &= z_\star \int_0^1 d\zeta \frac{1}{f} \left[\frac{1}{(\frac{f}{f_\star})(\frac{1}{\zeta})^4 - 1}\right]^{1/2} \\ &= \frac{L_x}{2} u(\chi) \end{aligned} \tag{4.8}$$

where $\zeta = z/z_\star$ and χ is related to the turning radius $z_\star$ of the minimal surface $\chi = (z_\star/z_h)^3$. The final form of u is:

$$u(\chi) = \frac{3\chi^{1/3}(1-\chi)^{1/2}}{2\pi} \int_0^1 \frac{d\zeta \zeta^2}{\sqrt{(1-\chi\zeta^3)}} \frac{1}{\sqrt{P(\chi,\zeta)}} \tag{4.9}$$

where $P(\chi, \zeta) = 1 - \chi\zeta^3 - (1-\chi)\zeta^4$.

By solving the above equation, we can obtain $u = L_A/L_x$ for different values of χ.

The area of the minimal surface equals to

$$\begin{aligned}\mathcal{A} &= 2L_y \int_\epsilon^{z_\star} dz \frac{1}{z^4}\left(\frac{1}{f/z^4 - E^2}\right)^{1/2} \\ &= \frac{2L_y}{z_\star}\int_{\epsilon/z_\star}^1 d\zeta \frac{1}{(f_\star)^{1/2}\zeta^4}\left[\frac{1}{(\frac{f}{f_\star})\frac{1}{\zeta^4} - 1}\right]^{1/2} \\ &= \frac{2L_y}{\epsilon} + \frac{8\pi L_y}{3L_x} j(\chi) \end{aligned} \tag{4.10}$$

where we have separated out the linearly divergent term, regulated by a cutoff close to boundary at $z = \epsilon$. The first term in $\mathcal{A}$ is the divergent area law and the second term is the finite subleading correction which can be calculated numerically using a parametric description for L_A and j in terms of $0 < \chi < 1$. The final form of j is:

$$j(\chi) = \chi^{-1/3}\left(\int_0^1 \frac{d\zeta}{\zeta^2}\left(\frac{1}{\sqrt{P(\chi,\zeta)}} - 1\right) - 1\right) \tag{4.11}$$

When u is small, $z_\star << z_h$ and in this case, the metric is the same as the metric for the usual AdS space and the subleading term $j(\chi)$ takes a simple scaling form $1/u$,

$$j(u) = -4\pi\left(\frac{\Gamma(\frac{3}{4})}{\Gamma(\frac{1}{4})}\right)^2 \frac{1}{u} \approx -1.4355\frac{1}{u} \tag{4.12}$$

This limit was first calculated in Ref. [Ryu and Takayanagi, 2006b].

In order to compare with the Dirac model we should normalize the coefficients in front of $1/u$ to be the same in the two cases. This requires some explanation - we are working in the classical gravity limit where $G_N \to 0$, so for the results we quoted to hold the coefficient in front of $1/u$ will be very large. This is certainly not the case for the Dirac model. In order to effectively compare these results we should then take a large number of copies of the Dirac model, with no interactions amongst each copy. The EE for the Dirac model then scales accordingly and in this way we can have a large $1/u$ coefficient to compare to the holographic model.

For comparison to the QBT model, a better holographic dual model will have a different metric (related to the $z = 2$ Lifshitz space-times introduced in [Kachru et al., 2008]). It is not hard to see that when u is small, it should have the same scaling behavior as the Dirac model. We leave comparison of the subheading terms in the $z = 2$ case to future work.

AdS soliton geometry with $L_y \leq L_x$

Similar expressions may be derived for the case where $L_y < L_x$. In this case the situation is complicated by the existence of a disconnected minimal surface that fills in the contractible L_y cycle of the AdS-soliton. This causes a saturation in the EE which we interpret as a gap for the lower dimensional system after a low energy reduction along the y direction. This saturation is related to the phase transition in holographic EE studied in Ref. [Nishioka and Takayanagi, 2007]. The appropriate scaling form is:

$$\mathcal{A} - \frac{2L_y}{\epsilon} = \frac{8\pi}{3}\widetilde{j}\left(\frac{L_x}{L_y}u\right), \quad 0 < u < \frac{L_y}{L_x}p \tag{4.13}$$

$$= -\frac{8\pi}{3}, \qquad \frac{L_y}{L_x}p < u < 1 - p\frac{L_y}{L_x} \tag{4.14}$$

$$= \frac{8\pi}{3}\widetilde{j}\left(\frac{L_x}{L_y}(1-u)\right), \quad 1 - p\frac{L_y}{L_x} < u < 1 \tag{4.15}$$

where $p \approx 0.19$ is a fixed number determined by where the saturation of EE occurs (the middle equation above). The function $\widetilde{j}$ is defined parametrically:

$$\widetilde{j}(\chi) = \chi^{-1/3}\left(\int_0^1 \frac{d\zeta}{\zeta^2}\left(\frac{\sqrt{1-\chi\zeta^3}}{\sqrt{P(\chi,\zeta)}} - 1\right) - 1\right) \tag{4.16}$$

$$\frac{L_x}{L_y}u = \frac{3}{2\pi}\chi^{1/3}(1-\chi)^{1/2}\int_0^1 \frac{d\zeta\zeta^2}{\sqrt{1-\chi\zeta^3}}\frac{1}{\sqrt{P(\chi,\zeta)}} \tag{4.17}$$

For completeness we plot the full set of scaling forms of $j(\chi)$ and $\widetilde{j}(\chi)$ for different values of L_x/L_y in Fig. 4.2.

We also plot the complete scaling forms of $J(u)$ with different aspect ratio L_x/L_y in Fig. 4.3. The $J(u)$ is defined in Eq. (4.12). [Stéphan et al., 2013b] As shown in Fig. 4.3, the $J(u)$ function has similar scaling behavior as the $j(u)$ and $\widetilde{j}(u)$ function. In the thin torus limit, $J(u)$ also shows the saturation behavior around $u = 0.5$.

4.3 Area law for QBT model

The fermionic QBT model in $2+1$-dimensions is a free fermionic spinor model with a quadratic energy dispersion. The Hamiltonian of the model has a similar structure as the Dirac fermion,

$$H = \int \frac{d^2k}{(2\pi)^2}\Psi^\dagger(\mathbf{k})\begin{pmatrix} k_x^2 - k_y^2 & -2ik_xk_y \\ 2ik_xk_y & -k_x^2 + k_y^2 \end{pmatrix}\mathbf{\Psi}(\mathbf{k}), \tag{4.18}$$

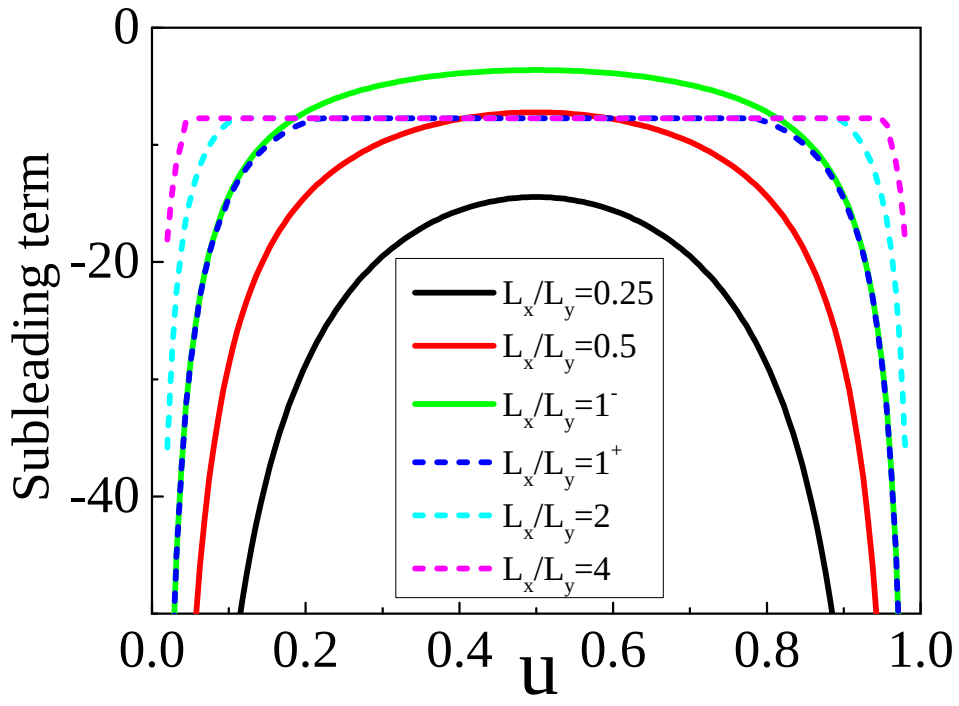

Figure 4.2: The subleading term for the minimal surface for various values of L_x/L_y. The solid curves are for $j(u)$ when $L_x \leq L_y$ and the dashed curves are for $\widetilde{j}(u)$ when $L_x > L_y$. See text for details.

with $\Psi(\mathbf{k}) = \begin{pmatrix} \psi_1(\mathbf{k}) & \psi_2(\mathbf{k}) \end{pmatrix}^{\mathbf{T}}$. The energy spectrum for this model is $E(\mathbf{k}) = \pm(\mathbf{k_x^2} + \mathbf{k_y^2})$. Different from a Dirac model, any local four-fermion term is marginally relevant,[Sun et al., 2009] which means that even an infinitesimally weak interaction leads to an instability of the free QBT point to the spontaneous breaking of either time-reversal invariance or the point group symmetry of the lattice. The QBT model, in this sense is a critical point [Sun et al., 2009]. In contrast, the Dirac model in $2+1$ dimensions is a stable fixed point since all local interactions are irrelevant at low energies. For the QBT model, at the band touching point $\mathbf{k} = (\mathbf{0}, \mathbf{0})$, there is a finite DOS. Since the origin of the violation of area law for the EE in a Fermi liquid is Fermi surface (which has a finite DOS), one might speculate that the QBT model may be a "Fermi liquid" of sorts with the Fermi surface replaced by a Fermi point and that it would also break the area law. To see if there is any violation of the area law in the EE of the QBT model, we first study the two-point equal-time correlation function for the fermionic QBT model. For the free fermion system, the entanglement entropy can be obtained by calculating the two-point correlation function, and hence the correlation function in the long distance limit can give information about the EE at the thermodynamic limit.

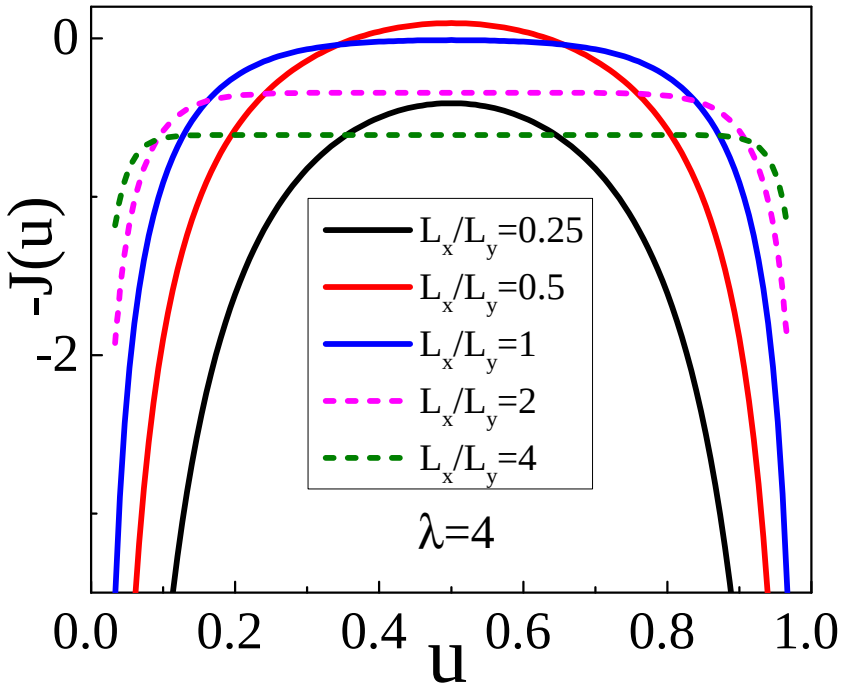

Figure 4.3: $-J(u)$ for various values of L_x/L_y. The solid curves are for $L_x \leq L_y$ and the dashed curves are for $L_x > L_y$.

The Lagrangian density for the QBT model is

$$\mathcal{L} = \bar{\Psi}\left[i\gamma_0\partial_0 - i(\partial_1^2 - \partial_2^2)\gamma_1 + 2i\partial_1\partial_2\gamma_2\right]\Psi. \tag{4.19}$$

where $\gamma_0 = \sigma_1$, $\gamma_1 = \gamma_0\sigma_3$ and $\gamma_2 = \gamma_0\sigma_2$ and $\bar{\Psi} = \Psi^\dagger\gamma_0$.

To calculate the correlation function of the QBT model, we first calculate the equal-time correlation function for the 2+1-dimensional QLM.[Ardonne et al., 2004] The equal-time two-point correlation function of the QLM has the asymptotic behavior in $|\mathbf{r}| = \sqrt{x^2+y^2} \to \infty$ with $|\mathbf{r}|$ as the spatial distance between the two points:

$$G_{\rm QLM}(\mathbf{r}) = \frac{\mathbf{1}}{\mathbf{4}\pi}\log(|\mathbf{r}|). \tag{4.20}$$

From this, we obtain the two point correlation function for the QBT model

$$\begin{aligned} G_{\rm QBT}(\mathbf{r}) &= ((\partial_1^2 - \partial_2^2)\gamma_1 - 2\partial_1\partial_2\gamma_2)G_{\rm QLM}(\mathbf{r}) \\ &= -\frac{2(x^2-y^2)\gamma_1 - 4xy\gamma_2}{4\pi r^4}. \end{aligned} \tag{4.21}$$

On the other hand, we can also calculate the correlation function for the Dirac fermion from the bosonic model. We calculate the equal-time correlation function of the relativistic free massless scalar field. In the limit $r \to \infty$:

$$G_0(r) \propto \frac{1}{|r|}. \tag{4.22}$$

Hence the two point correlation function for the Dirac fermion at equal time is

$$\begin{aligned} G_{\mathrm{D}}(\mathbf{r}) &= (\gamma_i \partial_i) G_0(\mathbf{r}) \\ &\propto -\frac{x\gamma_1 + y\gamma_2}{r^3}. \end{aligned} \tag{4.23}$$

For the QBT and Dirac models, we can see that the two-point correlation functions have asymptotically identical behavior in the long distance limit $|\mathbf{r}| \to \infty$. This implies that both the models will have the same scaling behavior for the leading term of the EE when the sizes of the subsystem is large enough compared to the UV cutoff. Since the Dirac model obeys the area law,[Ryu and Takayanagi, 2006b] the QBT model should also obey the area law and cannot have more divergent terms in the EE than the area law allows, in spite of having a finite DOS at zero energy.

Since the QBT model satisfies the area law, it is less entangled than the Fermi liquid. On the other hand, since the QBT model is a scale-invariant system with an IR unstable fixed point we expect it to have long-range entanglement in the form of scale-invariant contributions to the EE, which can only enter in the form of an $O(1)$ finite subleading correction to the area law. However, the correlation function argument itself cannot tell much information about the structure of the subleading term. To study the subleading term in EE for the QBT model we will need an explicit expression. Unfortunately it is not possible to write the EE as a closed analytic expression and we will use instead numerical methods to study its scaling behavior.

4.4 Entanglement entropy for Dirac and QBT fermions

The lattice model of the QBT model in momentum space can be written as

$$H_{\mathrm{QBT}} = \int_{BZ} \frac{d^2k}{(2\pi)^2} \Psi^\dagger(\mathbf{k}) \mathcal{H}_{\mathrm{QBT}}(\mathbf{k}) \mathbf{\Psi}(\mathbf{k}), \tag{4.24}$$

where BZ stands for the first Brillouin zone, $-\pi < k_x \leq \pi$ and $-\pi < k_y \leq \pi$. Here $\Psi^\dagger(\mathbf{k})$ is a two component spinor fermionic creation operator $\Psi^\dagger(\mathbf{k}) = (\psi_{\mathbf{1}}^\dagger(\mathbf{k}), \psi_{\mathbf{2}}^\dagger(\mathbf{k}))$. The one-particle Hamiltonian $\mathcal{H}_{\mathrm{QBT}}(\mathbf{k})$ has the

form

$$\mathcal{H}_{\mathrm{QBT}}(\mathbf{k}) = \mathbf{h_1}(\mathbf{k})\sigma_{\mathbf{1}} + \mathbf{h_3}(\mathbf{k})\sigma_{\mathbf{3}}, \tag{4.25}$$

where σ_1 and σ_3 are the usual two Pauli matrices, and

$$\begin{aligned} h_1(\mathbf{k}) &= -4t\cos(\frac{k_x}{2})\cos(\frac{k_y}{2}), \\ h_3(\mathbf{k}) &= -t'(\cos(k_x) - \cos(k_y)). \end{aligned} \tag{4.26}$$

The QBT point is at $\mathbf{k} = (\pi, \pi)$. Near the point, we can expand $\mathcal{H}_{\mathrm{QBT}}$ and find the continuum Hamiltonian Eq.(4.18). In the numerical calculation, we will set $t = t' = 1$.

Similarly, the lattice model for the Dirac fermion is a tight-binding model of spinless fermions on the square lattice with π flux on each plaquette. The Hamiltonian in momentum space is

$$H_D = \int_{BZ} \frac{d^2k}{(2\pi)^2} \Psi^\dagger(\mathbf{k})\mathcal{H}_{\mathbf{D}}(\mathbf{k})\mathbf{\Psi}(\mathbf{k}), \tag{4.27}$$

where BZ stands for the first Brillouin zone, $-\pi < k_x \leq \pi$ and $-\pi < k_y \leq \pi$. The one-particle lattice Dirac Hamiltonian $\mathcal{H}_D(\mathbf{k})$ takes the form

$$\mathcal{H}_D(\mathbf{k}) = h_1\sigma_1 + h_3\sigma_3, \tag{4.28}$$

with $h_1 = -2\cos(k_x)$ and $h_3 = 2\cos(k_y)$. The Dirac points are at $(\pm\frac{\pi}{2}, \pm\frac{\pi}{2})$.

$\mathcal{H}_D(\mathbf{k})$ can be diagonalized by a unitary transformation $V^{-1}\mathcal{H}_D V = M$ where M is the diagonal matrix with eigenvalues $E(\mathbf{k})_\pm = \pm\sqrt{\cos(k_x)^2 + \cos(k_y)^2}$. The V matrix equals to

$$\begin{aligned} V = &\frac{1}{\sqrt{(2\cos(k_y)^2 + 2\cos(k_x)^2 - 2\cos(k_y)\sqrt{\cos(k_y)^2 + \cos(k_x).^2}}} \\ &\times \begin{pmatrix} \cos(k_x) & -\cos(k_y) + \sqrt{\cos(k_y)^2 + \cos(k_x)^2} \\ -\cos(k_y) + \sqrt{\cos(k_y)^2 + \cos(k_x)^2} & -\cos(k_x) \end{pmatrix} \end{aligned} \tag{4.29}$$

In the numerical calculation, we put these two models on the torus as shown in Fig. 4.1 and calculate the two-cylinder entropy when the lower band is fully filled. In this geometry, the momentum k_y parallel to the cut is always a good quantum number, thus the $2+1$-dimensional model can be considered as a set of $1+1$-dimensional chains with an effective mass depending on the value of k_y. Thus we calculate the total two dimensional EE as the sum over the EE of the $1+1$-dimensional chains labelled by the momentum k_y. Furthermore, we notice the Rényi entropies S_n with different Rényi indices $n = 1, 2\ldots$ show similar

behavior and we will only consider the von Neumann entropy S_{vN} later in this chapter. By analogy with the QLM[Stéphan et al., 2011] , one might worry that there may be a phase transition between $n = 1$ and $n = 2$, but we find there is none in that the Rényi entropies S_n with different Rényi indices $n = 1, 2 \ldots$ can be fitted with the area law term supplemented by a single universal scaling form for the subleading term.

We first check that both models satisfy the area law numerically. To verify that the EE satisfies the area law, we change the length of L_y but fix the aspect ratio L_x/L_y to be a constant value. The numerical calculation for both the models are shown in Fig. 4.4(a) and (b). For the QBT and Dirac models, the von Neumann entropy and Rényi Entropy with Rényi index $n = 2$ are all linearly proportional to L_y, $S_E = \alpha L_y + \gamma$. The coefficient in front of L_y is invariant when we change the ratio $u = L_A/L_x$. This indicates that both models satisfy the area law.

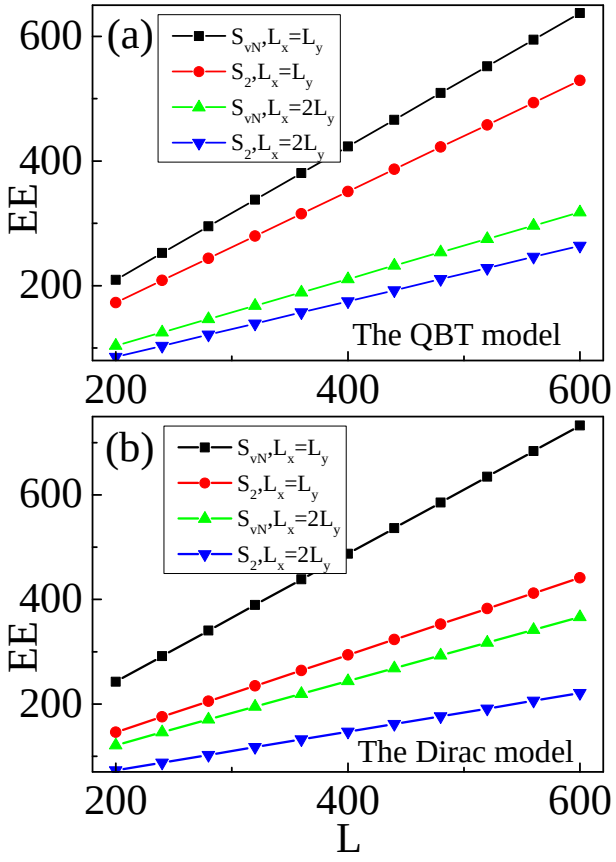

Figure 4.4: (a) The von Neumann entropy S_{vN} and Rényi entropy S_2 for the QBT model as a function of $L = L_x$. Both the EEs are linearly proportional to L when the aspect ratio L_x/L_y and the ratio $u = L_A/L_x$ are fixed. $u = 0.1$ and two different aspect ratios are considered. (b) The von Neumann entropy S_{vN} and Rényi entropy S_2 for the Dirac model. The setup of the bipartition geometry is the same as (a).

We will compute the finite subleading term and consider two different regimes for the aspect ratio

L_x/L_y of the torus: the thin torus limit $L_x << L_y$ and the two dimensional limit $L_x \approx L_y$. In the thin torus limit, the models are expected to behave effectively as the $1+1$-dimensional theory. For the Dirac model, the computation is sensitive to the boundary condition in the y direction (Fig. 4.1). For periodic boundary conditions, the zero mode $k_y = 0$ will contribute the logarithmic correction $\frac{1}{3}\log L_A$ to the total EE,[Calabrese and Cardy, 2004] while for anti-periodic boundary conditions there is no zero mode and no such logarithmic correction. In contrast, the QBT model is insensitive to the boundary condition. The zero mode $k_y = 0$ contributes nothing to the total EE (it contributes only finite $O((L_y)^0) = O(1)$ contribution to the total EE). This is because in $1+1$ dimensions the QBT model is not critical and is only short-ranged correlated. The two-point equal-time correlation function of the $1+1$ -dimensional QBT model is a delta-function. In particular, this also implies that here is no logarithmic subleading correction for the $2+1$-dimensional QBT model either. Thus, in the thin torus limit with periodic boundary condition, the Dirac model has a logarithmic subleading term correction while the QBT model does not. This result is verified by the numerical calculations shown in Fig. 4.5.

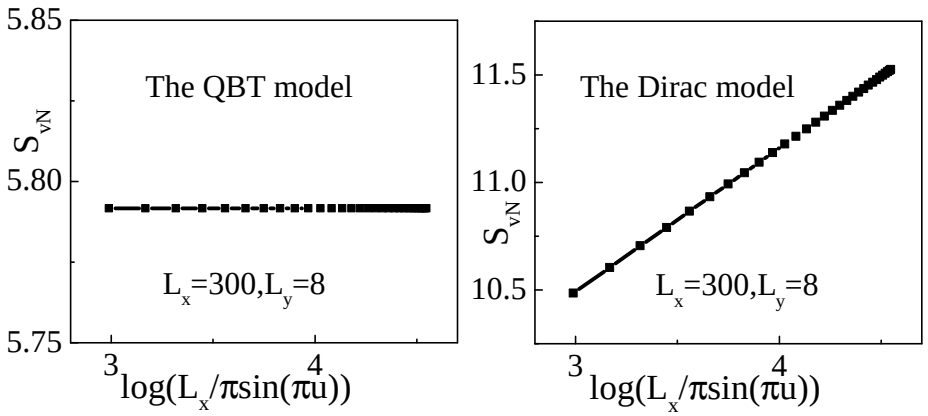

Figure 4.5: Left: The von Neumann entropy S_{vN} for the QBT model in the thin torus limit. Right: S_{vN} for the Dirac model in the thin torus limit with periodic boundary condition in y direction. The coefficient is 0.666 since there are two Dirac cone in the lattice model.

The above thin torus limit argument for the subleading term does not work in the two dimensional limit $L_x \approx L_y$ because of the complicated crossover behavior for the $1+1$-dimensional massive Dirac fermion with mass $k_y \approx L_A^{-1}$, which becomes analytically intractable. Instead, we directly calculate the subleading term numerically and fit the data with possible candidates for subleading terms. Since we are considering free fermion system, we will use Peschel's result to calculate the EEs.[Peschel, 2003]

The numerical results in the two dimensional limit show that the subleading term only depends on the aspect ratio of the torus L_x/L_y and on the ratio $u = L_A/L_x$.[Ju et al., 2012] For simplicity, we will fix

$L_x/L_y = 1$ (a square torus, and hence with modulus $\tau = i$) and only study the dependence of the subleading term on the aspect ratio u. We test three possible scaling functions for the subleading term defined in Sec.4.2,

$$S_{vN} = \alpha L_y + \beta J(u) \tag{4.30}$$

$$S_{vN} = \alpha L_y + \beta j(u) \tag{4.31}$$

$$S_{vN} = \alpha L_y + \beta \log(\sin(\pi u)) \tag{4.32}$$

where $J(u)$ in Eq.(4.30) is given by[Stéphan et al., 2013a]

$$J(u) = \log\Big(\frac{\theta_3(i\lambda u)\theta_3(i\lambda(1-u))}{\eta(2iu)\eta(2i(1-u))}\Big), \tag{4.33}$$

which is obtained from Eq. (4.2) by plugging $\tau = i$ and truncating $\log(\frac{\lambda\cdot\eta(i)^2}{2\theta_3(\lambda i)\theta_3(i/\lambda)})$, which is an O(1) constant. This scaling function was originally derived from the QLM. However, it was also found unexpectedly to fit well with the numerical results of the EE of the relativistic scalar field theories.[Stéphan et al., 2013b, Inglis and Melko, 2013] $j(u)$ in Eq. (4.31) is derived from the holographic calculation shown in Eq. (4.11), we will only check it for the Dirac fermion model. We also consider $\log(\sin(\pi u))$ as the possible subleading term because it is a natural extension of the thin torus limit.

As shown in Fig. 4.6 (c) and (d), when $L_y = L_x$ is fixed, for both the QBT and Dirac models, S_{vN} is linearly related to $J(u)$. For the Dirac model, S_{vN} is also linearly proportional to $j(u)$ as shown in Fig. 4.6 (b). It is clearly seen from Fig. 4.6 that the $J(u)$ and $j(u)$ fitting function works much better than the quasi-1D formula $\log(\sin(u))$. The $\log(\sin(\pi u))$ term which works well in the thin torus limit for the Dirac model is not linearly proportional to the numerical results in the two-dimensional limit (Fig. 4.6 (a)). For the $J(u)$ function, there is an additional tuning parameter λ. For the QBT model, λ decreases when the Rényi index n increases, while for the Dirac model, λ does not change when we increase the Rényi index, and it is found to be equal to $\lambda = 4.2$. Currently, we do not have a physical understanding for the meaning of λ for the fermionic models. In the case of the QLM, λ is the exponent of the two-point dimer correlation function[Fradkin, 2013] and thus is independent of the Rényi index $n > 1$.[Stéphan et al., 2013a]

The complete results are shown in Fig. 4.7 and Fig. 4.8, where the numerical calculations of S_{vN} for both the QBT and Dirac models fit with $J(u)$ for the whole range of the parameter $u \in [0, 1]$ within the numerical deviation 1% (deviation shown in the inset). Here we only study S_{vN} because the other Rényi entropies with different Rényi indices show the similar behaviors. The only difference between the QBT and Dirac

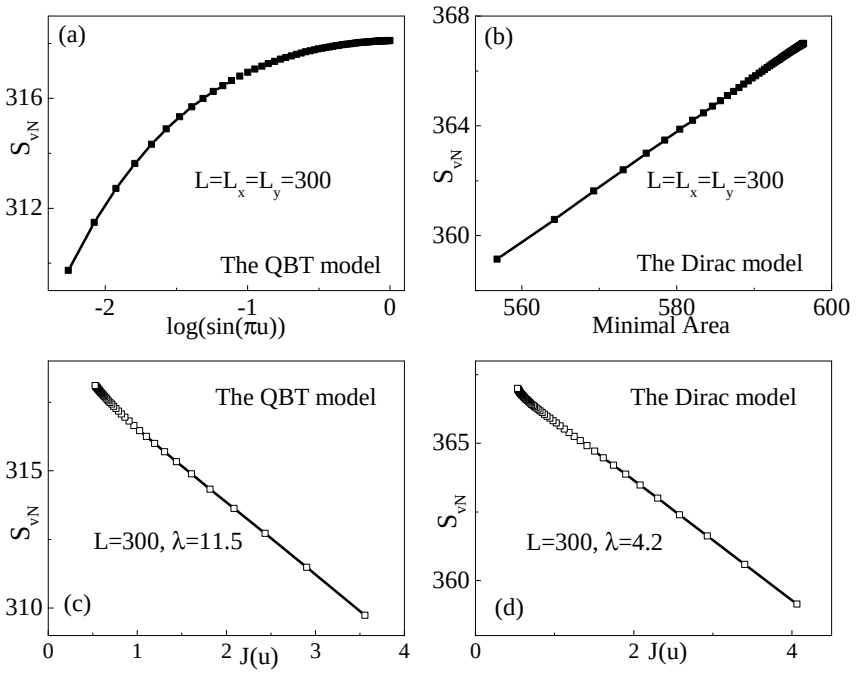

Figure 4.6: (a) S_{vN} for the QBT model in the function of $\log(\sin(\pi u))$. (b) S_{vN} for the Dirac model in the function of the minimal surface Eq. (4.10) for the AdS soliton geometry. (c) S_{vN} for the QBT model in the function of $J(u)$. (d) S_{vN} for the Dirac model in the function of $J(u)$.

models is that for the QBT model, the fitting parameter λ for S_{vN} is $\lambda = 11.5$ and for the Dirac model, $\lambda = 4.2$, so that the curve for the QBT model is more flat around $u = 0.5$ compared with the Dirac model (Fig. 4.7 and Fig. 4.8).

Furthermore, we notice that when u is small, $J(u)$ is linearly proportional to $1/u$. Similarly when $(L_x - L_A) \ll L_x$, $J(u)$ is linearly proportional to $1/(1-u)$. $J(u)$ is symmetric around $u = 0.5$. To illustrate this, we expand $J(u)$ for small $u << 1$, to obtain

$$J(u) \approx \frac{\pi}{24}\frac{L_y}{L_x}\frac{1}{u} + \log\left[\sqrt{\frac{2}{\lambda}}\frac{\theta_3(\lambda\tau)}{\eta(2\tau)}\right]. \tag{4.34}$$

The leading term in $J(u)$ is linearly proportional to $1/u$ and independent of λ. This result is consistent with the numerical results and the holographic entropy derived before. Indeed as we mentioned previously the coefficient of the $1/u$ term as $u \to 0$ is intrinsic to the critical theory, and it is a rough analog of the central charge in $1+1$-dimensional CFT. This statement can be further supported from the AdS/CFT calculation, where the coefficient only depends on the Newton constant G_N (see Eq. (4.4)). For the lattice Dirac model

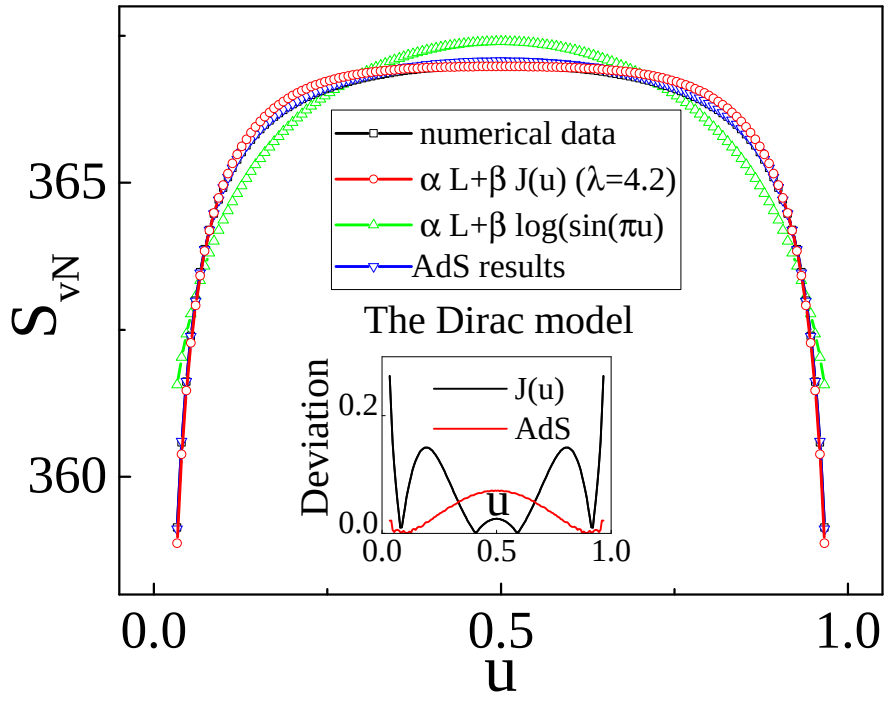

Figure 4.7: S_{vN} for the Dirac model as a function of u with $L = L_x = L_y = 300$. The red curve is the fitting function with the form $S_{vN} = \alpha L + \beta J(u)$. The numerical data is in black curve. The blue curve is the holographic entropy. (The black and blue curves are hard to see in the figure since they are almost overlapping with the blue curve) The inset is the absolute deviation for $S_{vN} = \alpha L + \beta J(u)$ (black curve) and the holographic entropy (red curve) with the numerical data. In both cases, the deviation is less than 1% for the whole region, but the holographic result appears to be the most accurate. The green curve is the fitting function with the form $S_{vN} = \alpha L + \beta \log(\sin(\pi u))$.

(which has two species of massless Dirac fermions), the numerical data shows that the coefficient of the $1/u$ is -0.3006, while for the QBT model, the coefficient is -0.3735. See Refs. [Ryu and Takayanagi, 2006a, Myers and Singh, 2012] for related studies of this quantity and how it flows under the RG. We use this coefficient to normalize the overall numerical coefficients β of the different scaling functions we compare.

4.4.1 EE for free boson CFT

Actually, we can also calculate the EE for free boson CFT on torus. In general, for the discrete free boson Hamiltonian defined on a lattice

$$H = \frac{1}{2}\left(\sum_{i=1}^{N} \Pi_i^2 + \sum_{i,j=1}^{N} \phi_i K_{ij} \phi_j\right) \tag{4.35}$$

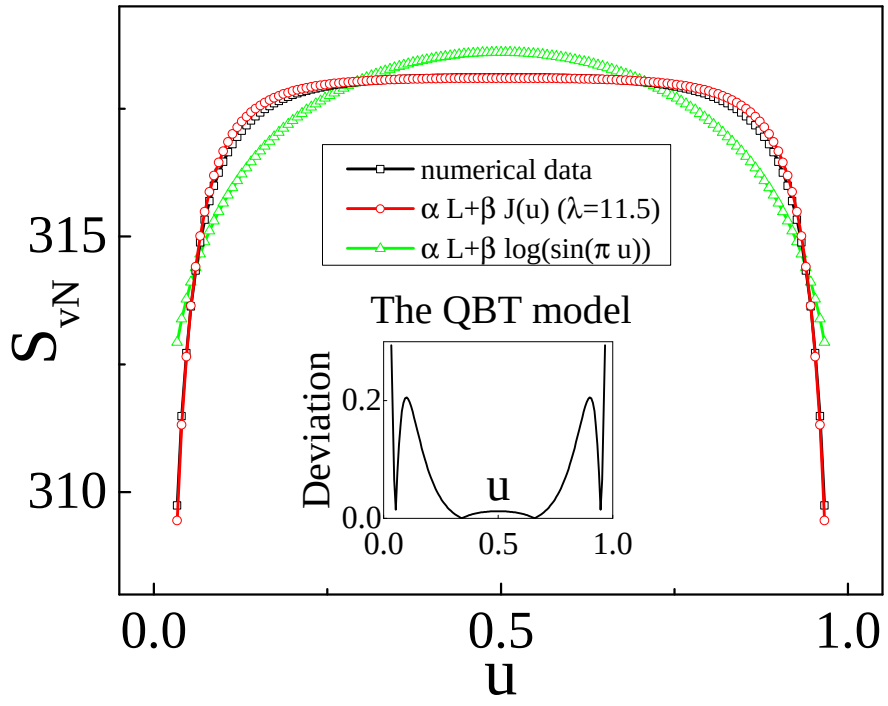

Figure 4.8: S_{vN} for the QBT model as a function of u. The bipartition geometry is the same as the Dirac model. The inset is the absolute deviation for the fitting function $S_{vN} = \alpha L + \beta J(u)$ with numerical data. The deviation is less than 1% for the whole region of u.

where they satisfy the canonical commutation relations

$$[\phi_i, \Pi_j] = i\delta_{ij}, \quad [\phi_i, \phi_j] = 0, \quad [\Pi_i, \Pi_j] = 0 \tag{4.36}$$

The ground state for this Hamiltonian is

$$|\Psi\rangle \sim e^{-\frac{1}{2}\sum_{ij}\phi_i K_{ij}^{\frac{1}{2}}\phi_j}|\phi\rangle \tag{4.37}$$

We will use this wave function to calculate the entanglement entropy

For free boson system, there is a very efficient numerical method to calculate the entanglement entropy. The details of this method can be found in the Ref. [Casini and Huerta, 2009]. Here is a short summary of this method.

The correlation functions for the ground state are

$$\langle \phi_i \phi_j \rangle = \frac{1}{2} K_{ij}^{-\frac{1}{2}} \equiv X_{ij}$$
$$\langle \pi_i \pi_j \rangle = \frac{1}{2} K_{ij}^{\frac{1}{2}} \equiv P_{ij} \tag{4.38}$$

The Von Neumann entanglement entropy for a subsystem A can be calculated by using these correlation functions,

$$S_A = (C + \frac{1}{2}) \log(C + \frac{1}{2}) - (C - \frac{1}{2}) \log(C - \frac{1}{2}) \tag{4.39}$$

where $C = \sqrt{X_A \cdot P_A}$. X_A and P_A are the correlation functions defined on subregion A. Similarly, Rényi entropy is

$$S_n = \frac{1}{n-1} \left[\log((C + 1/2)^n - (C - 1/2)^n) \right] \tag{4.40}$$

The Hamiltonian for the relativistic boson in $2 + 1$d is

$$H = \frac{1}{2} \int d^2x \left[\Pi^2 + (\nabla \phi)^2 + \frac{m^2}{2} \phi^2 \right] \tag{4.41}$$

The corresponding discrete lattice Hamiltonian (on the torus) is

$$H = \frac{1}{2} \sum_{i,j} \left[\Pi_{ij}^2 + (\phi_{i+1,j} - \phi_{i,j})^2 + (\phi_{i,j+1} - \phi_{i,j})^2 + m^2 \phi_{i,j}^2 \right] \tag{4.42}$$

In the momentum space, the Hamiltonian becomes

$$H = \frac{1}{2} \int_{-\pi}^{\pi} dk_1 \int_{-\pi}^{\pi} dk_2 \Pi(k) \Pi(-k) + \left[4 - 2\cos(k_1) - 2\cos(k_2) + m^2 \right] \phi(k) \phi(-k) \tag{4.43}$$

The two point correlation functions are

$$\langle \phi_{i,j} \phi_{i+n_1, j+n_2} \rangle = \frac{1}{8\pi^2} \int_{-\pi}^{\pi} dk_1 \int_{-\pi}^{\pi} dk_2 \frac{\cos(k_1 n_1) \cos(k_2 n_2)}{\sqrt{4 - 2\cos(k_1) - 2\cos(k_2) + m^2}}$$
$$\langle \pi_{i,j} \pi_{i+n_1, j+n_2} \rangle = \frac{1}{8\pi^2} \int_{-\pi}^{\pi} dk_1 \int_{-\pi}^{\pi} dk_2 \cos(k_1 n_1) \cos(k_2 n_2) \sqrt{4 - 2\cos(k_1) - 2\cos(k_2) + m^2} \tag{4.44}$$

Here we are interested in the subleading term in the massless limit $m \to 0$. However, in the numerical calculation, to avoid the singularity at $k_1 = k_2 = 0$, we add a small mass $m = 10^{-5}$ in the calculation for

the correlation functions. As we discussed in the previous section, in the thin slice limit $u \to 0$, the Von Neumann entanglement entropy for the critical system should take a simple form:

$$S_A = \alpha L_y - \beta \frac{1}{u} \tag{4.45}$$

We perform the numerical calculation on a torus with $L_x = L_y = 2000$ (the lattice spacing is equal to one) and we use the formula in Eq.(4.39) to calculate the entanglement entropy in the thin slice limit. We find the coefficient in front of $1/u$ is $\beta = 0.0406$. This result is consistent with Casini and Huerta's calculation in Ref.[Casini and Huerta, 2005]

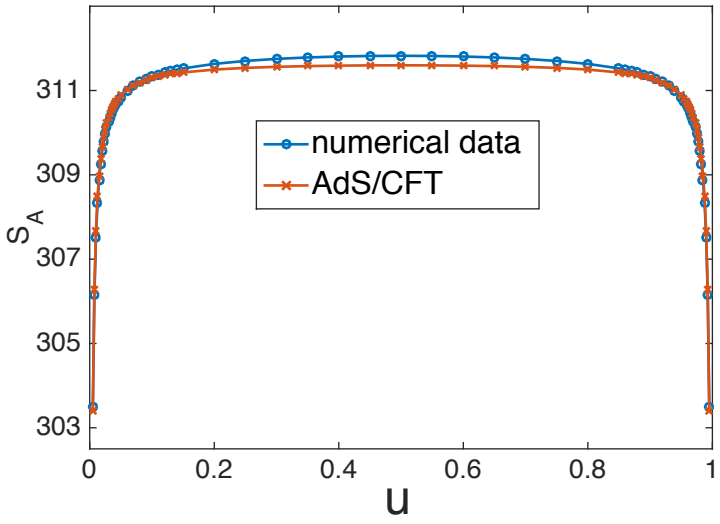

Figure 4.9: Von Neumann entanglement entropy S_{vN} as a function of the ratio u. The blue curve is the numerical result. The red curve is the holographic entanglement entropy $S_{vN} = \frac{1}{4G_N} j(u) + \alpha \frac{L_y}{\epsilon}$, where the prefactor $\frac{1}{4G_N} = 0.0283$ and the area law part $\alpha \frac{L_y}{\epsilon} = 311.7$. The square torus has $L_x = L_y = 2000$.

4.5 Conclusion and comments

The properties of a many-body state can be classified according to the scaling behavior of its EE. The critical system in $2+1$ dimensions is long-range entangled compared with the gapped system. Our results show that this difference can be detected in the subleading term in the two-cylinder EE, which includes both the von Neumann entropy and Rényi entropies. We calculate EEs of both the Dirac and quadratic band touching models numerically on the torus. We notice that the subleading term is linearly proportional to $1/u$ when the ratio u is small. We speculate that the coefficient in front of $1/u$ in the subleading term measures the number of the low-energy degrees of freedom of the system. Further calculations in

other models are necessary to pin down the physical meaning of this coefficient. For the whole region $0 < u < 1$, we use the subleading term for the QLM and find it fit well with both the QBT model and the Dirac model within a small numeric deviation $< 1\%$, even though these theories have different dynamical exponents, different DOS at low energies, and different behavior when the local four-fermion interactions are considered. We demonstrated that this similarity might come from the similar scaling behaviors between the two-point correlation functions at equal time for both the models. We also calculated the subleading term of the strongly-coupled models via the holographic AdS/CFT correspondence and find it consistent with the numerical results for the Dirac model.

Based on our calculation on the fermionic critical models, holographic calculations and previous works on the bosonic critical models in $2 + 1$ dimensions, there is strong evidence that the scaling form of the subleading term of EEs takes a robust form across a wide variety of $2+1$-dimensional critical systems on the torus geometry. It will be particularly interesting to test the holographic EE scaling we found here against other critical theories such as the quantum Ising model in $2 + 1$ dimensions.

Chapter 5

Bulk-boundary correspondence and EE in (3+1)-dimensional topological phases

5.1 Introduction

In this chatper, we will study the bulk-correspondence in $(3+1)$-dimensional topological phases and we will use this correspondence to study the entanglement entropy for topological phases. *The bulk-boundary correspondence* is one of the most salient features of topologically ordered phases of matter. In topologically ordered states in (2+1) dimensions [(2+1)d], all essential topological properties in their bulk can be derived and understood from their edge theories, such as quantized transport properties, properties of bulk quasi-particles (fractional charge and braiding statistics thereof), and the topological entanglement entropy, etc. [Halperin, 1982, Witten, 1989, Wen, 1992, Hatsugai, 1993, Cappelli et al., 2002, Cappelli and Zemba, 1997, Cappelli et al., 2010, Cappelli and Viola, 2011] Edge or surface theories also play an important role in symmetry-protected and symmetry-enriched topological phases. [Ryu and Zhang, 2012, Sule et al., 2013, Hsieh et al., 2014, Lu and Vishwanath, 2012, Cappelli and Randellini, 2013, Hsieh et al., 2015]

The purpose of this chapter is to study the bulk-boundary correspondence in the simplest (3+1)d topological field theory, the BF topological field theory [Horowitz, 1989, Horowitz and Srednicki, 1990, Blau and Thompson, 1991, Blau and Thompson, 1989, Birmingham et al., 1991, Oda and Yahikozawa, 1990, Bergeron et al., 1995], and its generalizations. The BF theory describes, among others, the long wave-length limit of BCS superconductors, and the deconfined phase of the $\mathbb{Z}_{\mathrm{K}}$ gauge theory. It is also relevant to the hydrodynamic description of (3+1)d symmetry-protected topological (SPT) phases including topological insulators and related systems. [Hansson et al., 2004, Banks and Seiberg, 2011, Cho and Moore, 2011, Vishwanath and Senthil, 2013, Chan et al., 2013, Tiwari et al., 2014, Ye and Gu, 2015, Gaiotto et al., 2015, Cirio et al., 2014]

To put our purpose in the proper context, let us give a brief overview of the bulk-boundary correspondence in (2+1)d topologically ordered phases. For (2+1)d topological phases, bulk topological phases can be characterized by the modular $\mathcal{S}$ and $\mathcal{T}$ matrices. The $\mathcal{S}$ and $\mathcal{T}$ transformations generate the basis transformation in the space of degenerate ground states, which appear when the system is put on a *spatial* two-dimensional

torus. Combined together, the $\mathcal{S}$ and $\mathcal{T}$ transformations form the group $SL(2,\mathbb{Z})$, the mapping class group of the two-dimensional torus T^2. Their geometric meanings are the 90° rotation and Dehn twist defined on the torus, respectively. In the basis in which the $\mathcal{T}$ matrix is diagonal (the so-called quasi-particle basis), the diagonal entries of the $\mathcal{T}$ matrix encode the information on the topological spin of quasi-particles. On the other hand, the $\mathcal{S}$ matrix contains the information of the braiding and fusion. For an Abelian topological phase, the elements of the $\mathcal{S}$ matrix are given by braiding phases between quasiparticles, up to an over all normalization factor $1/\mathcal{D}$, where $\mathcal{D}$ is the total quantum dimension.

On the other hand, at their boundary (edge), gapless boundary excitations supported by a (2+1)d topological phase can be described by a (1+1)d conformal field theory (CFT).[Francesco et al., 1997] There is one-to-one correspondence between quasi-particle excitations in the bulk and primary fields living on the edge. On the (1+1)d *spacetime* torus, one can form the character $\chi_j(\tau)$ from the tower of states built upon a primary field O_j:

$$\chi_j(\tau) = \mathrm{Tr}_{\mathcal{H}_j}\left[e^{2\pi i\tau_1 P_0 - 2\pi\tau_2 H_0}\right] \tag{5.1}$$

where H_0 and P_0 are the Hamiltonian and the momentum operators, respectively, the complex parameter $\tau = \tau_1 + i\tau_2$ is the modular parameter parameterizing the spacetime torus, and the trace is taken over all states in the Hilbert space $\mathcal{H}_j$ that is built upon the highest weight state associated with the primary field O_j. The characters χ_j transform into each other under the modular transformations of the spacetime torus. Under the modular $\mathcal{T}$ and $\mathcal{S}$ transformations, the characters $\chi_j(\tau)$ transform as

$$\begin{aligned}\chi_j(\tau+1) &= e^{2\pi i(h_j - \frac{c}{24})}\chi_j(\tau) = \mathcal{T}_{jj}\chi_j(\tau),\\ \chi_j(-1/\tau) &= \sum_{j'}\mathcal{S}_{jj'}\chi_{j'}(\tau),\end{aligned} \tag{5.2}$$

where the matrices $\mathcal{T}$ and $\mathcal{S}$ represent the action of the $\mathcal{T}$ and $\mathcal{S}$ modular transformations on the characters, respectively. The matrix $\mathcal{T}$ is a diagonal matrix and includes the conformal dimension h for each character and the central charge c for the CFT. The $\mathcal{T}$ and $\mathcal{S}$ matrices for the characters in the edge theory have the direct correspondence (and are essentially identical) to the the $\mathcal{T}$ and $\mathcal{S}$ matrices defined for the corresponding $(2+1)$d bulk topological theory.

Coming back to our main focus, i.e., $(3+1)$d topologically ordered phases, the bulk topological system can be defined on a spatial torus T^3 (while other choices are of course possible). The mapping class group of the three-dimensional torus is $SL(3,\mathbb{Z})$, and, as in the case of (2+1)d, is also generated by two transformations, which we also call the modular $\mathcal{S}$ and $\mathcal{T}$ transformations (see Sec. 5.2.1 for de-

tails). For $(3+1)$d topological phases defined on a spatial torus T^3, $\mathcal{S}$ and $\mathcal{T}$ matrices can be introduced to describe the basis transformation of degenerate ground states. As in (2+1)d, the $\mathcal{S}$ and $\mathcal{T}$ matrices encode the topological data of the bulk topological phase, such as the braiding and spin statistics of excitations. [Moradi and Wen, 2015, Jiang et al., 2014] In (3+1)d, the exchange statistics of particles has to be either fermionic or bosonic. On the other hand, a particle and a loop-like excitation, or two loop-like excitations in the presence of an additional background loop, can have non-trivial braiding and can obey non-trivial statistics. For the Abelian topological phase described by the BF theory, the $\mathcal{S}$ matrix describes the braiding phase between particle and loop excitations, while the $\mathcal{T}$ matrix has the physical meaning of a $(3+1)$d analogue of topological spins. [Moradi and Wen, 2015] It has been also proposed that there exist (3+1)d topological phases that are characterized by their three-loop braiding statistics. [Wang and Levin, 2014, Jiang et al., 2014, Wang and Wen, 2015, Jian and Qi, 2014, Wang and Levin, 2015, Lin and Levin, 2015, Wan et al., 2015]

We will demonstrate that these results, obtained and discussed previously from the bulk point of view, can be obtained solely from gapless boundary field theories. More specifically, taking various examples of (3+1)d topologically ordered phases and their surface states, which we put on the $(2+1)$d spacetime torus T^3, we compute the modular $\mathcal{S}$ and $\mathcal{T}$ matrices explicitly, and show that they agree with the $\mathcal{S}$ and $\mathcal{T}$ matrices obtained from the bulk considerations. We thereby establish the bulk-boundary correspondence in these (3+1)d topologically ordered phases. Along the course, we also propose a bulk continuum field theory which realizes non-trivial three-loop braiding statistics.

N.B. Our strategy adopted in this chapter is to utilize boundary field theories to learn about bulk excitations in (3+1)d topological phases, by establishing a bulk-boundary correspondence. One should however bear in mind that boundaries may have more "life" than their corresponding bulk, in that a given bulk topological phase can be consistently terminated by more than one boundary theory. Therefore, it would be more appropriate to consider a "stable equivalent class" of boundary theories for a given bulk theory. (See, for example, Ref.[Cano et al., 2014].) Nevertheless, one can expect universal topological properties of the bulk theories may be extracted from any boundary theory which consistently terminates the bulk.

5.1.1 Outline of this chapter

The rest of the chapter is organized as follows.

In Sec. 5.2, we consider the compactified free boson theory in $(2+1)$d defined on the 3d flat torus T^3 is computed. This (2+1)d theory is not necessarily tied to a particular (3+1)d bulk topological order but serves as a warm up for later sections. We will show its partition function is invariant under $SL(3,\mathbb{Z})$.

In Sec. 5.3, the surface theory of the (3+1)d BF theory at level K is studied. This theory can be subjected to twisted boundary conditions, which are induced by introducing quasi-particles in the (3+1)d bulk. We will show that the partition functions with different boundary conditions are transformed into each other under $SL(3,\mathbb{Z})$, and form a representation of $SL(3,\mathbb{Z})$. The extracted $\mathcal{S}$ and $\mathcal{T}$ matrices agree with the known result. [Moradi and Wen, 2015] We will also compute the thermal entropy in Sec. 5.3.4, and show that there is a constant negative contribution to the entropy. This contribution to the boundary thermal entropy is expected to capture the topological entanglement entropy defined in the corresponding (3+1)d bulk.

In Sec. 5.4, we introduce an additional term, the axion term or the theta term, to the (3+1)d BF theory. The theta angle has a texture (spatial inhomogeneity) and affects the boundary theory by twisting the quantum numbers. Being static, the texture in the theta angle is interpreted as a topological defect, and we will show that the introduction of the defect makes the surface theory non-modular invariant, in the sense that the action of modular transformations is not closed within the space of the partition functions.

This BF theory with the theta term motivates us to consider yet another theory in Sec. 5.5, which can be constructed by coupling two copies of the BF theory. Compared with the the defect system (the BF theory with the theta term) discussed in Sec. 5.4, in the coupled system, each copy can be interpreted as playing a role of a defect to the other. In this system, however, there is no externally imposed texture. We propose this continuum bulk field theory realizes three-loop braiding statistics discussed previously. [Wang and Levin, 2015, Wang and Levin, 2014, Lin and Levin, 2015, Jian and Qi, 2014] On the surface, we consider two copies of the BF surface theories, which are coupled together in their zero mode sectors. We will show that, by computing the modular $\mathcal{S}$ and $\mathcal{T}$ matrices explicitly, this system exhibits three-loop braiding statistics.

Finally, we conclude in Sec. 5.6.

5.2 The compactified free boson in $(2+1)$d

The compactified real scalar theory in $(2+1)$d is described by the Lagrangian density

$$\mathcal{L} = \frac{1}{(2\pi)^2}\left[(\partial_t\phi)^2 - (\partial_x\phi)^2 - (\partial_y\phi)^2\right], \tag{5.3}$$

where, for now, the spacetime is the "canonical" flat torus T^3 parameterized by (t,x,y). (We will consider, momentarily in Sec. 5.2.2, a generic torus parameterized by six modular parameters.) The boson field obeys

the compactification condition on a circle of radius r, i.e.,

$$\phi \equiv \phi + 2\pi \mathrm{r}. \tag{5.4}$$

This model can be exactly solved and is dual to the compact $U(1)$ gauge theory. Under the duality, the boson field ϕ is related to the $U(1)$ gauge field a_μ by

$$\epsilon^{\mu\nu\lambda}\partial_\nu a_\lambda \leftrightarrow \partial^\mu \phi, \quad f^{\mu\nu} f_{\mu\nu} \leftrightarrow \partial^\mu \phi \partial_\mu \phi. \tag{5.5}$$

Furthermore, quantized vortices on the boson side are dual to quantized charges in the $U(1)$ gauge theory. For the compact $U(1)$ gauge field theory, the monopole (instanton) proliferation leads to a confining phase and this process on the scalar boson side corresponds to adding a $\cos(\phi)$ term. [Polyakov, 1975, Polyakov, 1977] This process breaks the $U(1)$ symmetry in the compact boson theory, and the particle number is not conserved anymore. If we prohibit the monopoles, on the other hand, the Abelian $U(1)$ gauge theory is stably gapless.

The free boson theory can be canonically quantized: The corresponding Hamiltonian is

$$H = \frac{1}{(2\pi)^2} \int_0^{2\pi R_1} dx \int_0^{2\pi R_2} dy \left[\Pi^2 + (\partial_x \phi)^2 + (\partial_y \phi)^2\right], \tag{5.6}$$

where x and y are periodic with radius $2\pi R_1$ and $2\pi R_2$, respectively, and the canonical momentum is ($\mathsf{r} := (x, y)$)

$$\Pi(\mathsf{r}) := \partial_t \phi(\mathsf{r}). \tag{5.7}$$

The canonical commutation relation is given by

$$\begin{aligned} [\phi(t, \mathsf{r}), \Pi(t, \mathsf{r}')] &= \frac{i}{2}(2\pi)^2 \delta^{(2)}(\mathsf{r} - \mathsf{r}') \\ &= \frac{i}{2} \frac{1}{R_1 R_2} \sum_{s_{1,2} \in \mathbb{Z}} e^{i\mathsf{k}\cdot(\mathsf{r}-\mathsf{r}')}, \end{aligned} \tag{5.8}$$

where $\delta^{(2)}(\mathsf{r} - \mathsf{r}')$ is the periodic delta function and $\mathsf{k} = (s_1/R_1, s_2/R_1)$ is the 2d momentum ($s_i \in \mathbb{Z}$).

To specify the Hilbert space, we develop the mode expansion of the bosonic field ϕ. Due to the compactification condition (5.4), the bosonic field has the following expansion:

$$\phi(t, \mathsf{r}) = \frac{\mathrm{r} N_1}{R_1} x + \frac{\mathrm{r} N_2}{R_2} y + \frac{\phi_0 + \pi_0 t}{2\pi\sqrt{R_1 R_2}} + \phi_{osc}(t, \mathsf{r}), \tag{5.9}$$

where $N_{1,2} \in \mathbb{Z}$ characterize the winding zero modes in the x and y direction, respectively. The Fourier decomposition of the oscillator part $\phi_{osc}(t, \mathsf{r})$ is given by

$$\begin{aligned}\phi_{osc}(t,\mathsf{r}) = \frac{1}{\sqrt{R_1 R_2}} \sum_{\mathsf{k}\neq 0} \frac{1}{2\sqrt{\omega(\mathsf{k})}} \\ \times \left[a(\mathsf{k}) e^{-i\omega t - i\mathsf{k}\cdot\mathsf{r}} + a^\dagger(\mathsf{k}) e^{i\omega t + i\mathsf{k}\cdot\mathsf{r}}\right].\end{aligned} \tag{5.10}$$

According to Eq. (5.8), $a(\mathsf{k})$ satisfies the canonical commutation relation

$$\left[a(\mathsf{k}), a^\dagger(\mathsf{k}')\right] = \delta_{\mathsf{k},\mathsf{k}'}, \tag{5.11}$$

where $\omega(\mathsf{k})$ is the dispersion of the free boson on a Euclidean three-torus and given by

$$\omega(\mathsf{k}) = \sqrt{\left(\frac{s_1}{R_1}\right)^2 + \left(\frac{s_2}{R_2}\right)^2}. \tag{5.12}$$

On the other hand, the zero mode part satisfies

$$[\phi_0, \pi_0] = 2\pi^2 i. \tag{5.13}$$

Owing to the $2\pi\mathrm{r}$ periodicity of $\phi(t, \mathsf{r})$, the eigenvalues of π_0 needs to be quantized according to

$$\pi_0 = \frac{\pi N_0}{\mathrm{r}\sqrt{R_1 R_2}}, \quad N_0 \in \mathbb{Z}. \tag{5.14}$$

To summarize, the boson field $\phi(t, \mathsf{r})$ can be mode-expanded as

$$\begin{aligned}\phi(t,\mathsf{r}) = \frac{\phi_0}{2\pi\sqrt{R_1 R_2}} + \frac{N_0 t}{2\mathrm{r} R_1 R_2} + \frac{\mathrm{r} N_1}{R_1} x + \frac{\mathrm{r} N_2}{R_2} y \\ + \frac{1}{\sqrt{R_1 R_2}} \sum_{\mathsf{k}\neq 0} \frac{1}{2\sqrt{\omega(\mathsf{k})}} \\ \times \left[a(\mathsf{k}) e^{-i\omega t - i\mathsf{k}\cdot\mathsf{r}} + a^\dagger(\mathsf{k}) e^{i\omega t + i\mathsf{k}\cdot\mathsf{r}}\right].\end{aligned} \tag{5.15}$$

The Hilbert space $\mathcal{H}_0$ consists of, for each winding sector specified by $N_{1,2}$, the zero mode part and the bosonic Fock space for each $\mathsf{k} \neq 0$. States in the zero mode part are labeled by the eigenvalues of π_0, and hence by N_0. Furthermore, different winding sectors are summed over. In the following, the part of the partition function associated to the summation over $N_{0,1,2}$ is called the zero mode sector.

5.2.1 Modular transformations on T^3

We now consider the theory put on a generic flat torus. A flat three-torus is parameterized by six real parameters, $R_{0,1,2}$ and α, β, γ. For a flat three-torus T^3, the dreibein is given by [Hsieh et al., 2015]

$$e^A{}_\mu = \begin{pmatrix} R_0 & 0 & 0 \\ 0 & R_1 & 0 \\ 0 & 0 & R_2 \end{pmatrix} \begin{pmatrix} 1 & 0 & 0 \\ -\alpha & 1 & 0 \\ -\gamma & -\beta & 1 \end{pmatrix} \tag{5.16}$$

where R_0, R_1, and R_2 are the radii for the directions τ, x, and y, and α, β, and γ describe the angles between directions τ and x, x and y, and τ and y, respectively. The Euclidean metric is then given by

$$\begin{aligned} g_{\mu\nu} &= e^A{}_\mu e^B{}_\nu \delta_{AB} \\ &= \begin{pmatrix} R_0^2 + \alpha^2 R_1^2 + \gamma^2 R_2^2 & -\alpha R_1^2 + \beta\gamma R_2^2 & -\gamma R_2^2 \\ -\alpha R_1^2 + \beta\gamma R_2^2 & R_1^2 + \beta^2 R_2^2 & -\beta R_2^2 \\ -\gamma R_2^2 & -\beta R_2^2 & R_2^2 \end{pmatrix}, \end{aligned} \tag{5.17}$$

The group $SL(3, \mathbb{Z})$ is generated by two transformations:

$$U_1 = \begin{pmatrix} 0 & 0 & 1 \\ 1 & 0 & 0 \\ 0 & 1 & 0 \end{pmatrix}, \quad U_2 = \begin{pmatrix} 1 & 1 & 0 \\ 0 & 1 & 0 \\ 0 & 0 & 1 \end{pmatrix}. \tag{5.18}$$

Under the U_2 transformation, the metric is transformed as

$$g_{\mu\nu} \xrightarrow{U_2} \left(U_2 g U_2^T\right)_{\mu\nu} \tag{5.19}$$

which corresponds to the changes

$$\alpha \to \alpha - 1, \quad \gamma \to \gamma + \beta, \tag{5.20}$$

while R_0, R_1, R_2, and β are unchanged.

On the other hand, U_1 can be decomposed as

$$U_1 = U_1' M, \quad U_1' = \begin{pmatrix} 0 & -1 & 0 \\ 1 & 0 & 0 \\ 0 & 0 & 1 \end{pmatrix} \quad M = \begin{pmatrix} 1 & 0 & 0 \\ 0 & 0 & -1 \\ 0 & 1 & 0 \end{pmatrix} \tag{5.21}$$

where U_1' corresponds to the 90° rotation in the $\tau - x$ plane and M is the 90° rotation in the $x - y$ plane. The generator U_1' acts on the metric as

$$g_{\mu\nu} \xrightarrow{U_1'} (U_1' g U_1'^T)_{\mu\nu} \tag{5.22}$$

which corresponds to the changes

$$\begin{aligned} &R_0 \to R_0/|\tau|, \quad R_1 \to R_1|\tau|, \quad \tau_1 \to -\tau_1/|\tau|^2, \\ &\gamma \to -\beta, \quad \beta \to \gamma \quad \text{(while } R_2 \text{ is unchanged)}, \end{aligned} \tag{5.23}$$

where we have introduced

$$\tau \equiv \alpha + i r_{01}, \quad r_{01} \equiv R_0/R_1. \tag{5.24}$$

Observe also that under $R_0 \to R_0/|\tau|$ and $R_1 \to R_1|\tau|$, $\tau_2 \to \tau_2/|\tau|^2$. Hence, U_1' induces $\tau \to -1/\tau$.

The two transformations U_1' and U_2 correspond respectively to modular S and T^{-1} transformations in the $\tau - x$ plane, generating the $SL(2,\mathbb{Z})$ subgroup of $SL(3,\mathbb{Z})$ group. Combining with M, they generate the whole $SL(3,\mathbb{Z})$ group. In the following, we call $U_1' M$ as $\mathcal{S}$ transformation and U_2 as $\mathcal{T}^{-1}$ transformation.

Moreover, the two generators of $SL(3,\mathbb{Z})$, the U_1 and U_2 transformations defined in Eq. (5.18), satisfy [Wang and Wen, 2015]

$$U_1 U_1^\dagger = U_1^3 = R^6 = (U_1 R)^4 = (R U_1)^4 = 1, \tag{5.25}$$

$$(U_1 R^2)^4 = (R^2 U_1)^4 = (U_1 R^3)^3 = (R^3 U_1)^3 = 1, \tag{5.26}$$

$$(U_1 R^2 U_1)^2 R^2 = R^2 (U_1 R^2 U_1)^2 \quad \text{mod } 3, \tag{5.27}$$

where

$$R = (U_2 U_1)^2 U_2^{-1} U_1^2 U_2^{-1} U_1 U_2 U_1. \tag{5.28}$$

5.2.2 The partition function on T^3

In this section, we calculate the partition function of the compactified free boson theory on the three-torus in the presence of the generic flat metric. The Euclidean action is given by

$$\begin{aligned} S &= \frac{1}{(2\pi)^2}\int_0^{2\pi} d^3\theta\sqrt{|g|}g^{\mu\nu}\partial_\mu\phi\partial_\nu\phi \\ &= \frac{1}{(2\pi)^2}\int_0^{2\pi R_0} d\tau\int_0^{2\pi R_1} dx\int_0^{2\pi R_2} dy\left[(\partial_\tau\phi)^2+\left(\frac{\alpha^2R_1^2}{R_0^2}+1\right)(\partial_x\phi)^2+\left(\frac{R_2^2}{R_0^2}(\alpha\beta+\gamma)^2+\frac{R_2^2}{R_1^2}\beta^2+1\right)(\partial_y\phi)^2\right. \\ &\quad \left.+2\alpha\frac{R_1}{R_0}(\partial_\tau\phi)(\partial_x\phi)+2\frac{R_2}{R_0}(\alpha\beta+\gamma)(\partial_\tau\phi)(\partial_y\phi)+2\left(\frac{R_1R_2}{R_0^2}\alpha(\alpha\beta+\gamma)+\frac{R_2}{R_1}\beta\right)(\partial_x\phi)(\partial_y\phi)\right], \end{aligned} \tag{5.29}$$

where $0\le\theta^\mu\le 2\pi$ are angular variables and we noted $\sqrt{|g|}=R_0R_1R_2$, $\tau=R_0\theta^0$, $x=R_1\theta^1$ and $y=R_2\theta^2$. [1] The inverse metric $g^{\mu\nu}=(e_A^{\star\mu})^T\delta^{AB}(e_B^{\star\nu})$ ($e_A^\star$ is the inverse of e^A) is given by

$$g^{\mu\nu}=\begin{pmatrix} \frac{1}{R_0^2} & \frac{\alpha}{R_0^2} & \frac{\alpha\beta+\gamma}{R_0^2} \\ \frac{\alpha}{R_0^2} & \frac{\alpha^2}{R_0^2}+\frac{1}{R_1^2} & \frac{\alpha(\alpha\beta+\gamma)}{R_0^2}+\frac{\beta}{R_1^2} \\ \frac{\alpha\beta+\gamma}{R_0^2} & \frac{\alpha(\alpha\beta+\gamma)}{R_0^2}+\frac{\beta}{R_1^2} & \frac{(\alpha\beta+\gamma)^2}{R_0^2}+\frac{\beta^2}{R_1^2}+\frac{1}{R_2^2} \end{pmatrix}. \tag{5.30}$$

In the operator formalism, the partition function corresponding to the action (5.29) is given by the trace of the thermal density matrix $\exp(-2\pi R_0H')$ over the Hilbert space $\mathcal{H}_0$:

$$\mathcal{Z}=\mathrm{Tr}_{\mathcal{H}_0}\left[e^{-2\pi R_0H'}\right]. \tag{5.31}$$

The "boosted" Hamiltonian H' and the (untwisted) Hilbert space $\mathcal{H}_0$ are specified as follows. The boosted Hamiltonian H' consists of the "unboosted" Hamiltonian H (with $\alpha=\gamma=0$), and the momentum $P_{x,y}$, which induces the boost in x and y directions, respectively:

$$H'=H+i\frac{\alpha R_1}{R_0}P_x+i(\alpha\beta+\gamma)\frac{R_2}{R_0}P_y \tag{5.32}$$

[1] The Euclidean time coordinate τ should not be confused with the modular parameter.

where

$$H = \int \frac{dxdy}{(2\pi)^2} \left[\Pi^2 + G^{ij}\partial_i\phi\partial_j\phi\right],$$
$$P_i = \int \frac{dxdy}{(2\pi)^2} 2\Pi\partial_i\phi, \quad i = x, y. \tag{5.33}$$

and G^{ij} is defined as

$$g^{ij} = \begin{pmatrix} g_{11} & g_{12} \\ g_{21} & g_{22} \end{pmatrix} = \begin{pmatrix} \frac{1}{R_1^2} & \frac{\beta}{R_1^2} \\ \frac{\beta}{R_1^2} & \frac{\beta^2}{R_1^2} + \frac{1}{R_2^2} \end{pmatrix},$$
$$G^{ij} = R_i R_j g^{ij} = \begin{pmatrix} 1 & \beta\frac{R_2}{R_1} \\ \beta\frac{R_2}{R_1} & \frac{\beta^2 R_2^2}{R_1^2} + 1 \end{pmatrix} \tag{5.34}$$

(where i, j are not summed in $R_i R_j g^{ij}$). I.e.,

$$H' = \int \frac{dxdy}{(2\pi)^2} \Big[\Pi^2 + (\partial_x\phi + \beta\frac{R_2}{R_1}\partial_y\phi)^2 + (\partial_y\phi)^2$$
$$+2i\frac{\alpha R_1}{R_0}\Pi\partial_x\phi + 2i(\alpha\beta+\gamma)\frac{R_2}{R_0}\Pi\partial_y\phi\Big], \tag{5.35}$$

The mode expansion for the bosonic field ϕ is still given by Eq. (5.15), where the energy spectrum $\omega(\mathsf{k})$ is now given by

$$\omega(\mathsf{k}) = \sqrt{G^{ij}k_i k_j}$$
$$= \sqrt{g^{ij}s_i s_j} = \sqrt{\left(\frac{s_1}{R_1} + \beta\frac{s_2}{R_1}\right)^2 + \left(\frac{s_2}{R_2}\right)^2}. \tag{5.36}$$

The Hilbert space $\mathcal{H}_0$ is given as a direct product of the bosonic Fock spaces each built out of a given zero mode state specified by $N_{0,1,2}$.

Next, we proceed to compute the partition function and study its properties under modular transformations of the three-torus. The partition function can be split into the zero mode part, which we call Z_0, and the oscillator part, which we call Z_{osc}. The total partition function is $\mathcal{Z} = Z_0 Z_{osc}$.

The partition function of the zero mode part is

$$Z_0 = \sum_{N_{0,1,2}\in\mathbb{Z}} \exp\Big[-\frac{\pi\tau_2}{2\mathrm{r}^2 R_2}N_0^2 - 2\pi\mathrm{r}^2 R_2\tau_2(N_1+\beta N_2)^2 - \frac{2\pi\mathrm{r}^2 R_0 R_1}{R_2}N_2^2$$
$$+ 2\pi i\tau_1 N_0(N_1+\beta N_2) + 2\pi i\gamma N_0 N_2\Big] \tag{5.37}$$

where we recall $\tau_2 = R_0/R_1$, $\tau_1 = \alpha$ and $\tau = \tau_1 + i\tau_2$.

On the other hand, for the oscillator part, the Hamiltonian is

$$H'_{osc} = \sum_{\mathsf{k}\neq 0} \left[\omega(\mathsf{k}) + i\alpha\frac{R_1}{R_0}k_1 + i(\alpha\beta+\gamma)\frac{R_2}{R_0}k_2\right] a^\dagger(\mathsf{k})a(\mathsf{k}) + E_0, \tag{5.38}$$

where E_0 is the ground state energy and needs to be properly regularized:

$$E_0 = \sum_{\mathsf{s}\in\mathbb{Z}^2/(0,0)} \frac{1}{2}\sqrt{g^{ij}s_i s_j} = -\frac{\sqrt{\det(g)}}{2} \sum_{\mathsf{s}\in\mathbb{Z}^2/(0,0)} \frac{1}{|g^{ij}s_i s_j|^2}. \tag{5.39}$$

The partition function of the oscillator part can be decomposed into the product of the partition functions of one-dimensional non-compact bosons with "mass" given by s_2. When the "mass" $s_2 = 0$,

$$Z_{s_2=0} = e^{-2\pi R_0 E_0(s_2=0)} \prod_{s_1\neq 0\in\mathbb{Z}} \left[1 - e^{-2\pi R_0(\omega(\mathsf{k})+i\alpha\frac{s_1}{R_0})}\right]^{-1} = \left|\frac{1}{\eta(\tau)}\right|^2 \tag{5.40}$$

where $\eta(\tau)$ is the Dedekind eta function and τ is the 2-dimensional modular parameter:

$$\eta(\tau) := e^{\frac{\pi i\tau}{12}} \prod_{n=1}^{\infty}(1-q^n), \quad q := e^{2\pi i\tau}. \tag{5.41}$$

On the other hand, the other massive part equals to

$$\begin{aligned} Z_{s_2\neq 0} &= e^{-2\pi R_0 E_0(s_2\neq 0)} \prod_{s_2\neq 0, s_1\in\mathbb{Z}} \left[1 - e^{-2\pi R_0(\omega(\mathsf{k})+i\alpha\frac{s_1}{R_0}+i(\alpha\beta+\gamma)\frac{s_2}{R_0})}\right]^{-1} \\ &= \prod_{s_2\in\mathbb{Z}^+} \Theta^{-1}_{[\beta s_2,\gamma s_2]}\left(\tau, \frac{R_1}{R_2}s_2\right), \end{aligned} \tag{5.42}$$

where the massive theta function $\Theta_{[\beta s_2,\gamma s_2]}(\tau, \frac{R_1}{R_2}s_2)$ is defined as

$$\Theta_{[a,b]}(\tau, m) \equiv e^{4\pi\tau_2\Delta(m,a)} \prod_{n\in\mathbb{Z}} \left|1 - e^{-2\pi\tau_2\sqrt{m^2+(n+a)^2}+2\pi i\tau_1(n+a)+2\pi ib}\right|^2 \tag{5.43}$$

where

$$\Delta(m,a) \equiv \frac{1}{2}\sum_{n\in\mathbb{Z}} \sqrt{m^2+(n+a)^2} - \frac{1}{2}\int_{-\infty}^{\infty} dk(m^2+k^2)^{1/2} \tag{5.44}$$

Thus the partition function for the oscillator part equals to

$$Z_{osc} = Z_{s_2=0} Z_{s_2\neq 0} = \left|\frac{1}{\eta(\tau)}\right|^2 \prod_{s_2\in\mathbb{Z}^+} \Theta^{-1}_{[\beta s_2, \gamma s_2]}\left(\tau, \frac{R_1}{R_2} s_2\right). \tag{5.45}$$

Together with (5.37), we have completed the calculation of the total partition function, $\mathcal{Z} = Z_0 Z_{osc}$.

It is instructive to compare the above partition function with the partition function of the (1+1)d compactified free boson. Performing dimensional reduction, by taking $R_2 = 1, N_2 = 0$ and $s_2 = 0$, the partition function reduces to

$$\begin{aligned}\mathcal{Z} = \frac{1}{|\eta(\tau)|^2} \sum_{N_{0,1}\in\mathbb{Z}} \exp\Big(&- \frac{\pi\tau_2}{2\mathrm{r}^2} N_0^2 - 2\pi \mathrm{r}^2 \tau_2 N_1^2 \\ &+ 2\pi i \tau_1 N_0 N_1\Big).\end{aligned} \tag{5.46}$$

This is the partition function for the compactified free boson in $(1+1)$d.

Modular invariance

We now show that the total partition function is invariant under the $SL(3,\mathbb{Z})$ transformations.

For Z_0, under U_1' transformation, by using the Poisson resummation formula twice, we have

$$Z_0(\tau) \xrightarrow{U_1'} Z_0(-1/\tau) = |\tau| Z_0(\tau) \tag{5.47}$$

where the Poisson resummation formula is

$$\sum_{n\in\mathbb{Z}} e^{-\pi a n^2 + bn} = \frac{1}{\sqrt{a}} \sum_{k\in\mathbb{Z}} e^{-\frac{\pi}{a}\left(k + \frac{b}{2\pi i}\right)^2}. \tag{5.48}$$

For Z_{osc} part, under U_1' transformation, the massless $s_2 = 0$ component will contribute a $1/|\tau|$ prefactor. The massive part is invariant under U_1' transformation, since the massive theta function satisfies

$$\begin{aligned}\Theta_{[a,b]}\left(\tau, \frac{R_1}{R_2} s_2\right) &\xrightarrow{U_1'} \Theta_{[a,b]}\left(-\frac{1}{\tau}, \frac{R_1}{R_2} s_2 |\tau|\right) \\ &= \Theta_{[b,-a]}\left(\tau, \frac{R_1}{R_2} s_2\right)\end{aligned} \tag{5.49}$$

Thus the total partition function is invariant under U_1' transformation.

Under the M transformation which is basically a $\pi/2$ rotation in the $x-y$ plane, the partition function

for the zero mode part becomes

$$Z_0 \xrightarrow{M} Z_0 = \sum_{N_{0,1,2}\in\mathbb{Z}} \exp\Big(-\frac{\pi R_0}{2\mathrm{r}^2 R_1 R_2}N_0^2 \\ -2\pi\mathrm{r}^2 R_0 R_1 R_2\left[\left(\beta\frac{N_1}{R_1}-\frac{N_2}{R_1}\right)^2+\left(\frac{N_1}{R_2}\right)^2\right] \\ -2\pi i\alpha R_0[\beta N_1 - N_2]N_0 - 2\pi i\gamma N_1 N_0\Big). \tag{5.50}$$

Therefore the invariance of the zero mode part of the partition function can be seen from relabeling,

$$M:\begin{cases} N_1 \\ N_2 \\ N_0 \end{cases} \to \begin{cases} -N_2 \\ N_1 \\ N_0 \end{cases} \tag{5.51}$$

It is also straightforward to show that the oscillator part is invariant under M transformation and thus the total partition function is invariant under M transformation.

Finally, it is also easy to check that the partition function is invariant under U_2 transformation. Hence the partition function is invariant under the $SL(3,\mathbb{Z})$ transformation.

5.3 The surface theory of the (3+1)d BF theory

5.3.1 Bulk and surface theories

The bulk field theory The (3+1)-dimensional one component BF theory is described by the action

$$S_{bulk} = \int_{\mathcal{M}}\left[\frac{\mathrm{K}}{2\pi}b\wedge da - a\wedge J_{qp} - b\wedge J_{qv}\right] \\ = \int d^4x\left[\frac{\mathrm{K}}{4\pi}\varepsilon^{\mu\nu\lambda\rho}b_{\mu\nu}\partial_\lambda a_\rho - a_\mu j^\mu_{qp} - \frac{1}{2}b_{\mu\nu}j^{\mu\nu}_{qv}\right], \tag{5.52}$$

where $\mu,\nu,\ldots = 0,\ldots,3$, $a = a_\mu dx^\mu$ and $b = (1/2)b_{\mu\nu}dx^\mu dx^\nu$ are one and two form gauge fields; $\mathcal{M}$ is the bulk spacetime manifold. The "level" K is an integer. The three form J_{qp} and two form J_{qv} represent currents of zero-dimensional (point-like) quasi-particles and one-dimensional quasi-vortex lines, respectively. The BF theory furnishes the following (bulk) equations of motion

$$\frac{\mathrm{K}}{2\pi}da = J_{qv}, \quad \frac{\mathrm{K}}{2\pi}db = J_{qp}. \tag{5.53}$$

The BF theory implements a non-trivial fractional statistics between quasiparticles and quasivortices. To see this, we consider the following configuration of quasiparticles and quasivortices:

$$J_{qp} = \delta_3(\mathcal{C}), \quad J_{qv} = \delta_2(\mathcal{S}). \tag{5.54}$$

Here $\mathcal{C}$ and $\mathcal{S}$ represent the one-dimensional wold-line and the two-dimensional world-sheet of quasiparticles and quasivortices, respectively; $\delta_{D-n}(\mathcal{N})$ is the delta function $(D-n)$-form associated a submanifold $\mathcal{N} \subset \mathcal{M}$, where $D - n = \dim \mathcal{M} - \dim \mathcal{N}$. By definition, for any n-form A_n,

$$\int_{\mathcal{N}} A_n = \int_{\mathcal{M}} \delta_{D-n}(\mathcal{N}) \wedge A_n. \tag{5.55}$$

Hence, for example,

$$\int_{\mathcal{M}} J_{qp} \wedge a = \int_{\mathcal{C}} a, \quad \int_{\mathcal{M}} J_{qv} \wedge b = \int_{\mathcal{S}} b. \tag{5.56}$$

In the presence of these quasiparticles and quasivortices, we now integrate over a and b to derive the effective action for J_{qp} and J_{qv}. Since the theory is quadratic, this can be done by solving the equations of motion. These equations, up to a closed form, are solved by

$$b = \frac{2\pi}{\mathrm{K}} d^{-1} J_{qp}, \quad a = \frac{2\pi}{\mathrm{K}} d^{-1} J_{qv}. \tag{5.57}$$

(If the spacetime is trivial, by the Poincaré lemma, a closed form is exact. If so, such exact term does not affect our final result since, for an arbitrary closed submanifold $\mathcal{N}$, $\int \delta(\mathcal{N})(d\phi) \sim \int \delta(\partial\mathcal{N})\phi = 0$.) $d^{-1}J_{qp}$ and $d^{-1}J_{qv}$ are determined as

$$\begin{aligned} d^{-1} J_{qp} &= \delta_2(\mathcal{D}), \quad \text{where} \quad \partial\mathcal{D} = \mathcal{C}, \\ d^{-1} J_{qv} &= \delta_1(\mathcal{V}), \quad \text{where} \quad \partial\mathcal{V} = \mathcal{S}. \end{aligned} \tag{5.58}$$

where the two-dimensional manifold $\mathcal{D}$ and the three-dimensional manifold $\mathcal{V}$ are chosen such that $\partial\mathcal{D} = \mathcal{C}$ and $\partial\mathcal{V} = \mathcal{S}$. They are not unique, but different choices lead to different $d^{-1}J_{qp,qv}$ which differ by closed forms.

Substituting these solution into the action,

$$\begin{aligned} S_{bulk} &= -\frac{2\pi}{\mathrm{K}} \int (d^{-1} J_{qv}) \wedge J_{qp} \\ &= -\frac{2\pi}{\mathrm{K}} Lk(\mathcal{S}, \mathcal{C}), \end{aligned} \tag{5.59}$$

where Lk is the linking number between J_{qp} and J_{qv}. Hence,

$$\begin{aligned} \int \mathcal{D}[a,b] e^{iS_{bulk}} &= e^{-\frac{2\pi i}{\mathrm{K}} Lk(\mathcal{S},\mathcal{C})} \\ &= e^{-\frac{2\pi i}{\mathrm{K}} \sum_{ij} q_i \lambda_j Lk(\mathcal{S}_i, \mathcal{C}_j)}. \end{aligned} \tag{5.60}$$

In the last line, we assume the world-line $\mathcal{L}$ consists of trajectories $\mathcal{L}_i$ of many quasiparticles each carrying charge $q_i \in \mathbb{Z}$: $J_{qp} = \delta_3(\mathcal{C}) = \sum_i q_i \delta_3(\mathcal{C}_i)$. Similarly, the world-line $\mathcal{S}$ consists of trajectories $\mathcal{S}_i$ of many quasivortices each carrying charge $\lambda_i \in \mathbb{Z}$: $J_{qv} = \delta_2(\mathcal{S}) = \sum_i \lambda_i \delta_2(\mathcal{S}_i)$. The fractional phase (when $|\mathrm{K}| > 1$) in Eq. (5.60) represents statistical interactions between quasiparticles and quasivortices.

Once the coupling of the gauge fields to the currents is prescribed, it also specifies the set of Wilson loops and Wilson surfaces included in theory (see Eq. (5.56)). If the theory is canonically quantized on $\mathcal{M} = \mathbb{R} \times \Sigma$, the set of the Wilson loop and Wilson surface operators of our interest is

$$\exp im \int_L a, \quad \exp in \int_S b, \tag{5.61}$$

where m, n are integers, and L and S are arbitrary closed loops and surfaces in Σ. These operators satisfy the commutation relations,

$$\begin{aligned} \left[\textstyle\int_L a, \int_S b\right] &= \frac{2\pi i}{\mathrm{K}} I(L,S), \\ e^{im\int_L a} e^{in\int_S b} &= e^{\frac{2\pi i}{\mathrm{K}} I(L,S)} e^{in\int_S b} e^{im\int_L a}. \end{aligned} \tag{5.62}$$

where $I(L,S)$ is the intersection number of the loop L and the surface S.

The boundary theory On a closed manifold, the BF theory is invariant under gauge transformations $a \to a + d\varphi$, where φ is zero form, and $b \to b + d\zeta$, where ζ is one form. In the presence of a boundary (surface), the surface can be described by a gapless theory. The action describing the boundary degrees of freedom can be inferred by adopting the temporal gauge $a_0 = b_{i0} = b_{0i} = 0$ $(i = 1, 2, 3)$, solving the Gauss law constraints $\varepsilon^{ijk0} \partial_k b_{ij} = \varepsilon^{0ijk} \partial_j a_k = 0$ by $a_k = \partial_k \varphi$, $b_{ij} = \partial_i \zeta_j - \partial_j \zeta_i$, and then plugging these back to the action. The

resulting action is [Wu, 1991, Balachandran and Teotonio-Sobrinho, 1993, Amoretti et al., 2012]

$$S_{\partial\mathcal{M}} = \int_{\partial\mathcal{M}} dtdxdy \left[\frac{\mathrm{K}}{2\pi}\epsilon_{ij}\partial_i\zeta_j\partial_t\varphi - V(\varphi,\zeta)\right] \tag{5.63}$$

where $i,j = 1,2$. Here we have added the potential $V(\varphi,\zeta)$, which originates from microscopic details of the boundary and is non-universal. This boundary action can be obtained from the the free scalar and the $U(1)$ Maxwell theories by imposing a self-dual (or an anti-self-dual) constraint, $\epsilon^{\mu\nu\lambda}\partial_\nu\zeta_\lambda = \pm\partial^\mu\varphi$. [Balachandran and Teotonio-Sobrinho, 1993]

For the single-component Chern-Simons theory in $(2+1)$ dimensions, the boundary is described by the single-component chiral boson theory and cannot be gapped out. Different from the Chern-Simons theory, the boundary theory of BF theory in $(3+1)$ dimensions (also in $(2+1)$ dimensions) can be gapped out by adding some mass term (without symmetry protection). Although this gapless boundary theory is not stable at all, it does encode some topological data in the bulk as we will discuss later. Therefore, in this chapter, we will always assume that the surface state is gapless.

Let us now discuss, in more detail, the connection between the bulk excitations and the fields living on the boundary. In the following we choose $\mathcal{M} = S^1 \times \Sigma$, where the spatial manifold Σ is a solid torus, $\Sigma = D^2 \times S^1$, and hence $\partial\mathcal{M} = T^3$. Let us first consider a quasiparticle current consisting of a quasiparticle carrying n_0 units of charges ($n_0 \in \mathbb{Z}$):

$$j^\mu_{qp}(x) = n_0 \int_L d\tau \frac{dX^\mu(\tau)}{d\tau}\delta^{(4)}[x - X(\tau)] \tag{5.64}$$

where L is the world-line of the quasiparticle, and the coordinate $X^\mu(\tau)$ represents the trajectory of the particle. For the quasiparticle at rest, $X^{1,2,3}(\tau) = const. = X^{1,2,3}$,

$$j^0_{qp}(x) = n_0\delta^{(3)}(\vec{x} - \vec{X}). \tag{5.65}$$

Integrating the equation of motion over the total space,

$$\frac{\mathrm{K}}{4\pi}\int_\Sigma d^3x\, \varepsilon^{0ijk}\partial_i b_{jk} = \int_\Sigma d^3x\, j^0_{qp} = n_0. \tag{5.66}$$

Using Stokes' theorem, $\int_\Sigma db = \int_{\partial\Sigma} b = (1/2)\int_{\partial\Sigma} b_{ij}\epsilon^{ij}d^2x$, and substituting $b_{ij} = \partial_i\zeta_j - \partial_j\zeta_i$, this reduces

to

$$\int_{\partial\Sigma} d^2x\, \epsilon_{ij}\partial_i\zeta_j = \frac{2\pi}{\mathrm{K}} n_0. \tag{5.67}$$

Hence adding a quasiparticle in the bulk corresponds to introducing flux on the surface.

Similarly, let us consider to introduce a quasivortex source:

$$j^{\mu\nu}_{qv}(x) = n\int_S d^2\sigma\epsilon^{\alpha\beta}\frac{\partial X^\mu(\sigma)}{\partial\sigma^\alpha}\frac{\partial X^\nu(\sigma)}{\partial\sigma^\beta}\delta^{(4)}[x - X(\sigma)], \tag{5.68}$$

where S is the world-surface of the quasivortex, and the coordinate $X^\mu(\sigma)$ represents the trajectory of the particle in spacetime, and n is an integer. Let us consider a straight quasivortex at rest, stretching along a non-contractible cycle of the bulk solid torus. For convenience, this direction is taken as the x-direction (Fig. 5.1). Then, $j^{02}_{qv} = j^{03}_{qv} = 0$ and

$$j^{01}_{qv}(x) = n_2\delta(x^2 - X^2)\delta(x^3 - X^3). \tag{5.69}$$

where $X^{2,3}(\sigma) = const.$ and we have renamed the integer n as n_2. Integrating the equation of motion over space,

$$L_1 \times \frac{\mathrm{K}}{2\pi}\int dydz\, \varepsilon^{01ij}\partial_i a_j = n_2 \times L_1, \tag{5.70}$$

where $i, j = 1, 2$ and $L_1 = 2\pi R_1$ is the length of the quasivortex stretching in the x-direction, and we noted the flux $\varepsilon^{01ij}\partial_i a_j$ is independent of x_1. Using Stokes' theorem, and substituting $a_i = \partial_i\varphi$,

$$\oint dy\partial_y\varphi = \frac{2\pi}{\mathrm{K}} n_2. \tag{5.71}$$

Hence introducing a quasivortex (quasivortices) along the non-contractible loop in the bulk corresponds to introducing winding of the scalar boson on the surface.

One may wish to develop a similar argument for a quasivortex (quasivortices) stretching in the y-direction. (Fig. 5.1 (c)). It should however be noted that once we fix our geometry as above (Fig. 5.1 (b)), loops running in the y-direction are contractible in the bulk. In other words, if one constructs a solid torus by filling "inside" of a two-dimensional torus, one needs to specify one of non-contractible cycles on the two-dimensional torus, such that after filling, this cycle now is contractible in the sold torus.

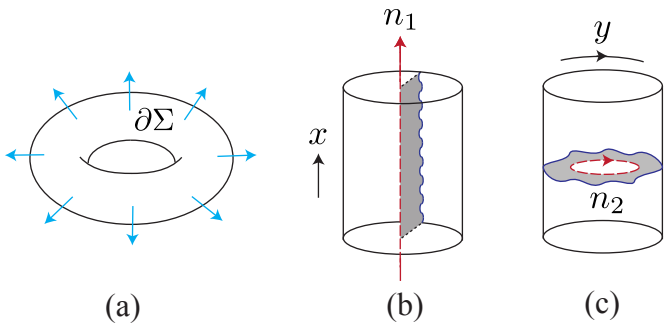

Figure 5.1: (a) The presence of a point-like quasiparticle in the bulk (solid torus) induces a fractional flux on the spatial boundary Σ (torus). (b) The presence of a quasivortex line in the bulk twists the boundary conditions of the surface theory. Here and in (c), the bulk is presented as a filled cylinder where the top and the bottom of the cylinder are identified. The shaded surface is a sheet of the branch cut which emanates from the quasivortex, and intersects with the spatial boundary (depicted by a wavy line). The surface excitations experience a twisted boundary condition as they go through the branch cut. (c) Similar to (b), a bulk quasivortex, which creates a branch cut on the surface which now goes along a different cycle of the surface, is depicted.

5.3.2 The surface theory and quantization

We now proceed to the canonical quantization of the surface theory. We start from the surface Lagrangian density

$$\begin{aligned}\mathcal{L} = &\frac{\mathrm{K}}{2\pi}(\epsilon_{ij}\partial_i\zeta_j)(\partial_t\varphi) \\ &- \frac{1}{2\lambda_1}(\epsilon_{ij}\partial_i\zeta_j)^2 - \frac{1}{2\lambda_2}G^{ij}\partial_i\varphi\partial_j\varphi.\end{aligned} \tag{5.72}$$

The boson field φ is compact and satisfy

$$\varphi \equiv \varphi + 2\pi. \tag{5.73}$$

I.e., physical observables are bosonic exponents

$$\exp[im\varphi(t,\mathsf{r})], \quad m \in \mathbb{Z}. \tag{5.74}$$

The winding number of φ is quantized, in the absence of bulk quasiparticles, according to

$$\oint dx^i \partial_i\varphi = 2\pi N_i, \quad N_i \in \mathbb{Z}, \tag{5.75}$$

where $i = 1, 2$ and i is not summed on the right hand side. On the other hand, the gauge field ζ_i is compact, meaning that physical observables are Wilson loops,

$$\exp im \int_C dx^i \zeta_i(t, \mathsf{r}), \quad m \in \mathbb{Z}, \tag{5.76}$$

where C is a closed loop on $\partial\Sigma = T^2$. The flux associated to ζ_i is quantized, in the absence of bulk quasiparticles, according to

$$\int dxdy\, \epsilon_{ij} \partial_i \zeta_j = 2\pi N_0 \tag{5.77}$$

where N_0 is an integer. The canonical commutation relation is

$$[\varphi(t, \mathsf{r}), \epsilon_{ij} \partial_i \zeta_j(t, \mathsf{r}')] = \frac{2\pi i}{\mathrm{K}} \delta^{(2)}(\mathsf{r} - \mathsf{r}') \tag{5.78}$$

In the following, we fix λ_1 and λ_2 according to

$$\frac{(2\pi)^2}{\mathrm{K}^2 \lambda_1 \lambda_2} = 1. \tag{5.79}$$

This choice is convenient since it gives rise to the same energy dispersion as the compactified free boson discussed in the previous section.

To proceed, we consider the mode expansion of the fields. The equations of motion are

$$\begin{aligned} &\frac{-\mathrm{K}}{2\pi} \epsilon_{ij} \partial_i \partial_t \zeta_j + \frac{1}{\lambda_2} G^{ij} \partial_i \partial_j \varphi = 0, \\ &\frac{-\mathrm{K}}{2\pi} \epsilon_{lk} \partial_l \partial_t \varphi + \frac{1}{\lambda_1} \epsilon_{lk} \partial_l (\epsilon_{ij} \partial_i \zeta_j) = 0. \end{aligned} \tag{5.80}$$

The mode expansion consistent with the equations of motion are

$$\begin{aligned}
\varphi(\mathsf{r}) &= \alpha_0 + \frac{\beta_1 x}{R_1} + \frac{\beta_2 y}{R_2} \\
&\quad + \frac{1}{\sqrt{R_1 R_2}} \sqrt{\frac{1}{2\mathrm{K}^2 \lambda_1}} \sum_{\mathsf{k}\neq 0} \frac{1}{\omega(\mathsf{k})^{1/2}} \\
&\qquad \times \left[a(\mathsf{k}) e^{-i\mathsf{k}\cdot\mathsf{r}} + a^\dagger(\mathsf{k}) e^{+i\mathsf{k}\cdot\mathsf{r}} \right], \\
\zeta_j(\mathsf{r}) &= \frac{\alpha_j}{2\pi R_j} + \frac{\beta_0}{2\pi R_1 R_2} x \delta_{j,2} \\
&\quad + \frac{1}{\sqrt{R_1 R_2}} \sqrt{\frac{\lambda_1}{8\pi^2}} \sum_{\mathsf{k}\neq 0} \frac{-1}{\omega(\mathsf{k})^{3/2}} \epsilon_{jm} G^{ml} k_l \\
&\qquad \times \left[a(\mathsf{k}) e^{-i\mathsf{k}\cdot\mathsf{r}} + a^\dagger(\mathsf{k}) e^{+i\mathsf{k}\cdot\mathsf{r}} \right],
\end{aligned} \tag{5.81}$$

where the eigenvalues of β_0 and $\beta_{1,2}$ describes the flux (associated with the gauge field a in the bulk), and the winding of the φ field, respectively. The quantization conditions of these variables will be discussed momentarily. Reflecting the compact nature of the φ and ζ_j fields, the zero modes are compact variable $\alpha_\mu \equiv \alpha_\mu + 2\pi$ $(\mu = 0, 1, 2)$; For α_0, the compactification condition comes from the fact that physical observables are given as bosonic exponents (5.74). Similarly, for $\alpha_{1,2}$, that physical observables are given in terms of Wilson loops (5.76), and that these Wilson loop operators must be invariant under large gauge transformations imposes the compactification condition, $\alpha_{1,2} \equiv \alpha_{1,2} + 2\pi$.

From the commutator $[\varphi(t, \mathsf{r}), \epsilon_{ij}\partial_i \zeta_j(t, \mathsf{r}')]$, we read off

$$\begin{aligned}
&[a(\mathsf{k}), a^\dagger(\mathsf{k}')] = \delta_{\mathsf{k},\mathsf{k}'}, \\
&[\alpha_0, \beta_0] = \frac{2\pi i}{\mathrm{K}} \frac{1}{2\pi}.
\end{aligned} \tag{5.82}$$

From the compactification condition $\alpha_0 \equiv \alpha_0 + 2\pi$, β_0 is quantized according to

$$\beta_0 = \frac{M_0}{\mathrm{K}}, \quad M_0 \in \mathbb{Z}. \tag{5.83}$$

This quantization condition translates into

$$\int dx dy\, \epsilon_{ij} \partial_i \zeta_j = \frac{2\pi M_0}{\mathrm{K}}. \tag{5.84}$$

Compared with the quantization condition (5.77), the flux is now quantized in the fractional unit. We will

separate M_0 into its non-fractional and fractional parts as

$$M_0 = \mathrm{K}N_0 + n_0, \quad N_0 \in \mathbb{Z}, \quad n_0 = 0, \ldots, \mathrm{K}-1, \tag{5.85}$$

and write the quantization condition of β_0 as

$$\beta_0 = N_0 + n_0/\mathrm{K}. \tag{5.86}$$

The quantization condition of $\beta_{1,2}$ can be discussed similarly. From the commutator $[\varphi(t,\mathsf{r}), \epsilon_{ij}\partial_i\zeta_j(t,\mathsf{r}')]$, we infer

$$[\epsilon_{ij}\partial_i\varphi(t,\mathsf{r}), \zeta_j(t,\mathsf{r}')] = -\frac{2\pi i}{\mathrm{K}}\delta^{(2)}(\mathsf{r}-\mathsf{r}'), \tag{5.87}$$

which implies

$$[\beta_1, \alpha_2] - [\beta_2, \alpha_1] = -\frac{2\pi i}{\mathrm{K}}\frac{1}{2\pi}. \tag{5.88}$$

One can choose, for example,

$$[\beta_1, \alpha_2] = 0, \quad [\beta_2, \alpha_1] = \frac{2\pi i}{\mathrm{K}}\frac{1}{2\pi}. \tag{5.89}$$

This choice may be consistent with the previous consideration from the bulk point of view, and in particular with the comment below (5.71). I.e., this choice may correspond to choosing which non-contractible loops on the surface are contractible in the bulk, when forming a solid torus starting from the two-dimensional torus by filling its "inside".

From the compactness of the gauge field ζ_i, the zero modes satisfy $\alpha_i \equiv \alpha_i + 2\pi$, which imposes the quantization condition

$$\beta_2 = \frac{M_2}{\mathrm{K}}, \quad M_2 \in \mathbb{Z}. \tag{5.90}$$

As before, we split M_2 into the fractional and non-fractional parts,

$$M_2 = \mathrm{K}N_2 + n_2, \quad N_2 \in \mathbb{Z}, \quad n_2 = 0, \ldots, \mathrm{K}-1. \tag{5.91}$$

With this, the boson field obeys the twisted boundary condition

$$\varphi(t, x, y + 2\pi R_2) = \varphi(t, x, y) + 2\pi \left(N_2 + \frac{n_2}{\mathrm{K}} \right). \tag{5.92}$$

While above consideration allows winding in the y-direction but not in the x-direction, in computing the partition functions of the surface theory in the next section, we consider winding in both directions,

$$\begin{aligned} \varphi(t, x + 2\pi R_1, y) &= \varphi(t, x, y) + 2\pi \left(N_1 + \frac{n_1}{\mathrm{K}} \right), \\ \varphi(t, x, y + 2\pi R_2) &= \varphi(t, x, y) + 2\pi \left(N_2 + \frac{n_2}{\mathrm{K}} \right), \end{aligned} \tag{5.93}$$

That is

$$\beta_{i=1,2} = N_{1,2} + n_{1,2}/\mathrm{K}. \tag{5.94}$$

To summarize, in the presence of twisted boundary conditions, the mode expansion of the fields are given by

$$\begin{aligned} \partial_i \varphi(t, \mathsf{r}) = & \frac{N_i + n_i/\mathrm{K}}{R_i} \\ & + \frac{-i}{\sqrt{R_1 R_2}} \sqrt{\frac{1}{2\mathrm{K}^2 \lambda_1}} \sum_{\mathsf{k} \neq 0} \frac{k_i}{\sqrt{\omega(\mathsf{k})}} \\ & \times \left[-a(\mathsf{k}) e^{-i\omega(\mathsf{k})t - i\mathsf{k}\cdot\mathsf{r}} + a^\dagger(\mathsf{k}) e^{+i\omega(\mathsf{k})t + i\mathsf{k}\cdot\mathsf{r}} \right], \\ \epsilon_{ij} \partial_i \zeta_j(t, \mathsf{r}) = & \frac{N_0 + n_0/\mathrm{K}}{2\pi R_1 R_2} \\ & + \frac{-i}{\sqrt{R_1 R_2}} \sqrt{\frac{\lambda_1}{8\pi^2}} \sum_{\mathsf{k} \neq 0} \sqrt{\omega(\mathsf{k})} \\ & \times \left[a(\mathsf{k}) e^{-i\omega(\mathsf{k})t - i\mathsf{k}\cdot\mathsf{r}} - a^\dagger(\mathsf{k}) e^{+i\omega(\mathsf{k})t + i\mathsf{k}\cdot\mathsf{r}} \right], \end{aligned} \tag{5.95}$$

The above consideration is somewhat analogous to the quantization of the chiral boson theory that appears at the edge of the (2+1)d Chern-Simons theory at level K. The (1+1)d chiral boson theory defined on a spatial circle of radius 2π is described by the Lagrangian density

$$\mathcal{L} = \frac{\mathrm{K}}{4\pi} \partial_x \Phi (\partial_t - \partial_x) \Phi, \tag{5.96}$$

where Φ is a single component boson theory compactified as $\Phi \equiv \Phi + 2\pi$, and obeys the canonical com-

mutation relation $[\Phi(x), \partial_x \Phi(x')] = (2\pi i/\mathrm{K})\delta(x - x')$. The zero mode part of Φ, defined by the mode expansion

$$\Phi(t, x) = \Phi_0 - p(t + x) + i \sum_{n \neq 0} b_n e^{-in(t+x)}, \tag{5.97}$$

satisfies $[\Phi_0, p] = i/\mathrm{K}$. This then suggests the quantization rule, $p = (\text{integer})/\mathrm{K}$, and the boundary condition of the chiral boson field

$$\Phi(t, x + 2\pi) = \Phi(t, x) - \frac{2\pi(\text{integer})}{\mathrm{K}}. \tag{5.98}$$

Thus, the canonical quantization naturally leads to the twisted boundary condition of the chiral boson field.

Quantization of the surface theory with the above twisted boundary conditions gives the spectrum of local as well as nonlocal (quasiparticles) excitations, which obey untwisted and twisted boundary conditions, respectively. Once we specify the boundary condition (with some integer vector $n_{\mu=0,1,2}$), the theory is quantized within one sector (labeled by the equivalence class $[\vec{n}]$ with the relation $\vec{n} \equiv \vec{n} + \mathrm{K}\vec{\Lambda}$ where $\vec{\Lambda}$ is a vector with integer entries) of the original spectrum. For this surface theory, there are K^3 sectors in this compactified theory and is consistent with the K^3 ground states of single component BF theory defined on T^3.

5.3.3 The partition functions and modular transformations

Now we compute the partition function (coupled to the T^3 metric):

$$\mathcal{Z}^{n_0 n_1 n_2} = \mathrm{Tr}_{\mathcal{H}_{n_0 n_1 n_2}} \left[e^{-2\pi R_0 H'} \right] \tag{5.99}$$

where $\mathcal{H}_{n_0 n_1 n_2}$ is the Hilbert space twisted by n_0, n_1, n_2 fractional quantum numbers, and

$$\begin{aligned} H' &= H + i\frac{\alpha R_1}{R_0} P_x + i(\alpha\beta + \gamma)\frac{R_2}{R_0} P_y, \\ H &= \int dxdy \, \frac{\mathrm{K}^2 \lambda_1}{8\pi^2} \left[\frac{4\pi^2}{\mathrm{K}^2 \lambda_1^2} (\epsilon_{ij} \partial_i \zeta_j)^2 + G^{ij} \partial_i \varphi \partial_j \varphi \right], \\ P_i &= \int dxdy \frac{\mathrm{K}}{2\pi} (\epsilon_{lm} \partial_l \zeta_m)(\partial_i \varphi). \end{aligned} \tag{5.100}$$

The calculation of the partition function goes in parallel with the calculation presented in the previous

section for the free boson theory. To see this, we note, from the equation of motion,

$$\epsilon_{ij}\partial_i\zeta_j = \frac{\mathrm{K}\lambda_1}{2\pi}\partial_t\varphi \tag{5.101}$$

up to a constant term. Thus, in terms of φ, the Hamiltonian density and the commutation relation are given by

$$\begin{aligned}\mathcal{H} &= \frac{1}{2}\frac{\mathrm{K}^2\lambda_1}{(2\pi)^2}\left[(\partial_t\varphi)^2 + G^{ij}\partial_i\varphi\partial_j\varphi\right], \\ [\varphi(t,\mathsf{r}),\partial_t\varphi(t,\mathsf{r}')] &= \frac{(2\pi)^2 i}{\mathrm{K}^2\lambda_1}\delta^{(2)}(\mathsf{r}-\mathsf{r}').\end{aligned} \tag{5.102}$$

By introducing the rescaled field,

$$\tilde{\phi} = \mathrm{K}\sqrt{\frac{\lambda_1}{2}}\varphi \tag{5.103}$$

the Hamiltonian and the commutation relation can be made isomorphic to those of the free boson theory. The compactification condition of the rescaled boson field is

$$\mathrm{r} = \mathrm{K}\sqrt{\frac{\lambda_1}{2}}. \tag{5.104}$$

The partition function $\mathcal{Z}^{n_0n_1n_2}$ can now be computed from the partition function of the free boson theory. The zero mode part of the partition function for each excitation sector is obtained from Z_0 (Eq. (5.37)) by making replacement $N_0 \to \mathrm{K}N_0 + n_0$ and $N_i \to N_i + n_i/\mathrm{K}$ $(i = 1, 2)$:

$$\begin{aligned}Z^{n_0n_1n_2} = \sum_{N_{0,1,2}\in\mathbb{Z}} \exp\Big\{ &-\frac{\pi\mathrm{K}^2\tau_2}{2\mathrm{r}^2R_2}\tilde{N}_0^2 - 2\mathrm{r}^2\pi R_2\tau_2\left[\tilde{N}_1+\beta\tilde{N}_2\right]^2 - \frac{2\mathrm{r}^2\pi R_0R_1}{R_2}\tilde{N}_2^2 \\ &+ 2\pi i\tau_1\mathrm{K}\tilde{N}_0\left[\tilde{N}_1+\beta\tilde{N}_2\right] + 2\pi i\gamma\mathrm{K}\tilde{N}_0\tilde{N}_2\Big\},\end{aligned} \tag{5.105}$$

where we have introduced the notation

$$\tilde{N}_\mu := N_\mu + n_\mu/\mathrm{K}. \tag{5.106}$$

For the oscillator part, since the Hamiltonian is the same as the oscillator part for the compact boson, the

partition function is exactly the same as the free boson case presented above. Thus we have

$$\begin{aligned} Z_{osc} &= Z_{s_2=0} Z_{s_2\neq 0} \\ &= \left|\frac{1}{\eta(\tau)}\right|^2 \prod_{s_2\in\mathbb{Z}^+} \Theta^{-1}_{[\beta s_2, \gamma s_2]}\left(\tau, \frac{R_1}{R_2} s_2\right). \end{aligned} \tag{5.107}$$

The total partition function for each sector is $\mathcal{Z}^{n_0 n_1 n_2} = Z^{n_0 n_1 n_2} Z_{osc}$.

Although the surface theory of the (3+1)d BF theory resembles the compactified free boson discussed in the previous section, these theories are physically different. For the compactified boson, the partition function is invariant under the $\mathcal{S}$ and $\mathcal{T}$ modular transformations: It is anomaly-free and a well-defined theory on the $(2+1)$d spacetime torus. On the other hand, for the surface theory, the partition function for each sector is not modular invariant and thus it is not a well-defined theory on the (2+1)d torus. It should be regarded as the boundary theory of a higher-dimensional topological phase. There are K^3 sectors determined by three quantum number $n_{0,1,2}$ and they form a complete basis under S and T modular transformations, as we will show now.

Under M transformation, quantum numbers are transformed as

$$M: \begin{cases} N_1 + \frac{n_1}{\mathrm{K}} \\ N_2 + \frac{n_2}{\mathrm{K}} \\ N_0 + \frac{n_0}{\mathrm{K}} \end{cases} \to \begin{cases} -N_2 - \frac{n_2}{\mathrm{K}} \\ N_1 + \frac{n_1}{\mathrm{K}} \\ N_0 + \frac{n_0}{\mathrm{K}} \end{cases} \tag{5.108}$$

To discuss U_1' transformation, we use the Poisson resummation to rewrite the summation over N_0 and N_1 in $Z^{n_0 n_1 n_2}$ and rewrite the zero-mode partition function as

$$\begin{aligned} Z^{n_0 n_1 n_2} = \frac{1}{\mathrm{K}|\tau|} \sum_{N_2, M_{0,1}\in\mathbb{Z}} \exp\Bigg\{ &- \frac{\pi\tau_2}{2r^2 R_2 |\tau|^2} M_1^2 - \frac{2r^2\pi R_2 \tau_2}{|\tau|^2}\left[\frac{M_0}{\mathrm{K}} - \gamma\tilde{N}_2\right]^2 - \frac{2\pi r^2 R_0 R_1}{R_2}\tilde{N}_2^2 \\ &- \frac{2\pi i \tau_1 \mathrm{K}}{|\tau|^2}\frac{M_1}{\mathrm{K}}\left[\frac{M_0}{\mathrm{K}} - \gamma\tilde{N}_2\right] + 2\pi i\beta\tilde{N}_2 M_1 + \frac{2\pi i n_1}{\mathrm{K}} M_1 + \frac{2\pi i n_0}{\mathrm{K}} M_0 \Bigg\}. \end{aligned} \tag{5.109}$$

Let us introduce

$$M_1 := \mathrm{K}N_0' + n_{0,}', \quad M_0 := \mathrm{K}N_1' + n_1' \tag{5.110}$$

Then, the partition function can be written as

$$Z^{n_0n_1n_2} = \frac{1}{K|\tau|}\sum_{N_2,M_{0,}\in\mathbb{Z}}\sum_{n'_{0,1}\in\mathbb{Z}_{\mathrm{K}}}\exp\Bigg[-\frac{\pi\tau_2K^2}{2r^2R_2|\tau|^2}\tilde{N}_0'^2-\frac{2r^2\pi R_2\tau_2}{|\tau|^2}\left[\tilde{N}_1'-\gamma\tilde{N}_2\right]^2-\frac{2\pi r^2R_0R_1}{R_2}\tilde{N}_2^2$$
$$-\frac{2\pi i\tau_1\mathrm{K}}{|\tau|^2}\tilde{N}_0'\left[\tilde{N}_1'-\gamma\tilde{N}_2\right]+2\pi i\mathrm{K}\beta\tilde{N}_2\tilde{N}_0'+\frac{2\pi in_1n_0'}{\mathrm{K}}+\frac{2\pi in_0n_1'}{\mathrm{K}}\Bigg], \tag{5.111}$$

where $\sum_{n\in\mathbb{Z}_{\mathrm{K}}} := \sum_{n=0}^{\mathrm{K}-1}$. From these expressions, under U_1' transformation,

$$(U_1'\mathcal{Z})^{n_0n_1n_2} = \frac{1}{\mathrm{K}}\sum_{n'_{0,1}\in\mathbb{Z}_{\mathrm{K}}} e^{\frac{2\pi i}{\mathrm{K}}(n_0n_1'+n_1n_0')}\mathcal{Z}^{n_0'n_1'n_2}. \tag{5.112}$$

Combined with the M transformation, we can write down the modular $\mathcal{S}$ and $\mathcal{T}$ matrices:

$$\mathcal{S}_{n_i,n_i'} = \frac{1}{\mathrm{K}}\delta_{n_1,n_2'}e^{-\frac{2\pi i}{\mathrm{K}}(n_0'n_2-n_0n_1')},$$
$$\mathcal{T}_{n_i,n_i'} = \delta_{n_0,n_0'}\delta_{n_1,n_1'}\delta_{n_2,n_2'}e^{\frac{2\pi i}{\mathrm{K}}n_0n_1}. \tag{5.113}$$

This result is consistent with previous works, Refs. [Moradi and Wen, 2015, Jiang et al., 2014], and also [Wang and Wen, 2015], where the action of the modular transformations are calculated in the bulk. In terms of the bulk physics, the $\mathcal{S}$ matrix describes the braiding phase between particle and loop excitations, whereas the $\mathcal{T}$ matrix encodes information related to $(3+1)$d analogue of topological spins. [Moradi and Wen, 2015] (See also Refs.[Wang and Levin, 2015, Wang and Levin, 2014, Lin and Levin, 2015, Jian and Qi, 2014].) The exact agreement between the $\mathcal{S}$ and $\mathcal{T}$ matrices calculated in the bulk and the boundary suggests there is one-to-one correspondence, the bulk-boundary correspondence in (3+1)d.

The computed $\mathcal{S}$ and $\mathcal{T}$ matrices (5.113) are expected to be consistent with the algebraic relations in Eq. (5.27): As in (1+1)d CFTs, together with the charge conjugation matrix $\mathcal{C}$, $\mathcal{S}$ and $\mathcal{T}$ matrices should obey essentially the same algebraic relations as Eq. (5.27). Assuming the charge conjugation matrix is unity, $\mathcal{C}=1$, we have checked, for the case of $\mathrm{K}=2,3,4,5$, the $\mathcal{S}$ and $\mathcal{T}$ matrices satisfy all the above constraints except the last equation in Eq. (5.27).

Before we leave this section, as we have done in the previous section, it is instructive to dimensionally reduce the partition functions of the surface theory of the (3+1)d BF theory. For each given sector, after

dimensional reduction, the partition function is given by

$$\begin{aligned}\mathcal{Z}^{n_0,n_1} = \frac{1}{|\eta(\tau)|^2}\sum_{N_{0,1}\in\mathbb{Z}} \exp\Big\{ & -\pi\tau_2 \mathrm{K}\left(N_0+\frac{n_0}{\mathrm{K}}\right)^2 \\ & -\pi\tau_2\mathrm{K}\left(N_1+\frac{n_1}{\mathrm{K}}\right)^2 \\ & +2\pi i\tau_1\mathrm{K}\left(N_0+\frac{n_0}{\mathrm{K}}\right)\left(N_1+\frac{n_1}{\mathrm{K}}\right)\Big\}. \end{aligned} \tag{5.114}$$

Here, we made a convenient choice $\lambda_1 = 1/\mathrm{K}$, i.e., $2\mathrm{r}^2 = \mathrm{K}$. This is the same as the character of the edge theory of the (2+1)d $\mathbb{Z}_\mathrm{K}$ gauge theory in its topological phase. The effective Lagrangian density of the edge CFT is by

$$\mathcal{L} = \frac{1}{4\pi}\partial_t\vec{\Phi}^T\mathbf{K}\partial_x\vec{\Phi} - \partial_x\vec{\Phi}^T\mathbf{V}\partial_x\vec{\Phi}, \tag{5.115}$$

where $\mathbf{K} = \mathrm{K}\sigma_x$ and $\mathbf{V}$ is a symmetric and positive definite matrix that accounts for the interaction on the edge and is non-universal. The characters defined in Eq. (5.114) can be simplified as

$$\chi_{ab}(\tau) = \frac{1}{|\eta(\tau)|^2}\sum_{s,t} q^{\frac{1}{4\mathrm{K}}(\mathrm{K}s+a+\mathrm{K}t+b)^2}\bar{q}^{\frac{1}{4\mathrm{K}}(\mathrm{K}s+a-\mathrm{K}t-b)^2} \tag{5.116}$$

where $a = n_0$ and $b = n_1$. There are K^2 characters in total. Under the $\mathcal{S}$ and $\mathcal{T}$ modular transformations, they are transformed as

$$\begin{aligned}\chi_{ab}(\tau+1) &= e^{2\pi i\frac{ab}{\mathrm{K}}}\chi_{ab}(\tau), \\ \chi_{ab}(-1/\tau) &= \frac{1}{\mathrm{K}}\sum_{a',b'}\chi_{a'b'}(\tau)e^{-2\pi i\frac{a'b+b'a}{\mathrm{K}}}. \end{aligned} \tag{5.117}$$

5.3.4 Entropy of the boundary theory

In this section, we compute the thermal entropy

$$S_T := \frac{d}{dT}\left[T\ln\chi_a\right], \tag{5.118}$$

obtained from the partition functions of the boundary theory discussed above. Here, χ_a is the partition function in the sector labeled by $a = (n_0, n_1, n_2)$, and

$$1/T = 2\pi R_0 \tag{5.119}$$

is the inverse temperature.

While S_T is defined for a system with a real (physical) boundary, it is expected to carry information on the universal topological part of the entanglement entropy (the topological entanglement entropy). The latter is defined for the bulk system (the BF theory) defined on a manifold without a physical boundary, and obtained by integrating out (tracing over) a subregion B (compliment to, say, subregion A). [Kitaev and Preskill, 2006, Fendley et al., 2007, Cappelli and Viola, 2011, Qi et al., 2012]

We are interested in the entropy S_T in the limit $R_1/R_0 \to \infty$ and $R_1/R_2 \to \infty$. (We could also equivalently take the limit with R_1 and R_2 exchanged, in which case, we have to resum differently but the result would be the same.) To evaluate the entropy in this limit, we first make use of the $\mathcal{S}$-modular transformation, [Affleck and Ludwig,] and write

$$S_T = \frac{d}{dT}\left[T \ln\left(\mathcal{S}_a^b \chi_b(-1/\tau)\right)\right]. \tag{5.120}$$

In the above limit, only the identity character gives rise to the dominant contribution, $\lim_{R_1/R_0\to\infty, R_1/R_2\to\infty} \chi_a(\tau) = \mathcal{S}_a^0 \chi_0(-1/\tau)$, as seen from Eq. (5.111). Hence

$$S_T|_{R_1/R_0\to\infty, R_1/R_2\to\infty} = \frac{d}{dT}\left[T \ln\left(\mathcal{S}_a^0 \chi_0\right)\right]. \tag{5.121}$$

Then using the modular $\mathcal{S}$ matrix computed in the previous section,

$$\begin{aligned} S_T|_{R_1/R_0\to\infty, R_1/R_2\to\infty} &= \frac{d}{dT}\left[T \ln\left(\frac{1}{\mathrm{K}}\chi_0\right)\right] \\ &= -\ln \mathrm{K} + \frac{d}{dT}\left[T \ln \chi_0\right]. \end{aligned} \tag{5.122}$$

The first term is the subleading term, and identical to the bulk topological entanglement entropy, although S_T and the entanglement entropy are defined differently. The second term is the extensive piece, which basically corresponds to the entropy of the free boson and is the usual leading order term. (When S_T is interpreted as the entanglement entropy, the second term corresponds to the area law term.)

5.4 The surface theory of the $(3+1)$d BF theory with the Θ term

Recall that in the surface theory of the BF theory discussed in the previous section, there are three quantum numbers $M_{0,1,2}$, which we wrote in terms of their non-fractional and fractional parts as

$$M_\mu = N_\mu + \frac{n_\mu}{\mathrm{K}}, \quad \mu = 0, 1, 2. \tag{5.123}$$

These quantum numbers in the surface theory can be interpreted as arising from the presence of bulk quasi-particles or quasi-vortices; $M_{1,2}$ represents the fractional winding number of the φ field induced by a bulk quaxi-vortex, whereas M_0 represents a fractionalized flux threading the surface induced by a bulk quasi-particle.

In this section, we consider the following "twist" of the quantum number

$$\begin{aligned} M_0 &\to M_0 + \frac{Q_1 M_2 - Q_2 M_1}{\mathrm{K}} \\ &= M_0 + \frac{Q \times M}{\mathrm{K}}, \end{aligned} \tag{5.124}$$

in the surface theory of the BF theory, where $Q_{1,2}$ are fixed integers, and we have introduced the notation

$$Q \times M := Q_1 M_2 - Q_2 M_1. \tag{5.125}$$

This twist can be induced by considering a modification of the BF theory by introducing the Θ term (axion term). In the next section, we will consider a similar twist to discuss three-loop braiding statistics.

5.4.1 The BF theory with the Θ-term in (3+1)d

We motivate the twist (5.124) by considering the following modification of the bulk BF theory by adding a Θ-term:

$$\begin{aligned} S_{bulk} = \int_{\mathcal{M}} \Big[&\frac{\mathrm{K}}{2\pi} b \wedge da - \frac{\mathrm{p}}{8\pi^2} d\Theta \wedge a \wedge da \\ &- a \wedge J_{qp} - b \wedge J_{qv} \Big]. \end{aligned} \tag{5.126}$$

In the second term (the-Θ term or axion term), p is a parameter, specific value of which will be discussed later, Θ is a non-dynamical background field, and we consider an inhomogeneous but time-independent configuration of Θ, which will be specified later. Compared to the standard form of the Θ term, $\Theta da \wedge da$,

we have done an integration by part and put the derivative acting on Θ. Since the Θ field is non-dynamical, we will interpret the presence of the Θ term as an introduction of a static *defect*. In Ref.[Lopes et al., 2015], a similar effective action has been proposed to describe the thermal and gravitational response of topological defects in superconducting topological insulators. [Chan et al., 2013] We also note that the BF theory with the Θ-term, $\Theta da \wedge da$, has been proposed to describe the fermonic and bosonic topological insulators. In Ref.[Jian and Qi, 2014], the BF theory with the Θ term was used to discuss three-loop braiding processes.

To see the Θ-term induces the twist (5.124), we assume the following configuration of the Θ-field:

$$\Theta(x, y, z) = \frac{Q_1 x}{R_1} + \frac{Q_2 y}{R_2}. \tag{5.127}$$

where $Q_{1,2}$ are fixed integers. From the equation of motion,

$$\begin{aligned} &\frac{\mathrm{K}}{2\pi}\varepsilon^{\mu\nu\lambda\rho}\partial_\lambda a_\rho = j^{\mu\nu}_{qv}, \\ &\frac{\mathrm{K}}{4\pi}\varepsilon^{\mu\nu\lambda\rho}\partial_\nu b_{\lambda\rho} + \frac{\mathrm{p}}{4\pi^2}\varepsilon^{\mu\nu\lambda\rho}\partial_\nu\Theta\partial_\lambda a_\rho = j^{\mu}_{qp}. \end{aligned} \tag{5.128}$$

By plugging the first equation into the second, these equations of motion reduce to

$$\begin{aligned} &\frac{\mathrm{K}}{2\pi}\varepsilon^{\mu\nu\lambda\rho}\partial_\lambda a_\rho = j^{\mu\nu}_{qv}, \\ &\frac{\mathrm{K}}{4\pi}\varepsilon^{\mu\nu\lambda\rho}\partial_\nu b_{\lambda\rho} = -\frac{\mathrm{p}}{2\pi\mathrm{K}}\partial_\nu\Theta j^{\mu\nu}_{qv} + j^{\mu}_{qp}. \end{aligned} \tag{5.129}$$

In the presence of quasiparticle and quasivortex sources, (5.65) and (5.69), the equations of motion integrated over space are

$$\begin{aligned} &\frac{\mathrm{K}}{2\pi}\int dydz\,\varepsilon^{01ij}\partial_i a_j = M_1, \\ &\frac{\mathrm{K}}{2\pi}\int dxdz\,\varepsilon^{02ij}\partial_i a_j = M_2, \\ &\frac{\mathrm{K}}{4\pi}\int_\Sigma d^3x\,\varepsilon^{0ijk}\partial_i b_{jk} = -\frac{\mathrm{p}}{\mathrm{K}}Q_i M_i + N_0, \end{aligned} \tag{5.130}$$

where $M_{1,2}, N_0 \in \mathbb{Z}$ and we noted

$$\partial_i\Theta\int d^3x\, j^{0i}_{qv} = \frac{Q_i}{R_i}M_i \times (2\pi R_i) = 2\pi Q_i M_i \tag{5.131}$$

(i is not summed over). These can be reduced to, by using Stokes' theorem,

$$\begin{aligned}
&\int dy \partial_y \varphi = \frac{2\pi}{\mathrm{K}} N_2, \\
&\int dx \partial_x \varphi = \frac{2\pi}{\mathrm{K}} N_1, \\
&\int d^2x \, \epsilon_{ij} \partial_i \zeta_j = \frac{2\pi}{\mathrm{K}} N_0 + \frac{2\pi \mathrm{p}}{\mathrm{K}^2} (Q \times N),
\end{aligned} \tag{5.132}$$

where $M_1 = -N_2$ and $M_2 = N_1$. Hence, upon choosing $\mathrm{p} = 1$, in the presence of the defect field Θ, the quantum number N_0 in the surface theory is "twisted" as in Eq. (5.124).

We observe that the following action

$$\begin{aligned}
S'_{bulk} = &\int d^4x \, \frac{\mathrm{K}}{4\pi} \varepsilon^{\mu\nu\lambda\rho} \partial_\nu b_{\lambda\rho} a_\mu \\
&- j^\mu_{qp} a_\mu - j^{\mu\nu}_{qv} \frac{1}{2} \left[b_{\mu\nu} - \frac{\mathrm{p}}{2\pi \mathrm{K}} (a_\mu \partial_\nu \Theta - a_\nu \partial_\mu \Theta) \right]
\end{aligned} \tag{5.133}$$

shares the same equations of motion, Eq. (5.129), as the BF theory with Θ terms, (5.126). Hence, the boundary theory derived from S'_{bulk} has the same quantization rules of the zero modes as the boundary theory of S_{bulk}. In the next section, we will consider the boundary theory derived from S'_{bulk}, and its partition functions.

To contrast the two theories S_{bluk} and S'_{bulk}, we note, in S_{bulk}, that the coupling to the currents are "normal" while the commutators are "abnormal", in the sense that the commutators among fields a, b are modified due to the presence of the theta term. On the other hand, in S'_{bulk}, the commutators are normal (the same as the ordinary BF theory) while the coupling to the current is "abnormal". (Since that the commutators are the same as the ordinary BF theory, S'_{bulk} and the corresponding boundary theory can be analyzed in a complete parallel with the BF theory – a practical reason why we will consider on S'_{bulk} in the following – expect for the zero mode part.)

In spite of these differences, these theories lead to the same quantization conditions (the same "lattice" of quantum numbers) of zero modes. To see how this is possible, we note that the quantization rule of the zero modes are determined both by (a) the canonical commutation relations and (b) the compactification conditions. The compactification condition is determined by declaring physically observable Wilson loop operators. This in term is determined from the coupling of the theory to the current. Therefore, in the original theory, (a) is abnormal but (b) is normal. In the modified theory, (a) is normal but (b) is abnormal. In the next section, we demonstrate this by deriving the quantization conditions (5.132), derived from the bulk point of view here, in terms of the boundary theory of S'_{bulk}.

5.4.2 The surface theory and partition functions

The compactification conditions and quantization rules

We now proceed to consider the surface theory of the bulk theory (5.133). Without sources, the surface theory is described by the same Lagrangian density as the surface of the BF theory, (5.72), and hence has the same canonical commutation relations. This immediately means that the oscillator part of the surface theory can be treated in exactly the same as before. On the other hand, reflecting the abnormal coupling of the gauge fields to the currents in the bulk action S'_{bulk}, the compactification conditions of the boundary fields φ and ζ are modified, as we will now discuss.

As we noted earlier, the coupling to the current can be written, e.g., $\int d^4x\, j^\mu_{qp} a_\mu = \oint_L a$. Thus, introducing a proper current corresponds to introducing a Wilson loop. If we now consider a Wilson line L that is spatial, and that ends at the boundary,

$$\int_L a = \int_L d\varphi = \int_{\partial L} \varphi = \varphi(\partial L) \tag{5.134}$$

where we noted ∂L is a point, and we have used the solution to the Gauss law constraint, $a_a = \partial_a \varphi$ $(a = 1, 2, 3)$. Thus,

$$\exp im \int_L a = \exp\left[im\varphi(\partial L)\right] \tag{5.135}$$

This means that φ is compactified with the radius 2π.

Let us repeat the same exercise for the coupling to the quasivortex current:

$$\begin{aligned} &\int d^4x\, j^{\mu\nu}_{qv} \frac{1}{2}\left[b_{\mu\nu} - \frac{\mathrm{p}}{2\pi\mathrm{K}}(a_\mu \partial_\nu \Theta - a_\nu \partial_\mu \Theta)\right] \\ &= \int_S \left[b - \frac{\mathrm{p}}{2\pi\mathrm{K}} a \wedge d\Theta\right], \end{aligned} \tag{5.136}$$

where S is the world surface of a quasivortex (quasivortices). In the presence of a boundary and using $b = d\zeta$, this is evaluated as

$$= \int_S \left[d\zeta - \frac{\mathrm{p}}{2\pi\mathrm{K}} d\varphi \wedge d\Theta\right] = \int_{\partial S} \left[\zeta - \frac{\mathrm{p}}{2\pi\mathrm{K}} \varphi \wedge d\Theta\right] \tag{5.137}$$

where the boundary of the world sheet is on the surface. We thus have a Wilson line on the surface:

$$\exp im \int_{\partial S} \left[\zeta - \frac{\mathrm{p}}{2\pi \mathrm{K}} \varphi \wedge d\Theta\right] \tag{5.138}$$

We now consider the case where ∂S is along the x- or y- cycles. Recalling the mode expansion Eq. (5.81), and noting $(\mathrm{p}/2\pi\mathrm{K}) \int_{L_i} \varphi d\Theta = (\mathrm{p}/\mathrm{K})\alpha_0 Q_i$ the zero modes enter into the integral $\int_{\partial S} \left[\zeta - \frac{\mathrm{p}}{2\pi \mathrm{K}} \varphi \wedge d\Theta\right]$ through the following combinations

$$\alpha_1 - \frac{\mathrm{p}}{\mathrm{K}} Q_1 \alpha_0, \quad \alpha_2 - \frac{\mathrm{p}}{\mathrm{K}} Q_2 \alpha_0. \tag{5.139}$$

Together with α_0, the following three linear combinations

$$v^a_\mu \alpha_\mu, \quad a = 0, 1, 2 \tag{5.140}$$

are angular variables, where

$$\begin{aligned} v^0 &= (1, 0, 0)^T, \\ v^1 &= \left(-\frac{\mathrm{p}Q_1}{\mathrm{K}}, 1, 0\right)^T, \quad v^2 = \left(-\frac{\mathrm{p}Q_2}{\mathrm{K}}, 0, 1\right)^T. \end{aligned} \tag{5.141}$$

Noting the commutation relations among zero modes,

$$[\alpha_0, \beta_0] = [\alpha_1, -\beta_2] = [\alpha_2, \beta_1] = \frac{i}{\mathrm{K}}, \tag{5.142}$$

we consider the linear combinations

$$w^\mu_a \bar{\beta}_\mu, \quad \bar{\beta} = (\beta_0, -\beta_2, \beta_1), \quad a = 0, 1, 2, \tag{5.143}$$

where w^a are translation vectors reciprocal to v^a:

$$w^\mu_a v^b_\mu = \delta^a_b. \tag{5.144}$$

Explicitly, they are given by

$$w_0 = \left(1, \frac{\mathrm{p}Q_1}{\mathrm{K}}, \frac{\mathrm{p}Q_1}{\mathrm{K}}\right), \ w_1 = (0, 1, 0), \ w_2 = (0, 0, 1). \tag{5.145}$$

Then, in the "rotated" basis, the commutation relation takes the following canonical form:

$$[v_\mu^a \alpha_\mu, w_b^\nu \bar{\beta}_\nu] = \frac{i}{\mathrm{K}} v_\mu^a w_b^\mu = \frac{i}{\mathrm{K}} \delta_b^a. \tag{5.146}$$

Due to the compacticity of $v_\mu^a \alpha_\mu$, $w_b^\nu \bar{\beta}_\nu$ takes on values

$$w_b^\nu \bar{\beta}_\nu = \frac{1}{\mathrm{K}} \times m_b, \quad m_{b=1,2,3} \in \mathbb{Z}. \tag{5.147}$$

Inverting this relation,

$$\bar{\beta}_\mu = \frac{1}{\mathrm{K}} u_\mu^a m_a, \quad u_\nu^a w_a^\mu = \delta_\nu^\mu \tag{5.148}$$

where

$$\begin{aligned} u_0 &= (1,0,0)^T, \\ u_1 &= \left(\frac{-\mathrm{p}Q_1}{\mathrm{K}}, 1, 0\right)^T, \quad u_2 = \left(\frac{-\mathrm{p}Q_2}{\mathrm{K}}, 0, 1\right)^T. \end{aligned} \tag{5.149}$$

Renaming the integers as $m_0 \to N_0$, $m_1 \to -N_2$, and $m_2 \to N_1$, Eq. (5.148) is nothing but the quantization rule (5.132).

The partition functions

With the twist (5.124), we can now write down the zero mode partition function. Let us recall the partition function of the BF surface without the theta term, $Z^{n_0 n_1 n_2}$, defined in Eq. (5.105). For later use, we write $Z^{n_0 n_1 n_2}$ as

$$\begin{aligned} Z^{n_0 n_1 n_2} &= \sum_{N_{0,1,2} \in \mathbb{Z}} f_{\mathrm{K}}\left(M_0, M_i\right) \\ &= \sum_{N_{0,1,2} \in \mathbb{Z}} f_{\mathrm{K}}\left(\mathrm{K}N_0 + n_0, \mathrm{K}N_i + n_i\right), \end{aligned} \tag{5.150}$$

where f_{K} is defined by the summand in Eq. (5.105), and recall $M_\mu = \mathrm{K}N_\mu + n_\mu$. We will call the partition function resulting from the twist $Z_{Q_1 Q_1}^{n_0 n_1 n_2}$. It is given by

$$Z_{Q_1 Q_2}^{n_0 n_1 n_2} = \sum_{N_{0,1,2} \in \mathbb{Z}} f_{\mathrm{K}}\left(\mathrm{K}N_0 + n_0 + \frac{Q \times M}{\mathrm{K}}, \mathrm{K}N_i + n_i\right). \tag{5.151}$$

To proceed, we write

$$\begin{aligned} M_i &= \mathrm{K}N_i + n_i = \mathrm{K}^2\bar{N}_i + \mathrm{K}t_i + n_i, \\ Q_i &= \mathrm{K}R_i + r_i = \mathrm{K}^2\bar{R}_i + \mathrm{K}s_i + r_i, \end{aligned} \tag{5.152}$$

where new integers $\bar{N}_i, \bar{R}_i, R_i$ and $\mathbb{Z}_{\mathrm{K}}$ variables t_i, s_i, r_i are introduced. In the following, we will show that the zero mode partition function depends on Q_i only through r_i, and hence can be denoted as $Z^{n_0 n_1 n_2}_{r_1 r_2}$, and that the partition function can be written as

$$Z^{n_0 n_1 n_2}_{r_1 r_2} = \sum_{t_{1,2} \in \mathbb{Z}_{\mathrm{K}}} X^{\bar{n}_0 \bar{n}_1 \bar{n}_2}, \tag{5.153}$$

where we have introduced

$$\begin{aligned} &\underline{\mathrm{n}}_0 := n_0 + s \times n + r \times t \mod \mathrm{K}, \\ &\begin{cases} \bar{n}_0 := \mathrm{K}\underline{\mathrm{n}}_0 + (r \times n) \\ \bar{n}_1 := \mathrm{K}t_1 + n_1 \\ \bar{n}_2 := \mathrm{K}t_2 + n_2, \end{cases} \end{aligned} \tag{5.154}$$

(i.e., $\underline{\mathrm{n}}_0 = (n_0 + s \times n + r \times t)\%\mathrm{K}$) and $X^{\bar{n}_0 \bar{n}_1 \bar{n}_2}$ is defined by

$$X^{\bar{n}_0 \bar{n}_1 \bar{n}_2} := \sum_{A_0, \bar{N}_{1,2} \in \mathbb{Z}} f_{\mathrm{K}}\left(\mathrm{K}A_0 + \frac{\bar{n}_0}{\mathrm{K}}, \mathrm{K}^2\bar{N}_i + \bar{n}_i\right). \tag{5.155}$$

To show Eq. (5.153), we start by writing the partition function in terms of variables introduced in Eq. (5.152):

$$\begin{aligned} Z^{n_0 n_1 n_2}_{Q_i = \mathrm{K}^2\bar{R}_i + \mathrm{K}s_i + r_i} &= \sum_{N_0, \bar{N}_{1,2} \in \mathbb{Z}} \sum_{t_{1,2} \in \mathbb{Z}_{\mathrm{K}}} \\ &\times f_{\mathrm{K}}\left(\mathrm{K}N_0 + n_0 + \frac{Q \times M}{\mathrm{K}}, \mathrm{K}^2\bar{N}_i + \mathrm{K}t_i + n_i\right). \end{aligned} \tag{5.156}$$

By further introducing

$$\begin{aligned} a_0 &= n_0 + s \times n + r \times t, \\ A_0 &= N_0 + (\mathrm{K}\bar{R} + s) \times N + \bar{R} \times n + r \times \bar{N}, \end{aligned} \tag{5.157}$$

and noting the equality

$$\mathrm{K}N_0 + n_0 + \frac{Q \times M}{\mathrm{K}} = \mathrm{K}A_0 + a_0 + \frac{r \times n}{\mathrm{K}} \tag{5.158}$$

Then,

$$\begin{aligned} Z^{n_0 n_1 n_2}_{Q_i = \mathrm{K}^2 \bar{R}_i + \mathrm{K}s_i + r_i} = & \sum_{N_0, \bar{N}_{1,2} \in \mathbb{Z}} \sum_{t_{1,2} \in \mathbb{Z}_{\mathrm{K}}} \\ & \times f_{\mathrm{K}} \left(\mathrm{K}A_0 + a_0 + \frac{r \times n}{\mathrm{K}}, \mathrm{K}^2 \bar{N}_i + \mathrm{K}t_i + n_i \right). \end{aligned} \tag{5.159}$$

We now fix $t_{1,2}$ and consider

$$\begin{aligned} X^{n_0 n_1 n_2, t_1 t_2}_{Q_i = \mathrm{K}^2 \bar{R}_i + \mathrm{K}s_i + r_i} = & \sum_{N_0, \bar{N}_{1,2} \in \mathbb{Z}} \\ & \times f_{\mathrm{K}} \left(\mathrm{K}A_0 + a_0 + \frac{r \times n}{\mathrm{K}}, \mathrm{K}^2 \bar{N}_i + \mathrm{K}t_i + n_i \right). \end{aligned} \tag{5.160}$$

Note that once $t_{1,2}$ are fixed, a_0 is fixed. Converting the summation over N_0 to a summation over A_0,

$$\begin{aligned} X^{n_0 n_1 n_2, t_1 t_2}_{Q_i = \mathrm{K}^2 \bar{R}_i + \mathrm{K}s_i + r_i} = & \sum_{A_0, \bar{N}_{1,2} \in \mathbb{Z}} \\ & \times f_{\mathrm{K}} \left(\mathrm{K}A_0 + a_0 + \frac{r \times n}{\mathrm{K}}, \mathrm{K}^2 \bar{N}_i + \mathrm{K}t_i + n_i \right). \end{aligned} \tag{5.161}$$

Note that the s and n_0 dependence of the right hand side comes only from a_0. Also, after converting the sum $\sum_{N_0} \to \sum_{A_0}$, the $\bar{R}_i$ dependence is gone. So, we write $X^{n_0 n_1 n_2, t_1 t_2}_{Q_i = \mathrm{K}^2 \bar{R}_i + \mathrm{K}s_i + r_i}$ simply as $X^{a_0 n_1 n_2, t_1 t_2}_{r_i}$. Observe that $X^{n_0 n_1 n_2, t_1 t_2}_{Q_i = \mathrm{K}^2 \bar{R}_i + \mathrm{K}s_i + r_i}$ appears to depend on nine $\mathbb{Z}_{\mathrm{K}}$-valued parameters, $n_{0,1,2}, t_{1,2}, s_{1,2}, r_{1,2}$ After the reorganization we have just done, we lost $s_{1,2}$, and we now only have six $\mathbb{Z}_{\mathrm{K}}$ parameters, $n_{1,2}, t_{1,2}, r_{1,2}$ and a_0. While a_0 is not $\mathbb{Z}_{\mathrm{K}}$-valued, we can shift a_0 such that

$$a_0 = \mathrm{K} \times (\text{integer}) + [a_0] \tag{5.162}$$

where the second term takes values $0, \ldots \mathrm{K} - 1$. Then,

$$\begin{aligned} X^{[a_0] n_1 n_2, t_1 t_2}_{r_1 r_2} = & \sum_{A_0, \bar{N}_{1,2} \in \mathbb{Z}} \\ & \times f_{\mathrm{K}} \left(\mathrm{K}A_0 + [a_0] + \frac{r \times n}{\mathrm{K}}, \mathrm{K}^2 \bar{N}_i + \mathrm{K}t_i + n_i \right). \end{aligned} \tag{5.163}$$

Observing that $X_{r_1 r_2}^{[a_0] n_1 n_2, t_1 t_2}$ depends on $[a_0], n_{1,2}, t_{1,2}$ only through $\bar{n}_{0,1,2}$ defined in Eq. (5.163), rewriting Eq. (5.163) in terms of $\bar{n}_{0,1,2}$ completes the derivation of Eq. (5.153).

Modular transformations

We now discuss the modular properties of the partition functions. Under the U_2 transformation, the zero-mode partition functions are transformed according to

$$(U_2 X)^{\bar{n}_0 \bar{n}_1 \bar{n}_2} = e^{-\frac{2\pi i}{\mathrm{K}^2} \bar{n}_0 \bar{n}_1} X^{\bar{n}_0 \bar{n}_1 \bar{n}_2}. \tag{5.164}$$

On the other hand, under the U_1' transformation, the partition functions are transformed as

$$(U_1' X)^{\bar{n}_0 \bar{n}_1 \bar{n}_2} = \frac{1}{|\tau| \mathrm{K}^2} \sum_{\bar{n}_{0,1}', \bar{r}_{0,1}'} e^{\frac{2\pi i}{\mathrm{K}^2} (\bar{n}_0 \bar{n}_1' + \bar{n}_1 \bar{n}_0')} X^{\bar{n}_0' \bar{n}_1' \bar{n}_2} \tag{5.165}$$

where $\bar{n}_0' \equiv \mathrm{K} \underline{\mathrm{n}}_0' + r_1' n_2 - r_2' n_1'$.

Observe that, upon the U_1' transformation, partition functions with new parameters r_1' and r_2' generated. Since r_1 and r_2 are the given quantum numbers from the Θ term, the action of modular transformations is not closed.

5.5 Coupling two BF theories – three-loop braiding statistics

In the twist (5.124), the integers $Q_{1,2}$ are fixed and treated as a background. I.e., Θ is a non-dynamical field. We have seen that the surface partition functions do not form a complete basis under modular transformations. To circumvent this issue, one may consider to treat Q_1 and Q_2 as dynamical variables, which may come from another copy of the BF theory. In this section, we will discuss two copies of the BF surface theories which are coupled via cubic terms.

Let us start from two decoupled copies of the BF surface theories. Let $M_{0,1,2}$ and $Q_{0,1,2}$ label different twisted sectors of the first and second copy, respectively. We consider to twist these quantum numbers by

$$\begin{aligned} M_0 &\to M_0 + \frac{Q \times M}{\mathrm{K}}, \\ Q_0 &\to Q_0 + \frac{M \times Q}{\mathrm{K}}. \end{aligned} \tag{5.166}$$

Here, unlike Eq. (5.124), both M and Q are dynamical variables.

In the next section, we start by introducing an (3+1)d bulk field theory, Eq. (5.167), or its alternative

form (5.173), which realizes precisely the twist (5.166). We will analyze the modular properties of the resulting zero mode partition functions at the surface. The oscillator part of the partition function is simply given by the partition function of the two decoupled copies of free boson theories. By computing the $\mathcal{S}$ and $\mathcal{T}$ matrices acting on the zero mode partitions, we argue that the action (5.167) realizes three loop braiding statistics.

5.5.1 The bulk field theory

The cubic theory Let us motivate the twist (5.166). We propose to work with the following bulk action:

$$\begin{aligned} S_{bulk} = \int_{\mathcal{M}} \Big[& \frac{\mathrm{K}}{2\pi} \delta_{IJ} b^I \wedge da^J \\ & + \frac{\mathrm{p}_1}{4\pi^2} a^1 \wedge a^2 \wedge da^2 + \frac{\mathrm{p}_2}{4\pi^2} a^2 \wedge a^1 \wedge da^1 \\ & - \delta_{IJ} b^I \wedge J^J_{qv} - \delta_{IJ} a^I \wedge J^J_{qp} \Big], \end{aligned} \tag{5.167}$$

where $I, J = 1, 2$ and $\mathrm{p}_{1,2}$ are, as the level K, constant parameters of the theory. Similar action has been discussed in Ref.[Kapustin and Thorngren, 2014, Wang et al., 2015, Wan et al., 2015, Ye and Gu, 2015]. The equations of motion are

$$\begin{aligned} & \frac{\mathrm{K}}{2\pi} da^I = J^I_{qv}, \\ & \frac{\mathrm{K}}{2\pi} db^1 + \frac{\mathrm{p}_1}{4\pi^2} a^2 \wedge da^2 \\ & \qquad - \frac{\mathrm{p}_2}{2\pi^2} a^2 \wedge da^1 + \frac{\mathrm{p}_2}{4\pi^2} da^2 \wedge a^1 = J^1_{qp}, \\ & \frac{\mathrm{K}}{2\pi} db^2 + \frac{\mathrm{p}_2}{4\pi^2} a^1 \wedge da^1 \\ & \qquad - \frac{\mathrm{p}_1}{2\pi^2} a^1 \wedge da^2 + \frac{\mathrm{p}_1}{4\pi^2} da^1 \wedge a^2 = J^2_{qp}. \end{aligned} \tag{5.168}$$

As in our previous discussion in the BF theory with and without the theta term, let us consider a fixed, static quasiparticle and quasivortex configuration and integrate the equation of motion over space. By solving the first equation of motion as $a^I = (2\pi/\mathrm{K})(d^{-1} J^I_{qv})$, plugging the solution to the second and the

third equations of motion, and integrating over space,

$$\begin{aligned}
\frac{\mathrm{K}}{2\pi}\int_\Sigma db^1 &= -\frac{\mathrm{p}_1}{\mathrm{K}^2}\int_\Sigma (d^{-1}J^2_{qv})\wedge J^2_{qv} \\
&\quad + \frac{\mathrm{p}_2}{\mathrm{K}^2}\int_\Sigma (d^{-1}J^2_{qv})\wedge J^1_{qv} + \int_\Sigma J^1_{qp}, \\
\frac{\mathrm{K}}{2\pi}\int_\Sigma db^2 &= -\frac{\mathrm{p}_2}{\mathrm{K}^2}\int_\Sigma (d^{-1}J^1_{qv})\wedge J^1_{qv} \\
&\quad + \frac{\mathrm{p}_1}{\mathrm{K}^2}\int_\Sigma (d^{-1}J^1_{qv})\wedge J^2_{qv} + \int_\Sigma J^2_{qp},
\end{aligned} \tag{5.169}$$

where note that in the static configurations considered here, J_{qv} is a delta function one form supporting a spatial loop, whereas J_{qp} is a delta function three form supporting a spatial point. Correspondingly, $d^{-1}J_{qv}$ is a delta function 0 form supporting a three dimensional manifold. The contributions to $\int_\Sigma db^I$ is coming from quasivortex loops, $\int_\Sigma (d^{-1}J^I_{qv})\wedge J^J_{qv}$, are given in terms of their linking number.

Considering now the specific geometry $\Sigma = D^2\times S^1$ with the boundary (surface) $\partial\Sigma = T^2$, we can derive the quantization rule of the zero modes of the boundary fields. Using the Gauss law constraint to write the boundary conditions in terms of φ^I and ζ^I, the bulk equations of motion translate in to

$$\begin{aligned}
&\frac{\mathrm{K}}{2\pi}\int_{S^1_i} d\varphi^1 = M_i, \quad \frac{\mathrm{K}}{2\pi}\int_{S^1_i} d\varphi^2 = Q_i, \\
&\frac{\mathrm{K}}{2\pi}\int_{\partial\Sigma} d\zeta^1 - \frac{\mathrm{p}_2}{4\pi^2}\int_{\partial\Sigma} d\varphi^2\wedge d\varphi^1 = M_0, \\
&\frac{\mathrm{K}}{2\pi}\int_{\partial\Sigma} d\zeta^2 - \frac{\mathrm{p}_1}{4\pi^2}\int_{\partial\Sigma} d\varphi^1\wedge d\varphi^2 = Q_0.
\end{aligned} \tag{5.170}$$

With $\mathrm{p}_1 = \mathrm{p}_2 = \mathrm{K}$, these correspond precisely to the twist (5.166).

Note that if we naively gauge transform as $b^I \to b^I + d\zeta^I$ and $a^I \to a + d\varphi^I$, we find that the theory is not gauge invariant. Moreover these gauge transformations are not generated by Gauss constraints. We propose the following alternate gauge transformations.

$$\begin{aligned}
b^1 \to b'^1 &= b^1 + d\zeta^1 - \frac{\mathrm{p}_2}{2\pi\mathrm{K}}\left(a^2\wedge d\varphi^1 + d\varphi^2\wedge a^1\right), \\
b^2 \to b'^2 &= b^2 + d\zeta^2 - \frac{\mathrm{p}_1}{2\pi\mathrm{K}}\left(a^1\wedge d\varphi^2 + d\varphi^1\wedge a^2\right), \\
a^I \to a'^I &= a^I + d\varphi^I.
\end{aligned} \tag{5.171}$$

Therefore the action with cubic term in Eq.(5.167) is gauge invariant. For the term coupling to the sources, by demanding the gauge invariance, we can get the new conservation law of currents.

On an open manifold, the action picks up a gauge anomaly on the boundary under these gauge transfor-

mations

$$
\begin{aligned}
S_{bulk}[b', a'] &= S_{bulk}[b, a] \\
&+ \frac{\mathrm{K}}{2\pi} \int_{\partial \mathcal{M}} \delta_{IJ} d\zeta^I \wedge a'^J \\
&+ \frac{1}{4\pi^2} \int_{\partial \mathcal{M}} \left(\mathrm{p}_1 d\varphi^1 \wedge d\varphi^2 \wedge a^2 + \mathrm{p}_2 d\varphi^2 \wedge d\varphi^1 \wedge a^1 \right).
\end{aligned} \tag{5.172}
$$

This anomaly then must be compensated by an appropriate boundary field theory.

The alternative quadratic theory Instead of tackling the cubic theory (5.167) and the corresponding surface theory, as in our discussion in the BF theory with theta term, we consider an alternative form of the theory. We note that the equations of motion (5.168) can be derived from the following alternative action:

$$
\begin{aligned}
S'_{bulk} = \frac{\mathrm{K}}{2\pi} \int \delta_{IJ} b^I \wedge da^J - \int \delta_{IJ} a^J \wedge J^I_{qp} \\
- \int \left[b^1 + \frac{\mathrm{p}_2}{2\pi \mathrm{K}} a^1 \wedge a^2 \right] \wedge J^1_{qv} \\
- \int \left[b^2 + \frac{\mathrm{p}_1}{2\pi \mathrm{K}} a^2 \wedge a^1 \right] \wedge J^2_{qv}.
\end{aligned} \tag{5.173}
$$

Unlike S_{bulk}, this theory is quadratic. Integrating over a^I and b^I, one obtains the effective action of the currents

$$
\int \mathcal{D}[a^I, b^I] e^{iS'_{bulk}} = e^{iS_{eff}} \tag{5.174}
$$

where

$$
\begin{aligned}
S_{eff} = -\frac{2\pi}{\mathrm{K}} \int (d^{-1} J^I_{qv}) \wedge J^I_{qp} \\
+ \left(\frac{2\pi}{\mathrm{K}} \right)^3 \mathrm{p}_1 \int (d^{-1} J^1_{qv}) \wedge (d^{-1} J^2_{qv}) \wedge J^2_{qv} \\
+ \left(\frac{2\pi}{\mathrm{K}} \right)^3 \mathrm{p}_2 \int (d^{-1} J^2_{qv}) \wedge (d^{-1} J^1_{qv}) \wedge J^1_{qv}.
\end{aligned} \tag{5.175}
$$

The first term in the effective action describes, as in the ordinary BF theory, the quasparticle-quasivortex braiding statistics while the second and third terms include interactions among three quasivortex lines.

From the coupling to the currents, we read off the Wilson loop and Wilson surface operators in the

theory:

$$\exp\left[im\int_L a^I\right], \quad \exp in\int_S\left[b^I+\frac{\mathrm{p}_{\bar{I}}}{2\pi\mathrm{K}}a^I\wedge a^{\bar{I}}\right], \tag{5.176}$$

where n and m are integers, L and S are arbitrary closed loop and surfaces, respectively, and we introduced the notation $\bar{1}=2$ and $\bar{2}=1$, and the repeated capital Roman indices are not summer over here. These operators (or rather their exponents) satisfy

$$\begin{aligned}\left[\textstyle\int_C a^I, \int_S B^J\right] &= \frac{2\pi i}{\mathrm{K}}\delta^{IJ}I(C,S),\\ \left[\textstyle\int_S B^I, \int_{S'} B^J\right] &= -\frac{2i\mathrm{p}_{\bar{J}}}{\mathrm{K}^2}\delta^{IJ}\textstyle\int_{S\#S'} a^{\bar{J}}+\frac{2i\mathrm{p}_{\bar{J}}}{\mathrm{K}^2}\delta^{I\bar{J}}\int_{S\#S'} a^J,\end{aligned} \tag{5.177}$$

where

$$B^I := b^I+\frac{\mathrm{p}_{\bar{I}}}{2\pi\mathrm{K}}a^I\wedge a^{\bar{I}}, \tag{5.178}$$

and as before the repeated capital Roman indices are not summed over. Note also the triple commutator among $\int_S B^I$ is computed as

$$\begin{aligned}&\left[\left[\textstyle\int_S B^I, \int_{S'} B^J\right], \int_{S''} B^K\right]\\ &\quad=\frac{4\pi\mathrm{p}_{\bar{J}}}{\mathrm{K}^3}\left(\delta^{IJ}\delta^{\bar{J}K}-\delta^{I\bar{J}}\delta^{JK}\right)I(S\#S',S'').\end{aligned} \tag{5.179}$$

To make a comparison between the cubic and quadratic theories, in the cubic theory, the canonical commutation relations differ from the ordinary BF theory, while they remain the same in the quadratic theory. In fact, in the cubic theory, the commutator among fields generates another field, $[b,b]\sim a$, schematically. On the other hand, the set of Wilson loop and surface operators in the cubic theory is conventional (i.e., identical to the ordinary BF theory) while it is modified in the quadratic theory as in (5.176). In spite of these differences, the algebra of Wilson loop and surface operators of the two theories appear to be identical. Therefore, we argue that the two theories are equivalent. In the following, we will proceed with the quadratic theory.

the quantization rule of the zero modes We now derive the compactification condition of the boundary fields from Eq.(5.176). In the presence of a boundary and using $b^I=d\zeta^I$ and $a^I=d\varphi^I$, the surface operators

reduce to

$$\begin{aligned}&\exp im\int_S\left[d\zeta^I+\frac{\mathrm{p}_{\bar{I}}}{2\pi\mathrm{K}}d\varphi^I\wedge d\varphi^{\bar{I}}\right]\\&=\exp im\int_{\partial S}\left[\zeta^I+\frac{\mathrm{p}_{\bar{I}}}{2\pi\mathrm{K}}\varphi^I\wedge d\varphi^{\bar{I}}\right]\end{aligned}\tag{5.180}$$

where the boundary of the world sheet is on the surface. We now consider the case where ∂S is along the x- or y- cycles on the surface. Recalling the mode expansion

$$\begin{aligned}\varphi^I(\mathsf{r})&=\alpha_0^I+\frac{\beta_1^I x}{R_1}+\frac{\beta_2^I y}{R_2}+\cdots,\\\zeta_j^I(\mathsf{r})&=\frac{\alpha_j^I}{2\pi R_j}+\frac{\beta_0^I}{2\pi R_1R_2}x\delta_{j,2}+\cdots,\end{aligned}\tag{5.181}$$

the zero modes enter into the integral $\int_{\partial S}[\zeta^I+(\mathrm{p}_{\bar{I}}/2\pi\mathrm{K})\varphi^I\wedge d\varphi^{\bar{I}}]$ through the combinations

$$\alpha_j^I+\frac{\mathrm{p}_{\bar{I}}}{\mathrm{K}}\alpha_0^I\beta_j^{\bar{I}}.\tag{5.182}$$

We thus conclude

$$v_\mu^{1a}\alpha_\mu^1,\quad v_\mu^{2a}\alpha_\mu^2,\tag{5.183}$$

are angular variables, where

$$\begin{aligned}v^{I0}&=(1,0,0)^T,\\v^{I1}&=(\mathrm{p}_{\bar{I}}\beta_1^{\bar{I}}/\mathrm{K},1,0)^T,\quad v^{I2}=(\mathrm{p}_{\bar{I}}\beta_2^{\bar{I}}/\mathrm{K},0,1)^T.\end{aligned}\tag{5.184}$$

The rest of the discussion is essentially identical to the analysis made in Sec. 5.4.2. We recall the commutation relations among zero modes

$$[\alpha_0^I,\beta_0^J]=[\alpha_1^I,-\beta_2^J]=[\alpha_2^I,\beta_2^J]=\frac{i}{\mathrm{K}}\delta_{IJ},\tag{5.185}$$

the following linear combinations of the zero modes are integer-valued

$$\mathrm{K}w_b^{I\nu}\bar{\beta}_\nu^I=m_b^I,\quad m_b^I\in\mathbb{Z},\tag{5.186}$$

where

$$w_0^I = \left(1, -\mathrm{p}_{\bar{I}}\beta_1^{\bar{I}}/\mathrm{K}, -p_{\bar{I}}\beta_2^{\bar{I}}/\mathrm{K}\right),$$
$$w_1^I = (0,1,0)\,, \quad w_2^I = (0,0,1)\,. \tag{5.187}$$

Inverting this relation, the eigenvalues are given by

$$\begin{aligned}
\mathrm{K}\beta_0^1 &= M_0 - \frac{\mathrm{p}_2}{\mathrm{K}}(Q\times M),\\
\mathrm{K}\beta_1^1 &= M_2, \quad \mathrm{K}\beta_2^1 = -M_1,\\
\mathrm{K}\beta_0^2 &= Q_0 - \frac{\mathrm{p}_1}{\mathrm{K}}(M\times Q),\\
\mathrm{K}\beta_1^2 &= Q_2, \quad \mathrm{K}\beta_2^2 = -Q_1,
\end{aligned} \tag{5.188}$$

where M_μ and Q_μ are integers.

5.5.2 The surface partition functions

With the twist (5.166), the two copies of the surface theories are coupled together. The partition functions are given by

$$Z^{n_0n_1n_2}_{r_1r_2} Z^{r_0r_1r_2}_{n_1n_2} \tag{5.189}$$

where, as before, we decompose the quantum numbers as

$$\begin{aligned}
M_\mu &= \mathrm{K}N_\mu + n_\mu, \quad n_\mu = 0,1,\ldots,\mathrm{K}-1, \quad N_\mu\in\mathbb{Z},\\
Q_\mu &= \mathrm{K}R_\mu + r_\mu, \quad r_\mu = 0,1,\ldots,\mathrm{K}-1, \quad R_\mu\in\mathbb{Z},
\end{aligned} \tag{5.190}$$

and noted, following the discussion in Sec. 5.4.2, the partition functions depend only on the fractional parts of M_μ/K and Q_μ/K. Following Sec. 5.4.2 further, we can write the partition functions as

$$Z^{n_0n_1n_2}_{r_1r_2} Z^{r_0r_1r_2}_{n_1n_2} = \sum_{t_{1,2},s_{1,2}\in\mathbb{Z}_\mathrm{K}} X^{\bar{n}_0\bar{n}_1\bar{n}_2} X^{\bar{r}_0\bar{r}_1\bar{r}_2}, \tag{5.191}$$

where

$$\begin{aligned}
&\underline{\mathrm{n}}_0 := n_0 + s \times n + r \times t \mod \mathrm{K},\\
&\underline{\mathrm{r}}_0 := r_0 + t \times r + n \times s \mod \mathrm{K},\\
&\begin{cases} \bar{n}_0 \equiv \mathrm{K}\underline{\mathrm{n}}_0 + (r \times n) \\ \bar{n}_1 \equiv \mathrm{K}t_1 + n_1 \\ \bar{n}_2 \equiv \mathrm{K}t_2 + n_2 \end{cases} \quad \begin{cases} \bar{r}_0 \equiv \mathrm{K}\underline{\mathrm{r}}_0 + (n \times r) \\ \bar{r}_1 \equiv \mathrm{K}s_1 + r_1 \\ \bar{r}_2 \equiv \mathrm{K}s_2 + r_2 \end{cases}
\end{aligned} \tag{5.192}$$

Under the U_2 transformation, the product $X^{\bar{n}_0\bar{n}_1\bar{n}_2}X^{\bar{r}_0\bar{r}_1\bar{r}_2}$ is invariant up to a phase,

$$\begin{aligned}
&(U_2X)^{\bar{n}_0\bar{n}_1\bar{n}_2}(U_2X)^{\bar{r}_0\bar{r}_1\bar{r}_2}\\
&= e^{-\frac{2\pi i}{\mathrm{K}}(\tilde{n}_0n_1+\tilde{r}_0r_1)-\frac{2\pi i}{\mathrm{K}^2}(r_1n_2-r_2n_1)(n_1-r_1)}X^{\bar{n}_0\bar{n}_1\bar{n}_2}X^{\bar{r}_0\bar{r}_1\bar{r}_2},
\end{aligned} \tag{5.193}$$

where we have introduced

$$\begin{aligned}
\tilde{n}_0 &\equiv \underline{\mathrm{n}}_0 - r_2t_1 + r_2s_1 \mod \mathrm{K},\\
\tilde{r}_0 &\equiv \underline{\mathrm{r}}_0 + n_2t_1 - n_2s_1 \mod \mathrm{K}.
\end{aligned} \tag{5.194}$$

For the above equation, if we write down the phase in terms of $\tilde{n}_0$ and $\tilde{r}_0$, it will be independent of t_i and s_i. In other words, for two different $X^{\bar{n}_0\bar{n}_1\bar{n}_2}X^{\bar{r}_0\bar{r}_1\bar{r}_2}$, if they have the same $\tilde{n}_0$, $\tilde{r}_0$, n_1, r_1, n_2 and r_2, the phases they acquire under the U_2 transformation are the same. This motivates us to combine these partition functions and define, for fixed $\tilde{n}_0, \tilde{r}_0 \in \mathbb{Z}_\mathrm{K}$,

$$\chi^{\tilde{n}_0n_1n_2}_{\tilde{r}_0r_1r_2} = \sum_{t_{1,2},s_{1,2}\in\mathbb{Z}_\mathrm{K}} X^{\tilde{n}_0\bar{n}_1\bar{n}_2}X^{\tilde{r}_0\bar{r}_1\bar{r}_2}, \tag{5.195}$$

where the sum is taken over all quartets $(t_{1,2}, s_{1,2})$ giving rise to given $\tilde{n}_0, \tilde{r}_0$. Observe that $X^{\bar{n}_0\bar{n}_1\bar{n}_2}$ is labeled by two $\mathbb{Z}_\mathrm{K}\times\mathbb{Z}_\mathrm{K}$-valued quantum numbers, and one $\mathbb{Z}_\mathrm{K}$-valued quantum number. On the other hand, $\chi^{\tilde{n}_0n_1n_2}_{\tilde{r}_0r_1r_2}$ depends on six $\mathbb{Z}_\mathrm{K}\times\mathbb{Z}_\mathrm{K}$-valued indices. There are K^6 sectors. From Eq. (5.193), it is straightforward to read off the transformation of χ under the U_2 transformation:

$$\begin{aligned}
&(U_2\chi)^{\tilde{n}_0n_1n_2}_{\tilde{r}_0r_1r_2}\\
&= e^{-\frac{2\pi i}{\mathrm{K}}(\tilde{n}_0n_1+\tilde{r}_0r_1)-\frac{2\pi i}{\mathrm{K}^2}(r_1n_2-r_2n_1)(n_1-r_1)}\chi^{\tilde{n}_0n_1n_2}_{\tilde{r}_0r_1r_2}.
\end{aligned} \tag{5.196}$$

As for the U_1' transformation, the product $X^{\bar{n}_0\bar{n}_1\bar{n}_2}X^{\bar{r}_0\bar{r}_1\bar{r}_2}$ transforms under U_1' as

$$\begin{aligned}&(U_1'X)^{\bar{n}_0\bar{n}_1\bar{n}_2}(U_1'X)^{\bar{r}_0\bar{r}_1\bar{r}_2}\\&=\frac{1}{|\tau|^2\mathrm{K}^4}\sum_{\bar{n}'_{0,1},\bar{r}'_{0,1}\in\mathbb{Z}_\mathrm{K}}e^{i\theta^{\bar{n}'_0\bar{n}'_1\bar{r}'_0\bar{r}'_1}}X^{\bar{n}'_0\bar{n}'_1\bar{n}_2}X^{\bar{r}'_0\bar{r}'_1\bar{r}_2}\end{aligned}\tag{5.197}$$

where the phase θ is given by

$$\begin{aligned}\theta^{\bar{n}'_0\bar{n}'_1\bar{r}'_0\bar{r}'_1}&=\frac{2\pi\bar{n}_0\bar{n}'_1}{\mathrm{K}^2}+\frac{2\pi\bar{n}_1\bar{n}'_0}{\mathrm{K}^2}+\frac{2\pi\bar{r}_0\bar{r}'_1}{\mathrm{K}^2}+\frac{2\pi\bar{r}_1\bar{r}'_0}{\mathrm{K}^2}\\&=\frac{2\pi}{\mathrm{K}}(\tilde{n}_0n'_1+\tilde{n}'_0n_1+\tilde{r}_0r'_1+\tilde{r}'_0r_1)\\&\quad+\frac{2\pi}{\mathrm{K}^2}\big[(r\times n)(n'_1-r'_1)\\&\qquad+(r'_1n_2-r_2n'_1)(n_1-r_1)\big].\end{aligned}\tag{5.198}$$

To derive this result, we note that n_2 and r_2 are invariant under the U_1' transformation. As in our previous discussion on the U_2 transformation, it is crucial to observe that the phase $\theta^{\bar{n}'_0\bar{n}'_1\bar{r}'_0\bar{r}'_1}$ is independent of $t_{1,2}, s_{1,2}$. We are thus led to consider the partition functions $\chi^{\tilde{n}_0n_1n_2}_{\tilde{r}_0r_1r_2}$ defined in Eq. (5.195), which transform, under the U_1' transformation, as

$$\begin{aligned}&(U_1'\chi)^{\tilde{n}_0n_1n_2}_{\tilde{r}_0r_1r_2}\\&=\frac{1}{|\tau|^2\mathrm{K}^2}\sum_{\tilde{n}'_0,n'_{1,2},\tilde{r}'_0,r'_{1,2}}e^{i\theta^{\bar{n}'_0\bar{n}'_1\bar{r}'_0\bar{r}'_1}}\chi^{\tilde{n}'_0n'_1n'_2}_{\tilde{r}'_0r'_1r'_2}\delta_{n_1,n'_2}\delta_{r_1,r'_2}\end{aligned}\tag{5.199}$$

Summarizing, the modular $\mathcal{S}$ and $\mathcal{T}$ matrices are given by

$$\begin{aligned}\mathcal{S}_{n_\mu,n'_\mu,r_\mu,r'_\mu}&=\frac{1}{\mathrm{K}^2}\delta_{n_1,n'_2}\delta_{r_1,r'_2}e^{-\frac{2\pi i}{\mathrm{K}}(\tilde{n}'_0n_2-\tilde{n}_0n'_1+\tilde{r}'_0r_2-\tilde{r}_0r'_1)}\\&\quad\times e^{-\frac{2\pi i}{\mathrm{K}^2}\left[(n_1+r_1)(n_2r'_1+n'_1r_2)-2n_2n'_1r_1-2n_1r_2r'_1\right]},\\\mathcal{T}_{n_\mu,n'_\mu,r_\mu,r'_\mu}&=\delta_{n_\mu,n'_\mu}\delta_{r_\mu,r'_\mu}\\&\quad\times e^{\frac{2\pi i}{\mathrm{K}}(\tilde{n}_0n_1+\tilde{r}_0r_1)+\frac{2\pi i}{\mathrm{K}^2}(r_1n_2-r_2n_1)(n_1-r_1)}.\end{aligned}\tag{5.200}$$

where $n_\mu=(\tilde{n}_0,n_1,n_2)$. Observe that a quick way to obtain this three loop braiding phase is to replace $n_0\to n_0+(r\times n)/\mathrm{K}$, $r_0\to r_0+(n\times r)/\mathrm{K}$, in the $\mathcal{S}$ and $\mathcal{T}$ matrices for the surface of the BF theory (Eq. (5.113)).

The first exponential in the $\mathcal{S}$ matrix, $e^{-2\pi i(\tilde{n}'_0n_2-\cdots)/\mathrm{K}}$, and the first term in Eq. (5.198) represents

$(n_1', r_1; n_2)$	$(n_1', r_1; r_2)$	$(r_1', r_1; n_2)$	$(n_1', n_1; r_2)$
$\frac{2\pi n_2 n_1' r_1}{\mathrm{K}^2}$	$\frac{2\pi r_2 n_1' r_1}{\mathrm{K}^2}$	$-\frac{4\pi n_2 r_1' r_1}{\mathrm{K}^2}$	$-\frac{4\pi r_2 n_1' n_1}{\mathrm{K}^2}$

Table 5.1: The braiding statistical phases (the second line) for the braiding processes between loop a and loop b with base loop c linking both of them (denoted by $(a, b; c)$ in the first line). Here, a, b and c are the quantum numbers for loop excitations.

the particle-loop braiding phase, which exists also in the ordinary BF theory. On the other hand, the second exponential in the $\mathcal{S}$ matrix, $e^{-2\pi i[(n_1+r_1)(n_2 r_1'+n_1' r_2)-\cdots]/\mathrm{K}^2}$, and the second term in Eq. (5.198) describes a topological invariant which can be considered as the higher dimensional generalization of the linking number of closed lines (in three dimensions), and is also related with the three-loop braiding process. [Jiang et al., 2014, Wang and Levin, 2014, Wang and Wen, 2015, Jian and Qi, 2014] More precisely, from the second term in Eq. (5.198), one can extract three-loop braiding statistical phases. For example, the phase factor $e^{2\pi i r_1 n_2 n_1'/\mathrm{K}^2}$ included in Eq. (5.198) can be interpreted as the three-loop braiding statistical phases associated to two loops running in the x-direction with quantum numbers r_1 and n_1' in the presence of a base loop running in the y-direction with quantum number n_2 (Table 5.1). The three-loop braiding statistics encoded in the $\mathcal{S}$-matrix can be further understood through dimensional reduction discussed below.

As for the $\mathcal{T}$ matrix, the first phase factor $e^{2\pi i(\tilde{n}_0 n_1+\tilde{r}_0 r_1)/\mathrm{K}}$ is proposed to be the topological spin for the composite particle-loop excitations in the BF theory. On the other hand, the second phase factor $e^{2\pi i(r_1 n_2 - r_2 n_1)(n_1 - r_1)/\mathrm{K}^2}$ can be considered as the topological spin for the loop excitations with a base loop threading through it. For instance, $e^{2\pi i r_1 n_2 n_1/\mathrm{K}^2}$ represents the topological spin for the loop excitation with quantum number (r_1, n_1) threaded by the loop excitation carrying quantum number n_2.

These results extracted from the boundary $\mathcal{S}$ and $\mathcal{T}$ matrices, (5.200), are consistent with the previous bulk calculations in the literature. [Jiang et al., 2014, Wang and Levin, 2014, Wang and Wen, 2015, Jian and Qi, 2014] In particular, in Ref.[Jiang et al., 2014] the $\mathcal{S}$ and $\mathcal{T}$ matrices in the bulk are calculated in the basis that is constructed from the so-called minimum entropy states (MESs) on the bulk spatial three torus. In Ref.[Wang and Wen, 2015], the bulk $\mathcal{S}$ and $\mathcal{T}$ matrices were constructed for $Z_{N_1} \times Z_{N_2} \times Z_{N_3}$ gauge theories.

Several comments are in order:

(i) The entropy S_T computed from these characters and the modular $\mathcal{S}$ matrix shows, in the limit $R_1/R_0 \to \infty$ and $R_1/R_2 \to \infty$, the asymptotic behavior $S_T = -2\ln \mathrm{K} + \cdots$, where $\cdots$ is the term proportional to the area of the surface. I.e., the constant piece in the (entanglement) entropy is the same as the two decoupled copies of the BF theories.

(ii) For $(3+1)$d topological phases (gauge theories) with $\mathbb{Z}_\mathrm{K} \times \mathbb{Z}_\mathrm{K}$ gauge symmetry, we expect there

$(n_1', r_1; n_2)$	$(n_1', r_1; r_2)$	$(r_1', r_1; n_2)$	$(n_1', n_1; r_2)$
$\frac{2\pi q_2 n_2 n_1' r_1}{K^2}$	$\frac{2\pi q_1 r_2 n_1' r_1}{K^2}$	$-\frac{4\pi q_1 n_2 r_1' r_1}{K^2}$	$-\frac{4\pi q_2 r_2 n_1' n_1}{K^2}$

Table 5.2: Same as Table 5.1, but for generic values of the parameter $q_{1,2} = 0, 1, 2, \ldots, K-1$.

are (at least) K^2 different topological phases that are differentiated by their three-loop braiding statistical phases. This is expected from the group cohomology classification (construction) of SPT phases; from $H^4[\mathbb{Z}_K \times \mathbb{Z}_K, U(1)] = \mathbb{Z}_K \times \mathbb{Z}_K$, we expect there are at least K^2 different SPT phases in (3+1)d protected by unitary on-site symmetry $G = \mathbb{Z}_K \times \mathbb{Z}_K$. Once the global symmetry is gauged, these different SPT phases give rise to K^2 different topologically ordered phases which are differentiated by the three-loop braiding phases.[Dijkgraaf and Witten, 1990, Chen and Fradkin, 2013] The model we studied in this section, the two copies of coupled BF surface theories, corresponds to the surface theory of one of the K^2 topological phases. The surface theories of all the other topological phases can be obtained by tuning the coefficient in the coupling terms. In our model, the coefficient p_1 and p_2 in front of the cubic terms are chosen to be K. In general, they can take value $q_1 K$ and $q_2 K$ with $q_{1,2} = 0, 1, \ldots, K-1$ [Gaiotto et al., 2015] which will lead to K^2 different topological phases with different $\mathcal{S}$ and $\mathcal{T}$ matrices. The three-loop braiding phases will be slightly modified and are shown in Table 5.2, which are consistent with Ref.[Wang and Levin, 2014].

Observe also that for $G = \mathbb{Z}_K$, $H^4[\mathbb{Z}_K, U(1)] = 0$, i.e., there is no non-trivial SPT phase protected by $G = \mathbb{Z}_K$ symmetry. Hence, there is essentially only one topologically ordered phase with $\mathbb{Z}_K$ gauge group, whose surface is described by the one-component surface theory studied in Sec. 5.3. On the other hand, the two-component surface theory studied in this section allows richer possibilities.

(iii) An insight on the three-loop braiding statistics phase can be obtained from dimensional reduction. For the trivial two-component BF theory, there is only a non-trivial particle and loop braiding phase described in Eq. (5.113). This model, after dimensional reduction, reduces to the $D(\mathbb{Z}_K \times \mathbb{Z}_K)$ quantum double model with the K-matrix given by $K\sigma_x \oplus K\sigma_x$.

For the topological phase with non-trivial three-loop braiding statistics phase, the dimensional reduction is more interesting. Here, we consider the simplest non-trivial example with $K = 2$. We perform dimensional reduction on U_1' and $\mathcal{T}$ defined in Eq. (5.199) and Eq. (5.200). When we do so, we need to fix the quantum numbers n_2 and r_2. For example, if we take $n_2 = 0$ and $r_2 = 0$, i.e., there is no third loop connecting the first and second loops, the $\mathcal{S}$ and $\mathcal{T}$ matrices after dimensional reduction are the same as those for the two copies of the toric code model.

On the other hand, if we take $n_2 = 1$ and $r_2 = 1$, the dimensional reduction results in the $\mathcal{S}$ and $\mathcal{T}$

matrices given by

$$\mathcal{S}^{n_i',r_i'}_{n_i,r_i} = \frac{1}{4} e^{\pi i(n_0 n_1' + n_0' n_1 + r_0 r_1' + r_0' r_1) + \pi i (r_1 - n_1)(n_1' - r_1')},$$
$$\mathcal{T}^{n_i',r_i'}_{n_i,r_i} = \delta_{n_i,n_i'} \delta_{r_i,r_i'} e^{\pi i (n_0 n_1 + r_0 r_1) - \frac{\pi i}{2}(n_1 - r_1)^2}. \tag{5.201}$$

This indicates that the (2+1)d topological order described by the K-matrix

$$\mathbf{K} = \begin{pmatrix} 2 & 2 & -2 & 0 \\ 2 & 0 & 0 & 0 \\ -2 & 0 & 2 & 2 \\ 0 & 0 & 2 & 0 \end{pmatrix}. \tag{5.202}$$

By an $SL(2,\mathbb{Z})$ similarity transformation, this K-matrix is equivalent to $\mathbf{K} = 2\sigma_z \oplus 2\sigma_z$, which represents two copies of the double semion model.

Similarly, if we choose $(n_2, r_2) = (1,0)$ and $(0,1)$, the corresponding (2+1)d topological order is described by the K-matrix

$$\mathbf{K} = \begin{pmatrix} 0 & 2 & -1 & 0 \\ 2 & 0 & 0 & 0 \\ -1 & 0 & 2 & 2 \\ 0 & 0 & 2 & 0 \end{pmatrix}, \tag{5.203}$$

and

$$\mathbf{K} = \begin{pmatrix} 2 & 2 & -1 & 0 \\ 2 & 0 & 0 & 0 \\ -1 & 0 & 0 & 2 \\ 0 & 0 & 2 & 0 \end{pmatrix}, \tag{5.204}$$

respectively. To summarize, after dimensional reduction, the original $(3+1)$d topological order with non-trivial three-loop braiding statistics "splits" into four different (2+1)d topological order, which are controlled by the quantum numbers n_2 and r_2. This result seems to be related with the group cohomology classification of symmetry-protected topological (SPT) phases in $(2+1)$d with $G = \mathbb{Z}_2 \times \mathbb{Z}_2$ symmetry, i.e., $H^3[\mathbb{Z}_2 \times \mathbb{Z}_2, U(1)] = \mathbb{Z}_2 \times \mathbb{Z}_2$.

5.6 Discussion

Let us summarize our main results.

– In the (3+1)d BF theory, we have demonstrated, through explicit calculations in the boundary field theories and by comparisons with known bulk results, there is a bulk-boundary correspondence in (3+1)d topological phases. In particular the modular $\mathcal{S}$ and $\mathcal{T}$ matrices are calculated from the gapless boundary field theory and shown to match with the bulk results.

– The surface theory of the (3+1)d BF theory with the theta term is introduced and solved. The action of the modular $\mathcal{S}$ and $\mathcal{T}$ transformations on the partition functions is calculated. It is shown that the partition functions do not form the complete basis under the modular $\mathcal{S}$ and $\mathcal{T}$ transformations.

– Finally, we propose a (3+1)d bulk field theory with cubic coupling that may realize three-loop braiding statistics. We discuss the twist that the cubic term of the field theory adds to the zero modes. By considering the alternative form of the bulk and boundary field theories, in which the quantization rule of the zero modes is twisted, we computed the surface partition functions, and the $\mathcal{S}$ and $\mathcal{T}$ matrices are constructed.

These results extend the well-established bulk-boundary correspondence in (2+1)d topological phases and their (1+1)d edge theories. Our approach from the surface field theories provide an alternative point of view to (3+1)d topological phases, and to recently discussed, novel braiding properties, such as three-loop braiding statistics.

There are, however, still some aspects in the (2+1)d-(1+1)d correspondence, which we do not know if have an analogue in the (3+1)d-(2+1)d correspondence. For example, in the case of the bulk-boundary correspondence connecting (2+1)d topological phases and (1+1)d edge theories, that the edge theories are invariant under an infinite-dimensional algebra seems to play a significant role: the Virasoro algebra or an extended chiral algebra of (1+1)d CFTs faithfully mirrors bulk topological properties of (2+1)d bulk phases. On the practical side, that edge theories enjoy an infinite-dimensional symmetry algebra provides many non-trivial solvable examples. For our example of (2+1)d surface theories of (3+1)d topological phases, on the other hand, we did not make use of such infinite-dimensional symmetry. In fact, the surface theories studied in this chapter are not conformal field theories. For example, the two-point correlation function of the boson field $\langle\phi(t,\mathsf{r})\phi(t',\mathsf{r}')\rangle$ in the free boson theory in (2+1)d decays algebraically. This should be contrasted with the logarithmic decay of the corresponding correlator in the (1+1)d compactified boson theory. As a consequence, the correlation functions of the bosonic exponents $\exp[im\phi(t,\mathsf{r})]$ ($m \in \mathbb{Z}$) do not decay algebraically in the (3+1)d free boson theory. Whether or not there exists a unified field theory framework in (2+1)d field theories that strongly resonates with topological properties of (3+1)d bulk topological phases requires further investigations.

References

[Affleck,] Affleck, I. Exact critical exponents for quantum spin chains, non-linear σ models at $\theta = \pi$ and the quantum hall effect. *Nucl. Phys. B*.

[Affleck, 1986] Affleck, I. (1986). Universal term in the free energy at a critical point and the conformal anomaly. *Phys. Rev. Lett.*, 56:746.

[Affleck and Ludwig,] Affleck, I. and Ludwig, A. W. W. *Phys. Rev. Lett.*

[Agarwal et al., 2015] Agarwal, K., Gopalakrishnan, S., Knap, M., Mueller, M., and Demler, E. (2015). *Phys. Rev. Lett.*, 114:160401.

[Amico et al., 2008] Amico, L., Fazio, R., Osterloh, A., and Vedral, V. (2008). Entanglement in many body systems. *Rev. Mod. Phys.*, 80:517.

[Amoretti et al., 2012] Amoretti, A., Blasi, A., Maggiore, N., and Magnoli, N. (2012). Three-dimensional dynamics of four-dimensional topological BF theory with boundary. *New Journal of Physics*, 14(11):113014.

[Anderson, 1958] Anderson, P. W. (1958). Absence of diffusion in certain random lattices. *Phys. Rev.*, 109:1492.

[Araki and Lieb, 1970] Araki, H. and Lieb, E. H. (1970). *Communications in Mathematical Physics*, 18:160.

[Ardonne et al., 2004] Ardonne, E., Fendley, P., and Fradkin, E. (2004). *Annals Phys.*, 310:493.

[Asplund et al., 2015] Asplund, C. T., Bernamonti, A., Galli, F., and Hartman, T. (2015). Entanglement scrambling in 2d conformal field theory. *J. High Energy Phys.*, 2015:110.

[Balachandran and Teotonio-Sobrinho, 1993] Balachandran, A. P. and Teotonio-Sobrinho, P. (1993). The Edge States of the BF System and the London Equations. *International Journal of Modern Physics A*, 8:723–752.

[Banks and Seiberg, 2011] Banks, T. and Seiberg, N. (2011). Symmetries and strings in field theory and gravity. *Phys. Rev. B*, 83(8):084019.

[Basko et al., 2006] Basko, D. M., Aleiner, I. L., and Altshuler, B. L. (2006). Metal–insulator transition in a weakly interacting many-electron system with localized single-particle states. *Ann. Phys.*, 321:1126.

[Bauer and Nayak, 2013] Bauer, B. and Nayak, C. (2013). Area laws in a many-body localized state and its implications for topological order. *Journal of Statistical Mechanics: Theory and Experiment*, 9:5.

[Bekenstein et al., 1973] Bekenstein, J. D., Koul, R. K., Lee, J., and Sorkin, R. D. (1973). *Phys. Rev. D*, 7:2333.

[Bergeron et al., 1995] Bergeron, M., Semenoff, G. W., and Szabo, R. J. (1995). Canonical BF-type topological field theory and fractional statistics of strings. *Nuclear Physics B*, 437:695–721.

[Bianchi and Myers, 2012] Bianchi, E. and Myers, R. C. (2012). On the architecture of spacetime geometry. *Class. Quantum Grav.*, 31:214002.

[Birmingham et al., 1991] Birmingham, D., Blau, M., Rakowski, M., and Thompson, G. (1991). Topological field theory. *Phys. Rept.*, 209:129–340.

[Bisognano and Wichmann, 1976] Bisognano, J. J. and Wichmann, E. H. (1976). On the duality condition for quantum fields. *J. Math. Phys.*, 17:303.

[Blau and Thompson, 1989] Blau, M. and Thompson, G. (1989). A New Class of Topological Field Theories and the Ray-singer Torsion. *Phys. Lett.*, B228:64.

[Blau and Thompson, 1991] Blau, M. and Thompson, G. (1991). Topological Gauge Theories of Antisymmetric Tensor Fields. *Annals Phys.*, 205:130–172.

[Blote et al., 1986] Blote, H. W., Cardy, J. L., and Nightingale, M. P. (1986). Conformal invariance, the central charge, and universal finite-size amplitudes at criticality. *Phys. Rev. Lett.*, 56:742.

[Bombelli et al., 1986] Bombelli, L., Koul, R. K., Lee, J., and Sorkin, R. D. (1986). Quantum source of entropy for black holes. *Phys. Rev. D*, 34:373.

[Bovier et al., 2002] Bovier, A., Kurkova, I., and Lowe, M. (2002). *Ann. Prob.*, 30:605.

[Bueno and Myers, 2015] Bueno, P. and Myers, R. C. (2015). Corner contributions to holographic entanglement entropy. *Journal of High Energy Physics*, 1508:068.

[Bueno et al., 2015] Bueno, P., Myers, R. C., and Witczak-Krempa, W. (2015). Universality of corner entanglement in conformal field theories. *Phys. Rev. Lett.*, 115:021602.

[Buffet, 1993] Buffet, E. (1993). *J. Phys. A*, 26:1823.

[Calabrese and Cardy, 2004] Calabrese, P. and Cardy, J. (2004). Entanglement entropy and quantum field theory. *J. Stat. Mech. JSTAT*, 04:P06002.

[Calabrese and Cardy, 2009] Calabrese, P. and Cardy, J. (2009). Entanglement Entropy and Conformal Field Theory. *JSTAT-J. Statist. Mech.: Theor. Exp.*, 42:504005.

[Calabrese et al., 2009] Calabrese, P., Cardy, J., and Tonni, E. (2009). Entanglement entropy of two disjoint intervals in conformal field theory. *JSTAT-J. Statist. Mech.: Theor. Exp.*, 2009:P11001.

[Calabrese et al., 2012] Calabrese, P., Cardy, J., and Tonni, E. (2012). Entanglement negativity in quantum field theory. *Phys.Rev.Lett.*, 109:130502.

[Callan and Wilczek, 1994] Callan, C. G. and Wilczek, F. (1994). *Phys. Lett. B*, 333:55.

[Cano et al., 2014] Cano, J., Cheng, M., Mulligan, M., Nayak, C., Plamadeala, E., and Yard, J. (2014). Bulk-edge correspondence in $(2 + 1)$-dimensional Abelian topological phases. *Phys. Rev. B*, 89(11):115116.

[Canovi et al., 2011] Canovi, E., Rossini, D., Fazio, R., Santoro, G. E., and Silva, A. (2011). *Phys. Rev. B*, 83:094431.

[Cappelli et al., 2002] Cappelli, A., Huerta, M., and Zemba, G. R. (2002). *Nucl. Phys. B*, 636:568.

[Cappelli and Randellini, 2013] Cappelli, A. and Randellini, E. (2013). *JHEP*, 12:101.

[Cappelli and Viola, 2011] Cappelli, A. and Viola, G. (2011). *J. Phys. A*, 44:075401.

[Cappelli et al., 2010] Cappelli, A., Viola, G., and Zemba, G. R. (2010). *Annals of Physics*, 325:465.

[Cappelli and Zemba, 1997] Cappelli, A. and Zemba, G. R. (1997). *Nucl. Phys. B*, 490:595.

[Caraglio and Gliozzi, 2008] Caraglio, M. and Gliozzi, F. (2008). Entanglement Entropy and Twist Fields. *JHEP-J. High Energy Phys.*, 0811:076.

[Cardy, 1996] Cardy, J. (1996). *Scaling and Renormalization in Statistical Physics*. Cambridge University Press, Cambridge, UK.

[Cardy, 2013] Cardy, J. (2013). Some results on the mutual information of disjoint regions in higher dimensions. *Journal of Physics A: Mathematical and Theoretical*, 46:285402.

[Casini and Huerta, 2005] Casini, H. and Huerta, M. (2005). Entanglement and alpha entropies for a massive scalar field in two dimensions. *Journal of Statistical Mechanics: Theory and Experiment*, 2005:P12012.

[Casini and Huerta, 2007] Casini, H. and Huerta, M. (2007). Universal terms for the entanglement entropy in $2+1$ dimensions. *Nuclear Physics B*, 764:183.

[Casini and Huerta, 2009] Casini, H. and Huerta, M. (2009). Entanglement entropy in free quantum field theory. *Journal of Physics A: Mathematical and Theoretical*, 42:504007.

[Casini and Huerta, 2010] Casini, H. and Huerta, M. (2010). Entanglement entropy for the n-sphere. *Physics Letters B*, 694:167.

[Casini and Huerta, 2012] Casini, H. and Huerta, M. (2012). On the RG running of the entanglement entropy of a circle. *Physical Review D*, 85:125016.

[Casini et al., 2011] Casini, H., Huerta, M., and Myers, R. C. (2011). Towards a derivation of holographic entanglement entropy. *JHEP-J. High Energy Phys.*, 2011:036.

[Casini et al., 2015] Casini, H., Huerta, M., Myers, R. C., and Yale, A. (2015). Mutual information and the F-theorem. *arXiv preprint arXiv:1506.06195*.

[Castelnovo and Chamon, 2007] Castelnovo, C. and Chamon, C. (2007). Entanglement and Topological Entropy of the Toric Code at Finite Temperature. *Phys. Rev. B*, 76:184442.

[Castelnovo and Chamon, 2008] Castelnovo, C. and Chamon, C. (2008). Quantum topological phase transition at the microiscopic level. *Phys. Rev. B*, 77:054433.

[Castelnovo et al., 2004] Castelnovo, C., Chamon, C., Mudry, C., and Pujol, P. (2004). From quantum mechanics to classical statistical physics: Generalized Rokhsar-Kivelson Hamiltonians and the "Stochastic Matrix Form" decomposition. *Annals of Physics*, 318:316.

[Castillo et al., 1997] Castillo, H. E., Chamon, C. C., Fradkin, E., Goldbart, P. M., and Mudry, C. (1997). Exact calculation of multifractal exponents of the critical wave function of dirac fermions in a random magnetic field. *Phys. Rev. B*, 56:10668.

[Chakravarty, 2010] Chakravarty, S. (2010). *Int. J. Mod. Phys. B.*, 24:1823.

[Chan et al., 2013] Chan, A., Hughes, T. L., Ryu, S., and Fradkin, E. (2013). Effective field theories for topological insulators by functional bosonization. *Phys. Rev. B*, 87(8):085132.

[Chandran et al., 2015] Chandran, A., Kim, I. H., Vidal, G., and Abanin, D. A. (2015). Constructing local integrals of motion in the many-body localized phase. *Phys. Rev. B*, 91:085425.

[Chen et al., 2015a] Chen, X., Cho, G. Y., Faulkner, T., and Fradkin, E. (2015a). Scaling of entanglement in $2+1$-dimensional scale-invariant field theories. *J. Stat. Mech.*, page P02010.

[Chen and Fradkin, 2013] Chen, X. and Fradkin, E. (2013). *J. Stat. Mech.*, page P08013.

[Chen et al., 2012] Chen, X., Hsu, B., Hughes, T. L., and Fradkin, E. (2012). *Phys. Rev. B*, 86:134201.

[Chen et al., 2015b] Chen, X., Tiwari, A., and Ryu, S. (2015b). Bulk-boundary correspondence in (3+1)-dimensional topological phases. *arXiv preprint arXiv:1509.04266*.

[Chen et al., 2015c] Chen, X., Yu, X., Cho, G., Clark, B., and Fradkin, E. (2015c). *Phys. Rev. B*, 92:214204.

[Cho and Moore, 2011] Cho, G. Y. and Moore, J. E. (2011). Topological BF field theory description of topological insulators. *Annals of Physics*, 326:1515–1535.

[Cho et al., 2014] Cho, G. Y., Teo, J. C. Y., and Ryu, S. (2014). Conflicting symmetries in topologically ordered surface states of three-dimensional bosonic symmetry protected topological phases. *Phys. Rev. B*, 89(23):235103.

[Cirio et al., 2014] Cirio, M., Palumbo, G., and Pachos, J. K. (2014). *Phys. Rev. B*, 90:085114.

[de C. Chamon et al., 1996] de C. Chamon, C., Mudry, and Wen, X. G. (1996). Gaussian field theories, random cantor sets and multifractality. *Phys. Rev. Lett*, 77:4194.

[Derrida, 1980] Derrida, B. (1980). *Phys. Rev. Lett.*, 45:79.

[Derrida, 1981] Derrida, B. (1981). *Phys. Rev. B*, 24:2613.

[Deutsch, 1991] Deutsch, J. M. (1991). *Phys. Rev. A*, 43:2046.

[Dijkgraaf and Witten, 1990] Dijkgraaf, R. and Witten, E. (1990). Topological gauge theories and group cohomology. *Communications in Mathematical Physics*, 129(2):393–429.

[Ding et al., 2012] Ding, W., Seidel, A., and Yang, K. (2012). Entanglememt entropy of fermi liquids via multidimensional bosonization. *Phys. Rev. X*, 2:011012.

[Dong et al., 2008] Dong, S., Fradkin, E., Leigh, R. G., and Nowling, S. (2008). Topological Entanglement Entropy in Chern-Simons Theories and Quantum Hall Fluids. *JHEP-J. High Energy Phys.*, 05:016.

[Dowker, 2010] Dowker, J. S. (2010). Entanglement entropy for odd spheres.

[Eisert et al., 2010] Eisert, J., Cramer, M., and Plenio, M. B. (2010). Colloquium: Area laws for the entanglement entropy. *Rev. Mod. Phys.*, 82:277.

[Emery et al., 2000] Emery, V. J., Fradkin, E., Kivelson, S. A., and Lubensky, T. C. (2000). *Phys. Rev. Lett.*, 85:2160.

[Evers and Mirlin, 2008] Evers, F. and Mirlin, A. (2008). Anderson transitions. *Rev. Mod. Phys.*, 80:1355.

[E.Witten, 1998] E.Witten (1998). Anti-de Sitter space, thermal phase transition, and confinement in gauge theories. *Adv. Theor. Math. Phys.*, 2:505.

[Fendley et al., 2007] Fendley, P., Fisher, M. P. A., and Nayak, C. (2007). Topological Entanglement Entropy from the Holographic Partition Function. *Journal of Statistical Physics*, 126:1111–1144.

[Fisher, 1994] Fisher, D. S. (1994). *Phys.Rev.B*, 50:3799.

[Fisher and Fradkin, 1985] Fisher, M. P. A. and Fradkin, E. (1985). Localization in a magnetic field: Tight binding model with one-half of a flux quantum per plaquette. *Nucl. Phys. B*, 251 [FS13]:457.

[Fradkin, 2013] Fradkin, E. (2013). *Field Theories of Condensed Matter Systems*. Cambridge University Press, Cambridge, UK.

[Fradkin et al., 2004] Fradkin, E., Huse, D., Moessner, R., Oganesyan, V., and Sondhi, S. L. (2004). On Bipartite Rokhsar-Kivelson points and Cantor Deconfinement. *Phys. Rev. B*, 69:224415.

[Fradkin and Moore, 2006] Fradkin, E. and Moore, J. (2006). Entanglement entropy of 2d conformal quantum critical points. *Phys. Rev. Lett.*, 97:050404.

[Francesco et al., 1997] Francesco, P., Mathieu, P., and Sénéchanl, D. (1997). *Conformal Field Theory*. Springer-Verlag, New York.

[Furukawa and Kim, 2011] Furukawa, S. and Kim, Y. B. (2011). Entanglement entropy between two coupled tomonaga-luttinger liquids. *Phys. Rev. B*, 83:085112.

[Furukawa and Misguich, 2007] Furukawa, S. and Misguich, G. (2007). Topological Entanglement Entropy in the Quantum Dimer Model on the Triangular Lattice. *Phys. Rev. B*, 75:214407.

[Gaiotto et al., 2015] Gaiotto, D., Kapustin, A., Seiberg, N., and Willett, B. (2015). Generalized global symmetries. *Journal of High Energy Physics*, 2:172.

[Gambassi and Calabrese, 2011] Gambassi, A. and Calabrese, P. (2011). *Europhys. Lett.*, 95:6607.

[Gioev and Klich, 2006] Gioev, D. and Klich, I. (2006). Entanglement entropy of fermions in any dimension and the widom conjecture. *Phys. Rev. Lett.*, 96:100503.

[Gogolin et al., 1998] Gogolin, A. O., Nersesyan, A. A., and Tsvelik, A. M. (1998). *Bosonization and Strongly Correlated Systems*. Cambridge University Press, Cambridge, UK.

[Goldstein et al., 2006] Goldstein, S., Lebowitz, J. L., Tumulka, R., and Zanghi, N. (2006). *Phys. Rev. Lett.*, 96:050403.

[Grover and Fisher, 2014a] Grover, T. and Fisher, M. P. A. (2014a). *J. Stat. Mech.*, page P10010.

[Grover and Fisher, 2014b] Grover, T. and Fisher, M. P. A. (2014b). Entanglement and the Sign Structure of Quantum States.

[Grover et al., 2011] Grover, T., Turner, A. M., and Vishwanath, A. (2011). *Phys. Rev. B*, 84:195120.

[Gruzberg et al., 2011] Gruzberg, I. A., Ludwig, A. W. W., Mirlin, A. D., and Zirnbauer, M. R. (2011). *Phys. Rev. Lett*, 107:086403.

[Halperin, 1982] Halperin, B. I. (1982). Quantized Hall conductance, current-carrying edge states, and the existence of extended states in a two-dimensional disordered potential. *Phys. Rev. B*, 25:2185–2190.

[Halsey et al., 1986] Halsey, T. C., Jensen, T., Kadanoff, L., Procaccia, I., and Shraiman, B. (1986). *Phys. Rev. A*, 33:114.

[Hamma et al., 2005a] Hamma, A., Ionicioiu, R., and Zanardi, P. (2005a). Bipartite entanglement and entropic boundary law in lattice spin systems. *Phys. Rev. A*, 71:022315.

[Hamma et al., 2005b] Hamma, A., Ionicioiu, R., and Zanardi, P. (2005b). Ground state entanglement and geometric entropy in the Kitaev model. *Physics Letters A*, 337:22.

[Hansson et al., 2004] Hansson, T. H., Oganesyan, V., and Sondhi, S. L. (2004). Superconductors are topologically ordered. *Annals of Physics*, 313:497–538.

[Hartman and Maldacena, 2013] Hartman, T. and Maldacena, J. (2013). Evolution of entanglement entropy in one-dimensional systems. *J. High Energy Phys.*, 1305:014.

[Hastings et al., 2010] Hastings, M. B., González, I., Kallin, A. B., and Melko, R. G. (2010). Measuring renyi entanglement entropy in quantum monte carlo simulations. *Phys. Rev. Lett.*, 104:157201.

[Hatsugai, 1993] Hatsugai, Y. (1993). Chern number and edge states in the integer quantum Hall effect. *Physical Review Letters*, 71:3697–3700.

[Hawking, 1975] Hawking, S. W. (1975). *Commun. Math. Phys.*, 43:199.

[Henley, 2004] Henley, C. (2004). From classical to quantum dynamics at Rokhsar-Kivelson points. *Journal of Physics: Condensed Matter*, 16:S891.

[Holzhey et al., 1994] Holzhey, C., Larsen, F., and Wilczek, F. (1994). Geometric and renormalized entropy in conformal field theory. *Nucl. Phys. B*, 424:443.

[Horowitz, 1989] Horowitz, G. T. (1989). Exactly soluble diffeomorphism invariant theories. *Communications in Mathematical Physics*, 125:417–437.

[Horowitz and Myers, 1998] Horowitz, G. T. and Myers, R. C. (1998). The AdS/CFT Correspondence and a New Positive Energy Conjecture for General Relativity. *Phy. Rev. D*, 59:026005.

[Horowitz and Srednicki, 1990] Horowitz, G. T. and Srednicki, M. (1990). A quantum field theoretic description of linking numbers and their generalization. *Communications in Mathematical Physics*, 130:83–94.

[Hsieh et al., 2015] Hsieh, C.-T., Cho, G. Y., and Ryu, S. (2015). Global anomalies on the surface of fermionic symmetry-protected topological phases in (3+1) dimensions. *Phys. Rev. B*, 92:075128.

[Hsieh et al., 2014] Hsieh, C.-T., Sule, O. M., Cho, G. Y., Ryu, S., and Leigh, R. G. (2014). Symmetry-protected topological phases, generalized Laughlin argument, and orientifolds. *Phys. Rev. B*, 90(16):165134.

[Hsu and Fradkin, 2010] Hsu, B. and Fradkin, E. (2010). *J. Stat. Mech.*, P09004.

[Hsu et al., 2009] Hsu, B., Mulligan, M., Fradkin, E., and Kim, E.-A. (2009). *Phys. Rev. B*, 79:115421.

[Huse and Oganesyan, 2014] Huse, D. A. and Oganesyan, V. (2014). *Phys. Rev. B*, 90:174202.

[Imbrie, 2014] Imbrie, J. Z. (2014). On Many-Body Localization for Quantum Spin Chains.

[Inglis and Melko, 2013] Inglis, S. and Melko, R. G. (2013). Entanglement at a Two-Dimensional Quantum Critical Point: a $T = 0$ Projector Quantum Monte Carlo Study . *New. J. Phys.*, 15:073048.

[Jaefari and Fradkin, 2012] Jaefari, A. and Fradkin, E. (2012). Pair-density-wave superconducting order in two-leg ladders. *Phys. Rev. B*, 85:035104.

[Jafferis et al., 2011] Jafferis, D., Klebanov, I., Pufu, S., and Safdi, B. (2011). Towards the F-theorem: $\mathcal{N} = 2$ field theories on the three-sphere. *Journal of High Energy Physics*, 2011(6):102.

[Jensen et al., 1987] Jensen, M. H., Kadanoff, L., and Procaccia, I. (1987). *Phys. Rev. A*, 36:1409.

[Jia et al., 2008] Jia, X., Subramaniam, A. R., Gruzberg, I. A., and Chakravarty, S. (2008). *Phys. Rev. B*, 77:014208.

[Jian and Qi, 2014] Jian, C.-M. and Qi, X.-L. (2014). Layer Construction of 3D Topological States and String Braiding Statistics. *Physical Review X*, 4(4):041043.

[Jiang et al., 2014] Jiang, S., Mesaros, A., and Ran, Y. (2014). Generalized Modular Transformations in (3+1)D Topologically Ordered Phases and Triple Linking Invariant of Loop Braiding. *Physical Review X*, 4(3):031048.

[Jin and Korepin, 2004] Jin, B. and Korepin, V. E. (2004). Quantum spin chain, toeplitz determinants and fisher-hartwig conjecture. *J. Stat. Mech.*, 116:79.

[Ju et al., 2012] Ju, H., Kallin, A. B., Fendley, P., Hastings, M. B., and Melko, R. G. (2012). Entanglement scaling in two-dimensional gapless systems. *Phys. Rev. B*, 85:165121.

[Kachru et al., 2008] Kachru, S., Liu, X., and Mulligan, M. (2008). Gravity duals of Lifshitz-like fixed points. *Phys.Rev.*, D78:106005.

[Kallin et al., 2014] Kallin, A. B., Stoudenmire, E. M., Fendley, P., Singh, R. R. P., and Melko, R. G. (2014). Corner contribution to the entanglement entropy of an $O(3)$ quantum critical point in 2+1 dimensions. *J. Stat. Mech.*, page P06009.

[Kapustin and Thorngren, 2014] Kapustin, A. and Thorngren, R. (2014). Anomalies of discrete symmetries in various dimensions and group cohomology. *ArXiv e-prints*.

[Katsura et al., 2010] Katsura, H., Kawashima, N., Kirillov, A. N., Korepin, V. E., and Tanaka, S. (2010). *Journal of Physics A: Mathematical and Theoretical*, 43:255303.

[Khemani et al., 2014] Khemani, V., Chandran, A., Kim, H., and Sondhi, S. L. (2014). *Phys. Rev. E*, 90:052133.

[Khemani et al., 2015] Khemani, V., Pollmann, F., and Sondhi, S. (2015). Obtaining highly-excited eigenstates of many-body localized Hamiltonians by the density matrix renormalization group.

[Kitaev and Preskill, 2006] Kitaev, A. and Preskill, J. (2006). Topological entanglement entropy. *Phys. Rev. Lett.*, 96:110404.

[Kitaev, 2003] Kitaev, A. Y. (2003). Fault-tolerant quantum computation by anyons. *Annals of Physics*, 303:2.

[Kjall et al., 2014] Kjall, J. A., Bardarson, J. H., and Pollmann, F. (2014). *Phys. Rev. Lett.*, 113:107204.

[Klebanov et al., 2011] Klebanov, I. R., Pufu, S. S., and Safdi, B. R. (2011). F-theorem without supersymmetry. *JHEP*, 2011(10):38.

[Kogut and Susskind, 1975] Kogut, J. and Susskind, L. (1975). Hamiltonian formulation of Wilson's lattice gauge theories. *Phys. Rev. D*, 11:395.

[Kravtsov et al., 2015] Kravtsov, V. E., Khaymovich, I. M., Cuevas, E., and Amini, M. (2015). A random matrix model with two localization transitions.

[Lauchli and Schliemann, 2012] Lauchli, A. and Schliemann, J. (2012). Entanglement spectra of coupled s=1/2 spin chains in a ladder geometry. *Phys. Rev. B*, 85:054403.

[Laumann et al., 2014] Laumann, C. R., Pal, A., and Scardicchio, A. (2014). Many-body mobility edge in a mean-field quantum spin glass. *Phys. Rev. Lett.*, 113:200405.

[Levin and Wen, 2006] Levin, M. and Wen, X.-G. (2006). Detecting topological order in a ground state wave function. *Phys. Rev. Lett.*, 96:110405.

[Lewkowycz and Maldacena, 2013] Lewkowycz, A. and Maldacena, J. (2013). Generalized gravitational entropy. *JHEP*, 1308:090.

[Li and Haldane, 2008a] Li, H. and Haldane, F. (2008a). Entanglement spectrum as a generalization of entanglement entropy: identification of topological order in non-abelian fractional quantum Hall effect states. *Phys. Rev. Lett.*, 101:010504.

[Li and Haldane, 2008b] Li, H. and Haldane, F. D. M. (2008b). Entanglement spectrum as a generalization of entanglement entropy. *Phys. Rev. Lett.*, 101:010504.

[Lin and Levin, 2015] Lin, C.-H. and Levin, M. (2015). Loop braiding statistics in exactly soluble 3D lattice models. *ArXiv e-prints*.

[Lopes et al., 2015] Lopes, P. L. e. S., Teo, J. C. Y., and Ryu, S. (2015). Effective response theory for zero-energy Majorana bound states in three spatial dimensions. *Phys. Rev. B*, 91(18):184111.

[Lou et al., 2011] Lou, J., Tanaka, S., Katsura, H., and Kawashima, N. (2011). *Phys. Rev. B*, 84:245128.

[Lu and Vishwanath, 2012] Lu, Y.-M. and Vishwanath, A. (2012). Theory and classification of interacting integer topological phases in two dimensions: A Chern-Simons approach. *Phys. Rev. B*, 86:125119.

[Luca and Scardicchio, 2013] Luca, A. D. and Scardicchio, A. (2013). Ergodicity breaking in a model showing many-body localization. *Europhys. Lett.*, 101:37003.

[Luitz et al., 2014] Luitz, D. J., Alet, F., and Laflorencie, N. (2014). Universal behavior beyond multifractality in quantum many-body systems. *Phys. Rev. Lett.*, 112:057203.

[Luitz et al., 2015] Luitz, D. J., Laflorencie, N., and Alet, F. (2015). Many-body localization edge in the random-field heisenberg chain. *Phys. Rev. B*, 91:081103.

[Lundgren et al., 2012] Lundgren, R., Chua, V., and Fiete, G. A. (2012). *Phys. Rev. B*, 86:224422.

[McMinis and Tubman, 2013] McMinis, J. and Tubman, N. (2013). Renyi entropy of the interacting fermi liquid. *Phys. Rev. B*, 87:081108(R).

[Metlitski et al., 2009] Metlitski, M. A., Fuertes, C. A., and Sachdev, S. (2009). Entanglement entropy in the $O(N)$ model. *Phys. Rev. B*, 80:115122.

[Metlitski and Grover, 2011] Metlitski, M. A. and Grover, T. (2011). Entanglement Entropy in Systems with Spontaneously Broken Continuous Symmetry. arXiv:1112.5166 (unpublished).

[Mezard and Montanari, 2009] Mezard, M. and Montanari, A. (2009). *Information, Physics, and Computation*. Oxford University press, Oxford, UK.

[Moessner and Sondhi, 2001] Moessner, R. and Sondhi, S. L. (2001). Resonating Valence Bond Phase in the Triangular Lattice Quantum Dimer Model. *Phys. Rev. Lett.*, 86:1881.

[Monthus and Garel, 2010] Monthus, C. and Garel, T. (2010). Many-body localization transition in a lattice model of interacting fermions: Statistics of renormalized hoppings in configuration space. *Phys. Rev. B*, 81:134202.

[Moradi and Wen, 2015] Moradi, H. and Wen, X.-G. (2015). Universal topological data for gapped quantum liquids in three dimensions and fusion algebra for non-Abelian string excitations. *Phys. Rev. B*, 91(7):075114.

[Morong and DeMarco, 2015] Morong, W. and DeMarco, B. (2015). Simulation of anderson localization in two-dimensional ultracold gases for pointlike disorder. *Phys. Rev. A*, 92:023625.

[Myers and Singh, 2012] Myers, R. C. and Singh, A. (2012). Comments on Holographic Entanglement Entropy and RG Flows. *JHEP*, 1204:122.

[Nandkishore and Huse, 2015] Nandkishore, R. and Huse, D. A. (2015). Many-Body Localization and Thermalization in Quantum Statistical Mechanics. *Annual Review of Condensed Matter Physics*, 6:15.

[Nishioka and Takayanagi, 2007] Nishioka, T. and Takayanagi, T. (2007). AdS Bubbles, Entropy and Closed String Tachyons. *JHEP*, 0701:090.

[Oda and Yahikozawa, 1990] Oda, I. and Yahikozawa, S. (1990). Linking Numbers and Variational Method. *Phys. Lett.*, B238:272.

[Oganesyan and Huse, 2007] Oganesyan, V. and Huse, D. A. (2007). Localization of interacting fermions at high temperature. *Phys. Rev. B*, 75:155111.

[Oshikawa, 2010] Oshikawa, M. (2010). Boundary Conformal Field Theory and Entanglement Entropy in Two-Dimensional Quantum Lifshitz Critical Point. *arXiv:1007.3739 [cond-mat, physics:hep-th]*. arXiv: 1007.3739.

[Pal and Huse, 2010] Pal, A. and Huse, D. A. (2010). *Phys.Rev.B*, 82:174411.

[Papanikolaou et al., 2007] Papanikolaou, S., Raman, K. S., and Fradkin, E. (2007). Topological phases and topological entropy of two-dimensional systems with finite correlation length. *Phys. Rev. B*, 76:224421.

[Peschel, 2003] Peschel, I. (2003). Calculation of reduced density matrices from correlation functions. *J. Phys. A.*, 36:L205.

[Peschel and Chuang, 2011] Peschel, I. and Chuang, M.-C. (2011). On the relation between entanglement and subsystem hamiltonians. *Europhys. Lett.*, 96:50006.

[Peschel and Eisler, 2009] Peschel, I. and Eisler, V. (2009). *J. Phys. A: Math. and Theor.*, 42:504003.

[Poilblanc, 2010] Poilblanc, D. (2010). Entanglement spectra of quantum heisenberg ladders. *Phys. Rev. Lett.*, 105:077202.

[Polyakov, 1975] Polyakov, A. M. (1975). Compact Gauge Fields and the Infrared Catastrophe. *Phys. Lett.*, B59:82–84.

[Polyakov, 1977] Polyakov, A. M. (1977). Quark Confinement and Topology of Gauge Groups. *Nucl. Phys.*, B120:429–458.

[Popescu et al., 2006] Popescu, S., Short, A. J., and Winter, A. (2006). *Nature Phys.*, 2:754.

[Potter et al., 2015] Potter, A. C., Vasseur, R., and Parameswaran, S. A. (2015). Universal properties of many-body delocalization transitions. *Phys. Rev. X*, 5:031033.

[Qi et al., 2012] Qi, X.-L., Katsura, H., and Ludwig, A. W. W. (2012). General relationship between the entanglement spectrum and the edge state spectrum of topological quantum states. *Phys. Rev. Lett.*, 108:196402.

[Reed and Simon, 1981] Reed, M. and Simon, B. (1981). *I: Functional Analysis*. Methods of Modern Mathematical Physics. Academic Press, London, UK, revised edition.

[Refael and Moore, 2009] Refael, G. and Moore, J. (2009). *Phys. Rev. B*, 42:504010.

[Rokhsar and Kivelson, 1988] Rokhsar, D. S. and Kivelson, S. A. (1988). Superconductivity and the quantum hard-core dimer gas. *Phys. Rev. Lett.*, 61:2376.

[Ros et al., 2015] Ros, V., Müller, M., and Scardicchio, A. (2015). Integrals of motion in the many-body localized phase. *Nuclear Physics B*, 891:420.

[Ryu and Takayanagi, 2006a] Ryu, S. and Takayanagi, T. (2006a). Aspects of Holographic Entanglement Entropy. *JHEP*, 0608:045.

[Ryu and Takayanagi, 2006b] Ryu, S. and Takayanagi, T. (2006b). Holographic derivation of entanglement entropy from ads/cft. *Phys.Rev.Lett.*, 96:181602.

[Ryu and Zhang, 2012] Ryu, S. and Zhang, S.-C. (2012). Interacting topological phases and modular invariance. *Phys. Rev. B*, 85:245132.

[Semenoff, 1984] Semenoff, G. W. (1984). Condensed-Matter Simulation of a Three-Dimensional Anomaly. *Phys. Rev. Lett.*, 53:2449.

[Serbyn et al., 2013] Serbyn, M., Papic, Z., and Abanin, D. A. (2013). *Phys. Rev. Lett.*, 110:260601.

[Sherrington and Kirkpatrick, 1975] Sherrington, D. and Kirkpatrick, S. (1975). *Phys. Rev. Lett.*, 35:1792.

[Srednicki, 1993] Srednicki, M. (1993). Entropy and Area. *Phys. Rev. Lett.*, 71:666.

[Srednicki, 1994] Srednicki, M. (1994). *Phys. Rev. E*, 50:888.

[Stéphan et al., 2009] Stéphan, J. M., Furukawa, S., Misguich, G., and Pasquier, V. (2009). Shannon and entanglement entropies of one and two-dimensional critical wave functions. *Phys. Rev. B*, 80:184421.

[Stéphan et al., 2013a] Stéphan, J.-M., Ju, H., Fendley, P., and Melko, R. G. (2013a). Entanglement in gapless resonanting-valence-bond states. *New. J. Phys.*, 15:015004.

[Stéphan et al., 2013b] Stéphan, J.-M., Ju, H., Fendley, P., and Melko, R. G. (2013b). Entanglement spectra of quantum heisenberg ladders. *New. J. Phys*, 15:015004.

[Stéphan et al., 2011] Stéphan, J.-M., Misguich, G., and Pasquier, V. (2011). Phase transition in the Rényi-Shannon entropy of Luttinger liquids. *Phys. Rev. B*, 84:195128.

[Stéphan et al., 2012] Stéphan, J. M., Misguich, G., and Pasquier, V. (2012). Rényi entanglement entropies in quantum dimer models: from criticality to topological order. *JSTAT-J. Statist. Mech.: Theor. Exp.*, 2012:P02003.

[Stoudenmire et al., 2014] Stoudenmire, E., Gustainis, P., Johal, R., Wessel, S., and Melko, R. G. (2014). Corner contribution to the entanglement entropy of strongly-interacting $O(2)$ quantum critical systems in 2+1 dimensions.

[Sule et al., 2013] Sule, O. M., Chen, X., and Ryu, S. (2013). *Phys. Rev. B*, 88:075125.

[Sun et al., 2009] Sun, K., Yao, H., Fradkin, E., and Kivelson, S. A. (2009). *Phys. Rev. Lett.*, 103:046811.

[Swingle, 2010] Swingle, B. (2010). Entanglement entropy and the fermi surface. *Phys. Rev. Lett.*, 105:050502.

[Tasaki, 1998] Tasaki, H. (1998). *Phys. Rev. Lett.*, 80:1373.

[Thouless, 1974] Thouless, D. J. (1974). Electrons in Disordered Systems and the Theory of Localization. *Physics Reports*, 13:93.

[Tiwari et al., 2014] Tiwari, A., Chen, X., Neupert, T., Santos, L. H., Ryu, S., Chamon, C., and Mudry, C. (2014). Topological BF theory of the quantum hydrodynamics of incompressible polar fluids. *Phys. Rev. B*, 90(23):235118.

[Torres-Herrera and Santos, 2015] Torres-Herrera, E. J. and Santos, L. F. (2015). Dynamics at the many-body localization transition. *Phys. Rev. B*, 92:014208.

[Vasseur and Moore, 2015] Vasseur, R. and Moore, J. E. (2015). Multifractal orthogonality catastrophe in one-dimensional random quantum critical points. *Phys. Rev. B*, 92:054203.

[Vidal et al., 2003] Vidal, G., Latorre, J. I., Rico, E., and Kitaev, A. (2003). *Phys.Rev.Lett.*, 90:227902.

[Vishwanath and Carpentier, 2001] Vishwanath, A. and Carpentier, D. (2001). *Phys. Rev. Lett.*, 86:676.

[Vishwanath and Senthil, 2013] Vishwanath, A. and Senthil, T. (2013). Physics of Three-Dimensional Bosonic Topological Insulators: Surface-Deconfined Criticality and Quantized Magnetoelectric Effect. *Physical Review X*, 3(1):011016.

[Vosk et al., 2014] Vosk, R., Huse, D. A., and Altman, E. (2014). Theory of the many-body localization transition in one dimensional systems. *Phys. Rev. X*, 5:031032.

[Wan et al., 2015] Wan, Y., Wang, J., and He, H. (2015). *Phys. Rev. B*, 92:045101.

[Wang and Levin, 2014] Wang, C. and Levin, M. (2014). Braiding Statistics of Loop Excitations in Three Dimensions. *Physical Review Letters*, 113(8):080403.

[Wang and Levin, 2015] Wang, C. and Levin, M. (2015). Topological invariants for gauge theories and symmetry-protected topological phases. *Phys. Rev. B*, 91(16):165119.

[Wang et al., 2015] Wang, J., Gu, Z.-C., and Wen, X.-G. (2015). Twisted gauge theory model of topological phases in three dimensions. *Phys. Rev. Lett.*, 114:031601.

[Wang and Wen, 2015] Wang, J. C. and Wen, X.-G. (2015). Non-Abelian string and particle braiding in topological order: Modular SL (3 ,Z) representation and (3 +1) -dimensional twisted gauge theory. *Phys. Rev. B*, 91(3):035134.

[Wegner, 1980] Wegner, F. (1980). Inverse participation Ratio in $2 + \epsilon$ Dimensions. *Zeitschrift für Physik B Condensed Matter*, 36:209.

[Wen, 1992] Wen, X.-G. (1992). Theory of the edge states in fractional quantum Hall effects. *Int. J. Mod. Phys.*, B6:1711–1762.

[Wen, 2012] Wen, X.-G. (2012). Topological order: from long-range entangled quantum matter to an unification of light and electrons. *arXiv: 1210.1281*.

[Witczak-Krempa et al., 2015] Witczak-Krempa, W., Sierens, L. E. H., and Melko, R. G. (2015). Cornering gapless quantum states via their torus entanglement. *arXiv:1603.02684 [cond-mat, physics]*.

[Witten, 1989] Witten, E. (1989). Quantum field theory and the Jones polynomial. *Communications in Mathematical Physics*, 121:351–399.

[Wolf, 2006] Wolf, M. (2006). Violation of the entropic area law for fermions. *Phys. Rev. Lett.*, 96:010404.

[Wolf et al., 2008] Wolf, M. M., Verstraete, F., Hastings, M. B., and Cirac, J. I. (2008). Area laws in quantum systems: mutual information and correlations. *Phys. Rev. Lett.*, 100:070502.

[Wu, 1991] Wu, S. (1991). Topological quantum field theories on manifolds with a boundary. *Communications in Mathematical Physics*, 136:157–168.

[Ye and Gu, 2015] Ye, P. and Gu, Z.-C. (2015). Vortex-Line Condensation in Three Dimensions: A Physical Mechanism for Bosonic Topological Insulators. *Physical Review X*, 5(2):021029.

[Yu et al., 2015] Yu, X., Pekker, D., and Clark, B. K. (2015). Finding matrix product state representations of highly-excited eigenstates of many-body localized Hamiltonians.

[Zaletel et al., 2011] Zaletel, M. P., Bardarson, J. H., and Moore, J. E. (2011). Logarithmic Terms in Entanglement Entropies of 2D Quantum Critical Points and Shannon Entropies of Spin Chains. *Phys. Rev. Lett.*, 107:020402.

[Zhang et al., 2012] Zhang, Y., Grover, T., Turner, A., Oshikawa, M., and Vishwanath, A. (2012). Quasiparticle statistics and braiding from ground-state entanglement. *Phys. Rev. B*, 85:235151.

[Zozulya et al., 2009] Zozulya, O. S., Haque, M., and Regnault, N. (2009). Entanglement signatures of quantum Hall phase transitions. *Phys. Rev. B*, 79:045409.

[Zozulya et al., 2007] Zozulya, O. S., Haque, M., Schoutens, K., and Rezayi, E. H. (2007). Bipartite entanglement entropy in fractional quantum Hall states. *Phys. Rev. B*, 76:125310.